Universität Basel

Fakultät für Psychologie

The brain's functional architecture and its links to emotion processing and episodic memory during the resting-state and an encoding task

A cumulative dissertation

Submitted to the Faculty of Psychology, University of Basel, in partial fulfillment of the requirements for the degree of Doctor of philosophy

by

M.Sc. Léonie Geissmann

from Basel, Basel-Stadt, Switzerland

Basel, 2022

First supervisor: Prof. Dr. med Dominique J.-F. de Quervain

Second supervisor: Prof. Dr. med. Andreas Papassotiropoulos

Universität
Basel

Fakultät für
Psychologie

Year of graduation: 2022

Approved by the Faculty of Psychology at the request of

Prof. Dr. med. Dominique de Quervain

Prof. Dr. med. Andreas Papassitoropoulos

Basel,

Prof. Dr. phil. Jens Gaab

Summary

Episodic memory, i.e., the conscious memory for personally experienced events within a particular spatio-temporal context, and emotion processing represent salient features of the clinical picture of many mental disorders, and are tightly intertwined with cognitive functioning.

Over the past three decades, cognitive neuroscience research using functional magnetic resonance imaging (fMRI) has seen two major shifts: firstly, a shift away from region-based to network-based modeling of brain function, and, secondly, more credit is given to the state of the brain during rest. Alongside this progress, substantial advances in fMRI technology and analysis methods have been achieved. There has also been an increase in awareness of the importance of statistical power and inter-individual variability in brain function. The acknowledgment that the brain works as a network consisting of interacting subnetworks and brain regions, a concept falling under the term functional connectivity, has been a milestone in the field of fMRI-based cognitive neuroscience.

This PhD project sought to combine these developments to investigate the brain's functional architecture in relation to episodic memory and emotion processing in healthy young adults.

To investigate whether exposure to emotionally aversive pictures affects subsequent resting-state networks differently from exposure to neutral pictures, Study 1 incorporated a resting-state EEG-fMRI study (n = 34), in which we focused on investigating (i) patterns of amygdala whole-brain and hippocampus connectivity, (ii) whole-brain resting-state networks, and (iii) the amygdala's regional low-frequency fluctuations, all while EEG-recording potential fluctuations in vigilance. Despite the successful emotion induction, none of the resting-state measures was differentially affected by picture valence.

In Study 2, the major aim was to address the extent to which differential brain responsivity during encoding might explain inter-individual differences in episodic memory performance. For this purpose, we analyzed a large sample of adults (n = 1,434) who underwent a picture encoding task in a single MR scanner. Complementing a voxel-based with a network-based approach, Study 2 found that responsivity in some of the regions implicated in successful encoding, as well as responsivity of six functional connectivity networks (FCN), were associated with inter-individual differences in memory performance.

Alongside these two core projects, two other studies, based on the sample from Study 2, looked into emotional memory. Study 3 aimed at investigating the involvement of functional activation clusters and their interactions in the effect of emotional memory enhancement (*n* = 1,418). The results underline the involvement of cortico-cerebellar interactions and localized cerebellar activity. Finally, Study 4 used prediction modeling to investigate FCN responsivity to negative pictures and its links to behavior (*n* = 1,147). The primary objectives were to (i) assess which FCNs are important for negative picture encoding, (ii) detect subjects with peculiarities in FCN responsivity, and (iii) find links between peculiarities between this measure and emotion-related behavioral phenotypes. The main finding was that individuals with peculiarities in network responsivity to negative pictures tend to also have peculiarities in an emotion-related behavioral phenotype.

Overall, this work has strengthened the central assumption that the brain functions as a network during states of resting and episodic memory encoding. The temporal unfolding of emotion processing seems to be not reflected in a subsequent state of rest (Study 1). Brain activity during a task of encoding can be summarized to robust FCNs. The responsivity of six of these FCNs is linked to later free recall performance of the encoded stimuli (Study 2). The cerebellum and its interactions with the cerebrum are involved in emotional memory enhancement (Study 3). Among the healthy, there are individuals with peculiar emotion responsivity on a neurofunctional level (Study 4), a finding which sets the path for future studies to investigate whether it could be a neurofunctional marker for being in an antecedent stage to develop a mental disorder. Together, the findings point to a multifactorial nature of complex behavior. Identifying neurofunctional markers based on inter-individual differences in memory and emotion processing may open the possibility for studying associations with other phenotypes, such as psychological traits, genetic or epigenetic makeup, or individual metabolomic profiles. Our work contributes to the growing understanding of the neurofunctional underpinnings of emotion processing and episodic memory.

Acknowledgments

I would like to thank my supervisor, Prof. Dr. Dominique de Quervain, for his guidance and support through each stage of my PhD project, as well as Prof. Dr. Andreas Papassitoropoulos for his inspirational input and continuous support.

My heartfelt thanks goes to Dr. David Coynel and Dr. Leo Gschwind, whom I have had the pleasure to have countless inspirational conversations with and who have offered me invaluable input and support. Along this way, I have also met my colleagues at the Division of Cognitive Neuroscience and the Division of Molecular Psychology, without whom this project would not have been feasible.

My time as a student and member of the Division of Cognitive Neuroscience has defined my journey as a researcher and will continue to do so. This PhD position has enabled me to research the topic that interests me the most; had I had the chance to build a PhD project from scratch, there would not have been many differences.

I greatly appreciate the support of family and friends. I would also like to thank all other individuals not mentioned by name without whom I would not have been able to complete this dissertation successfully.

Table of contents

Preface

Research articles

The following research articles with first authorship are included in this thesis and discussed in depth:

- Geissmann, L., Gschwind, L., Schicktanz, N., Deuring, G., Rosburg, T., Schwegler, K., Gerhards, C., Milnik, A., Pflueger, M. O., Mager, R., de Quervain, D. J. F., & Coynel, D. (2018). Resting-state functional connectivity remains unaffected by preceding exposure to aversive visual stimuli. *NeuroImage*, *167*, 354–365. https://doi.org/10.1016/j.neuroimage.2017.11.046
- Geissmann, L., Coynel, D., Papassotiropoulos, A., & de Quervain, D. J. F. (n.d.). *Neurofunctional underpinnings of individual differences in visual episodic memory*. [Manuscript submitted for publication]. Division of Cognitive Neuroscience, University of Basel.

The following research article with co-authorship is also included in this thesis and not discussed extensively:

- Fastenrath, M., Spalek, K., Coynel, D., Loos, E., Milnik, A., Egli, T., Schicktanz, N., Geissmann, L., Roozendaal, B., Papassotiropoulos, A., & de Quervain, D. J. F. (n.d.). *Human cerebellum and cortico-cerebellar connections are involved in emotional memory enhancement*. [Manuscript submitted for publication]. Division of Cognitive Neuroscience, University of Basel.

Minor modifications to these research articles include:

- Numeration and format of figures and tables
- All references are provided together in one joint reference section
- The supplementary materials of the manuscripts are provided at the end of this thesis

Any deviation from style format is due to the strive to minimize changes to the original versions. The above-mentioned research articles are referred to as Study 1, Study 2, and Study 3. For improved understanding, some abbreviations may not be introduced at first mention.

Other content

Research project

Study 4 was an important part of the PhD project. It has not been submitted for publication.

Figures

Photographs were taken with an iPhone 11 Pro. Figures representing brain images in the Introduction and Discussion are based on the sample from Study 2 and were created with Nilearn (V. 0.8.1; https://nilearn.github.io/stable/index.html).

"Courage is not the absence of fear,

but rather the assessment that something else is more important than fear"

– Franklin D. Roosevelt

Introduction

Adaptive behavior

Adaptive behavior and the brain

Individuals who can react to the natural environment in ways favorable for long- and short-term survival are more likely to pass their gene line to the next generation.

Throughout evolution, all organisms have developed a repertoire of adaptive responses to evade threats (Perusini & Fanselow, 2015), reflected in evolutionarily well-conserved neurogenic pathways (Mohammad et al., 2016; Narayanan & Rothenfluh, 2016; Wahlstrom et al., 2018). Humans are distinguished from other close species by their highly developed brain. Driven by cell number expansion, morphology changes and cell composition changes, the expansion of the human cerebral cortex and the appearance of new brain regions are unique to humans (Geschwind & Rakic, 2013). Shared core characteristics of fear-related brain circuits across many species include analogies in amygdala circuitry (Janak & Tye, 2015). Different species face different challenges. Consequently, humans are experts at rapidly recognizing, interpreting (Bunford et al., 2020; Okon-Singer et al., 2015; Pascalis et al., 2011), and responding to (El Zein et al., 2015) facial expressions. To disentangle mechanisms of individual variation, an understanding of between-species variation is essential, because individual variation emerges from extreme within-species variation (Darwin, 1979; Insel, 2006). Characteristics of common occurrence and approximate normal distribution within a species may set a basis for the manifestation of extreme forms, such as increased vulnerability for or presence or absence of a mental disorder.

Ontogenetic brain development: Genetics, environment and timing

Throughout prenatal and postnatal development, the brain undergoes marked changes (Chakraborty et al., 2021; Nakagawa & Shimogori, 2012) as a complex function of genetics, environmental factors, and timing (Geschwind & Rakic, 2013). Inter-individual differences in the fine-tuning of brain maturation impact the subsequent brain development. For example, threat responding, linked to the concurrent development of reward and threat circuitry, is differentially expressed as a function of age (Gerhard et al., 2021). Adolescent cocaine exposure can elicit an enduring state of medial prefrontal cortex (PFC) disinhibition suggested to increase susceptibility to mental disorders in adulthood (Cass et al., 2013). In humans, prenatal cannabis exposure has been linked to fetal alterations in hippocampal functional

connectivity as well as distinguishable functional connectivity patterns related to mental disorders at age five (Thomason et al., 2021).

The development of inter-individual differences in brain structure versus brain function

Individual variability in cortical networks' size and topographic organization are under genetic control (Anderson et al., 2021). Localized structural properties give rise to structural connectivity (Nakagawa & Shimogori, 2012). Early thalamic afferents, for example, which are largely genetically programmed, impact the development of cortical morphology and size in a pathway-specific manner (Moreno-Juan et al., 2017). Given their protracted ontogenetical development, functional properties of the brain, as opposed to structural properties, may be less influenced by genetics, and, therefore, be comparatively richer in inter-individual variability (Sydnor et al., 2021). Given the cumulative effect of environmental factors over time, developments most distal from early developmental processes may underlie most inter-individual differences (Sydnor et al., 2021). Ontogenetically later developing brain characteristics, such as functional maturation, may introduce inter-individual differences relevant to adaptive behavior. Higher-level cognitive functions, e.g., attention and working memory, linked to higher-order brain regions, such as the PFC, are among the most distal from both early embryonic signaling gradients and thalamus-mediated sensory inputs (Anderson et al., 2021; Sydnor et al., 2021). Functional connectivity and localized brain activation may be related to inter-individual differences in cognitive functions, yet only for functional connectivity may this brain-behavior association be moderated by age (Tsvetanov et al., 2018).

Functional connectivity

The brain is a network

The brain is organized as a network (van den Heuvel & Hulshoff Pol, 2010). A distinctive feature of the human brain is its ability to flexibly reconfigure interactions within and between populations of neurons. These functional interactions, a term used to describe co-activity of brain regions, indicate communication and coordination of brain activity (Buckner et al., 2008; Shin & Jadhav, 2016), anchored in the notion that the functional expression of cognitive functions requires coactivation of an ensemble of interconnected local area networks (Bressler & Tognoli, 2006). For target regions to respond, the joint action of an assembly of

several tens of thousands of neurons, rather than a single isolated neuron, is necessary (Bressler & Tognoli, 2006). Functional connectivity (FC) reflects the temporal dependence of neural activity patterns of separated brain regions (van den Heuvel & Hulshoff Pol, 2010). The arrangements by which functionally connected brain regions abide can be used to summarize the whole-brain FC architecture into large-scale functional connectivity networks (FCN), offering a means for the examination of links between human behavior and information integration. The functional architecture in the brain is assumed to undergo refinement over the lifespan by sculpting of phylogenetically established pathways (Bressler & Tognoli, 2006). There is still much to learn about the exact mechanisms that underlie functionally interacting brain regions.

Nevertheless, one can assume that FC roots back to bundles of long-distance axonal interconnections between large groups of spatially separated neurons that provide the infrastructure for information transmission in the brain (van den Heuvel & Hulshoff Pol, 2010). Importantly, there is no one-to-one correspondence between structural and functional connectivity (Deco et al., 2011; Whitesell et al., 2021). This is assumed to partly be due to the mutiplexing nature of FCNs that arises from the level of cell populations and fine-grained cytoarchitectonic organization of network members (Whitesell et al., 2021). Phase synchronization of oscillatory neuronal assembly activity might be a mechanism for the fast-time long-range coordination of cortical neuronal assemblies (Chan et al., 2017).

Low-frequency fluctuations in the brain

A distinguishing quality of the mammalian neocortex is patterns of brain-wide slow oscillations (~0.01 – 0.1 Hz) that occur spontaneously in the absence of sensory stimulation (Chan et al., 2017), a state commonly referred to as the resting-state. More precisely, the resting-state is defined as a state of nonattendance in an active task and the absence of external stimulation (Barkhof et al., 2014). The repertoire of FCNs utilized by the brain in action may persist in the resting-state, where they can be mapped as overlapping resting-state networks (RSN) (Biswal et al., 2010; Damoiseaux et al., 2006; Laird et al., 2011; S. M. Smith et al., 2009; van den Heuvel & Hulshoff Pol, 2010). The presence of a meaningful functional network architecture during the resting-state has been described and investigated in depth. Studies leading to this widely recognized validity of RSNs have included modalities beyond fMRI, such as EEG (Deligianni et al., 2014), revealing associations to stable as well as relatively transient characteristics, such

as age (Fransson et al., 2007; Varangis et al., 2019), species adherence (Zhang et al., 2010), psychiatric disorders (Gaudio et al., 2015; Jung et al., 2013; Sorg et al., 2013; Whitfield-Gabrieli & Ford, 2012), cognitive state (Salehi et al., 2020), and drug-specific states (Klumpers et al., 2012; Scheidegger et al., 2012). At least six RSNs have been robustly detected, depending on factors beyond the scope of this paragraph (Uddin et al., 2019; van den Heuvel & Hulshoff Pol, 2010). Commonly used as templates and as a reference for quality checks are the RSNs reported by Smith and colleagues (2009) and region-of-interest-based networks such as those from the Power atlas (Power et al., 2011).

The first documented finding on resting-state (rs) FC traces back to 1995, when Biswal and colleagues (Biswal et al., 1995) demonstrated that rs-BOLD signals are temporally correlated within the somatomotor system. Initially, intrinsic low-frequency oscillations in the brain had been regarded as noise (Purdon & Weisskoff, 1998). The field of neuroscience has come a long way ever since. These days, rs-fMRI studies sparkle with their comparatively easy implementation and relatively simple data aggregation, seemingly comprehensible interpretation and a multitude of analysis approaches available. Brain activity during that unique state is thought to display the intrinsic core of the brain (Uddin et al., 2019), with ion concentration dynamics mediated by neuronal and glial activity as likely contributors in the generation of very slow spontaneous fluctuations (Krishnan et al., 2018).

Adaptive behavior, episodic memory and emotion processing

Memory and emotion processing are key elements for adaptive behavior and mental well-being. Many mental disorders are characterized by difficulties regulating emotional states elicited by memories or thoughts, but such difficulties or peculiarities may also affect non-clinical populations (Kret & Ploeger, 2015). An emotion is defined as an affective state with psychological, experiential, behavioral, and visceral components (Seth, 2013). Emotion regulation is the ability to interrupt or alter the generation of emotional states (Engen & Anderson, 2018). Emotion processing is interlocked with perception, cognition, motivation and action. Emotion states are reactions to external or internal emotional cues and vary depending on arousal, valence, stimulus-specificity (i.e., generalized or specific), and persistence (i.e., enduringness) (Kunwar et al., 2015). Emotion states play a causative role in driving behavior (Kunwar et al., 2015) and are closely linked to episodic memory (Dolcos et al., 2017).

Human episodic memory, the conscious memory for personally experienced events within a particular spatio-temporal context, is unique (Tulving & Markowitsch, 1998). Its content is a self-conscious (re-)construction of a past episode with temporal, spatial, and self-referential context. Episodic memory involves multiple brain systems during encoding, consolidation and retrieval. Several essential steps are included in an efficient retrieval system (Nenert et al., 2014). The encoding phase, during which a stimulus is encountered for the first time, relies on receiving information through sensory modalities and cognitive integration, such as content processing, attention attribution and storage (Kim et al., 2011).

Fundamental neurobiological background

Encoding

The processing cascade of encoding visual stimuli starts with the extraction of lower-level visual properties (e.g., color, contrast), then that of more complex texture information, to the extraction of superordinate categories and up to abstract conceptual and semantic information (Zhang et al., 2020). After being processed by sensory receptors and thalamic nuclei, information from the external world reaches the primary sensory areas of the neocortex. The integration of the representation into a single event with its distinctive contextual and spatiotemporal information critically depends on the hippocampus (Allen & Fortin, 2013). Multimodal representations are funneled into the parahippocampal region, mediating communications between the neocortex and hippocampus.

The hippocampus

The parahippocampal region, which includes the entorhinal cortex, perirhinal cortex, and parahippocampal cortex, is the main interface for cortical-hippocampal connectivity (Murray et al., 2018; Schultz & Engelhardt, 2014; Sekeres et al., 2018). See Figures 1.1 and 1.2 for the illustration of brain regions. The hippocampus contains cytoarchitectonically and functionally distinct subregions, jointly forming a directional circuit, including the subiculum, dentate gyrus, and cornu ammonis (CA) fields, all of which receive major inputs from the parahippocampal region. The dentate gyrus projects to CA3, which projects to itself and CA1, leading to the major hippocampal output originating from the CA1 and subiculum, which terminate in the entorhinal cortex and are connected indirectly and directly to the PFC (Yang et al., 2014).

Figure 1.1

Illustration of brain regions in the left brain hemisphere

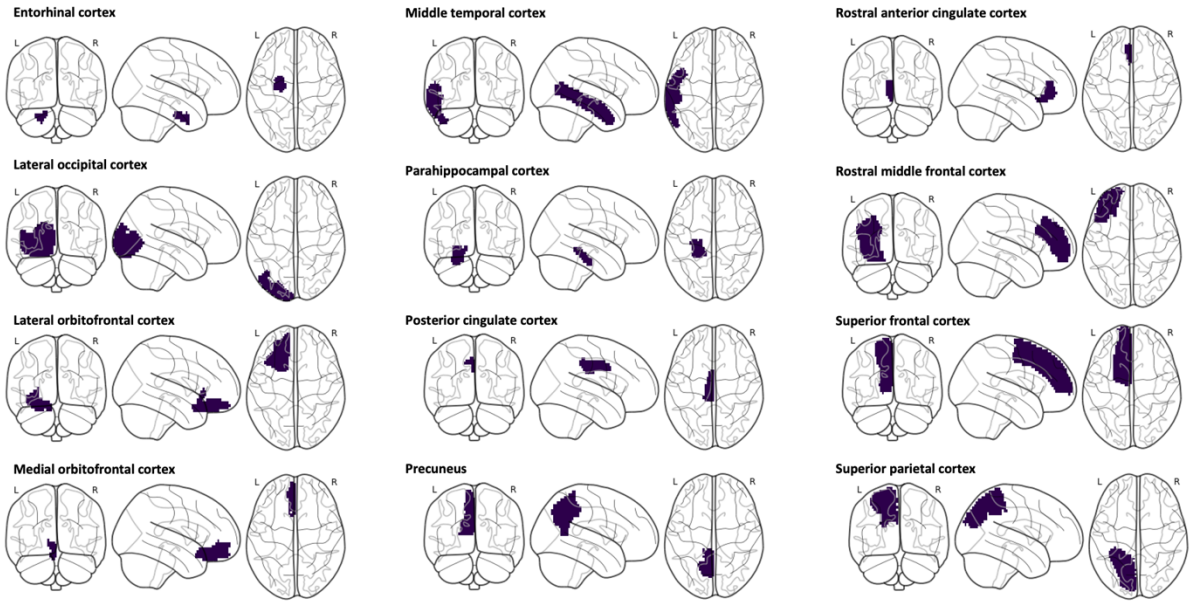

Note. These glass brains are based on an in-house group-based probabilistic atlas of subjects from Study 2.

The process by which memories can guide behavior is thought to critically depend on coordination with the PFC. For example, during anxiety, theta-frequency firing within the ventral hippocampus is synchronized with medial PFC discharge (Adhikari et al., 2011), and prefrontal theta oscillations promote selective encoding of behaviorally relevant events (Jarovi et al., 2018). Both contribute to guiding acutely adaptive anxiety-related behaviors (Padilla-Coreano et al., 2016). With the dynamic character of environmental and internal demands, the ability to flexibly select suitable behaviors is essential, and damage to the PFC impairs that flexibility (Schoenbaum & Roesch, 2005; Sotres-Bayon et al., 2006).

Stimuli and cues that indicate imminent biological significance must be processed differently than situationally irrelevant cues. For acute response selection and efficient future processing, a stimulus or event needs to be recalled with its emotional significance and its spatio-temporal context and updated and integrated into the context of new memories.

Figure 1.2

Illustration of brain regions in the left brain hemisphere

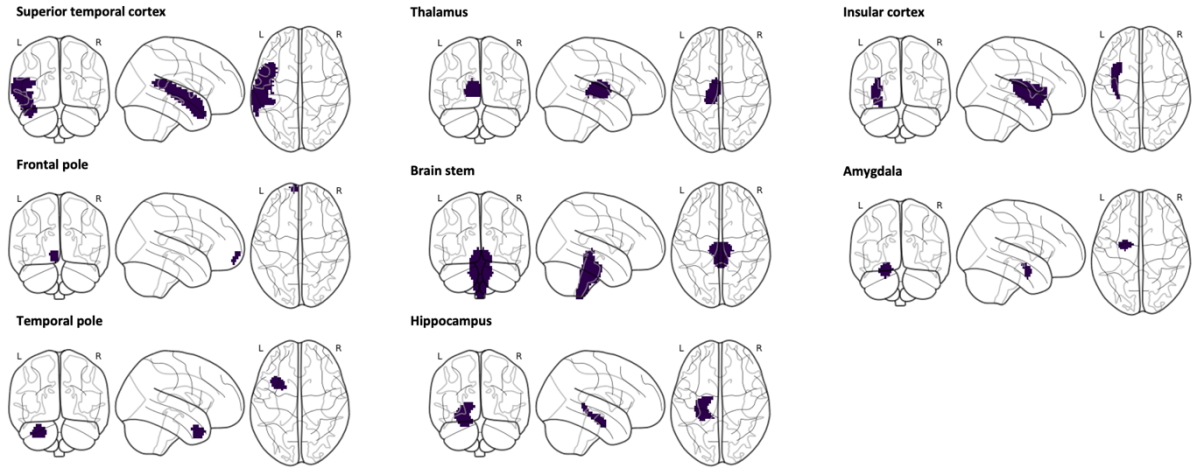

Note. These glass brains are based on an in-house group-based probabilistic atlas of subjects from Study 2.

The amygdala

A critical distinction between neutral and emotional memory formation is the amygdala's involvement (McGaugh, 2004). The amygdala strongly reacts to emotional stimuli and there is ample evidence that functional interactions of the amygdala with other brain regions are critically implicated in emotion processing upon acute emotional stimuli (Banks et al., 2007; Eippert et al., 2007; Erk et al., 2010; Kanske et al., 2011; Townsend et al., 2013). The amygdala receives input from all sensory systems and polymodal cortices. Behavioral responses are generated primarily through amygdala projections to hypothalamic and brainstem centers involved in autonomic control. Among these is the locus coeruleus, a primary norepinephrine synthesis site. Norepinephrine pathways are important in maintaining arousal and level-setting for gathering sensory information and storing emotional memories (Venkatraman et al., 2017). Connections between the amygdala and hippocampal complex contribute to the memory-enhancing effect of emotional arousal (Fastenrath et al., 2014; Richardson et al., 2004; Roozendaal et al., 2009). During an instance of emotional upheaval, the central amygdala activates neurons in hippocampal CA3, which can shut down the activity of nearby CA3 pyramidal neurons that do not receive amygdalar input to affect mnemonic processes.

Connections from the basolateral amygdala (BLA) to ventro-hippocampal CA1 drive approach behavior to exert an anxiolytic effect (Pi et al., 2020).

The PFC plays a role in cognitively and emotionally interpreting affectively valenced stimuli and controlling the subsequent behavioral responses (Höistad & Barbas, 2008), allowing for flexible emotion regulation (Sotres-Bayon & Quirk, 2010). In humans, top-down and bottom-up mechanisms orchestrated by interactions between the amygdala and medial PFC have been discussed extensively in the context of anxiety and emotion regulation (Kim et al., 2011; Park et al., 2018; Sussman et al., 2016).

The BLA has widespread connections across the brain. It has reciprocal connections with the hippocampus (Pi et al., 2020), unidirectional outputs to the striatum (including nucleus accumbens), bed nucleus of the stria terminalis (BNST) and central amygdala translating BLA signals into behavioral output. Activation of glutamatergic somata in the BLA has anxiogenic effects (Tye et al., 2011), while stimulation of the BLA terminals in the central amygdala and the BNST has anxiolytic effects (Kim et al., 2013). Other neurons of the BLA bypass the central amygdala and directly project to the periaqueductal gray and paraventricular nucleus of the thalamus. The amygdala is involved in avoidance and defensive behaviors, appetitive and approaching behaviors, and weighing the relative value of biologically significant outcomes depending on emotional valence.

Valence and salience are encoded in neural circuits that include the amygdala but also other regions such as the nucleus accumbens and PFC (Tye, 2018). In coalescence with the amygdala, the cerebellum integrates multiple internal presentations with external stimuli, thereby maintaining behavior around a homeostatic baseline, serving as an unconscious oscillation dampener to optimize performance to context (Schmahmann et al., 2019). The amygdala thus is a composite of parallel circuits that contribute to imperative cognitive functions in downstream regions.

After the encoding phase, over time, internal representations gained through experience are constructed via long-lasting physical changes to the brain (Yang et al., 2014), which can be reactivated by recapitulating the initial spatio-temporal pattern of neural activity that occurred during the experience (Josselyn & Frankland, 2018). In the BLA and the CA1 subregion, one experience is allocated to a small subset of neurons. The magnitude of intrinsic neuronal excitability is decisive for how and where information is encoded in the lateral amygdala, and the same applies to the hippocampus. Once allocated, neurons become

essential for subsequent expression of that specific memory. It can be recapitulated by artificial reactivation to the neurons allocated to an engram, even in the absence of external retrieval cues (Josselyn & Frankland, 2018). Learning itself initiates the reconstruction processes of an engram via an increase of neuronal excitability and an increase in CREB function. Contextual memories acquired in temporal proximity to each other become functionally linked via co-allocation, as illustrated in engram overlaps for acquired memories after up to 6 hours but not after 18 hours (Josselyn & Frankland, 2018). This exemplifies that the simple reactivation of distinct engrams during memory retrieval may link them together. Synaptic plasticity mechanisms within the amygdala have been identified as a key component underlying the ability to learn and store specific emotional experiences (Rodrigues et al., 2004). After the initial synaptic strengthening ocurrs during learning-related plasticity, i.e., during encoding, other processes take over to maintain the potentiation of synapses and ensure long-term storage (Fonseca et al., 2006). During memory retrieval, synapses undergo re-strengthening, called reconsolidation (Alberini & LeDoux, 2013), at the same time rendering memories labile to editing. This allows current memories to interact with the retrieved ones, and new information to be integrated, such as if the cue was present in a different context from the initial experience (Bravo-Rivera & Sotres-Bayon, 2020). Memory formation is highly complex and depends on factors before, during and after encoding (Urgolites et al., 2020).

Memory-enhancing effects during encoding

Hippocampal dynamics in close temporal proximity to initial encoding are predictive of better memory, such as pre-encoding and peri-encoding hippocampal spike activity indicative of “ready-to-encode” hippocampal mode 1,000 to 2,000 ms before stimulus presentation to directly after presentation (Urgolites et al., 2020), increase in intra-hippocampal phase coherence during the first 1,000 ms after item presentation linked to better encoding (Lin et al., 2017), and locus coeruleus activation supporting Schaffer collateral-CA1 mechanisms relevant for memory promoting encoding of spatial information (Lemon et al., 2009). During encoding, presence of neuromodulators, such as norepinephrine and cortisol, triggers an increase in activity and connectivity in brain regions such as the hippocampus, amygdala, and PFC (Vaisvaser et al., 2013; Veer et al., 2012). Activation of the locus coeruleus increases CA1 noradernaline levels to facilitate selecting relevant information to prioritize during encoding

(Lemon et al., 2009). Modulation of acetylcholine receptors on cortico-amygdala glutamatergic synapses is boosted by activation of BLA cholinergic terminals (Jiang et al., 2016).

Memory-enhancing effects after encoding

The effects of these neuromodulators affect encoding as well as temporally less proximal consolidation stages (e.g., sleep), serving as emotional tagging entities (Kim & Payne, 2020). Sleep architecture is a mediator of stress levels during encoding emotional stimuli to affect memory, which is affected by neuromodulators (Denis et al., 2021). The emotional tone of an experience is reduced over time (Dolcos et al., 2005), yet its influence endures far beyond the initial encoding phase. Even after one year, recognition performance has been shown to still be better for emotional versus neutral stimuli, supported by specific neurofunctional activation patterns (Dolcos et al., 2005). Aversive memories stored in defensive survival circuits can last a lifetime (Gale et al., 2004). Event-specific reactivation of encoding processes during rest assist in successful memory consolidation (Staresina et al., 2013), with general wakeful rest following immediate encoding being beneficial for memory (Martini et al., 2018).

General overview of the PhD project

Main objectives

This PhD project primarily addressed FC in relation to emotion processing and episodic memory.

Study 1: The effects of emotion processing on resting-state functional connectivity

The first emphasis was on emotion processing and its impact on rs-FC.

This was realized in Study 1, which looked into the effects of encoding aversive pictures on subsequent FC measures during the resting-state. This study used a two-group repeated-measures EEG-rs-fMRI paradigm, wherein emotions were elicited in a picture encoding task in the experimental group. In constrast, the control group viewed neutral pictures. A versatility of analysis methods was implemented to showcase the functional network architecture during the resting-state and relate it to the neurofunctional consequences of emotion processing.

Study 2: Task-based functional connectivity, basic neurofunctional underpinnings of episodic memory and inter-individual differences in memory performance

The second key focus was on episodic memory.

Data of task-based functional activation during picture encoding was modeled in both voxel-based and network-based ways to unravel the basic neurofunctional underpinnings of episodic memory and inter-individual differences in memory performance. To chart whole-brain FCNs, methods commonly used for rs-fMRI were tested and validated. To unlock inter-individual differences in episodic memory, a brain-behavior correlational approach was used.

Study 3: Emotional memory enhancement and cortico-cerebellar interactions

The third study looked into the effect of emotional memory enhancement.

The procedure was to (i) check for the involvement of functional activation clusters in this effect. From there, (ii) interactions between these activation clusters were investigated.

Study 4: Task-based functional connectivity and emotion-related behavioral phenotypes

Study 4 looked into in emotion processing.

Based on data from Study 2, we looked into associations between peculiarities in FCN responsivity to negative pictures and emotion-related behavioral variables. The objective was to find neurofunctional markers for presumed vulnerability to developing a mental disorder in healthy individuals.

Methods: General overview

Experimental paradigm

In humans, viewing unpleasant pictures generates defensive reactions, which may account for the emotional modulation of memory (Perusini & Fanselow, 2015). Picture tasks are widely used in human brain activation studies, and viewing emotional pictures acutely increases activation in several brain regions, including the amygdala and hippocampus (Fastenrath et al., 2014; Murty et al., 2010; Rasch et al., 2009).

Both studies involved a picture encoding task. IAPS pictures (Lang et al., 2005) and geometrical figures (Spreen & Strauss, 1991) were presented and rated for either arousal and valence or shape and size, respectively.

Neuroimaging

To measure brain activity, we used functional magnetic resonance (fMRI). The fMRI technique makes use of the differential physical properties of the blood oxygenation status, which changes as a function of brain activity (Logothetis, 2003).

Electroencephalography (EEG), which measures the electrical activity of large, synchronously firing populations of neurons in the brain (Light et al., 2010), was used simultaneously with fMRI in Study 1 to track fluctuations in vigilance and wakefulnes. As these may co-vary with changes in rs-FC (Olbrich et al., 2009; Tagliazucchi et al., 2012), this was vital to ensure rs-fMRI data quality.

Study 1: Resting-state functional connectivity remains unaffected by preceding exposure to aversive visual stimuli

Title:

Resting-state functional connectivity remains unaffected by preceding exposure to aversive visual stimuli

Authors:

Léonie Geissmann[1,2], Leo Gschwind[1,2,3], Nathalie Schicktanz[1,2], Gunnar Deuring[4], Timm Rosburg[4], Kyrill Schwegler[1,2,5], Christiane Gerhards[1,2], Annette Milnik[2,3,5], Marlon O. Pflueger[4], Ralph Mager[4], Dominique J. F. de Quervain[1,2,5], David Coynel[1,2]

Affiliations:

[1]Division of Cognitive Neuroscience, Department of Psychology, University of Basel, Birmannsgasse 8, 4055 Basel, Switzerland, [2]Transfaculty Research Platform Molecular and Cognitive Neurosciences (MCN), University of Basel, Birmannsgasse 8, 4055 Basel, Switzerland, [3]Division of Molecular Neuroscience, Department of Psychology, University of Basel, Birmannsgasse 8, 4055 Basel, Switzerland, [4]Department of Forensic Psychiatry, University Psychiatric Clinics Basel, Wilhelm Klein-Strasse 27, 4002 Basel, Switzerland, [5]Psychiatric University Clinics, University of Basel, 4055 Basel, Switzerland.

Abstract

While much is known about immediate brain activity changes induced by the confrontation with emotional stimuli, the subsequent temporal unfolding of emotions has yet to be explored. To investigate whether exposure to emotionally aversive pictures affects subsequent resting-state networks differently from exposure to neutral pictures, a resting-state fMRI study implementing a two-group repeated-measures design in healthy young adults (*N*=34) was conducted. We focused on investigating (i) patterns of amygdala whole-brain and hippocampus connectivity in both a seed-to-voxel and seed-to-seed approach, (ii) whole-brain resting-state networks with an independent component analysis coupled with dual regression, and (iii) the amygdala's fractional amplitude of low-frequency fluctuations, all while EEG recording potential fluctuations in vigilance. In spite of the successful emotion

induction, as demonstrated by stimuli rating and a memory-facilitating effect of negative emotionality, none of the resting-state measures was differentially affected by picture valence. In conclusion, resting-state networks connectivity as well as the amygdala's low-frequency oscillations appear to be unaffected by preceding exposure to widely used emotionally aversive visual stimuli in healthy young adults.

Keywords

Resting-state, functional connectivity, fMRI, amygdala, emotion, resting-state networks

Highlights:

- The short-term effect of emotional stimuli on resting-state measures was explored
- Subjects were exposed to either neutral or negative emotional pictures
- None of the resting-state measures were differentially affected by picture valence
- EEG-monitored fluctuations in vigilance did not act as confounders
- On a behavioral level, a memory-enhancing effect of negative valence was observable

Introduction

Emotions are closely tied to cognitive, attentional and motivational processes. The amygdala strongly reacts to emotional stimuli and there is ample evidence that functional interactions of the amygdala with other brain regions are critically implicated in emotion processing upon acute emotional stimuli (Banks et al., 2007; Eippert et al., 2007; Erk et al., 2010; Townsend et al., 2013). The amygdala receives input from all sensory systems and polymodal cortices. Behavioral responses are generated primarily through amygdala projections to hypothalamic and brainstem centers involved in autonomic control. Among these is the locus coeruleus (LC), a major norepinephrine synthesis site. Norepinephrine pathways are important in maintaining arousal and level-setting for gathering sensory information and storing emotional memories (Venkatraman et al., 2017). Connections between the amygdala and the hippocampal complex contribute to the memory-enhancing effect of emotional arousal (Fastenrath et al., 2014; Richardson et al., 2004; Roozendaal et al., 2009), while, the prefrontal cortex (PFC) plays a role in cognitively and emotionally interpreting affectively valenced stimuli, and in controlling the subsequent behavioral responses (Höistad & Barbas, 2008). In humans, top-down and bottom-up mechanisms orchestrated by interactions between the amygdala and

medial PFC have been discussed extensively in the context of anxiety and emotion regulation (Kim et al., 2011).

Whereas much is known about the immediate effects of emotions on brain activations measured with blood-oxygen-level dependent contrast (BOLD) functional imaging during the acute emotional state (Murty et al., 2010; Verduyn et al., 2015; Waugh & Schirillo, 2012), little is known about the further temporal unfolding of emotions and their long-term neural consequences. On the behavioral level, there is ample evidence for such long-term consequences. For example, pathological anxiety may be expressed in excessive apprehension subsequent to immediate emotion processing (Calhoon & Tye, 2015). Moreover, in animals it has been shown that the amygdala plays a key role in enhancing memory consolidation processes and, thereby, long-term memory of emotionally arousing information (Phelps & LeDoux, 2005; Roozendaal et al., 2009).

One possibility to investigate delayed neural consequences of emotional stimuli is to analyze functional connectivity (FC) in a resting-state period after an emotional task. The resting-state is defined as a state of nonattendance in an active task and absence of external stimulation (Barkhof et al., 2014), while FC reflects the temporal dependence of neural activity patterns of separated brain regions (van den Heuvel & Hulshoff Pol, 2010). The repertoire of functional networks utilized by the brain in action may persist in the resting-state, where they can be mapped as overlapping resting-state networks (RSN) (Biswal et al., 2010; Damoiseaux et al., 2006; Laird et al., 2011; Smith et al., 2009) using resting-state functional magnetic resonance imaging (rs-fMRI). Among the most commonly used approaches for identifying functionally interacting brain regions from rs-fMRI data are independent component analysis (ICA), seed-to-voxel, and seed-to-seed approaches (Smith et al., 2014; Whitfield-Gabrieli, & Nieto-Castanon, 2012). Besides network measures, BOLD signal changes in regional spontaneous activity are valuable complements for characterizing resting-state low-frequency oscillations (LFO), e.g. fractional amplitude of low-frequency fluctuations (fALFF) (Zou et al., 2008).

Whereas initial cognitive theories have regarded the resting-state as a “default state of mind”, it is becoming clearer now that cognitive activity also affects later rs-FC. Studies in healthy subjects have already indicated that the time following acute stressors is characterized by particular patterns of amygdala-FC, e.g. increased amygdala-FC after watching highly aversive video clips (van Marle, Hermans, Qin, & Fernández, 2010). More

precisely, female subjects not used to violent media watched a movie of 1.5 min duration while inside the MRI scanner. Directly afterwards, enhanced amygdala-FC with a set of predefined regions was observed (van Marle et al., 2010). Among those was the dorsal anterior cingulate cortex (dorsal ACC) and anterior insula (AI), which are implicated in the subjective experience of emotion, and the LC, which contributes to arousal by noradrenergic innervations to the amygdala. In another study, as much as 1 hour after a well-established psychosocial stress task, increased amygdala-FC with cortical midline structures, pertaining to the default mode network (DMN), and the medial PFC was found (Veer et al., 2011). The authors discuss the increased amygdala-FC with DMN regions as reflecting stress-induced facilitation of self-evaluative processes under emotionally salient experiences. The enhancements in amygdala-medial PFC coupling may be an indicator of top-down processes (Kim et al., 2011; Veer et al., 2011).

Here we investigated if emotionally arousing pictures similar to stressful events can also induce changes in rs-FC. We chose a picture task because such tasks are widely used in human brain activation studies, and because viewing emotional pictures acutely increases activation in several brain regions, including the amygdala and hippocampus (Fastenrath et al., 2014; Murty et al., 2010; Rasch et al., 2009). Since emotional arousal is known to enhance not only memory encoding but also memory consolidation processes (Roozendaal et al., 2009), we hypothesized that such long-term effects may be reflected in increased amygdala rs-FC with brain regions like the hippocampus.

Implementing a repeated-measures mixed design with two experimental groups of equal size (total *N*=34), a neutral-picture and a negative-picture group, we focused on the between-groups comparison in terms of changes in rs-FC from baseline (pre-intervention) to post-intervention (time point*group interaction). In a first step, we investigated FC of the amygdala with the whole brain in a seed-to-voxel approach, as well as with the hippocampus only in a ROI-to-ROI analysis. In a second step, we used ICA coupled with dual regression to assess functional connectivity changes in the brain in a more explorative way to address the diversity of networks potentially involved in emotion regulation. To get a complementary view on the amygdala's regional resting-state activity, we additionally extracted its mean fALFF. For validation purposes, the seed-based analyses done with amygdala masks were conducted with two segmentation procedures. Upon a more explorative background, we secondarily investigated FC of the hippocampus with the whole brain. Due to the uncontrolled nature of

vigilance in rs-fMRI (Tagliazucchi & Laufs, 2014), we utilized simultaneous electroencephalography (EEG)-fMRI recordings to take into account in a post-hoc manner potential fluctuations in vigilance.

Materials and methods

Subjects

Thirty-four healthy, normal-weight (BMI 19 to 25) subjects aged 18 to 25 participated in this study (M = 22.5, SD = 2.06 range = 18.4 to 25.8). Male (N_{male} = 14) and female (N_{female} = 20) subjects did not significantly differ in age ($t(31.3) = 0.94$, $p = 0.35$). Participation was not possible if one or more of the following applied: regular intake of medical drugs with the exception of oral contraceptives, currently pregnant or breastfeeding, known or suspected non-compliance, drug or alcohol abuse, inability to follow the procedures of the study (e.g. due to language problems), present diagnosis of acute or chronic mental and/or somatic disorder, presently doing psychotherapy, not fulfilling MRI eligibility criteria. Previous participation in another study of the Transfaculty Research Platform Molecular and Cognitive Neurosciences (MCN), University of Basel, Switzerland (< 2 years ago), if concordant visual stimuli employed, was also an exclusion criterion. For eligibility clarification, a psychologist screened subjects by telephone. When in doubt, assertion was obtained through medical counseling. Written informed consent was given at the study visit day. The study was conducted in approval with the local Ethics Committee, Ethikkommission Nordwest- und Zentralschweiz (EKNZ), Switzerland. The study took place between March and June 2015.

The method of allocating participants to a picture valence group (negative-group vs. neutral-group) was quasi-random: there was an alternation per participant in the order they were included in the study. Indispensably, towards the end of the study, three exceptions had to be made in order to equalize the ratio of experimental group within the factor sex. Subjects were instructed to refrain from caffeine intake and cigarette smoking at least 2 h, cannabis intake at least 2 weeks, alcohol and medical drug intake at least 24 h prior to commencement of the experiment, and to adhere to their personal sleeping habits the night before the examination.

Depression scores were measured with a screening questionnaire, the long version of the Allgemeine Depressionsskala (ADS) (Hautzinger & Bailer, 1993) (supplementary Table A1). Generally, there were no scores indicative for presence of depression (Table 2.1). However,

two female subjects and one male subject met or surpassed the clinical threshold of 23 points. As exclusion of these subjects did not alter the results of the main brain imaging analyses (section Seed-to-voxel analyses), we retained them in the analyses while controlling for depression score by including it as a covariate (section Brain imaging analysis).

Experimental procedure

The experimental procedure is illustrated in Figure 2.1. Upon arrival, written informed consent was acquired and the participant was made familiar with the MRI environment. After this, about 50 min were spent filling out questionnaires while the investigator was attaching the EEG electrodes. Participants wore the EEG cap during the entire experiment. EEG was recorded in five sessions: shortly before the first MRI as a brief quality check, during both MRI sessions, during the pictorial rating task and throughout the free recall task. After satisfactory quality check of the EEG signal (impedances well below 20 kΩ; for reference and ground electrodes below 10 kΩ), the first MRI session followed, which took about 20 min. This started with the structural imaging.

Figure 2.1

Illustration of the experimental procedure

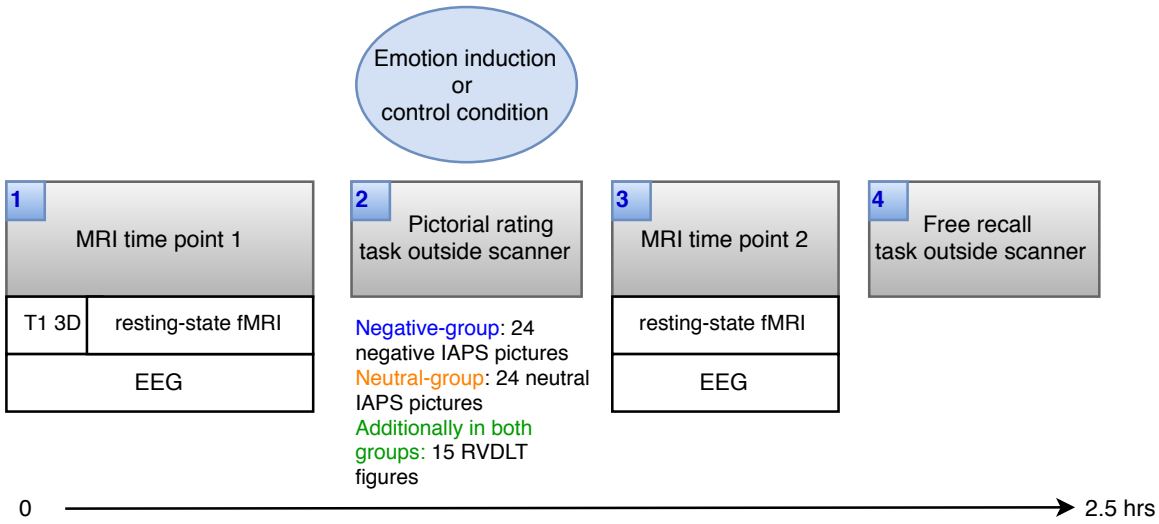

Note. Not depicted in this figure are the questionnaires that were completed before and after the first MRI, as well as three of the total of five EEG recordings.

In between the first and second MRI sessions, subjects accomplished the pictorial rating task, which served as the emotion induction intervention, outside the MRI-scanner, for about 10

min. Information about stimuli valence was kept from the subjects until the pictorial rating task. From the study descriptions, subjects were aware that they might view emotionally aversive stimuli. Subsequent to the second rs-fMRI measurement, which lasted about 10 min, there was an unannounced free recall task, followed by follow-up questionnaires. Participation compensation was CHF 60.-. The study visit took approximately 2.5 h.

Behavioral measures

Pictorial rating task

The software Presentation® (Neurobehavioral Systems, Inc., Berkeley, CA, www.neurobs.com) was used for the pictorial rating task. Stimuli consisted of a total of 53 pictures selected from the International Affective Picture System (IAPS; Lang, Bradley, & Cuthbert, 2005) and 16 geometrical figures taken from the Rey Visual Design Learning Task (RVDLT) (Spreen & Strauss, 1991). On the basis of normative valence and arousal scores of an American sample, pictures were assigned either to an emotionally neutral or emotionally negative category (Supplementary Table S2). For the training session (see below), we exclusively used neutral pictures.

Depending on the experimental condition, for the main task either 24 neutral or 24 negative pictures were employed (neutral-group vs. negative-group) (Supplementary Table S2). Negative emotional pictures were of various sorts, e.g., mutilated bodies, fearful faces, threatening animals, scenes depicting accidents and environmental pollution. Each of the 24 negative pictures matched one of the 24 neutral pictures corresponding to the following criteria: species (e.g., human, ungulate), perspective (scenery, single object, portrait), color spectrum, and number of individuals shown (e.g. portraits with neutral facial expression matched to a seriously injured face).

In addition to the emotional pictures (negative or neutral IAPS-pictures), the pictorial rating task included 16 geometrical figures (the same were used in both study groups) chosen from the RVDLT-set (Spreen & Strauss, 1991) and presented on a colored scrambled background we created using Adobe Photoshop CS3 (©2007 Adobe Systems Incorporated). It was composed of the task IAPS-images positioned next to one another, edited with a distortion and crystal filter in such a way that the motives were no longer perceivable.

Participants were instructed to subjectively and intuitively rate the emotional pictures for valence (negative/positive) and arousal (calm/arousing), and the geometrical figures for

form (height/width) and size (big/small) on a dimensional scale. The task was performed on a computer screen located at eye height about 40 cm away from the subject. Subjects submitted their ratings using a computer mouse on a visual-analog scale with a range of rating values ranging from -200 to +200. Each picture was presented for 2.5 s in a quasi-randomized order, with two pictures maximum in succession from any one category (IAPS-pictures vs. RVDLT-figures). The first and last two pictures presented were IAPS-pictures and the same for all individuals within their experimental group. Due to expected presentation order effects, these primacy and recency pictures were excluded from the analysis of the free recall and pictorial rating tasks. There was no time limit for rating.

To ensure clarity of the instructions, the task was preceded by a training session, in which five neutral IAPS-pictures and one RVDLT-figure were used. The task itself comprised 24 IAPS-pictures and 15 geometrical figures. All geometrical figures, as well as the IAPS-pictures of the training session, were the same for all subjects.

Free recall task

In a memory task after the second rs-fMRI, participants were given 10 min to freely recall as many photographs and geometrical figures as possible. They were instructed to describe briefly and precisely the remembered photographs in writing on the computer and to draw the geometrical figures on a blank paper. After 10 min had passed, participants were given the option of prolonging the time provided by 5 min, and then again by 5 min. The descriptions were rated for recall success independently by three trained investigators, the third of which then took a final decision about the score. Scores were calculated by summing the correctly remembered items, individually for photographs and figures, respectively. Due to misunderstanding of the instructions for the figure recall task two subjects were excluded from statistical analyses involving RVDLT-recall performance but included in all other analyses.

Questionnaires

A battery of self-report questionnaires in German language was used, including the long version of the Allgemeine Depressionsskala (Hautzinger & Bailer, 1993) for assessment of depression scores, the German version of the Affect intensity measure (Larsen & Diener, 1987) that assesses the intensity of a person's affective experiencing, the Edinburgh Handedness Inventory for evaluation of handedness (Oldfield, 1971), the Epworth Sleepiness Scale (Johns,

1991) for chance of dozing, and the NEO-FFI (Borkenau & Ostendorf, 1993) as a measure of personality dimensions. In order to measure anxiety levels the STAI state and trait versions (Laux, Glanzmann, Schaffner, & Spielberger, 1981) were used (Supplementary Table S1). Additionally, a brief in-house questionnaire was filled in to check for adherence to study rules and to get some complementary information (e.g., thoughts during MRI, previous MRI examinations).

Brain imaging acquisition

All functional and structural MR images were acquired with a General Electric Discovery MR750w 3.0 T MRI scanner (General Electric Company, Milwaukee, USA) at bilddiagnostik.ch (Basel, Switzerland), equipped with a GE-28-elements GEM head and neck unit (General Electric Company, USA). The first MRI session started with the structural imaging (T1-weighted) and was directly followed by the first rs-fMRI acquisition (2D gradient-echo T2*-weighted echo-planar images). The second MRI session took place about 15 min after the end of the first MRI session, comprising an identical rs-fMRI sequence. In order to reduce head motion and dampen scanner noise, the subject was outfitted with ear protection and air cushions at each side of the head. For structural analysis, a T1 high-resolution anatomical sequence, 3D BRAVO (brain volume imaging), was performed, established with an oblique plane in an interleaved manner with the following scan parameters: 256 x 256 matrix, flip angle = 15°, field of view (FOV) = 250 mm and a bandwidth of 31.25, repetition time (TR) = 8.5 ms, echo time (TE) = 3 ms. To cover the entire brain, 164 slices, 1 mm thick, were implemented, leading to an in-plane resolution of 1 mm in all three directions. An inversion preparation pulse with a preparation time of 450 ms was also applied to increase T1-weighting.

Shortly before starting the rs-fMRI sequence, subjects were instructed to keep their eyes closed, to let their mind wander, not to fall asleep, and to move as little as possible. Functional images were acquired in an interleaved slice-order along the anterior commissure–posterior commissure with a single-shot, gradient-recalled echo-planar imaging sequence (TR = 3000 ms, TE = 30 ms, flip angle = 90°), consisting of 37 axial slices (slice thickness = 4 mm, slice spacing = 0.4 mm, FOV = 240 mm, in-plane matrix = 96 x 96, in-plane resolution = 2.5 mm^2). Two hundred volumes were acquired per scan. Additionally, four dummy samples were

acquired before the actual start of the experiment to allow magnetization to reach a steady state, for a total acquisition time of 10.2 min.

Brain imaging analysis

Preprocessing of anatomical brain imaging data

Anatomical images were segmented into gray matter (GM), white matter (WM), and cerebrospinal fluid (CSF) by using SPM12 (Statistical Parametric Mapping, Wellcome Trust Centre for Neuroimaging, London). A diffeomorphic non-linear registration algorithm (diffeomorphic anatomical registration through exponentiated lie algebra; DARTEL) (Ashburner, 2007) was used to spatially normalize the segmented images to an in-house template brain (Heck et al., 2014), based on a sample of 1,000 healthy subjects aged 18 to 35 comparable to the current study sample. The resulting flow fields were combined with an affine spatial transformation to normalize the images to the MNI space in order to render the findings comparable to other studies. Subject-specific amygdala and hippocampus masks were created for each hemisphere separately through segmentation with FreeSurfer (v.5.3.0; http://surfer.nmr.mgh.harvard.edu/). The segmented ROIs were normalized to the MNI space by applying the previous normalization parameters, and mean functional time series of the amygdalae and hippocampi were then calculated by averaging across all voxels within each mask, respectively. To take into account potential divergences in amygdala segmentation between different methods (Morey et al., 2009), we complemented the amygdala's segmentation by using FSL's FIRST segmentation tool in a subject-specific manner (Patenaude et al., 2011). While subcortical segmentation in FIRST proceeds with Bayesian shape and appearance models, FreeSurfer assigns a neuroanatomical label to each voxel based on probabilistic information automatically estimated from a large training set of expert measurements (Fischl et al., 2002; Morey et al., 2009; Patenaude et al., 2011). Unless specified otherwise, amygdala segmentations obtained with FreeSurfer were used.

Preprocessing of functional brain imaging data

The preprocessing pipeline prior to the analyses (section Brain imaging analysis) included motion and slice-timing correction, normalization to the MNI space by using the transformation computed on the anatomical data, and smoothing with an 8 mm FWHM isotropic Gaussian Kernel. The experimental setup for all second-level analyses encompassed

two second-level covariates of interest (negative- and neutral-group) and three of no interest (sex, age and depression score, all mean-centered), which were incorporated in consideration of their associations with measures of rs-FC (Andrews-Hanna et al., 2007; Fair et al., 2008; Ferreira & Busatto, 2013; Hjelmervik et al., 2014; Sheline et al., 2010). ART (Artifact Detection Tools; developed by Stanford Medicine, Center for Interdisciplinary Brain Sciences Research), an analysis software for detection of motion artifact sources in fMRI time series, was implemented to provide movement regressor files as covariates in the first-level analyses. These are called "art_regression_outliers_and_movement.mat" per default and contain regressors to describe three translation, three rotation, one composite motion score and a variable number of outliers. Time points exceeding the movement threshold of 2 mm, or a *z*-value of 9 in the *z*-normalized global BOLD, were defined as outliers. Composite motion describes the maximal movement of any voxel within the brain bounding box in mm. For baseline and post-intervention resting-state, there were outliers in six and five subjects with maximum counts of 15 and 18 time points, respectively.

Seed-to-voxel and seed-to-seed analysis with bivariate correlation

For the seed-to-voxel approach, the functional connectivity toolbox Conn v.15c (www.nitrc.org/projects/conn) was used (Whitfield-Gabrieli & Nieto-Castanon, 2012). WM and CSF masks obtained from the segmentation of the anatomical images were coregistered to the functional space and considered subject- and session-specific noise regions of interest (ROI). Their respective time series were decomposed into 2 principal components by using a principal component analysis of the multivariate BOLD signal within each ROI with the CompCor method (Behzadi et al., 2007), and then regressed from the BOLD time series at each voxel. Such a flexible method is particularly appropriate for fMRI noise sources as cardiac and respiratory effects do not show a common spatial distribution across the brain (Behzadi et al., 2007). The temporal time series characterizing subject motion (three rotation and three translation parameters, and their first-order derivatives, i.e., ART motion parameters) were also removed from the BOLD data as temporal first-level covariates. The data were then band-pass filtered (0.01 Hz<*f*<0.1Hz).

For main and secondary analyses, mean time series of the bilateral amygdala and bilateral hippocampus, respectively, were used as seed-ROI. There are two reasons for using the bilateral amygdala. First, previous studies investigating amygdala-FC (section

Introduction) used the bilateral amygdala as seed-ROI. Second, studies have shown robust effects in bilateral amygdala activation when viewing negative IAPS pictures (section Discussion). The first-level step comprised a whole-brain bivariate correlation analysis between the residual voxel-wise BOLD time series and the ROI time series. In case of amygdala-hippocampus ROI-to-ROI analysis, FC was defined as bivariate Pearson's correlation between mean time series of the respective ROI pair. Second-level analyses consisted of a linear model including the first-level estimates for both rs-fMRI sessions (within-subjects factor: time point), both groups (between-subjects factor: group), and their interaction. The main contrast of interest was the interaction time point*group. The threshold for significance was set at voxel-*p*-uncorrected < 0.001 and cluster-*p*-FWE-corrected < 0.05, as has been used previously (Chai et al., 2011, 2014; Manning et al., 2015).

Spatial decomposition into independent components and dual regression

FSL's MELODIC 3.0 (Jenkinson et al., 2012) uses independent component analysis (ICA) to decompose a single or multiple 4D datasets into different spatial and temporal components (http://fsl.fmrib.ox.ac.uk/fsl/fslwiki/MELODIC/). We implemented MELODIC's spatial ICA to decompose the brain's low-frequency fluctuations at resting-session 1 for all 34 subjects. In consideration of our intention to pursue a data-driven, explorative approach, it has been recommended to include the whole set of ICs in subsequent tests for between-group differences (http://fsl.fmrib.ox.ac.uk/fslcourse/lectures/practicals/melodic/). Based on recent reports (Biswal et al., 2010), and in order to maintain a reasonable level of overview, we manually set the number of dimensions to be estimated with MELODIC to d = 20. Under the assumption that the 10 consistently reported networks (e.g., Biswal et al., 2010; Damoiseaux et al., 2006; Laird et al., 2011) will be subsumed to interpretable ICs in this solution, this allowed us to proceed with a pertinent quantity of ICs. Then, the set of spatial maps from the group-level analysis of the 20 dimensions solution was used to generate subject-specific versions of the spatial maps, and associated time series, using dual regression (Filippini et al., 2009). First, for each subject, the group-average set of spatial maps (from baseline resting-state) was regressed (as spatial regressors in multiple regression) into the subject's 4D space-time dataset from each rs-fMRI session. This resulted in a set of subject-specific time series, one per group-level spatial map (from baseline resting-state) for each rs-fMRI session. Next, those time series were regressed (as temporal regressors, again in multiple

regression) into the same 4D dataset, resulting in a set of subject-specific maps, one per group-level spatial map for each subject. We predicted that one or more of the 20 spatial networks would underlie a different change from pre-intervention resting-state to post-intervention resting-state depending on the emotionality of the presented pictures. For each subject, we calculated the difference between session 2 and session 1 (i.e., subtracting session 2 from session 1). Those files were the input to FSL's randomise permutation-testing tool (Winkler et al., 2014). The model comprised the mean-centered covariates of no interest sex, age, and depression score (ADS). The two contrasts of interest were (i) negative-group > neutral-group and (ii) neutral-group > negative-group. The *p*-FWE-voxel-corrected output files from FSL's randomise were further corrected for the amount of RSNs with the Bonferroni method.

Quality control of the independent components

MELODIC's decomposition will result in both functionally coherent RSNs as well as spatially structured artifacts (Smith et al., 2014) not necessarily represented by delimited components. An initial quality control of the 20 networks' spatial patterns was performed. The ICs' time courses, frequency spectra and spatial distributions were visually compared with previous reports (Damoiseaux et al., 2006; Smith et al., 2009). We further quantified the similarity of the networks to resting-state templates of 10 RSNs, available on http://www.fmrib.ox.ac.uk/datasets/brainmap+rsns/ (retrieved 07/07/16), described in Smith and colleagues (2009). These template networks circumscribe three visual networks (medial, occipital pole, lateral visual areas; 1-3), the default mode network (DMN) a cerebellum network (CN), the sensorimotor network (SMN), the auditory network (ADT), executive control network (ECN) and left/right frontoparietal networks (LFPN, RFPN; 9-10). These RSNs have been robustly detected in a number of independent studies (e.g., Biswal et al., 2010; Damoiseaux et al., 2006; Laird et al., 2011). We identified the template RSN that had the highest spatial correlation to our networks by using FSL's spatial cross-correlation, after binarizing the inputs at $z > |2|$.

Fractional amplitude of low-frequency fluctuations

As a method to measure LFO, fALFF has recently been shown to be superior to the originally used ALFF due to its higher sensitivity and specificity of detecting spontaneous brain activity

(Zou et al., 2008). Extraction of fALFF was performed by using the Data Processing Assistant for Resting-State fMRI (DPARSF) (Chao-Gan & Yu-Feng, 2010), which is based on SPM and the toolbox for Data Processing & Analysis of Brain Imaging (DPABI). Specific preprocessing of structural and functional images was conducted in DPARSF. This included normalization with DARTEL for structural images, slice timing correction, realignment, smoothing, head motion correction with Friston 24 head motion parameters (Friston, Williams, Howard, Frackowiak, & Turner, 1996) and removal of WM and CSF signals for functional images. FSL's fslmeants was used to extract the mean of the time course of fALFF in rs-fMRI session 2 in the left and right amygdala, respectively, for each subject. These values were then subjected to group-level analyses of variance to test for time point*group interaction effects with the mean-centered covariates of no interest sex, age and depression score (ADS), as implemented in R (R Core Team, 2015).

Electroencephalography

EEG recording

The EEG recordings, conducted with a similar setting as Zotev, Phillips, Yuan, Misaki and Bodurka (2014), were performed simultaneously with the rs-fMRI acquisitions by using the Brain Products' MR-compatible EEG system. Each subject wore an MR-compatible EEG cap (BrainCap MR from EASYCAP GmbH) throughout the experiment. The cap is fitted with 32 EEG electrodes (including the reference electrode), arranged according to the international 10-20 system, and one electrocardiographic (ECG) electrode placed on the subject's back. The EEG amplifier (BrainAmp MR plus from Brain Products GmbH) was positioned just outside the MRI scanner bore near the axis of the magnet. The electrical cable connecting the EEG cap to the amplifier was fixed in place by using a sandbag. The amplifier was connected to the PC interface outside the scanner room via fiber optic cable. The EEG system's clock was synchronized with the 10 MHz MRI-scanner's clock by using Brain Products' SyncBox device. The EEG signal acquisition was performed in BrainVision Recorder Professional (v. 1.20.0801) with 16-bit analog-to-digital conversion and 5000 Hz sampling rate, providing 0.2 ms temporal and 0.5 µV measurement resolution. The EEG signals were measured relative to FCz and filtered online between 0.016 Hz (10 s time constant) and 250 Hz (Zotev et al., 2014).

EEG preprocessing

All EEG data were processed in EEGLAB (v. 13.5.4b) running on Matlab R2014a (Mathworks). The large steady magnetic field B_0 and the fast time varying fields generated by the MR imaging sequence induce substantial artifacts in EEG data collected in an MRI-environment (Moosmann et al., 2009). Therefore, correction for gradient-related and ballistocardiographic (BCG) artifacts is required. We accomplished this correction with the Bergen plugin for EEGLAB (Allen et al., 2000; Moosmann et al., 2009). First, the fMRI volume onsets were detected via an autocorrelation method on the basis of an automatically selected channel premised on its median variance. This automatically detected channel was then manually checked and accepted. The threshold defining the occurrence of an fMRI gradient artifact was based on the first derivative (gradient value) of the EEG signal, specified in percentage relative to the maximum value of the gradient of the artifact signal. The artifact duration was defined as the time between the volume onset and the time point immediately before the subsequent volume onset marker (i.e., start = 0, end = TR; continuous recording). Next, baseline correction of the artifact periods defined in the previous step was done by using the mean of the artifact period itself. A realignment parameter-informed algorithm was used for correction for the gradient artifacts (Moosmann et al., 2009). This algorithm is based on an extension of template subtraction and performs particularly well in case of abrupt head movements. Following the fMRI gradient-artifact correction, the data was resampled to 500 Hz, QRS events were detected, and BCG artifacts removed with an artifact subtraction method, implemented in the FMRIB plug-in for EEGLAB, provided by the University of Oxford Centre for Functional MRI of the Brain (Iannetti et al., 2005; Niazy et al., 2005). Unsatisfactory cleaning of the gradient-related artifacts, as well as recording problems in one individual, led to valid EEG data for a total of 31 and 32 subjects for each rs-fMRI session, respectively.

Assessment of vigilance

Vigilance at different time points was dichotomously divided into relaxed wakefulness and drowsiness, henceforth referred to respectively as stage A and B, following an established procedure (Hegerl et al., 2008; Olbrich et al., 2009). This procedure retains much of a standard vigilance and sleep scoring (Rechtschaffen & Kales, 1968). Briefly put, this extended approach for vigilance scoring (Hegerl et al., 2008; Olbrich et al., 2009) centers on the concept of spatial redistribution of spectral alpha power and its diminishment during the transition from

wakefulness to drowsiness. Building upon this, the procedure was as follows: for each subject and each resting-session, we split the whole rs-EEG according to the TR of the rs-fMRI sequence (3 s) leading to a total of 204 bins of 3 s duration (1,500 EEG sampling points). Spectra for each bin were calculated with EEGLAB's spectopo-function, which uses Matlab's pwelch-function for obtaining Welch's power spectral density estimates. Bins were defined as an A-stage if at least one of channels O1, O2, F3, and F4 showed a higher power for the range 8 to 12 Hz than for 2 to 8 Hz; else, the bin was considered a B-stage. The former two electrodes correspond to the occipital, the latter two to the frontal parts of the brain.

Before vigilance staging, a first-level outlier correction was applied to the spectral power of the two frequency bands for each channel and each resting-session in two stages: (i) linear interpolation (R function approx from the stats-package), (ii) remaining outliers (i.e., those that could not be interpolated because they were either at the end or beginning of the sequence) were replaced by the respective channel's mean spectral power. Outliers were defined as time points below or above the tenth and ninetieth percentiles, respectively. Since the spectral estimations obtained from the Welch's method may take on negative values, those values were then log-transformed to positive values in order to form interpretable ratios.

Effect of vigilance fluctuations on the BOLD signal

With SPM12, we tested the extent to which the EEG-derived vigilance regressor was associated with the BOLD signal. First, the fully preprocessed images, i.e., after performing standard and resting-state-specific preprocessing using Conn, for each subject were used as input to estimate first-level contrast images with the HRF-convolved binary covariate vigilance stage (A = 0, B = 1) to test for voxels that would show a significantly (i) higher or (ii) lower activity change jointly with this regressor in a second-level analysis. Model parameters were estimated by using Restricted Maximum Likelihood specified with an autoregressive error model.

Statistical analysis of behavioral data

Analyses of behavioral data, unless specified otherwise, were performed in R Studio (R Core Team, 2015). For inferential statistics of behavioral data, the threshold of significance was set to $p < 0.05$. Between-group differences were tested for by means of two-sided Welch-*t*-tests

for independent samples. Repeated-measures between-group differences and corresponding interactions were analyzed in mixed linear models with group as between-subjects factor and session as within-subjects factor, implemented in the R library nlme (v. 3.1-131). Non-directional associations of quantitative variables were tested for with pairwise-complete Pearson's correlation.

Results

Behavioral data

Pictorial rating task

As expected, subjects in the negative-group rated task IAPS pictures as less pleasurable and more arousing than did subjects in the neutral-group ($t(31.4) = 8.72$, $p < 0.001$ for valence; $t(29.8) = -4.36$, $p < 0.001$ for arousal). Size and form rating of geometrical figures did not significantly differ between the groups *(*$t(29) = 0.69$, $p = 0.49$; $t(27.1) = 1.73$, $p = 0.1$) (Table 2.1).

Free recall task

In recalling task IAPS-pictures, subjects in the negative-group performed better than subjects in the neutral-group ($t(31.1) = -2.17$, $p = 0.04$), with an average of 10.5 freely recalled task IAPS-pictures in the neutral-group ($SD_{neu} = 3.68$), and 13.1 in the negative-group ($SD_{neg} = 3.09$). In contrast, there were no between-group differences in the number of correctly recalled RVDLT-figures ($t(30) = -0.25$, $p = 0.81$) (Table 2.1), nor was there an association in recall performance between these two types of visual stimuli ($t(32) = -1.25$, $p = 0.22$, Pearson's $r = -0.216$).

Table 2.1

Descriptive statistics for demographical data and the measures of the three behavioral domains

	Measure	Negative-group *M(SD)* (*N* = 17)	Neutral-group *M(SD)* (*N* = 17)	*t(df)*	*p*-value
Demographical data	Female	10	10		
	Male	7	7		
	Age	22.5(1.97)	22.6(2.20)	0.040(31.6)	
Pictorial rating task	IAPS arousal	11.4(12.4)	-5.09(9.40)	-4.36(29.8)	**<0.001**
	IAPS valence	-22.7(9.27)	7.25(10.7)	8.72(31.4)	**<0.0001**
	RVDLT size	16.7(12.2)	20.2 (17.0)	0.691(29.0)	0.495
	RVDLT form	-0.875(10.2)	7.05(16.0)	1.73(27.1)	0.096
Free recall task	IAPS correctly recalled	13.1(3.09)	10.5 (3.68)	-2.17(31.1)	**0.038**
	RVDLT correctly recalled	3.12(1.45)	3.00(1.41)	-0.25(30.0)	0.807
Questionnaires	NEO-neuroticism	16.0(6.48)	17.1 (4.83)	0.568(29.5)	0.575
	NEO-extraversion	31.8(6.02)	30.1(5.93)	-0.846(30.9)	0.404
	NEO-openness	29.2(6.40)	31.6 (6.67)	1.07(30.7)	0.291
	NEO-agreeableness	32.9(5.94)	33.9(5.02)	0.514(29.2)	0.611
	NEO-conscientiousness	31.9(7.35)	30.9(6.06)	-0.420(29)	0.678
	AIM-positive intensity	23.5(3.74)	26.7 (5.91)	1.91(27.1)	0.067
	AIM-negative intensity	19.9(7.29)	24.3(6.43)	1.87(31.5)	0.071
	AIM-serenity	18.8(5.29)	22.0(4.12)	1.99(30.2)	0.056
	STAI trait	35.7(6.76)	35.8 (6.49)	0.052(32.0)	0.959
	STAI state 1	29.5(9.27)	29.4 (4.76)	-0.021(20.3)	0.984
	STAI state 2	33.4(5.30)	30.5 (7.51)	-1.29(28.8)	0.206
	ADS-L	10.4(7.61)	11.2(6.63)	0.313(31.4)	0.757
	ESS	10.8(2.59)	8.81(2.97)	-2.01(29.8)	0.054

Note. Numbers represent the mean (*M*) and standard deviation (*SD*) of the negative- and neutral-groups individually. Between-group inferential statistics were obtained with Welch's two-sided *t*-tests for independent samples and denoted in *t*-statistic (*t*) and degrees of freedom (*df*). Sex counts are given in absolute numbers. For detailed description of the questionnaires please refer to Supplementary Table S1. Note some minor deviations from the number of subjects: for the NEO-subscales and the STAI state 1, data for two subjects was not available. There was missing data in the ESS for one subject. Two subjects were excluded from statistical tests involving RVDLT-recall performance.

Questionnaires

There were no significant group differences in NEO-FFI, AIM subscales, or in STAI trait anxiety (Table 2.1). With regard to state anxiety (STAI state), there was no significant time point*group interaction ($F(1,30) = 0.91$, $p = 0.35$), and no main effect of group or session ($F(1,31) = 2.88$, $p = 0.42$; $F(1,32) = 0.68$, $p = 0.42$).

Resting-state fMRI

Seed-to-whole brain and seed-to-seed functional connectivity

Overall, baseline FC of the bilateral amygdala showed widespread connectivity clusters across the whole brain ($F_{min}(4,58) = 5.33$, minimum number of voxels in one cluster = 63), e.g. covering the temporal poles, precentral gyri, frontal orbital cortices, right middle frontal gyrus, insular cortices (Figure 2.2a). There was no significant time point*group interaction. There was also no main effect of time point (group-invariant effect of the task, see Figure 2.2b for amygdala-WB-FC at post-intervention), nor a main effect of any of the dimensional behavioral variables NEO-neuroticism, STAI trait anxiety, AIM affect reactivity, and ADS depression score. Post-hoc tests showed that the groups did not diverge in amygdala-FC either at the baseline or at the post-intervention rs-fMRI after the pictorial rating task. Furthermore, amygdala-hippocampus-FC did not reveal a significant time point*group interaction. All these results remained non-significant also if the right and left amygdala, and in case of the ROI-to-ROI analysis left and right hippocampus, served as separate seed-ROIs.

When using FIRST's instead of FreeSurfer's amygdala segmentations, there was still no time point*group interaction and no main effect of time point. While there was a main effect of segmentation method for baseline amygdala-FC ($F_{min}(2,29) = 8.85$, minimum number of voxels in one cluster = 56), including regions spanning temporal poles, subcallosal cortex, frontal orbital cortices, frontal medial cortex (Supplementary Figure S1), the interaction time point*segmentation (mean of bilateral amygdala FIRST vs. FreeSurfer) was non-significant.

Figure 2.2

Brain maps thresholded at F > 7 depicting amygdala-whole brain functional connectivity clusters across both groups ***(a)*** *at baseline and* ***(b)*** *after the pictorial rating task (p-voxel-uncorrected < 0.001 and p-cluster-FWE-corrected < 0.05; $F_{min}(4,58) = 5.33$ for both sessions), depicted in axial slices (Z = 26.40 to Z = 57.20 in MNI space). Abbreviations: FWE=family-wise error rate; F=F-statistic.*

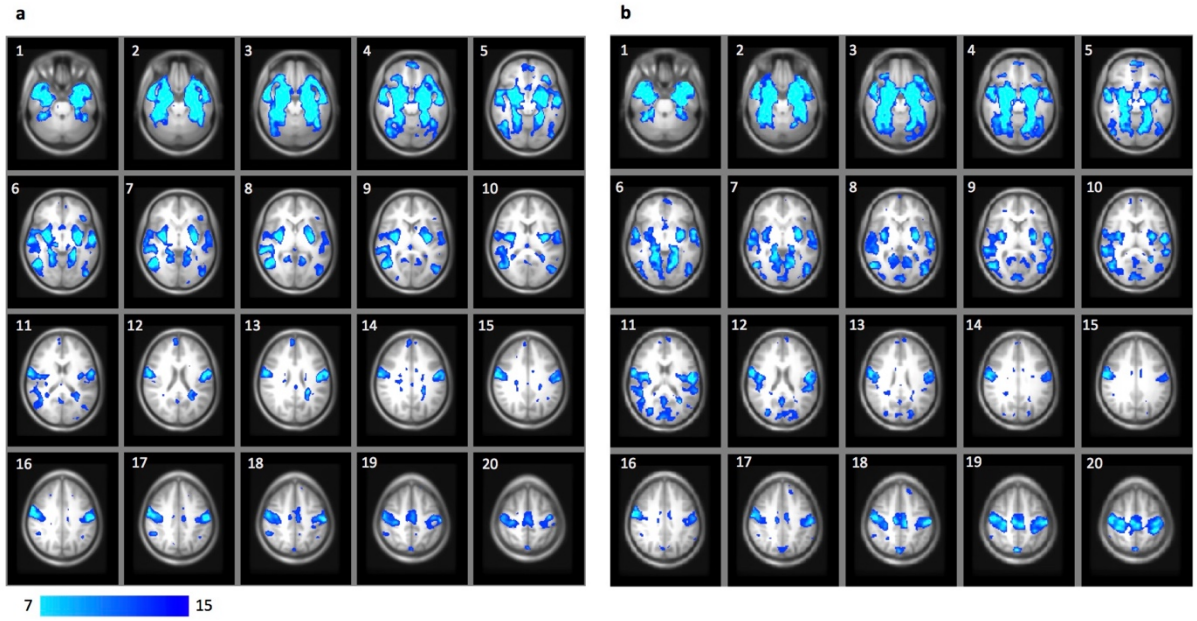

Figure 2.3

Brain maps thresholded at F > 7 showing hippocampus-whole brain functional connectivity clusters across both groups ***(a)*** *at baseline and* ***(b)*** *after the pictorial rating task (p-voxel-uncorrected < 0.001 and p-cluster-FWE-corrected < 0.05; $F_{min}(4,58) = 5.33$ for both sessions), depicted in axial slices (Z = 26.40 to Z = 57.20 in MNI space). Abbreviations: FWE=family-wise error rate; F=F-statistic.*

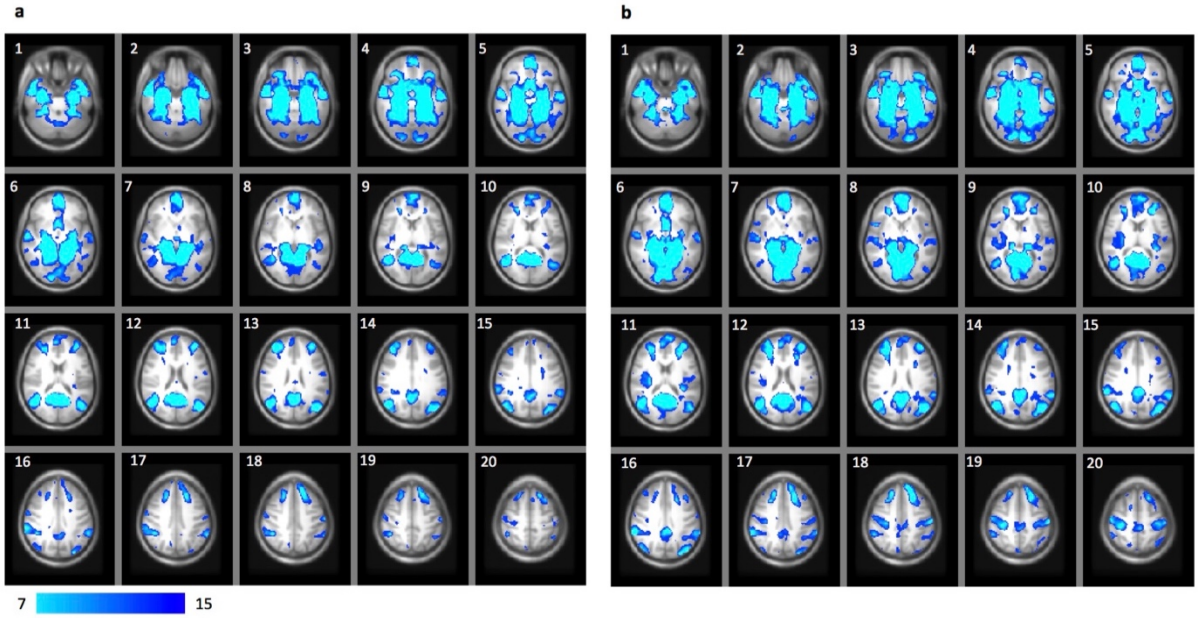

The bilateral hippocampus was extensively functionally connected to other brain regions at baseline ($F_{min}(4,58) = 5.33$, minimum number of voxels in one cluster = 51), e.g. frontal and temporal poles, lingual gyri, OFC, cingulate gyrus, thalamus, subcallosal cortex, insular cortex (Figure 2.3a; Figure 2.3b for post-intervention rs-fMRI). The same negative findings as for the amygdala apply to the hippocampus. Note that the hippocampus was segmented uniquely with FreeSurfer.

Spatial decomposition into independent components and dual regression

Upon visual inspection of the 20 ICs' time courses, frequency spectra and spatial distributions, we regarded some ICs as nuisance while others as reflecting actual brain activation, based on previous reports (Damoiseaux et al., 2006; Smith et al., 2009).

Figure 2.4

Brain maps illustrating the 20 ICs as estimated with FSL's MELODIC for spatial decomposition of all subjects' 4D data sets of baseline resting-state functional connectivity.

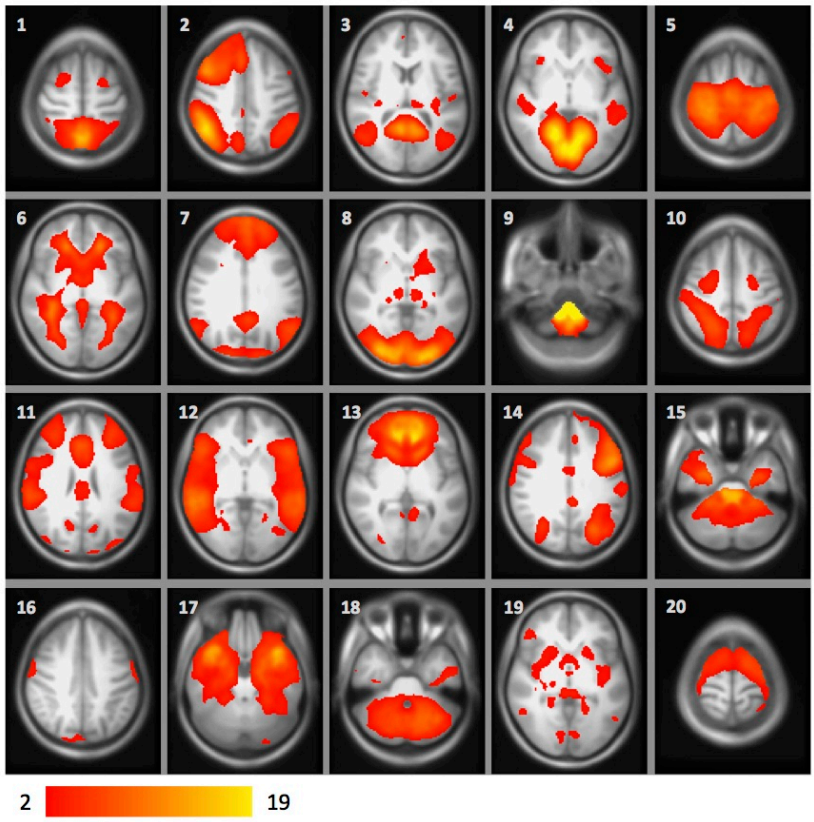

Note. The enumeration of these ICs corresponds to the ones used in Table 2.2. Abbreviations: IC=independent component.

The validity of the 20 networks (Figure 2.4) was further investigated by comparing them to templates of 10 validated RSNs. The template networks VN1, VN3, CBN, ECN, and RFPN each were related to two networks, while each of the remaining five matched one (Table 2.2, Supplementary Figure S2A-O). Testing the contrasts (i) negative-group > neutral-group, and (ii) neutral-group > negative-group showed that none of the 20 networks exhibited an emotionality-dependent change from resting-session 1 to resting-session 2 (even at nominal significance level, i.e., without correcting for the number of networks tested).

Table 2.2

Table demonstrating the spatial overlap of the independent components from resting-session 1 with 10 robust template resting-state networks, obtained with cross-correlation

Template network	IC	*r*	Index
VN1	4	0.760	1A
VN1	8	0.222	1B
VN2	8	0.701	1C
VN3	10	0.398	1D
VN3	12	0.387	1E
DMN	3	0.445	1F
CN	15	0.238	1G
CN	18	0.672	1H
SMN	5	0.681	1I
ADT	12	0.472	1J
ECN	2	0.245	1K
ECN	7	0.318	1L
LFPN	2	0.349	1M
LFPN	11	0.490	1N
RFPN	14	0.633	1O

Note. Brain maps of these spatial overlaps can be found in Supplementary Figures S2A-O (as indexed in the table). Abbreviations: VN=visual network; DMN=default mode network; CN=cerebellum network; SMN=sensorimotor network; ADT=auditory network; ECN=executive control network; LFPN=left frontoparietal network; RFPN=right frontoparietal network.

Fractional amplitude of low-frequency fluctuations

There was no time point*group interaction in in fALFF for either left ($F(1,32) = 0.28$, $p = 0.6$) or right ($F(1,32) = 1.15$, $p = 0.291$) amygdala (Figure 2.5).

Figure 2.5

Bar charts showing baseline and post-intervention fALFF values of the left ***(a)*** *and right* ***(b)*** *amygdala for each group separately.*

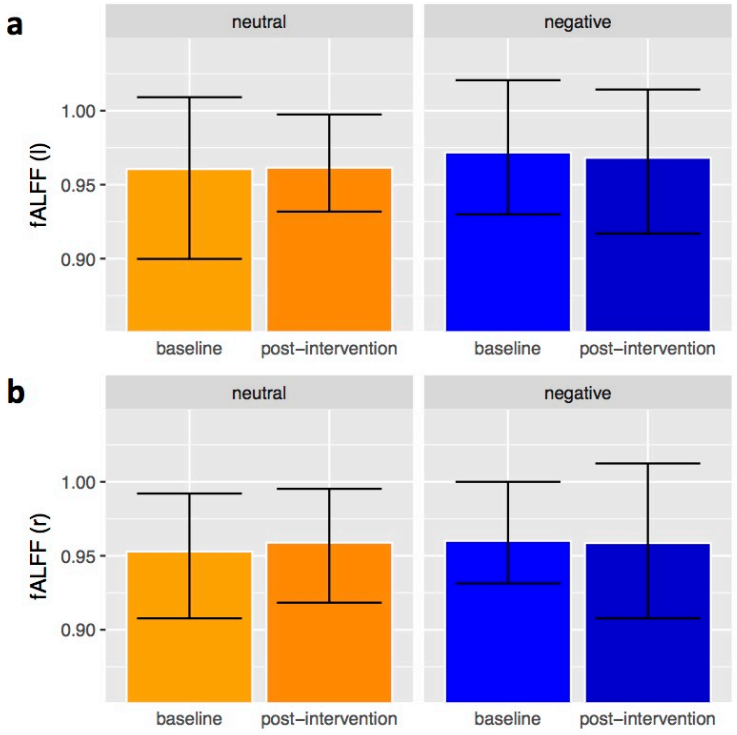

Note. Error bars depict standard error of the mean. Abbreviations: fALFF=fractional amplitude of low-frequency fluctuations; l=left; r=right.

Motion outliers

There was no main effect in the amount of motion outliers (section Preprocessing of functional brain imaging data) for the factors group ($F(1,32) = 0.492$, $p = 0.488$) and time point ($F(1,32) = 0.126$, $p = 0.725$), nor was there an interaction time point*group ($F(1,32) = 0.04$, $p = 0.842$).

Resting-state EEG

EEG data collection

To warrant our subjects the highest safety possible, in 15 subjects, the EEG electrodes had to be mended in between the MRI sessions due to poor electrode impedances. This was the case for four, eight, and five subjects before the first rs-fMRI, after the first rs-fMRI, and after the pictorial rating task, respectively. This prolonged the experiment by about 3 min for the subjects concerned.

Frequency of vigilance stage A and B

As described in section Assessment of vigilance, vigilance was classified into the two discrete stages wakefulness and drowsiness (stages A and B, respectively) (Hegerl et al., 2008; Olbrich et al., 2009). For resting-session 1, the majority of participants showed a higher proportion of A- stages than B-stages for the total of that resting-session (*M* = 0.70, *SD* = 0.29, range = 0.15 to 0.99). This tendency remained approximately the same at resting-session 2 (*M* = 0.76, *SD* = 0.26, range = 0.18 to 1). There was no time point*group interaction *(F*(1,28) = 1.86, *p* = 0.18). Of note, all subjects except for two stated having been awake at all times.

Effect of vigilance fluctuations on the BOLD signal

There was no significant effect of the binary first-level regressor vigilance at any voxel at *p*-FDR-corrected at neither resting-session 1 nor resting-session 2.

Discussion

We implemented a two-group repeated-measures rs-fMRI design to investigate functional networks and functional connectivity of the amygdala in healthy young adults. The present study aimed to reveal the brain states that characterize delayed emotion regulation following exposure to visual stimuli of negative compared to neutral valence. Overall, the amygdala showed widespread connectivity clusters across the whole brain, e.g. covering temporal poles, precentral gyrus, frontal orbital cortices, right middle frontal gyrus, and insular cortices, in line with previous findings from rs-fMRI in humans (Roy et al., 2009). This was applicable for both rs-fMRI sessions. Compliant with these findings, tracer studies in rhesus monkeys provide strong evidence for projections from specific orbitofrontal, medial prefrontal and temporal cortical pathways onto excitatory and inhibitory pathways in the amygdala, suggested to interact in emotion mechanisms (Ghashghaei & Barbas, 2002; Höistad & Barbas, 2008).

Whereas we expected to observe distinct bilateral amygdala-FC between-session changes in subjects who had viewed negative pictures, as compared to those who had viewed neutral pictures (time point*group interaction), there was no such effect, not even in amygdala-hippocampus FC. In the light of the plurality of cognitive processes in which the amygdala is involved (e.g., impulsivity, appetitive motivation) (Kerr et al., 2015; Passamonti et al., 2008; C. Xie et al., 2011) and the many brain regions implicated in affective processes, e.g.,

the cerebellum (Baumann & Mattingley, 2012; Riedel et al., 2015), and medial prefrontal regions (Phan et al., 2002), we intended to account for this presumable complexity of networks involved in emotion regulation. This was accomplished by spatial decomposition of BOLD activation patterns of the baseline resting-state into 20 spatial networks. Statistical comparisons to recently and robustly reported resting-state networks (RSN) (Damoiseaux et al., 2006; Smith et al., 2009; Smith et al., 2014) confirmed their validity. Mapping them into each individual subject's space each for resting-session 1 and 2 and consecutively performing group comparisons with dual regression disclosed that none of the 20 RSNs was differentially affected by picture emotionality.

Remarkably, complementing evidence for this apparent non-susceptibility towards emotional pictures in amygdala-FC and RSNs in the time following immediate emotion processing was given by our finding that the fractional amplitude of low-frequency fluctuations (fALFF) in the amygdala showed no relation to picture valence.

As opposed to the neurofunctional data, behavioral measures were differentially affected by picture valence. Compared to neutral pictures, negative pictures were rated as more negative and arousing, and were remembered better. Since the recall of geometrical figures was independent of picture emotionality, this memory-facilitating effect was not ascribable to general memory performance. Research designed to look into memory consolidation has revealed that rs-FC directly after encoding may be predictive both of later recall performance of visual stimuli, e.g. associations between post-encoding rs-FC of the hippocampus and memory performance about 60 minutes afterwards (Tambini et al., 2010), and of links between inter-network-FC and memory performance 6.5 weeks later (Sneve et al., 2017). In the current experimental paradigm, which is not primarily aimed at investigating memory dynamics, we found no valence-dependent effects on hippocampus-whole brain-FC. However, for hippocampus-FC to be related to later memory performance, time window may be particularly important. In line with this, rs-FC between the parietal memory network and DMN after encoding correlates with memory capacity when tested 6.5 weeks but not 1.5 hours later (Sneve et al., 2017). These findings indicate that rs-FC is hardly susceptible to preceding processing of visual emotional stimuli.

Fluctuations in vigilance (Olbrich et al., 2009) and different sleep stages (Tagliazucchi et al., 2012) may co-vary with changes in rs-FC. There was a report of a reliable loss of wakefulness within 3 min rs-fMRI in one third of subjects, grounded on an analysis of 1,147

datasets (Tagliazucchi & Laufs, 2014). Notably, in the current study, out of 31 and 32 subjects during resting-session 1 and 2, respectively, for whom we had valid EEG data, the large majority of subjects was in a state of relaxed wakefulness at most time points (summarized over 3 s). The binary first-level regressor vigilance had no impact on the BOLD signal. It is thus unlikely that vigilance, a physiological state defined according to previously adapted concepts (Hegerl et al., 2008; Olbrich et al., 2009), operated as a confounder in this study. Owing to the risk of oversimplification of the dynamic and gradual process of sleep onset (Prerau et al., 2014) and due to subjective reports of wakefulness from our subjects, we refrained from a discrete categorization of wake/sleep.

Prolonged activation in amygdala-FC networks following acute stressors has been reported, an effect suggested to constitute an extended state of hypervigilance (Clewett, Schoeke, & Mather, 2013; van Marle et al., 2010; Veer et al., 2011). In accordance with this stress perspective, stress-induced neuroendocrine levels may regulate amygdala-FC in the recovery phase from acute stressors (Quaedflieg et al., 2015), and acute painful stressors alter amygdala-FC with frontal and anterior cingular cortex (ACC) regions 15 to 30 min after stressor onset (Clewett et al., 2013). This framework differs from ours in that we did not apply acute stressors (e.g., psychological stress test, painful interventions). Even if a substantial increase in corticosteroids were elicited by the emotion induction peak levels could be expected only after 30 min. Yet, one study reported enhanced amygdala-FC with the dorsal ACC, AI, and LC after viewing a highly aversive movie clip for 1.5 min highly aversive movie clip (van Marle et al., 2010). In contrast to our study design, the movie clip might have induced a stressful state reflected in lasting changes in rs-FC. Moreover, they conducted the rs-fMRI without time delay after cessation of the movie, which was presented inside the scanner. Importantly, the stress induction paradigms used in these studies substantially differ from our emotion induction paradigm.

The present study has several limitations: Due to the setting of the pictorial rating task at the computer outside the scanner, we could not measure BOLD-related brain activity during the pictorial rating task. Although EEG data during this task was available, it could not be properly analyzed due to major movement-related artifacts. Yet, a multitude of studies has demonstrated the amygdala to be activated upon viewing negative pictures (Banks et al., 2007; Eippert et al., 2007; Erk et al., 2010; Fastenrath et al., 2014; Radua et al., 2014; Townsend et al., 2013; Walter et al., 2009). Moreover, the memory-facilitating effect of

picture emotionality also found in our study is known to rely on the amygdala's initial involvement (e.g., Fastenrath et al., 2014; Kim, 2011; McGaugh, 2004). Nonetheless, future studies should include brain activation measures also during the emotion induction task. Furthermore, we cannot generalize to other emotional tasks. It may well be that stronger and more ecologically valid emotion induction paradigms (Schilbach, 2016; Xie et al., 2016) might have induced alterations in the resting-state measures applied in the present study. A further limitation is the number of subjects (*N* = 34), which may be regarded relatively small given the unconstrained nature of the resting-state (Finn et al., 2017). Therefore, the negative results should be treated with caution and tested for replication in larger samples.

The progress towards incorporation of rs-FC measures as clinical biomarkers (Camchong, Stenger, & Fein, 2013; Drysdale et al., 2017; Gong et al., 2014; Sorg et al., 2013; Verduyn et al., 2015; Whitfield-Gabrieli et al., 2016; Wilcox et al., 2016; Yang et al., 2014; Zotev et al., 2013) will require minimization of confounding factors to allow for a standardized setting. Concerning this, it is essential to unveil factors affecting rs-FC. Factors eliciting emotional responses in everyday life, like negative emotional stimuli and daily hassles, may be hard to control for by clinicians. In this line of thoughts, we believe our findings provide important insight into the requirements for measurement standardization, a key challenge for rs-fMRI. Yet, rs-fMRI-specific confounds may vary with mental health status, which is particularly important given the planned implication of rs-fMRI in patients with tentative diagnoses. The pathological correlates of mental disorders that have been associated with traumatic experiences, such as post-traumatic stress disorder (PTSD) and borderline personality disorder (Bandelow et al., 2005; Golier et al., 2003), have been proposed to be escalates of brain activation patterns observed in the healthy confronted with ethically acceptable aversive emotional stimuli. PTSD, as an example, may be regarded as a disorder of recovery from the early responses to traumatic events (Shalev, 2009). In cases of pathological anxiety, excessive apprehension occurs upon minimally threatening stimuli, implying dysfunction at the level of interpretation (Calhoon & Tye, 2015). It is important to understand what factors exacerbate or protect against disadvantageous reactions to emotional stimuli. Amygdala-FC may form a critical juncture for affective reactivity, culminating in individual patterns of immediate emotion processing and emotion regulation. Future studies may want to investigate those transient states of emotion regulation in clinical samples.

Conclusions

In summary, our findings demonstrate that several resting-state measures, which had been hypothesized to be involved in the temporal dynamics of emotion processing following exposure to emotional pictorial stimuli, transpired unaffected by such an intervention. Future research should include additional emotion induction paradigms and might investigate if resting-state functional connectivity in patients with problems in emotion regulation, as it is commonly observed in depression or anxiety disorders, might be more susceptible to emotion induction.

Acknowledgements and funding source declaration

This project has mainly been sponsored by Bilddiagnostik.ch, directed at the time by Alfred Geissmann, who generously provided the MRI materials and personnel assistance, by the MCN, University of Basel, head of which is Prof. de Quervain, in providing personnel and the funds for participant reimbursement, and the UPK Basel, in providing EEG materials and professional support. Our gratitude also goes particularly to Amanda Aerni and Franck Girard.

Legal statements

All authors certify that this work has been submitted in accordance with their agreement. They warrant that the article is the authors' original work and has not been published previously. Part of this work has been presented in a poster on the Fifth Biennial Conference of Resting State and Brain Connectivity 2016 in Vienna, Austria, by the first author (L.G.). The authors further declare that there are no conflicts of interest. The study has been conducted in accordance with the Declaration of Helsinki.

Study 2: Neurofunctional underpinnings of individual differences in visual episodic memory performance

Title:

Neurofunctional underpinnings of individual differences in visual episodic memory performance

Short title:

Brain activity linked to individual differences in episodic memory

Teaser:

The study reports links between memory and brain activity by unifying network-based and region-localizationist approaches.

Authors:

Léonie Geissmann[1,5], David Coynel[1,5], Andreas Papassotiropoulos[2,3,4,5]*, Dominique J.-F. de Quervain[1,4,5]*

Affilitations:

[1]Division of Cognitive Neuroscience, Faculty of Psychology, University of Basel, CH, [2]Division of Molecular Neuroscience, Faculty of Psychology, University of Basel, CH, [3]Life Sciences Training Facility, Department Biozentrum, University of Basel, CH, [4]University Psychiatric Clinics Basel, CH, [5]Transfaculty Research Platform, University of Basel, CH

* These authors jointly supervised this work.

Abstract

Episodic memory, i.e., the ability to consciously recollect information along with its context, is a significant element of human cognition. Numerous fMRI studies on subjects' group-level activity reported brain regions implicated in successful memory encoding. It is widely unknown, however, to what extent differential responsivity of these regions explain inter-individual differences in memory performance. We analyzed a large sample of 1,434 adults

who underwent a picture encoding task in a single MR scanner. Complementing a voxel-based with a network-based approach, we found that responsivity in some of the regions implicated in successful encoding as well as responsivity of six functional connectivity networks were associated with inter-individual differences in memory performance. This study offers new insights into brain regions and networks involved in inter-individual differences in episodic memory.

Introduction

Human episodic memory (EM) refers to the conscious memory for personally experienced events within a particular spatio-temporal context (Tulving & Markowitsch, 1998). It involves multiple brain systems during encoding, consolidation and retrieval. The encoding phase relies on receiving information through sensory modalities and on cognitive integration, like content processing, attention attribution and storage (Kim, 2011).

Extensive fMRI research has resulted in solid knowledge about neural activity related to successful EM encoding. Most studies used the subsequent memory paradigm, in which one compares subjects' group-level average voxel activations of successful encoding (i.e., later remembered stimuli) with voxel activations of stimuli not later remembered. A meta-analysis of visual EM reported subsequent memory effects in the left inferior frontal cortex, bilateral fusiform gyrus, bilateral medial temporal lobe, bilateral premotor cortex, and bilateral posterior parietal cortex (Cohen et al., 2015; Gilmore et al., 2015; Kim, 2011, 2019; Xue, 2018). Even though the meta-analysis (Kim, 2011) was well-powered with 72 studies, sample sizes of the individual studies ranged from 12 to 25 participants. To the best of our knowledge, a substantially powered single-sample study (i.e., sample size well above 500 subjects) of subsequent memory effects with regard to episodic memory is still lacking.

While group-based activation studies provide insight into the neurofunctional architecture that is common across a group of individuals for a given cognitive task, they allow no inferences about the substantial subject-to-subject variability and its association with inter-individual differences in cognitive performance (Majerus et al., 2013). In another words: It is unclear to what extent brain regions that are essential for successful memory encoding also show higher activity in individuals with better memory performance. While one could hypothesize that people with better memory performance also show more activity in brain regions involved in successful encoding, there are findings from previous studies that

challenge this hypothesis. It has been shown, for example, that subjects with mild cognitive impairment show significantly greater hippocampal activation in an associative memory encoding task as compared to healthy controls (Dickerson et al., 2005). Further, it has been proposed that for a given performance level, subjects more skilled and more efficient in dealing with cognitive load would show less brain activation due to a higher neural efficiency (Bernardi et al., 2013; Train the Brain Consortium, 2017).

In order to address individual differences by investigating brain-behavior correlations, typical fMRI sample sizes of individual studies need to be scaled up substantially (Dubois & Adolphs, 2016). While much is known about the associations between inter-individual cognitive performance and properties of brain structure (Kranz et al., 2018; Martı & Colom, 2013; Razlighi et al., 2017), and between inter-individual cognitive performance and resting-state activity (Fjell et al., 2015; Liu et al., 2015; Nyberg et al., 2016; Oertel-Knöchel et al., 2015; Reineberg et al., 2018), there are no large-scale studies investigating the relationship between task-based functional brain profiles and inter-individual performance in episodic memory.

In the present study we explored the neurofunctional basis of inter-individual differences in episodic memory performance by including both a region-localized approach and a network-based approach in a large cohort of 1,434 adults. A distinctive feature of the human brain is its ability to flexibly reconfigure interactions within and between populations of neurons. These functional interactions, a term used to describe co-activity of brain regions, indicate communication and coordination of brain activity (Buckner et al., 2008; Shin & Jadhav, 2016). Even in the absence of structural connections, abnormal activity at one region can cause dysfunction at other regions in a network (Bostan & Strick, 2018). Functional interactions are disregarded by the conventional region-localizationist approach, which assigns functional roles to separate brain regions and provides only a partial account of brain function (Di & Biswal, 2015; Fornito et al., 2015; Tsvetanov et al., 2018). Therefore, a more thorough understanding of the neural basis of inter-individual differences in EM can benefit from a network-based approach as a complement to the well-established region-localizationist voxel-based approach. We used independent component analysis (ICA) to extract task-specific activity of functional networks (FCNs) for our network-based analysis. This data-driven procedure allows taking into account the non-universality of FCNs across tasks and different populations of individuals (Fornito et al., 2012; Laird et al., 2011; Utevsky et al., 2014).

The current work used data of a large sample of healthy young adults (*n* = 1.434) who performed an EM task, comprising a picture encoding task in the same MRI scanner and a subsequent free recall task. First, we investigated the classical group-based subsequent memory effect in this sample. Second, we investigated the association between inter-individual differences in task-based functional brain profiles and EM in a voxel-based as well as a network-based approach. Additionally, we compared the subsequent memory effects of the two approaches by verifying their spatial overlaps and checked for reliability of the network extraction (ICA).

The present study aims at exploring the similarities and differences of neurofunctional underpinnings of successful memory encoding and inter-individual differences in memory performance.

Results

Behavior

We found substantial variability in EM performance across subjects (*M* = 30.61, *SD* = 8.35). No ceiling or floor effects were detected (Figure 3.1). The number of pictures freely recalled ranged from 5 to 55 (of 72 presented ones).

Figure 3.1

Free recall performance

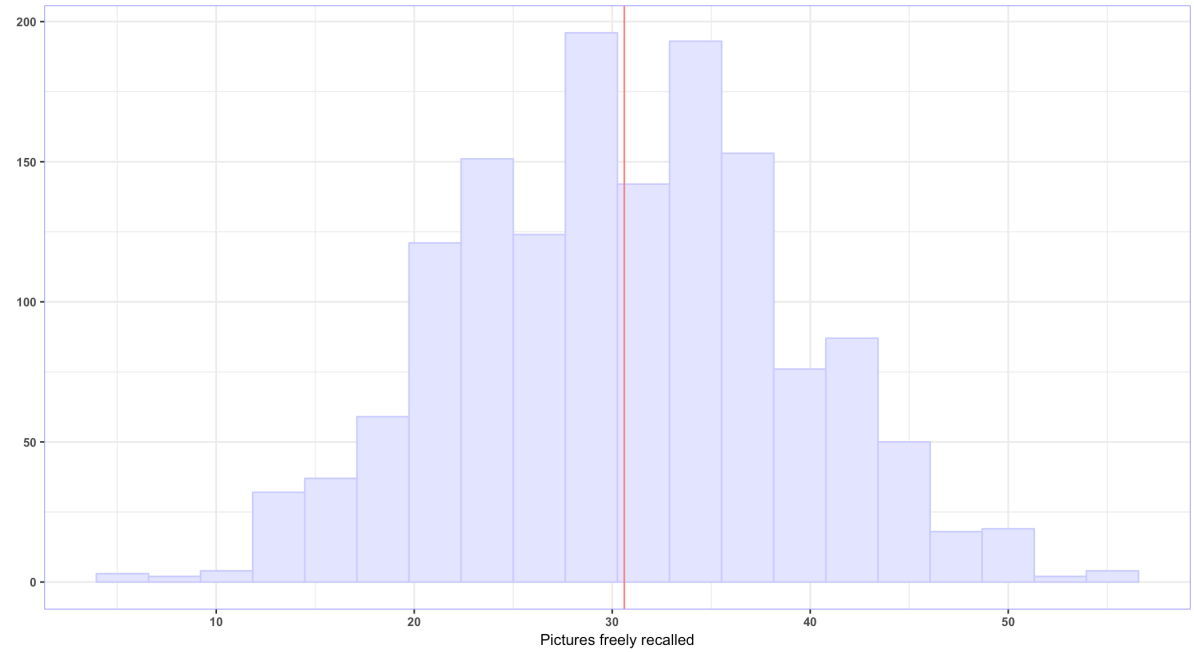

Note. The histogram illustrates free recall performance, defined as number of pictures freely recalled (*M* = 30.61, *SD* = 8.35, range = 5 to 55).

Subsequent memory effect: voxel-based

We first ran a group-based subsequent-memory analysis. We could replicate subsequent memory effects known from the literature (Kim, 2011) in the left inferior frontal cortex, bilateral fusiform gyrus, bilateral medial temporal lobe, bilateral premotor cortex, and bilateral posterior parietal cortex. Moreover, there were additional findings of subsequent memory effects, located in the precuneus, lingual gyrus, cerebellum, thalamus, orbitofrontal cortex, anterior cingulate cortex and large parts of the frontal cortex, all bilaterally (Figure 3.2; Figure S1).

Responsivity during encoding and inter-individual differences in memory: voxel-based

At the voxel-level, we detected positive brain-behavior associations between brain responsivity to pictures and later EM free recall in the left precuneus/left posterior cingulate cortex (PCC), orbitofrontal cortex (OFC), superior frontal cortex (SFC), left cerebellum, and bilaterally in the hippocampal formation (two-sided *FWE*-corrected $p < 0.05$; 510 voxels; Figure 3.3A). There were no negative correlations.

Figure 3.2

Statistical brain map of the group-based subsequent memory effects

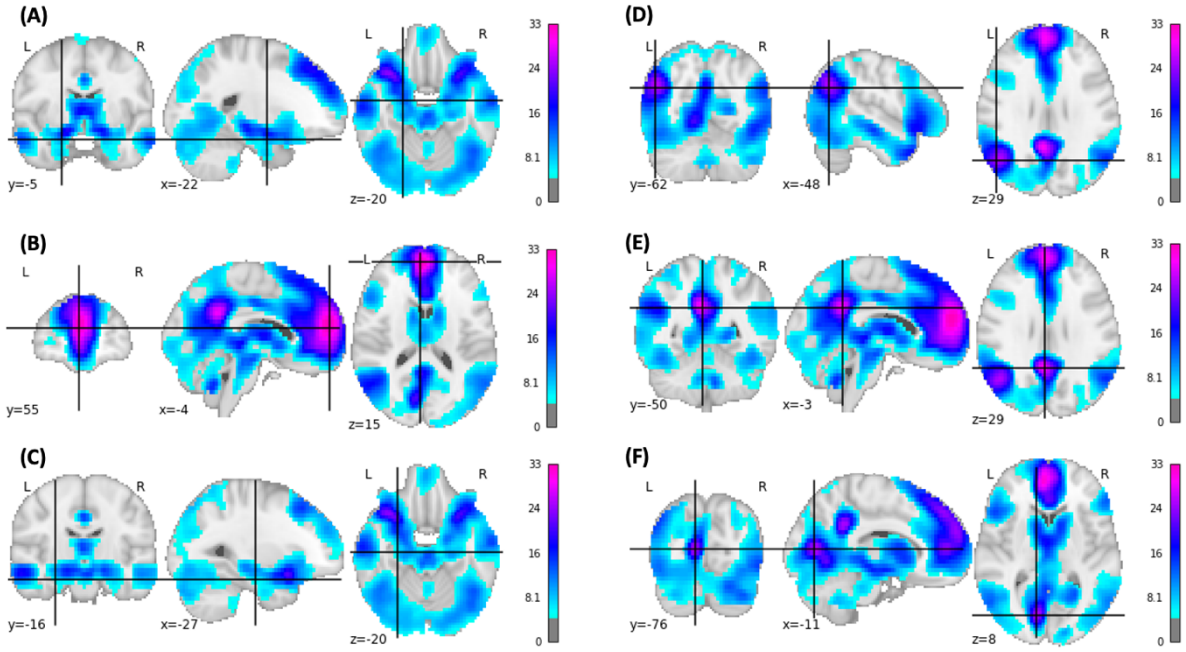

Note. For illustrative purposes, coordinates were placed in left-hemispheric brain regions: **(A)** amygdala (t = 13.34), **(B)** caudal anterior cingulate (t = 18.3), **(C)** hippocampus (t = 7.5), **(D)** inferior-parietal cortex (t = 25.67), **(E)** isthmus-cingulate (t = 28.53), **(F)** pericalcarine cortex (t = 26.09). The images are corrected for multiple comparison at the whole-brain level (two-sided *FWE* $p < 0.05$).

Responsivity during encoding and inter-individual differences in memory: voxel-based

At the voxel-level, we detected positive brain-behavior associations between brain responsivity to pictures and later EM free recall in the left precuneus/left posterior cingulate cortex (PCC), orbitofrontal cortex (OFC), superior frontal cortex (SFC), left cerebellum, and bilaterally in the hippocampal formation (two-sided *FWE*-corrected $p < 0.05$; 510 voxels; Figure 3.3A). There were no negative correlations.

A cluster analysis decomposed the voxel-based brain-behavior correlations into 15 clusters based on the t-values of its statistical image, six of which consisted of at least 20 voxels (range for all clusters' size: 1 to 133 voxels) (Table 3.1; Figure 3.3B). There were two MTL clusters (one in each hemisphere), three cerebellar clusters, one in the medial prefrontal cortex (MPFC), one in the superior frontal gyrus (SFG), one in the precuneus/isthmus cingulate, and one in the anterior cingulate cortex/subcallosal cortex. The biggest clusters were located in the left MTL, precuneus, and right MTL, consisting of 133, 108, and 83 voxels, respectively.

Table 3.1

Clusters of the voxel-based brain-behavior correlations

VBA-BBC-Cluster index	Voxels	MAX X (mm)	MAX Y (mm)	MAX Z (mm)	*t*-value VBA-BBC	*t*-value SME	*t*-value SME 10 mm sphere (min)	*t*-value SME 10 mm sphere (max)	*t*-value SME 10 mm sphere (median)	*t*-value SME 5 mm sphere (min)	*t*-value SME 5 mm sphere (max)	*t*-value SME 5 mm sphere (median)
1	133	-24.80	-19.20	-16.00	6.45	12.51	2.62	17.13	10.16	7.70	14.91	11.63
2	107	-2.75	-46.80	28.00	5.64	26.37	3.92	29.52	20.53	17.44	29.52	24.71
3	82	22.00	-19.20	-20.00	5.82	10.37	1.18	16.23	7.78	3.91	14.32	9.45
4	82	5.50	55.00	-16.00	6.90	9.54	2.72	22.75	9.37	5.93	16.94	9.88
5	43	19.20	-85.20	36.00	5.12	11.21	0.00	13.15	10.58	8.57	12.39	10.85
6	29	-8.25	41.20	40.00	5.43	19.52	8.89	25.45	19.32	14.94	23.72	19.67

Note. The columns illustrate each cluster's size in voxels, maximum value of intensity (*t*-value VBA-BBC), and location of the maximum intensity voxel, given as X/Y/Z coordinate values in standard space (MAX X (mm), MAX Y (mm), MAX Z (mm)). The *t*-values of the subsequent memory effects (SME) are provided at the voxel location (*t*-value SME) as well as the minimum, maximum and median in the respective spheres of 10 and 5 mm size, respectively. Only clusters with at least 20 voxels are listed.

Figure 3.3

Inter-individual correlations between brain responsivity during encoding and free recall performance using a voxel-based approach

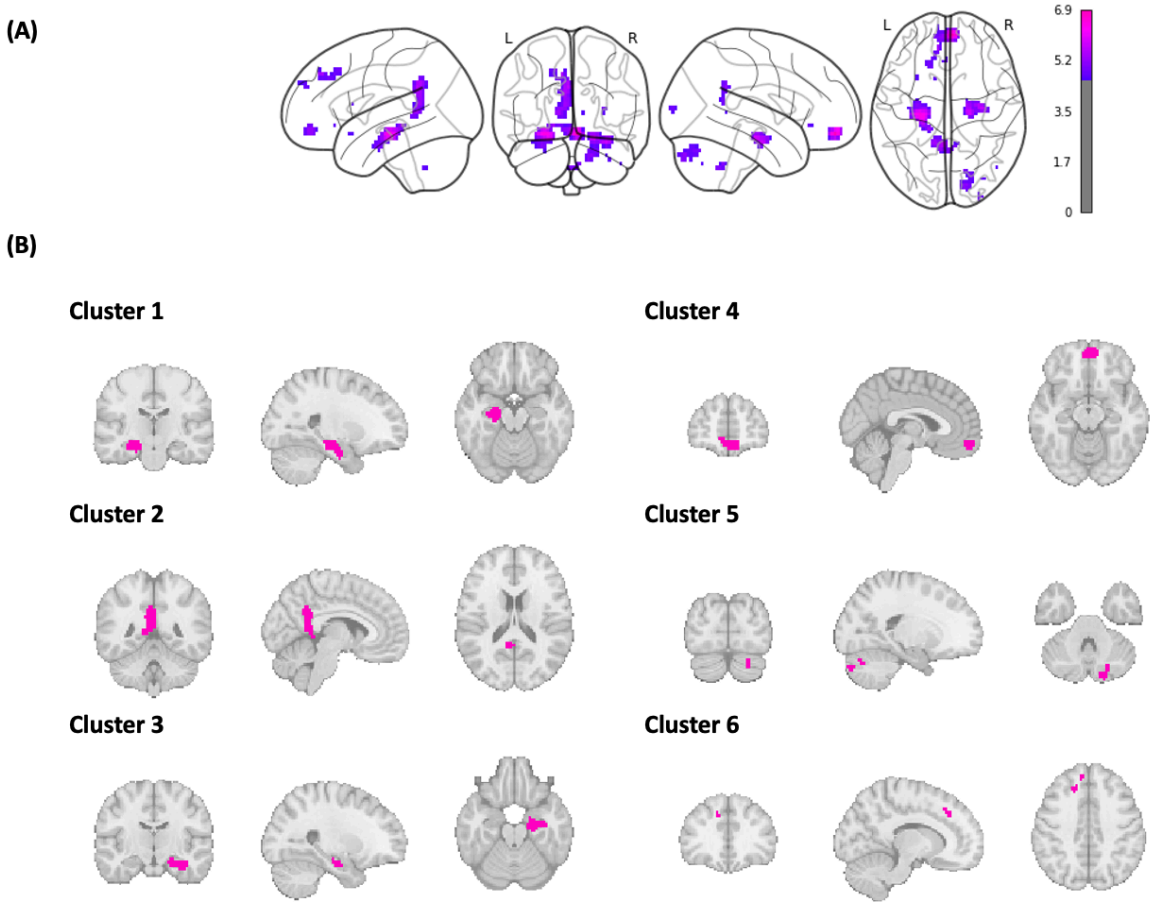

Note. **(A)** Glass brain visualization (two-sided *FWE* $p < 0.05$ correction for multiple comparison). **(B)** Activations comparted into 15 clusters, mapped on anatomical slices. The six largest clusters are shown. Cluster 1: left hippocampus; cluster 2: isthmus of cingulate cortex; cluster 3: right hippocampus; cluster 4: medial orbitofrontal cortex; cluster 5: right cerebellum; cluster 6: left superior frontal cortex.

Comparison of the voxel-based subsequent memory effects and the voxel-based brain-behavior correlations

A cluster analysis comparted the subsequent memory effect map into 14 clusters (Table 3.2, Figure 3.4, Figure S2). Two of those clusters' peak voxels were also prominently represented in the voxel-based brain-behavior correlation map (Table 3.2). The larger of the two, cluster 2, encompasses 2307 voxels and is located in the posterior cingulate gyrus and precuneus. The second one, cluster 9, is situated in the right hemisphere of the Crus I, Crus II and IX of the

cerebellum. On the other hand, for several clusters (e.g., clusters 5 and 10) there was no evidence for representation in the brain-behavior correlation map.

In contrast, all clusters from the voxel-based brain behavior correlation map were located in regions that also exhibited significant subsequent memory effects (Table 3.1).

Figure 3.4

Clusters of the subsequent memory effects at voxels with T-values above the 75th percentile of all subsequent memory effects

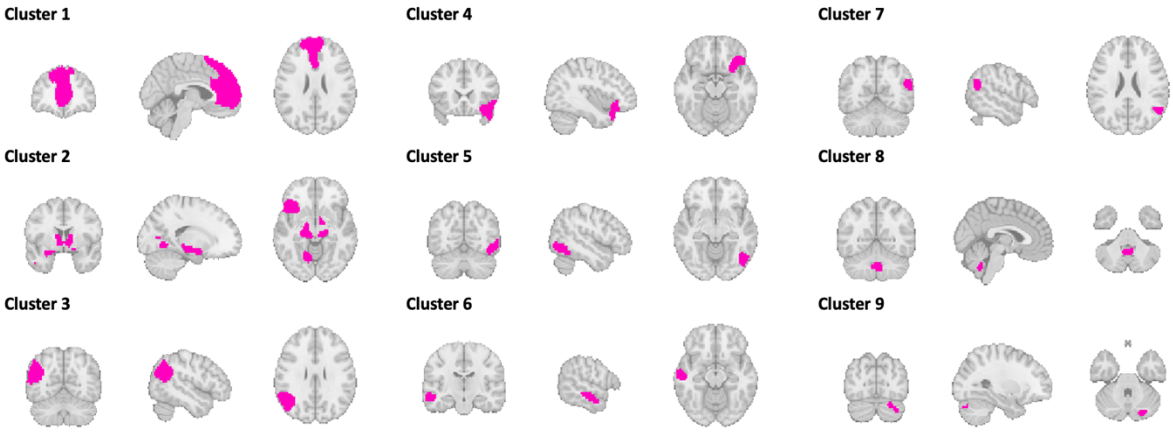

Note. The nine largest clusters are shown. Cluster 1: superior frontal gyrus, paracingulate gyrus, frontal pole; cluster 2: posterior cingulate gyrus, precuneus; cluster 3: lateral occipital cortex, angular gyrus; cluster 4: orbitofrontal cortex, insula; cluster 5: lateral occipital cortex; cluster 6: middle temporal gyrus; cluster 7: lateral occipital cortex, angular gyrus; cluster 8: right cerebellar cortex; cluster 9: right cerebellar cortex.

Table 3.2

Clusters of the voxel-based subsequent memory effect

SME Cluster index	Voxels	MAX X (mm)	MAX Y (mm)	MAX Z (mm)	*t*-value SME	*t*-value VBA-BBC	*t*-value VBA-BBC 10 mm sphere (min)	*t*-value VBA-BBC 10 mm sphere (max)	*t*-value VBA-BBC 10 mm sphere (median)	*t*-value VBA-BBC 5 mm sphere (min)	*t*-value VBA-BBC 5 mm sphere (max)	*t*-value VBA-BBC 5 mm sphere (median)
1	2564	-2.75	55.00	16.00	32.60	2.92	1.65	4.06	2.93	2.39	3.19	2.82
2	2307	-5.50	-49.50	28.00	29.50	5.41	1.93	5.64	4.25	4.70	5.64	5.19
3	600	-49.50	-63.20	32.00	26.00	3.21	1.43	3.66	2.57	2.48	3.58	3.00
4	388	30.20	16.50	-16.00	21.10	2.88	-1.49	3.81	1.29	0.45	3.81	2.17
5	202	49.50	-68.80	-8.00	16.90	-1.46	-2.11	1.70	-0.88	-1.84	-0.23	-1.20
6	167	-57.80	-19.20	-12.00	18.70	2.03	0.08	3.46	1.76	1.29	2.95	2.02
7	90	55.00	-60.50	28.00	15.60	1.32	-0.28	2.28	1.11	0.73	1.79	1.31
8	66	5.50	-55.00	-44.00	17.40	3.71	-0.44	5.07	2.25	1.09	5.00	3.28
9	56	22.00	-79.80	-28.00	13.60	4.75	1.39	4.95	3.67	3.77	4.95	4.43
10	30	-46.80	-71.50	-12.00	13.20	0.52	-2.23	1.45	-0.05	-0.92	0.75	0.178
11	27	63.20	-5.50	-24.00	14.50	3.31	0.36	3.64	2.26	1.64	3.64	2.95
12	23	0.00	-11.00	36.00	14.80	0.21	-2.02	1.88	-0.13	-1.18	1.16	0.14
13	21	22.00	-55.00	4.00	14.10	1.18	-0.72	3.84	1.04	0.30	2.10	1.16

Note. The columns illustrate each cluster's size in voxels, maximum value of intensity (*t*-value SME), and location of the maximum intensity voxel, given as X/Y/Z coordinate values in standard space (MAX X (mm), MAX Y (mm), MAX Z (mm)). The *t*-values of the voxel-based brain-behavior correlations (VBA-BBC) are provided at the voxel location (*t*-value VBA-BBC) as well as the minimum, maximum and median in the respective spheres of 10 and 5 mm size, respectively. Only clusters with at least 20 voxels are listed.

Network-based analyses

We used ICA to extract group-based functional connectivity networks in a data-driven manner and implemented validation steps.

ICA decomposition and network validation

For the purpose of ICA decomposition and network validation, we split our sample into two comparably large sub-samples (see materials and methods). This validation step involved comparing the solution of the ICA conducted in subsample 1 (n = 590) with the solution of the ICA conducted in subsample 2 (n = 580). Among 60 ICs (Figure S3), between-sample spatial voxel correlations were high ($|r|_{max} > 0.6$) for 50 ICs, with a median of r = 0.856 (Supplementary Table S1, Supplementary Figure S4) and 25th and 75th quantiles at r = 0.716 and 0.915, respectively.

Network characterization: similarity to resting-state networks

We checked for similarity of our task-based ICs with typical resting-state networks (RSN), as previously done (Geissmann et al., 2018). We did so by calculating cross-correlations between the ICs obtained from our sample and ten typical RSN (Smith et al., 2009), using a lenient and a more stringent threshold ($|r| > 0.1$ and $|r| > 0.2$, respectively). The mean number of matching RSNs per IC was $M_{lenient}$ = 2.083 and $M_{stringent}$ = 1.5 ($SD_{lenient}$ = 1.204 and $SD_{stringent}$ = 0.682). RSNs with high similarity to the ICs for which brain-behavior correlations were found (see below) were the cerebellum network, sensorimotor network, auditory network, and left fronto-parietal network in case of the stringent threshold, and additionally the default mode network when considering the lenient threshold (Figure S5, Figure S6).

Network-based analysis: network responsivity during encoding and inter-individual differences in memory

Responsivity of 7 ICs was associated with the number of pictures freely recalled (ICs 5, 6, 21, 29, 42, 50, 54), i.e., showed brain-behavior correlations (Figure 3.5, Figure S7). Responsivity of IC 6 demonstrated a negative association with the numbers of pictures freely recalled, while the other significant ICs showed a positive association. Variance explained by each of these

IC's responsivity was small to medium (J. Cohen, 1988), ranging from 3.3 % to 6 % (Supplementary Table S3).

Network characterization: visual inspection and characterization of the independent components with brain-behavior correlations

Close inspection of spatial distribution (see below) showed that ICs 5, 6, 21, 29, 42 and 50 may be understood as functional connectivity networks (Supplementary Figure S7). Since IC 54, in addition to grey matter involvement, has a spatial distribution indicative of noise components (large involvement of ventricles) (Supplementary Figure S8), we refrained from further interpreting IC 54.

Figure 3.5

The ICs with brain-behavior correlations

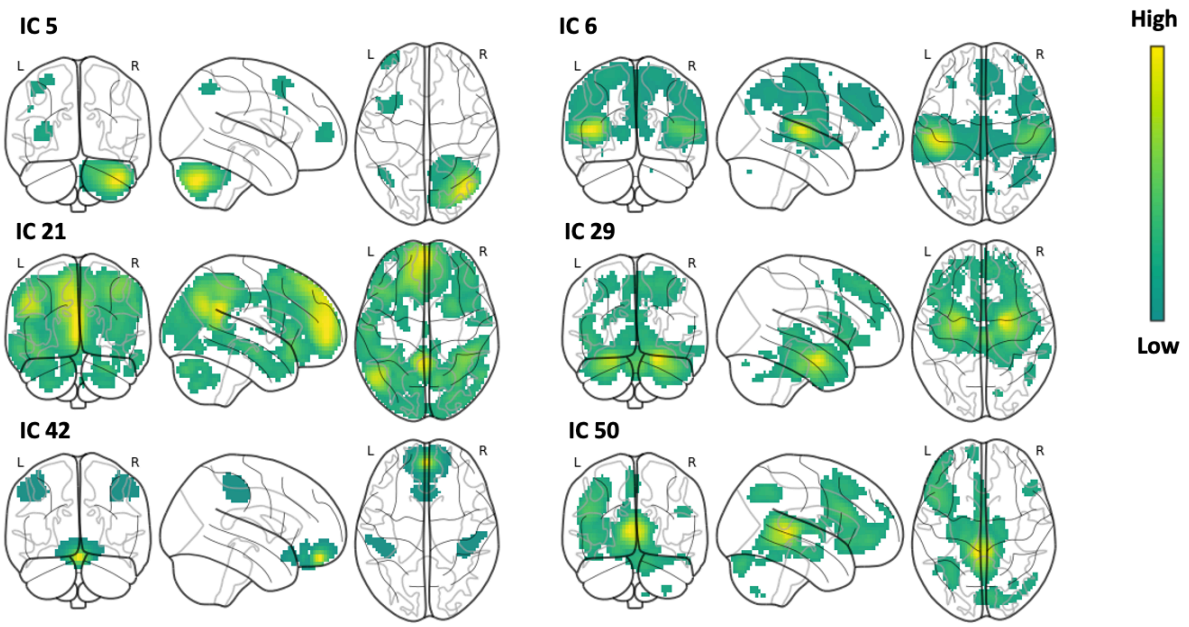

Note. Z-values run along a spectrum from yellow to dark green, respectively, high to low values. These values indicate the contribution of brain regions within their IC irrespective of their link to behavior. Please note: IC 6 was negatively associated with numbers of pictures freely recalled, while the other ICs were positively associated.

IC 5: Cortico-cerebellar network

For the most part, IC 5 encompasses the right cerebellum as well as left fronto-opercular, fronto-caudal and fronto-rostral parts, temporal and parietal regions. The right cerebellum is

important in cognitive processes like error processing, response inhibition, performance monitoring, memory, emotional responding, and other brain regions of this IC are involved in memory integration, information binding, and planning (Baumann & Mattingley, 2012; Brissenden et al., 2016; Peterburs & Desmond, 2016; Yazar et al., 2017). Given its structural connections and functional implications, the cerebellum has been suggested as an add-on to the dorsal attention network (Brissenden et al., 2016), suggesting a cortico-cerebellar network.

IC 6: Multi-modal integration network

IC 6 overlays sensory-motor and sensory-auditory areas. It includes the anterior and posterior cingulate cortices and the posterior insula. These brain regions, especially the posterior insula, have wide-spanning cognitive and sensory functions and wide-ranging structural connections, including cholinergic, dopaminergic, serotonergic, and noradrenergic systems (Gogolla, 2017; Laird et al., 2011). Accordingly, we propose to label it multi-modal integration network.

IC 21: Medial-frontoparietal network

IC 21 resembles not only the DMN but also contains additional clusters. Anatomically, it includes the frontal pole, anterior-medial OFC, superior frontal cortex, rostral ACC, PCC, precuneus, isthmus cingulate cortex, occipital cortices and angular gyrus. Among these regions' recognized functional roles are episodic memory retrieval, higher-order cognition, visuo-spatial imagery, self-processing, and memory integration (Laird et al., 2011).

IC 29: MTL network

Centered on the MTL, IC 29 includes the parahippocampal gyrus, hippocampus, entorhinal cortex and amygdala bilaterally. Additional brain regions are the brainstem, thalamus, and right cerebellum. These regions share fundamental roles in memory and emotion (Murty et al., 2010; Salay et al., 2018; Sved et al., 2002). To a comparatively smaller extent, IC 29 includes non-neural areas.

IC 42: OFC network

IC42 is characterized by two clusters in the medial OFC and one in the bilateral postcentral and precentral gyrus, IC 42 has a remarkably compact appearance. Covered brain regions are

implicated in autobiographical memory recall, recollection of self-relevant information, emotion regulation, imagery, representational memory, behavior-outcome-expectancy (Kim et al., 2019; Schoenbaum & Roesch, 2005). This network is novel in that it has not been reported in the literature yet.

IC 50: Extended left fronto-parietal network

IC 50 spans the superior frontal cortex, opercular cortex, lateral OFC, rostral and caudal frontal cortex, opercular cortex, inferior frontal cortex, cerebellum, precuneus, posterior cingulate cortex, brainstem, thalamus, angular gyrus, thereby sharing overlap with the left fronto-parietal network. Among the included brain regions' functions are executive function, affective and interoceptive processing, and memory integration (Laird et al., 2011; Smith et al., 2009). Besides coverage of brain regions, IC 50 includes ventricular parts.

Discussion

The present single-center study in 1,434 individuals allowed to perform both analyses on group-level, focusing on the neural underpinnings of successful memory encoding, as well as brain-behavior correlations, focusing on neural underpinnings of inter-individual differences in memory performance. With regard to the group-level analyses, we replicated and extended the findings from a meta-analysis (Kim, 2011) on the neural underpinnings of the subsequent memory effect. With regard to brain-behavior correlations, we found both brain regions and brain networks that were associated with inter-individual differences in memory performance.

Subsequent memory effect

In line with numerous studies (Kim, 2011), the subsequent memory effects in this study were located in the left inferior frontal cortex, bilateral fusiform gyrus, bilateral medial temporal lobe (MTL), bilateral premotor cortex, and bilateral posterior parietal cortex. Regions not consistently reported previously included the precuneus, lingual gyrus, cerebellum, thalamus, orbitofrontal cortex (OFC), anterior cingulate cortex (ACC) and large parts of the frontal cortex. Those novel findings are likely due to the high statistical power of our large single-center sample. While these additional findings apply to free recall of picture memory, it remains to be determined whether they also apply to EM involving other sensory modalities.

Brain-behavior correlations: voxel-based approach

Inter-individual differences in memory performance were associated with responsivity of voxels in the left precuneus/left posterior cingulate cortex, OFC, SFC, left cerebellum, and bilaterally in the hippocampal formation. These regions largely overlap with the medial fronto-parietal network, also referred to as core recollection network, which has recently been suggested to be among the six macro-scale FCNs according to a cortico-centric taxonomy (Uddin et al., 2019).

The voxel-based brain-behavior correlations were decomposable into at least 9 clusters of brain regions, the three largest of which were located in the left MTL, precuneus/isthmus cortex, and right MTL, and largely covered by functional connectivity networks that accounted for inter-individual differences in EM in our study, namely the MTL network and default mode network (DMN). Voxel-based brain-behavior correlations in the cerebellum were parted into three clusters, the largest of which was located in the right lateral crus I and II, which have recently been related to autobiographical memory (King et al., 2019).

Comparison of the two voxel-based approaches

A novel finding lies in the identification of brain regions that were either exclusively or non-exclusively related to successful memory encoding or to inter-individual differences in memory performance. While all brain regions with voxel-based brain-behavior correlations exhibited a significant subsequent memory effect, the opposite was not true: only a few subsequent memory effect clusters were involved in the inter-individual analysis. This was the case for cluster 2, involving MTL regions, and cluster 9 in the right cerebellar cortex. In other words, among the brain regions involved in explaining inter-individual differences in EM, all appeared to be relevant for successful memory encoding, while there were brain regions relevant for successful memory encoding that did not explain inter-individual differences in EM.

Brain-behavior correlations: network-based approach

Network responsivity during encoding of 6 FCNs was associated with later free recall. The current state of research on functions of brain regions and their structural and functional connectivity supports the associations of the 6 ICs with EM. These ICs only partly match

previously described FCN or RSN, in line with state-specific and task-specific flexibility in network configuration (Greene et al., 2020). Labels for this set of ICs with brain-behavior correlations were selected based on previous literature and the ICs' spatial representation in the brain. We found positive correlations of EM performance and network responsivity for a cortico-cerebellar network (IC 5), the medial-frontoparietal network (IC 21), MTL network (IC 29), orbitofrontal cortex (OFC) network (IC 42) and extended left fronto-parietal network (IC 50). The multi-modal integration network (IC 6) demonstrated a negative correlation in its responsivity with EM performance.

Among the FCNs for which higher responsivity is associated with improved recall is the cortico-cerebellar network (IC 5). Its brain regions are implicated in visual working memory, emotion, visual attention, executive functions, memory, cortico-striatal plasticity, and conscious representation of memory (Baumann & Mattingley, 2012; Brissenden et al., 2016; Peterburs & Desmond, 2016; Yazar et al., 2017). IC 21 consists of regions in the frontal pole, OFC, superior frontal cortex, ACC, PCC, precuneus, isthmus CC, occipital cortex, lingual gyrus, parahippocampal gyrus, temporal gyrus and opercular cortex. Given the overlap with the DMN, this network is presumably involved in internally-oriented processing and memory. The DMN's setup is assumed to be task-dependent and may consist of multiple subnetworks (Salehi et al., 2020). IC 29 consists of MTL regions, including amygdala, hippocampus, parahippocampal gyrus, entorhinal cortex, and brainstem, but also ventricular regions. The MTL is known for its role in memory (Murty et al., 2010; Salay et al., 2018; Sved et al., 2002). The FCN that makes up IC 42 is novel in that it has not been reported as an FCN so far. It consists of the medial OFC, and postcentral and precentral gyrus. The OFC is important for outcome expectancy, representational memory, impulsivity, decision making (Kim et al., 2019; Schoenbaum & Roesch, 2005), and has functional connections to the DMN, limbic regions, hippocampus, striatum, and thalamus. As opposed to IC 42's compact appearance, IC 50 consists of a large number of brain regions, that is, the superior frontal cortex, opercular cortex, right inferior frontal cortex, left lateral OFC, opercular cortex, inferior and caudal frontal cortex, cerebellum, precuneus, PCC, brainstem, and thalamus. It overlaps with the left frontoparietal network, which is implicated in language, executive function, inhibitory control, pain, and sensory processing (Smith et al., 2009).

Network responsivity of IC 6 was negatively associated with memory performance, i.e., the stronger this FCN responds to stimuli, the less pictures were remembered later. IC 6

consists of extensively connected regions, such as sensory-motor, and sensory-auditory areas, ACC, PCC, juxtapositional cortex, and posterior insula. The insula is important for interoception, emotions, memory, sensory processing and integration, and attention (Gogolla, 2017; Kurth et al., 2010). The involvement of the insula in IC 6 could be therefore seen as beneficial for memory function. However, the involvement of sensory-auditory areas could reflect auditory processing in an environment with high-volume auditory input (i.e., the auditory noise from the rapidly switching gradients in the MRI environment). It is therefore possible that processing and integrating auditory signals may interfere with the visual memory task and therefore result in lower memory performance.

It is noteworthy that almost all ICs with brain-behavior correlations were largely included in the brain regions whose brain activity during encoding, on group-level, have been found to be associated with successful recollection (i.e., subsequent memory effect). Outstanding in this regard is the cortico-cerebellar network (IC 5). Since the cerebellum does not have the same microscopic structure as the cerebral cortex (Schmahmann et al., 2019), its functional specialization may be better represented in variations in anatomical connectivity rather than variations in local microstructure (Guell et al., 2018; Schmahmann et al., 2019). This indicates that investigations of cerebellar implications in EM in particular may benefit from a network-based approach rather than mass-univariate voxel-based group-level analyses. Cerebellar FCNs have been shown to clearly reconfigure during states of cognitive tasks compared to resting conditions and be highly flexible depending on the cognitive task (Salehi et al., 2020), highlighting the benefit of using FCNs based on the functional architecture present during a specific task such as to best capture associations with a relevant behavioral phenotype.

The significance of using the two complementary approaches is further evidenced by the opposing quest in neuroscience to unravel both basic mechanisms as well as inter-individual differences (Lebreton et al., 2019). While the former, in order to explain a shared basic mechanism, wishes to minimize inter-individual variance by group-averaging, the latter wishes to maximize variability to describe the association between behavior and neural underpinnings. This variability can be gathered only within the limited scope of the phenotypes measured. For that reason, it is essential to rely on well-defined phenotypes and large samples (Dubois & Adolphs, 2016). The large sample size and the fact that all subjects were investigated in the same scanner in our study is therefore beneficial with regards to

statistical power and suitability for the inter-individual approach used here. However, the need of large samples and the necessity to minimize memory-unrelated variability (e.g., differences between scanners) is a limitation of the inter-individual approach with regard to integrating the results in meta-analytic methods and with regard to generalizability of the findings.

Novelty

In the present study, we compared the neural underpinnings of successful memory encoding with those explaining inter-individual differences in EM and identify both similarities and differences. Additionally, our analyses allow for the comparison of voxel-based and network-based approaches for brain-behavior relationships, which are complementary to each other. Using a data-driven network-based approach, we show that inter-individual differences in EM are partly explained by the way task-related FCNs respond to stimuli during encoding. In conclusion, the study offers new insights into brain regions and networks involved in inter-individual differences in EM. The identification of neurofunctional markers based on inter-individual differences in memory may open the possibility for studying associations with other individual phenotypes, such as psychological traits, genetic or epigenetic makeup, or individual metabolomic profiles.

Materials and Methods

Experimental Design

Sample and study

Data presented in this paper comes from a large single-center study aimed at uncovering neurobiological mechanisms underlying episodic memory and working memory by combining genetic, behavioral, eye-tracking and neuroimaging data (Egli et al., 2018; Heck et al., 2014). The sample (n = 1.485) consists of healthy young adults aged 18 to 35, with the majority being aged between 20 and 24 (M = 22.36, SD = 3.25). The study encompassed cognitive tasks inside the scanner, outside the scanner, and sampling of genetic and blood markers. After a short introduction, subjects were guided inside the MRI scanner to perform a picture encoding task, followed by a working memory task, whilst fMRI data was being collected. Then followed an unannounced free recall (FR) task outside the scanner. After this, subjects once again lay inside the scanner to complete a picture recognition task. Upon the second fMRI session followed

an anatomical scan and, in some subjects, a DTI scan. The following data is presented in this paper: fMRI data during encoding, behavioral data of the free recall task (number of pictures recalled), and demographic information.

Behavioral tasks: encoding task

Seventy-two pictures selected from the International Affective Picture System (IAPS) (Lang et al., 2005) were used for the episodic memory tasks (encoding, free recall, recognition), valenced either neutral, negative, or positive. During the encoding, the IAPS pictures were presented for 2.5 seconds each in a sequential randomized manner and rated for arousal and valence on a dimensional scale. Additionally, intermingled in between the IAPS pictures, so that a maximum of two IAPS pictures were presented in succession, 25 geometrical figures (Spreen & Strauss, 1991) were presented on a colored scrambled background and rated for size and shape on a dimensional scale. The scrambled background was created using Adobe Photoshop CS3 (©2007 Adobe Systems Incorporated) and composed of the task IAPS-images positioned one next to another, edited with a distortion and crystal filter in such a way that the motives were no longer perceivable. Subjects were kept uninformed about the upcoming memory tasks.

Behavioral tasks: free recall task

In the free recall task, subjects were instructed to describe in writing as many of the previously seen pictures as possible. There was no time limit for completion. Three independent raters were responsible for the scoring to guarantee inter-rater validity. The amount of correctly recalled pictures was our behavioral variable of interest.

Statistical analysis

fMRI preprocessing

fMRI data was preprocessed using SPM12 (Statistical Parametric Mapping, Wellcome Trust Centre for Neuroimaging; http://www.fil.ion.ucl.ac.uk/spm/) implemented in MATLAB R2016b (MathWorks).

Volumes were slice-time corrected to the first slice, realigned using the 'register to mean' option, and coregistred to the anatomical image by applying a normalized mutual information 3-D rigid-body transformation. Successful coregistration was visually verified for

each subject. Subject-to-template normalization was done using DARTEL (Ashburner, 2007), which allows registration to both cortical and subcortical regions and has been shown to perform well in volume-based alignment (Klein et al., 2009). Normalization incorporated the following four steps: 1) Structural images of each subject were segmented using the 'New Segment' procedure in SPM12. 2) The resulting gray and white matter images were used to derive a study-specific group template. The template was computed from a subgroup of 1.000 subjects, which were part of the subjects included in the present study. 3) An affine transformation was applied to map the group template to MNI space. 4) Subject-to-template and template-to-MNI transformations were combined to map the functional images to MNI space. The functional images were smoothed with an isotropic 8 mm full-width at half-maximum (FWHM) Gaussian filter.

Normalized functional images were masked using information from their respective T1 anatomical file as follows. At first, the three-tissue classification probability maps of the "Segment" procedure (grey matter, white matter, and CSF) were summed to define the mask. The mask was binarized, dilated and eroded with a 3 × 3 × 3 voxels kernel using fslmaths (FSL) to fill in potential small holes. The previously computed DARTEL flowfield was used to normalize the brain mask to MNI space, at the spatial resolution of the functional images. The resulting non-binary mask was thresholded at 50% and applied to the normalized functional images. Consequently, the implicit intensity-based masking threshold usually employed to compute a brain mask from the functional data during the first level specification (spm_get_defaults('mask.thresh'), by default fixed at 0.8) was not needed any longer and set to a lower value of 0.05.

Subsequent memory effect

As in typical subsequent memory analyses, we proceeded in a standard hierarchical GLM implemented in SPM 12. First-level analyses were conducted to identify subject-specific activations. Regressors modeling the onsets and duration of stimulus events were convolved with a canonical hemodynamic response function (HRF). More precisely, the model comprised regressors for button presses modeled as stick/delta functions, picture presentations (IAPS pictures later recalled, IAPS pictures later not recalled, primacy and recency) modeled with an epoch/boxcar function (duration: 2.5 s), and rating scales modeled with an epoch/boxcar function of variable duration (depending on when the subsequent button press occurred).

Serial correlations were removed using a first-order autoregressive model, and a high-pass filter (128 s) was applied to remove low-frequency noise. Six movement parameters were also entered as nuisance covariates. The contrast estimates "IAPS pictures later recalled - IAPS pictures later not recalled" were used as input for a group-level analysis, including age, sex, and batch effects (two MR gradient changes and one MR software upgrade) as regressors, implemented in MRTools' GLM Flex Fast2 (http://mrtools.mgh.harvard.edu).

Network extraction and validation in two subsamples: ICA

Using group probabilistic spatial ICA (Jenkinson et al., 2012), we first decomposed brain activity during encoding into 60 spatially independent components (IC). This number of ICs yielded an optimal balance between dimensionality reduction and loss of information. ICA input data consists of all subjects' data concatenated in the time dimension (60.638 voxels x 420 time points of *n* subjects). Importantly, the algorithm is not given any information about the task but instead separates signal into independent spatial sources that together explain brain activity in a purely data-driven manner.

The resulting spatial maps were thresholded using an alternative hypothesis test-based on fitting a mixture model to the distribution of voxel intensities within spatial maps, using the default parameters (https://fsl.fmrib.ox.ac.uk/fsl/fslwiki/MELODIC#MELODIC_report_output) (Beckmann & Smith, 2004).

Network extraction was done for two subsamples independently, consisting of 590 and 580 subjects each (subsamples 1 and 2, respectively). Network extraction calculations were performed on sciCORE (http://scicore.unibas.ch/) scientific computing center at the University of Basel, Switzerland, on a single node with 128 GB of RAM. Due to characteristics inherent to FLS's MELODICS, the job was running on a single core. Based on these computational backgrounds, this analysis did not use the full sample size. This allowed us to validate the decomposition in subsample 1 and to proceed with replicable networks only. For each of both subsamples' decompositions, we extracted all unthresholded IC's voxel loadings, and cross-correlated them with all IC's voxel loadings of the other sample. ICs with $|r|_{max} \geq 0.7$ were regarded as replicable. ICs with $|r|_{max} \geq 0.6$ and $|r|_{max} < 0.7$ were visually inspected to make a judgement on their replicability. All other ICs were treated as insufficiently replicable and were therefore not considered for interpretation. The value $|r|_{max}$ describes

the maximum correlation value of an IC of subsample 1 with any IC of subsample 2, i.e., regardless of the number of matches passing the threshold.

Network time course calculation in all subjects: dual regression

The next step was to get subject-specific time-courses for the 60 ICs obtained from subsample 1 running dual regression in FSL v.5.0.9 (Jenkinson et al., 2012). The set of spatial maps from the group-average analysis was used to generate subject-specific versions of the spatial maps, and associated time-series, using dual regression (Beckmann et al., 2009; Filippini et al., 2009). First, for each subject, the group-average set of spatial maps is regressed (as spatial regressors in a multiple regression) into the subject's 4D space-time dataset. This results in a set of subject-specific time-series, one per group-level spatial map, for the total sample (n = 1,434).

Network and voxel responsivity

Functional modulation of each component for each subject was estimated in a first-level analysis including the following regressors: IAPS pictures, geometrical figures, primacy and recency pictures, stimuli rating, button press, six movement parameters. The dependent variable was each IC's subject-specific time course. The difference between IAPS pictures and geometrical figures estimates (standardized betas) was used as a measure of task-related functional responsivity of each IC (Samu et al., 2017).

Those contrast estimates were used to examine their relationship with inter-individual differences in memory, by means of linear models. Each model included all subjects' contrasts as the independent variable of interest, number of correctly recalled pictures as the dependent variable, and the covariates sex, age, and batch effect. The batch effect variable was coded according to one of two rooms in which subjects completed the free recall task.

A similar approach was used for the voxel-based analysis, but instead of network responsivity (network betas), voxel responsivity (voxel betas) was used as independent variable of interest. All results were corrected for multiple comparisons to reduce the burden of false positives. In the case of the voxel-based approach, a whole-brain *FWE*-correction was applied, with a significance threshold of $p < 0.05$. In the case of the network-based approach, a Bonferroni correction was applied by dividing the statistical threshold by the number of ICs, resulting in a threshold of $p < 8.33e\text{-}04$ (0.05/60).

Network characterization

Anatomical labeling was based on an in-house standard anatomical atlas, which is most representative of the sample at hand.

Similarity of the voxel-based and network-based brain-behavior correlations

In order to compare the spatial coverage of the voxel-based and network-based results (6 and 1 brain map for the network-based appoach and voxel-based approach, respectively), we quantified their overlap with FSL's fslmaths tools. The procedure included binarization of the spatial 3D brain maps, multiplication of each of 6 the resultant 6 network-based brain maps with the voxel-based brain map, and based thereupon counting of overlapping voxels between each pair.

Using FSL's fslmaths tools and in particular FSL's cluster function, a cluster analysis decomposed the voxel-based brain-behavior correlations voxel effects into 15 clusters based on the *t*-values of its statistical image. These were used to describe the overlap between voxel-based and network-based brain-behavior correlations in more detail, following the same principles as described in the previous paragraph.

Voxel-based approaches: comparison of the subsequent memory effects and the voxel-based brain-behavior correlations

For the purpose of a descriptive comparison of the second-level results of the two voxel-based approaches, we comparted subsequent memory effects into clusters. More specifically, we ran a cluster analysis on the statistical t-map of the subsequent memory effect, wherein only voxels with a *t*-value above the 75th percentile of all *FWE*-corrected voxels were included. This threshold was chosen to avoid a two cluster solution when only considering the FWE threshold. As described in the above paragraph, we used FLS's cluster function. To scale up the spatial level of these comparisons from one voxel in the brain-behavior correlations to a group of voxels, spheres of 5 mm and 10 mm were created around the peak voxel of the SME cluster (Table 3.2). The idea of this was to avoid focusing on single voxels when drawing conclusions on brain regions.

Network characterization: similarity to resting-state networks

As done previously (Geissmann et al., 2018), we quantified the similarity of our task-related ICs to a set of 10 resting-state templates, which have been robustly detected in a number of independent studies (Biswal et al., 2010; Damoiseaux et al., 2006; Laird et al., 2011), available on http://www.fmrib.ox.ac.uk/dazasezs/brainmap+rsns/ (retrieved 07/07/2016), described in Smith et al. (2009). These template RSNs circumscribe three visual networks (medial, occipital pole, lateral visual areas; 1-3), the default mode network (DMN), a cerebellum network (CN), the sensorimotor network (SMN), auditory network (ADT), executive control network (ECN) and left/right fronto-parietal networks (LFPN, RFPN). We identified the template RSNs that had the highest spatial correlation with our task-based ICs using FSL's spatial cross-correlation.

Network characterization: similarity to the subsequent memory effect

The procedure was the same as the one for calculation of similarity between the VBA and NBA brain-behavior correlations (see above).

Network characterization: visual inspection and characterization of the independent components with brain-behavior correlations

ICA separates the data into a set of spatial maps that together compose the whole-brain data (McKeown & Sejnowski, 1998; S. M. Smith et al., 2009). Due to its ability to simultaneously denoise as well as capture variances in the BOLD signal (Greene et al., 2020), careful visual inspection of the ICs is a critical step to reap its full benefits. We carefully visually inspected the ICs such as to be sure to draw valid conclusions based on the findings from the network-based brain behavior correlations, keeping in mind the drawbacks and benefits of the data-driven approach of ICA. Examples of noise components are: strong loadings in the ventricular system, movement-related ring artifacts at the periphery of the cortex. We further provide detailed descriptions of which brain regions are included in the ICs and what their implications are.

Brainmaps: figure creation

Figures were created with Nilearn (V. 0.8.1; https://nilearn.github.io/stable/index.html). Cross-section slicing positions, if applicable (Figure 3.2, Supplementary Figure S2,

Supplementary Figure S3), were calculated with default settings, which works by iteratively locating peak activations that are separated by a certain distance in voxels, wherein the default is 0.5 / 7. This function has been designed to find good cross-section slicing positions.

Study 3: Human cerebellum and cortico-cerebellar connections involved in emotional memory enhancement

Title:

Human cerebellum and cortico-cerebellar connections involved in emotional memory enhancement

Authors:

Matthias Fastenrath[1,2,], Klara Spalek[1,2,3], David Coynel[1,2], Eva Loos[1,2], Annette Milnik[2,3], Tobias Egli[2,3], Nathalie Schicktanz[1,2], Léonie Geissmann[1,2], Benno Roozendaal[4], Andreas Papassotiropoulos[2,3,5,6*], Dominique J F de Quervain[1,2,5*]

Affiliations:

[1]Division of Cognitive Neuroscience, Department of Psychology, University of Basel, Switzerland, [2]Transfaculty Research Platform Molecular and Cognitive Neuroscience, University of Basel, Switzerland, [3]Division of Molecular Neuroscience, Department of Psychology, University of Basel, Switzerland, [4]Department of Cognitive Neuroscience, Radboud university medical center, and Donders Institute for Brain, Cognition and Behaviour, Radboud University, Nijmegen, The Netherlands, [5]Psychiatric University Clinics, University of Basel, Switzerland, [6]Department Biozentrum, Life Sciences Training Facility, University of Basel, Switzerland

* These authors jointly supervised this work

Author contributions:

A.P., D.J.F.Q. and M.F. were in charge of conceptualization, project administration and funding acquisition. E.L. and K.S. performed study participant recruitment and data acquisition. A.M., D.C., D.J.F.Q, M.F. and T.E. were involved in methodology, formal analysis and data curation. A.M., A.P., B.R., D.C., D.J.F.Q., E.L., K.S., L.G., M.F., N.S., and T.E. were involved in writing.

Competing interest statement:

The authors declare no competing interests.

Classification: Major: Biological Sciences, minor: Neuroscience; major: Social Sciences, minor: Psychological and Cognitive Sciences

Keywords: Cerebellum, dynamic causal modelling, emotional memory enhancement, episodic memory

Significance Statement

Enhanced memory for emotional stimuli is crucial for survival, but may also contribute to the development and maintenance of fear-related disorders in case of highly aversive experiences. This large-scale functional brain imaging study identifies the cerebellum and cerebello-cerebral connections to be involved in the phenomenon of superior memory for emotionally arousing visual information. These findings expand the knowledge on the role of the cerebellum in complex cognitive and emotional processes and may be relevant for the understanding of psychiatric disorders with aberrant emotional circuitry, such as post-traumatic stress disorder or autism spectrum disorder.

Abstract

Emotional information is better remembered than neutral one. Extensive evidence indicates that the amygdala and its interactions with other cerebral regions play an important role in the memory-enhancing effect of emotional arousal. While the cerebellum has been found to be involved in fear conditioning, its role in the emotional enhancement of episodic memory is less clear. To address this issue, we used a whole-brain fMRI approach in 1418 healthy subjects. First, we identified clusters significantly activated during enhanced memory encoding of emotional pictures. In addition to the well-known emotional memory-related cerebral regions, we identified a cluster in the cerebellum. We then used dynamic causal modeling and identified several cerebellar connections with increased connection strength corresponding to enhanced emotional memory, including one to a cluster covering the amygdala and hippocampus, and bidirectional connections with the anterior cingulate cortex. The present findings indicate that the cerebellum and cerebello-cerebral connections are

involved in the phenomenon of superior episodic memory for emotionally arousing visual information.

Introduction

Enhanced memory for emotionally arousing information is a well-recognized phenomenon, which has adaptive value in evolutionary terms, as it is vital to remember both dangerous and favorable situations (de Quervain et al., 2017; McGaugh, 2003). From studies in rodents it is well-established that emotional arousal leads to noradrenergic activation of the amygdala, which in turn activates the hippocampus and other brain regions to enhance memory consolidation of emotionally arousing information (LaBar & Cabeza, 2006; McGaugh, 2000; Roozendaal & Mcgaugh, 2011). Moreover, there is evidence from human studies that emotional arousal and noradrenergic activation regulates memory processes already during encoding (Canli et al., 2000; Cole et al., 2013; S. B. Hamann et al., 1999; Todd et al., 2013; van Stegeren et al., 2005) and that the connection strength from the amygdala to the hippocampus is rapidly increased during the encoding of emotionally arousing information compared to neutral information (Fastenrath et al., 2014). Apart from the amygdala and hippocampus, two meta-analyses of human brain activation studies using functional magnetic resonance imaging (fMRI) indicated the potential relevance of several additional brain regions for enhanced encoding of declarative memory by emotional arousal, including the middle occipital gyrus, middle frontal gyrus, fusiform gyrus, inferior frontal gyrus, supramarginal gyrus, orbitofrontal cortex, parietal cortex, the claustrum, the caudate and the insula (Dahlgren et al., 2020; Murty et al., 2010). Even though the cerebellum has been occasionally listed in fMRI studies on emotional memory enhancement (Cahill et al., 2004; Mickley Steinmetz & Kensinger, 2009), a meta-analysis including 15 studies did not list it (Murty et al., 2010). A more recent meta-analysis including 25 studies did find the cerebellum significantly activated, but after excluding 3 studies showing no behavioral enhancement effect, the significance vanished (Dahlgren et al., 2020). Potential reasons for this ambiguity include that the cerebellum may have shown only subthreshold significance levels in individual studies or that the cerebellum has a-priori not been included in the analysis (Talmi et al., 2008).

The cerebellum is typically known for its important role in controlling motor functions (Ito, 1984). However, there is evidence that the output of the cerebellum targets not only cortical motor areas but also several non-motor cortical and subcortical regions that are

involved in higher brain functions, including emotion and cognition (Damasio et al., 2000; Koziol et al., 2014; Strata, 2015; Strick et al., 2009), and that the cerebellum itself holds robust representations of multiple networks involved in these functions (Habas et al., 2009; Xue et al., 2020). Importantly, it is known from animal and human studies that the cerebellum plays an important role in fear conditioning (Adamaszek et al., 2017; Lange et al., 2015; Sacchetti et al., 2005; Strata, 2015; Timmann et al., 2010), which is traditionally categorized as an unconscious or non-declarative form of learning with a strong emotional component (LaBar & Cabeza, 2006; LeDoux, 2014). It is less clear, however, if the cerebellum is also involved in the enhancing effect of emotional arousal on episodic memory, a declarative form of memory that requires conscious memory encoding and enables conscious recollection of information along with its context (LaBar & Cabeza, 2006; Squire & Zola, 1998; Tulving & Markowitsch, 1998). Animal and human lesion studies and human neuroimaging studies indicate that fear conditioning and emotional enhancement of episodic memory partly depend on the same neural underpinnings, such as the amygdala (James L. et al., 1996; LaBar & Cabeza, 2006; LeDoux, 2003; Murty et al., 2010). Therefore, it is possible that the cerebellum is not only involved in fear conditioning but also in emotional enhancement of episodic memory. In the present study, we investigated if the cerebellum and cerebello-cerebral connections are involved in the phenomenon of superior episodic memory for emotionally arousing visual information.

We used an fMRI sample of 1,418 healthy human subjects who performed a picture encoding task containing positive and negative emotional and neutral pictures, followed by a free recall test, which assesses episodic memory (Squire & Zola, 1998; Tulving & Markowitsch, 1998), 20 min after the end of encoding. Since emotional arousal rather than valence is driving the memory-enhancing effect of salient information on episodic memory (LaBar & Cabeza, 2006; Sutherland & Mather, 2018), we focused on the identification of emotional arousal effects irrespective of valence. The large sample size allowed us to divide the sample into a discovery (*N*=945 subjects) and replication sample (*N* = 473 subjects; see materials and methods). To measure the neural correlates of superior memory for emotional information during encoding, we used the subsequent emotional memory paradigm (Murty et al., 2010). This paradigm assesses the difference between encoding activity of later successfully recalled emotional items vs. non-recalled emotional items, compared to successfully recalled neutral items vs. non-recalled neutral items (termed “enhanced emotional memory encoding”). At

first, we identified voxels with significantly increased activity during enhanced emotional memory encoding in the discovery sample. We performed this analysis for the entire brain, including the cerebellum. From the voxels that showed increased activity during enhanced emotional memory encoding, we defined regions of interest (ROIs) for the dynamic casual modeling (DCM) analysis. We defined ROIs functionally, rather than anatomically, as the sensitivity of detecting the presence of connections can be increased by using regions of interest (ROIs) that match actual functional boundaries (Smith et al., 2011). Specifically, we combined voxels with a similar response profile to create spatially coherent and temporal homogenous ROIs by using a clustering approach (Craddock et al., 2012). We then tested if the identified ROIs show increased activity during enhanced emotional memory encoding also in the replication sample. With the replicated ROIs (i.e. one cerebellar ROI, 26 cerebral ROIs) we finally explored the directed connectivity between the cerebellar ROI and the cerebral ROIs using DCM (Friston et al., 2003; Stephan et al., 2010) in both samples. We focused on increases rather than decreases in connection strength, since ROIs were defined based on voxels with increased activity.

Results

Behavioral data: emotional memory enhancement

The behavioral results in both the discovery and replication sample indicated that participants freely recalled more emotional pictures than neutral pictures. Discovery sample: 4.50 $\pm$ 2.76 (*mean* ± *SD*), T = 50.01, P = 7.53e10-268, N = 945; replication sample: 4.65 $\pm$ 2.60 (*mean* ± *SD*), T = 38.82, P = 7.03e10-149, N = 473. For A detailed description of the behavioral data see (Fastenrath et al., 2014). This emotional memory enhancement was not significantly associated with age or sex (P > 0.05; two-sided).

Activity related to enhanced emotional memory encoding

For the contrast representing enhanced emotional memory encoding, 7,708 voxels with increased activity were identified in the discovery sample (N = 945, $P_{\text{whole-brain-FWE-corrected}}$ < 0.05, Figure S2, Table S3). We did not observe significant positive or negative associations between activity and the effects of sex, age, changes in scanner software or changes in gradient coils ($P_{\text{whole-brain-FWE-corrected}}$ > 0.05). Voxels related to enhanced emotional memory encoding were parcellated into 30 clusters (i.e. regions of interest, ROIs) to reduce the dimensionality of the

data (Figure 4.1, Figures S3-S7, see methods for details on the parcellation method). One cluster (ROI 11) contained isolated voxels and small clusters of voxels that were not spatially coherent and was therefore removed from further analysis.

Figure 4.1

Clusters showing an increased activation for enhanced emotional memory encoding within the discovery sample

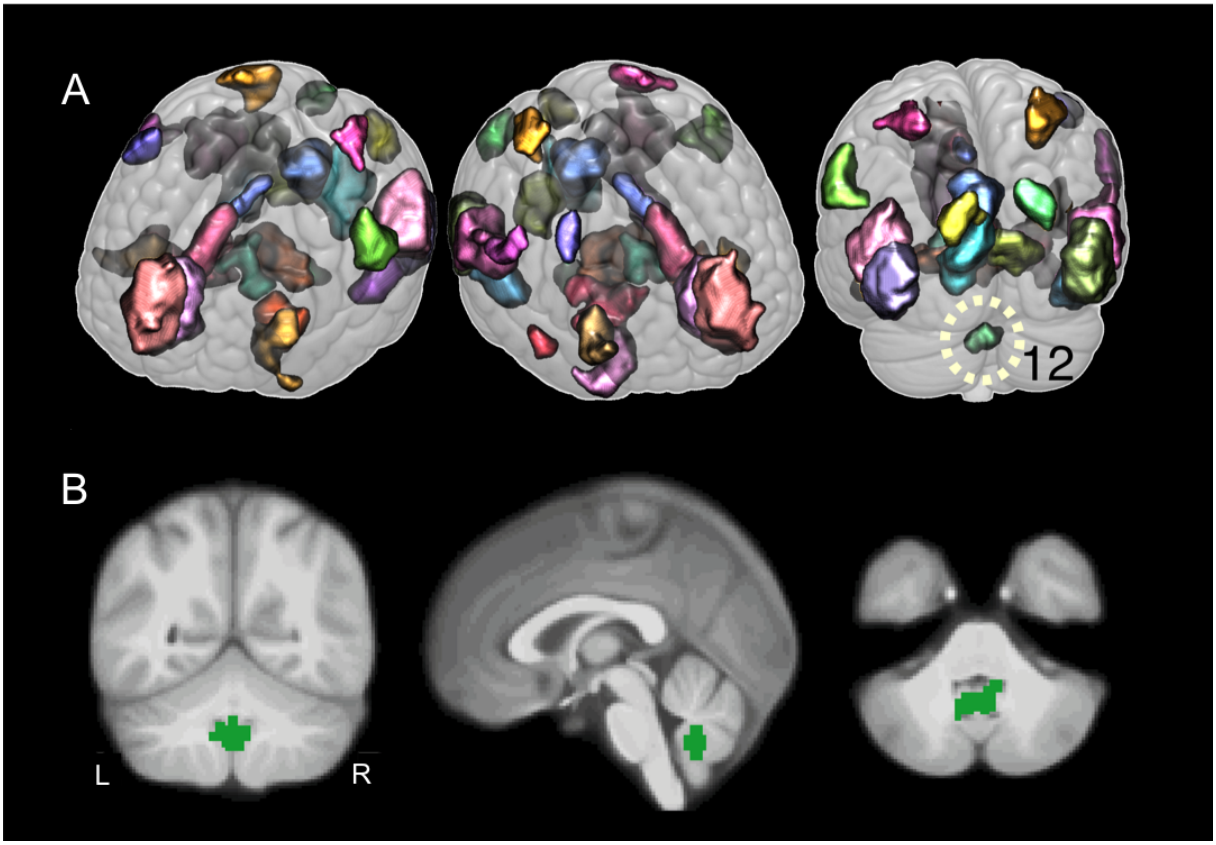

Note. Clusters span voxels significantly activated during enhanced emotional memory encoding ($P_{\text{whole-brain-FWE-corrected}} < 0.05$, $N = 945$). These clusters were used as regions of interest (ROIs) to explore the connectivity of the cerebellar cluster (ROI 12). Different colors denote different clusters. Panel A displays 3D images of the 29 clusters. Panel B depicts sagittal, coronal and horizontal views, focusing on the cluster located in the cerebellum (ROI 12). See Figure S3 – S7 for additional representations.

Out of the 29 remaining ROIs, 28 ROIs were located in neocortical and subcortical regions of the cerebrum and one cluster in the cerebellum (Figure 4.1, see Table S5 for details on number of voxels as well as anatomical correspondence per cluster). According to a probabilistic MR atlas of the human cerebellum (Diedrichsen et al., 2009) the cerebellar cluster in the discovery sample mapped mainly onto the vermis (local maximum by 76 % in lobule IX, and by 22 % in the replication sample) of the cerebellum. Out of the 29 ROIs

identified in the discovery sample, 26 ROIs (including the cerebellum) were also significantly activated during enhanced emotional memory encoding in the replication sample (significance threshold for ROI-maxima $T = 4.41$, $P < 0.05$, one-sided, Bonferroni corrected for all significant voxels of the 29 ROIs identified in the discovery sample). Maxima for ROI 7, 13 and 25 did not reach significance in the replication sample and were therefore not considered for the DCM analysis. In summary, the replicated 26 ROIs mapped onto the occipital, temporal, parietal, and frontal cortex as well as onto the amygdala/hippocampus, the cingulate, thalamus, brain stem and cerebellum (Figure 4.1, see Table S5).

DCM: connection strength during enhanced emotional memory encoding

The replicated 26 ROIs related to enhanced emotional memory encoding entered the DCM analysis. To investigate changes in connection strengths during enhanced emotional memory encoding between the cerebellar ROI and the remaining 25 cerebral ROIs, we used a series of two-node (cerebellum to all others) DCMs to explore all pairwise (bidirectional) connections (note that the large number of model parameters precluded the inclusion of all 26 ROIs into a single DCM model).

Within the discovery sample, 25 connections (out of the 50 possible unidirectional connections) showed an increased strength during enhanced emotional memory encoding (*posterior probability* > 0.99). Considering the number of tests, we applied a conservative probability threshold of 0.99 and replicated the results in an independent sample using the same threshold (Friston et al., 2003; Kass & Raftery, 1995; Masson, 2011). Fifteen out of the 25 connections also had an increased strength in the replication sample (*posterior probability* > 0.99) (Figure 4.2). Out of those 15 replicated connections, 11 connections showed increased connection strengths from the cerebellum to cerebral regions. Of particular interest is the strong connection from the cerebellar ROI to the amygdala/hippocampal ROI (Figure 4.2). Four connections showed increased connection strengths from cerebral regions to the cerebellum (Figure 4.2). The connections between the cerebellar ROI and the rostral anterior cingulate ROI and between the cerebellar ROI and the frontal ROI showed increased strength in both directions.

Figure 4.2

Increase in the strength of cerebellar connections during enhanced emotional memory encoding

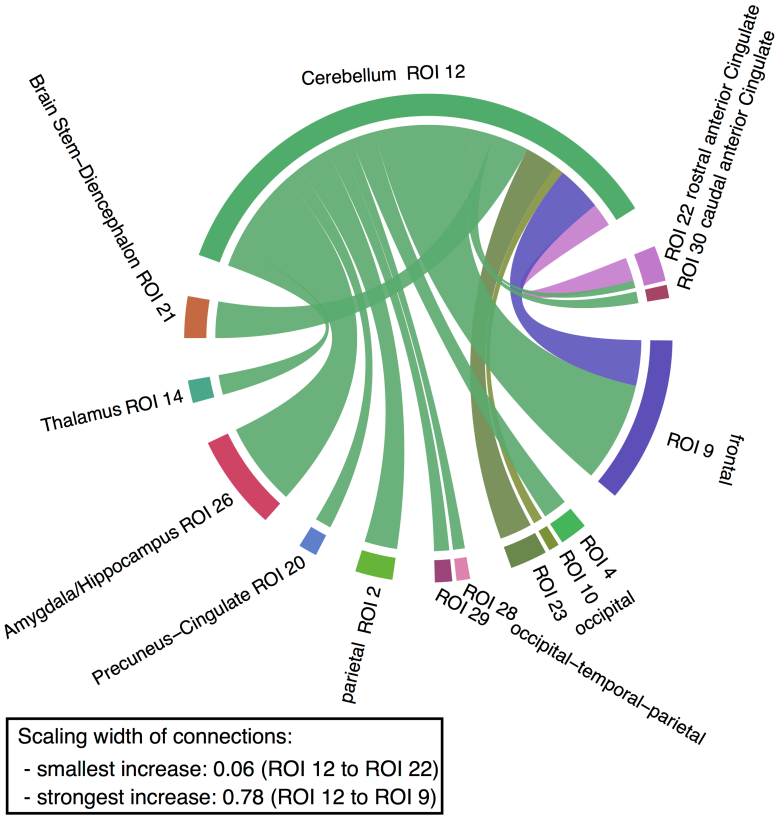

Note. Green edges indicate an increased connection from the cerebellum to a target ROI, while the other colors represent an increased connection from the ROI to the cerebellum. The width of the edges denotes the strength of the increase in connectivity in the replication sample. Only replicating connections are depicted (discovery sample N_{max} = 902, N_{mean} = 887, N_{min} = 798; replication sample N_{max} = 433, N_{mean} = 426, N_{min} = 378; *posterior probability* > 0.99; Table S1). For a detailed breakdown on anatomical localization per ROI, see Table S5. For connection strength values, see Tables S6-S9.

Discussion

The aim of the present study was to investigate if the cerebellum and cerebello-cerebral connections are involved in the phenomenon of superior episodic memory for emotionally arousing visual information. In the first step, we identified clusters showing increased activity during enhanced encoding of emotional pictures. The cerebral clusters map onto the occipital, temporal, parietal, and frontal cortex as well as onto the amygdala/hippocampus, the cingulate and thalamus. These brain activation results are largely in line with the findings of two meta-analyses of enhanced emotional memory encoding in humans (Dahlgren et al.,

2020; Murty et al., 2010) and extensive experimental work in animals (James L. et al., 1996; Phelps & LeDoux, 2005; Roozendaal & Mcgaugh, 2011). In addition to these cerebral regions, we found robust evidence for a cluster located mainly in the vermis of the cerebellum showing increased activity during enhanced emotional memory encoding in two large samples. Interestingly, the midline cerebellum has been found activated during recalling emotional personal life episodes, indicating a role of this region in emotional memory retrieval (Damasio et al., 2000).

There is accumulating evidence that the cerebellum, in particular the cerebellar vermis, is crucially involved in fear conditioning (Adamaszek et al., 2017; Sacchetti et al., 2005; Strata, 2015; Timmann et al., 2010). In rodents, it has been shown that lesions of the vermis abolish heart rate conditioning (Supple & Leaton, 1990) and that the vermis is necessary for intact fear conditioning (Sacchetti et al., 2002). In humans, it has been reported that patients with lesions of the cerebellar vermis show impaired acquisition of fear conditioned bradycardia (Maschke et al., 2002). Moreover, an fMRI study in healthy participants found the vermis to be involved in eyeblink classical conditioning (Cheng et al., 2014). The vermis has efferent projections to limbic regions, including the amygdala and hippocampus, structures involved in delay conditioning and trace conditioning, respectively (Cheng et al., 2008). The connection of the vermis with the amygdala and hippocampus would also allow an influence of the vermis on the enhancement of episodic memories by emotional arousal, which depends on both structures (LaBar & Cabeza, 2006). The findings of the present study indeed indicate that the vermis is not only involved in fear conditioning but also in the phenomenon of superior memory for emotionally arousing visual information.

The subsequent DCM connectivity analysis indicated that several cerebellar-cerebral connections showed increased strength during enhanced emotional memory encoding. Interestingly, we found 11 connections with increased connection strengths from the cerebellum to cerebral regions. In the context of enhanced emotional memory encoding, the connection to the amygdala/hippocampus seems of special interest. It has been shown that the cerebellum and the amygdala are functionally interconnected during fear conditioning (Lee & Kim, 2004; Sacchetti et al., 2007). Moreover, studies in rats and cats showed that electrical stimulation of the vermis (outside of a learning context) modulates (i.e. some units being facilitated and others inhibited) amygdala and hippocampus activity (Heath, 1973; Heath et al., 1978), indicating that the vermis is functionally connected with these limbic

regions. These findings fit with the direction found in the current DCM analysis, indicating an influence of the vermis on amygdala/hippocampus. There is ample evidence that the amygdala and hippocampus, as well their interactions, are crucially involved in the enhancing effect of emotional arousal on episodic memory (Fastenrath et al., 2014; Hamann, 2001; LaBar & Cabeza, 2006; Roozendaal & Mcgaugh, 2011).

We also found evidence for the involvement of bidirectional connections of the cerebellum with the cingulate cortex (anterior part) in emotional memory enhancement. A resting-state functional connectivity MRI study in healthy humans has shown that the cingulate is functionally connected with the cerebellum (Habas et al., 2009). Furthermore, the anterior cingulate has been related to emotion, reward valuation, and value representations (Vogt, 2014). It has been postulated that the anterior cingulate cortex, in addition to the amygdala and the insula, is a fundamental part of a large-scale salience network, which functions to segregate the most relevant among internal and extrapersonal stimuli in order to guide behavior (Menon & Uddin, 2010; Seeley et al., 2007). Moreover, the salience network has been reported to be activated by noradrenergic activation (Hermans et al., 2011), a neurotransmitter system crucially involved not only in arousal and attentional processes but also in emotional memory enhancement (Roozendaal & Hermans, 2017). Interestingly, the locus coeruleus, the principal site for brain synthesis of norepinephrine, also projects to areas throughout the cerebellum (Samuels & Szabadi, 2008). Whether the cerebellum gets activated directly by the locus coeruleus or indirectly by the salience network has yet to be determined. Finally, we found a bidirectional connection of the cerebellum with the frontal cortex (mainly precentral), which may be related to the regulation of motor functions (Coffman et al., 2011), possibly motor learning, in the context of emotional memory enhancement.

The current findings may contribute to a better understanding of the network involved in emotional memory enhancement in adaptive conditions. Furthermore, the findings may also have implications for pathological conditions, since it has been shown that genetic factors related to enhanced memory for emotional pictures are also related to stronger traumatic memories and to increased risk for posttraumatic stress disorder (de Quervain et al., 2007, 2012). As we found that the cerebello-cerebral connections are involved in emotional memory enhancement, future studies might investigate in how far the cerebellum and its connections are involved in the formation of overly aversive episodic memories in patients with fear-related disorders. We hypothesize a hyperactivity of the cerebellum in fear-related disorders,

since we found that the cerebellum was activated during emotional memory enhancement. In contrast, a cerebellar hypoactivity could be related to a reduced emotional memory enhancement. Indeed, clinical studies indicate that the pathologies affecting vermal functioning are associated with a range of cognitive and emotional impairments, including symptoms of autism spectrum disorder (Courchesne et al., 1988; Tavano et al., 2007). Interestingly, patients with autism spectrum disorder show deficits in emotional enhancement of episodic memories (Beversdorf et al., 1998; Deruelle et al., 2008). It is likely that this deficit partially originates from structural and functional abnormalities of the amygdala often observed in this disorder (Baron-Cohen et al., 2000; Bauman & Kemper, 2005). However, based on the present results, the vermal hypoplasia in autism spectrum disorder might also contribute to impaired enhancement of episodic memory by emotional arousal in this disorder. It is therefore possible that a network of connected brain areas rather than isolated structures is responsible for specific behavioral phenomena.

There is mounting evidence indicating that the cerebellum, in particular the cerebellar vermis, and its connections to several cerebral regions, including the limbic system, are involved in emotional functions, including emotional perception, emotional recognition, emotional processing fear conditioning (Adamaszek et al., 2017; Stoodley & Schmahmann, 2010). The present findings now indicate that the cerebellum is part of a circuitry involved in emotional enhancement of episodic memory. Within this circuitry, the cerebellum receives input from several cerebral regions including the cingulate, while the amygdala/hippocampus and cingulate receive input from the cerebellum. These findings expand the knowledge on the role of the cerebellum in complex cognitive and emotional processes and may be relevant for the understanding of psychiatric disorders with aberrant emotional circuitry, such as post-traumatic stress disorder or autism spectrum disorder.

Materials and methods

Participants

We recruited healthy, young subjects (872 females, 546 males, mean age = 22.39 years, *SD* = 3.27). Advertising was done mainly at the University of Basel and in local newspapers. The subjects were free of any neurological or psychiatric illness, did not take any medication at the time of the experiment (except hormonal contraceptives), and were between 18 and 35 years old. Physical and mental health was assessed based on standard questionnaires. The

experiment was approved by the ethics committee of the Canton of Basel, Switzerland. All subjects gave written informed consent before participating in the study. Prior to the analysis, the sample was divided into a discovery sample (*N* = 945, 2/3 of all subjects) and a replication sample (*N* = 473, 1/3 of all subjects) by randomly assigning subjects to one of the samples. Randomization was performed using the Matlab function randperm. There were no significant differences between the discovery and replication samples in terms of age, sex or emotional memory enhancement (*P* >= 0.33, two-sided testing, *N* = 1,418).

Experiment: procedure

Subjects underwent four consecutive tasks, i.e. a picture encoding task, a working memory task, a free recall memory test and a recognition task. Participants were first instructed and then trained on the picture encoding and working memory tasks. After training, they were positioned in the scanner and received earplugs and headphones to reduce scanner noise. Their heads were fixated in the coil using small cushions, and they were told not to move. Pictures were presented in the scanner using MR-compatible liquid crystal display goggles (VisualSystem; NordicNeuroLab, Bergen, Norway). Eye correction was used when necessary. The picture encoding task lasted for approximately 20 minutes. Immediately afterwards, subjects performed a letter n-back working memory task in the scanner for approximately 10 minutes. In the current study, the working memory task is used as a distraction task between encoding and recall of memory testing. Hence, we did not analyze the data from the working memory task itself (see (Heck et al., 2014) for description of the task). After leaving the scanner, participants were given an unannounced free recall memory test of the pictures in a separate room (no time limit was set for this task). After the free recall, participants were repositioned in the scanner and performed a recognition task (see (Gediminas et al., 2015) for description of the task). Participants received 25 CHF/h for participation. Due to organizational constraints, we had to change the room in which pictures were recalled, which means that some subjects recalled pictures in a slightly different setting.

Experiment: design of picture encoding task

Stimuli consisted of 72 pictures (24 positive, 24 negative, 24 neutral) that were selected from the International affective picture system (IAPS) (Lang et al., 2005), as well as from in-house standardized picture sets that allowed us to equate the pictures for visual complexity and

content (e.g., human presence). Pictures received from IAPS were classified according to the IAPS valence rating. Eight out of the 24 neutral pictures were not received from IAPS. These pictures were rated based on an in-house valence rating (Fastenrath et al., 2014). On the basis of normative valence scores (from 1 to 9), pictures were assigned to negative (2.3 ± 0.6), neutral (5.0 ± 0.3), and positive (7.6 ± 0.4) conditions, resulting in 24 pictures for each valence. Positive stimuli were initially selected to match arousal ratings of negative stimuli based on data of a pilot study in 20 subjects. Four additional pictures showing neutral objects were presented. Two of these pictures were presented in the beginning and two at the end of the picture task. These pictures were excluded from recall performance evaluation to control for primacy and recency effects in memory. Examples of pictures are: erotica, sports and appealing animals for the positive valence; bodily injury, snake, attack scenes for the negative valence; and neutral faces, household objects and buildings for the neutral condition. In addition, 24 scrambled pictures were used. The background of the scrambled pictures contained the color information of all pictures used in the experiment (except primacy and recency pictures), overlaid with a crystal and distortion filter (Adobe Photoshop CS3). In the foreground, a mostly transparent geometrical object (rectangle or ellipse of different sizes and orientations) was shown. For the present study, the scrambled pictures were of no interest.

The pictures were presented for 2.5 s in a quasi-randomized order so that at maximum four pictures of the same category occurred consecutively. A fixation cross appeared on the screen for 500 ms before each picture presentation. The stimulus onset time was jittered within 3 s [1 repetition time (TR)] per valence category with regard to the scan onset. During the intertrial period, participants rated each of the 72 pictures according to valence (negative, neutral, positive) and arousal (large, medium, small) on a three-point scale (self assessment manikin, SAM) by pressing a button with their dominant hand. For scrambled pictures, participants rated form (vertical, symmetric or horizontal) and size (large, medium, small) of the geometrical object in the foreground. The software Presentation® (Neurobehavioral Systems, Inc., Berkeley, CA, www.neurobs.com) was used for the picture presentation.

Behavioral data: emotional memory enhancement

To document free recall, subjects had to write down a description of the recalled pictures. A picture was scored as correctly recalled if the rater could identify the presented picture on the basis of the subject's description. Two trained investigators independently rated the

descriptions for recall success (inter-rater reliability > 99%). A third independent rater decided on pictures that were rated differently. For each subject, we computed how often emotional pictures were recalled compared to neutral pictures: *((recalled positive – recalled neutral) + (recalled negative – recalled neutral))/2*. Data points were plotted and were found to be approximately normal distributed (Figure S1). Two-sided *t*-tests were applied to test if emotional memory performance was significantly different from zero. In addition, we tested for the effects of potential confounders. We used a two-sample *t*-test to assess if emotional memory performance depends on sex. We used Pearson's linear correlation coefficients to associate recall performance with age. Two-sided *t*-tests were applied to test if the correlation coefficient was significantly different from zero.

Imaging: MRI acquisition

Measurements were performed on a Siemens Magnetom Verio 3 T whole-body MR unit equipped with a twelve-channel head coil. Functional time series were acquired with a single-shot echo-planar sequence using parallel imaging (GRAPPA). We used the following acquisition parameters: TE (echo time) = 35 ms, FOV (field of view) = 22 cm, acquisition matrix = 80 × 80, interpolated to 128 × 128, voxel size: 2.75 × 2.75 × 4 mm^3, GRAPPA acceleration factor R = 2.0. Using a midsaggital scout image, 32 contiguous axial slices placed along the anterior–posterior commissure (AC–PC) plane covering the entire brain with a TR = 3000 ms (α = 82°) were acquired using an ascending interleaved sequence. The first two acquisitions were discarded due to T1 saturation effects. A high-resolution T1-weighted anatomical image was acquired using a magnetization prepared gradient echo sequence (MPRAGE, TR=2000 ms; TE=3.37 ms; TI=1000 ms; flip angle=8; 176 slices; FOV= 256 mm; voxel size = 1 x 1 x 1 mm^3).

Imaging: software package for statistical analysis of imaging data

We used SPM12 v6685 (Statistical Parametric Mapping, Wellcome Trust Centre for Neuroimaging, London, UK; http://www.fil.ion.ucl.ac.uk/spm/) implemented in Matlab R2016a.

Imaging: preprocessing and normalization of EPI volume

Volumes were slice-time corrected to the first slice, realigned using the 'register to mean' option, and coregistered to the anatomical image by applying a normalized mutual

information 3-D rigid-body transformation. Successful coregistration was visually verified for each subject. Each volume was masked with the subject's T1 anatomical image to exclude voxels outside of the brain. The EPI volumes were normalized to MNI space and smoothed with an 8 mm full width at half maximum (FWHM) Gaussian kernel by applying DARTEL. DARTEL leads to an improved registration between subjects (Ashburner, 2007; Klein et al., 2009).

The interleaved sequence used to acquire functional time series made it a prerequisite to use slice-time correction as a first preprocessing step (Kiebel et al., 2007) . Slice-timing correction methods can successfully compensate for slice-timing effects (Sladky et al., 2011). Importantly, in DCM for fMRI, the direction of causality is not identified by temporal precedence. Instead, causality is embodied by the mathematical form of the differential state equation of each region. The state equations of a given model define the systems structure (e.g. the connectivity between regions), prescribing explicitly how dynamics arise within the system (Stephan et al., 2010). Therefore, a number of DCM studies with similar TRs were previously conducted (Leff et al., 2008; Richardson et al., 2011; Seghier & Price, 2010).

Imaging: modeling of voxel-wise activity

General linear models (GLMs) were specified for each subject to identify voxels activated by task. Regressors modeling the onsets and duration of stimulus events were convolved with a canonical hemodynamic response function (HRF). More precisely, the model comprised regressors for button presses modeled as stick/delta functions, picture presentations (positive, neutral, negative, scrambled, primacy and recency) modeled with an epoch/boxcar function (duration: 2.5 s), and rating scales modeled with an epoch/boxcar function of variable duration (depending on when the subsequent button press occurred). Serial correlations were removed using a first-order autoregressive model, and a high-pass filter (128 s) was applied to remove low-frequency noise. Six movement parameters were also entered as nuisance covariates. We defined two different types of GLMs. One type of GLM was used to identify voxels related to successful emotional memory encoding. Here, positive, negative and neutral stimuli were modeled separately depending on whether they were subsequently recalled or not. The resulting parameter estimates were contrasted to identify voxels that are associated with successful emotional memory encoding [*(recalled emotional pictures – non-recalled emotional pictures) – (recalled neutral pictures – non-recalled neutral pictures)*]. Another type

of GLM was specified to identify voxels associated to encoding of emotional pictures, irrespective of memory. We specified regressors for positive, neutral and negative pictures, irrespective of whether the pictures were recalled or not, and contrasted the resulting parameter estimates (*emotional pictures – neutral pictures*).

Imaging: group statistics of voxel-wise activity

To determine activity related to "successful emotional memory encoding" and to "encoding of emotional pictures", contrast maps were entered in a random effects model (second level analysis) using GLM Flex (Martinos Center & Mass General Hospital, Charlestown, MA, USA; http://nmr.mgh.harvard.edu/harvardagingbrain/People/AaronSchultz/GLM_Flex.html). We controlled for the effect of sex, age, one change in scanner software and two changes in gradient coils by including them as covariates. We used GLM Flex as EPI sequences suffer from signal loss in the presence of magnetic field inhomogeneities that can occur close to air-tissue boundaries. The normalization procedure applied in DARTEL accurately transforms both voxels with signal and voxels with signal loss to MNI space. In SPM, signal loss at a MNI coordinate in a functional image of only one subject leads to the exclusion of the voxel at this coordinate from the group level analysis. Consequently, the probability of a voxel being excluded increases with sample size. GLM Flex circumvents this problem by allowing a variable number of subjects at each voxel. The minimum number of subjects per voxel was set to 2/3 of all subjects.

Imaging: definition of ROIs – functionally defined mask

Since the sensitivity of detecting the presence of connections can be increased by using ROIs that match actual functional boundaries (Smith et al., 2011), we defined ROIs functionally, rather than anatomically. Specifically, within the discovery sample (N = 945), we used a functionally derived mask and then used a data-driven group level clustering approach to parcellate preprocessed and normalized EPI volumes into spatially coherent and temporal homogenous regions (Craddock et al., 2012). The mask consisted of voxels that were positively associated to successful emotional memory encoding within the discovery sample ($P_{\text{whole-brain-FWE-corrected}} < 0.05$). The identified voxels were then additionaly masked with the encoding of emotional pictures contrast ($P_{\text{whole-brain-FWE-corrected}} < 0.05$) to assure that all included voxels also show a positive effect for emotion encoding (99% of all voxels significant in the "successful

emotional memory encoding contrast" were also significant in the "encoding of emotional pictures contrast").

Imaging: definition of ROIs – parcellation procedure

Voxels within the functionally defined mask were combined into ROIs such that the similarity between voxels within the same cluster was maximized compared to the similarity between voxels in different clusters, using a normalized cut method incorporating a spatial constrain (Craddock et al., 2012) . For computational expedience, parcellation was performed based on the EPI-volumes of 200 subjects that were randomly drawn from the whole population. These volumes were smoothed with a 6 mm FWHM Gaussian kernel in line with a recent paper (Craddock et al., 2012). Clustering was first performed within each subject, followed by a second level group clustering, as recommended by Craddock et al. (Craddock et al., 2012). We parcellated the voxels within the mask into 30 ROIs, as we found that this number leads to sufficient spatial specificity, while still being manageable with regard to the computational burden induced by the computation of connectivity with DCM. One of these ROIs contained isolated voxels and discrete small clusters that were not spatially coherent. This ROI (ROI 11), which contained 60 voxels, was thus removed from further analysis.

Connectivity analysis: time-course extraction

We extracted time courses per subject and ROI from unsmoothed and unnormalized data using the procedure as described below. Note that we extracted from unsmoothed data as smoothing can be damaging to connectivity estimation as it leads to a mixing of blood oxygenation level dependent (BOLD) time courses between regions in close proximity (Smith et al., 2011).

1. Mapping functional ROIs from MNI space to native subject space: The ROIs as determined in the parcellation procedure were generated in MNI space. We therefore mapped their location to native subject space by inverting the normalization warp field of each subject.

2. Time course extraction from functional and anatomical ROIs: Before the actual modeling of connectivity within the DCM framework, time courses were extracted from each ROI. A time course consists of the BOLD responses measured during the course of the experiment. The

ROI summary time courses were derived by computing the first principal eigenvariate of the data across all significantly activated voxels within each ROI. The extracted time courses were mean corrected and corrected for movement artifacts. We used the "encoding of emotional pictures contrast" to identify significant voxels at the single subject level (Emotional > neutral, $P < 0.05$ uncorrected, minimum cluster size 3). Note that the purpose of this significance threshold is to find voxels with task-related signal and to exclude voxels with noisy signal. The encoding of emotional pictures contrast had a larger effect than the "successful emotional memory encoding contrast", facilitating the differentiation between voxels with task-related signal and voxels with noisy signal at the single subject level. Importantly, we only extracted time courses from regions showing a significant group-level effect for the "successful memory encoding of emotional pictures contrast" (see paragraph "*Definition of ROIs – Functionally defined mask"*).

Across all 29 functional ROIs, time courses were successfully extracted in 97.88% of all cases in the discovery sample, and in 97.57% of all cases in the replication sample, as they showed robust task-dependent activation in accordance with our significance threshold outlined above. Data from all ROIs in all subjects is a prerequisite to run DCM, as the purpose of DCM is to compare different models for an observed activation (Friston et al., 2003; Stephan et al., 2010). Hence, we excluded a subject from a particular DCM if a ROI did not show activation in line with the criteria defined above. Out of all ROIs, ROI 9 showed the smallest proportion of subjects with robust activation (discovery sample 88.36%; replication sample 85.84%). See Table S1 for number of subjects per DCM and Table S2 for percentages of excluded subjects per ROI. Potential reasons for the lack of sufficiently strong activation in some subjects pertain to noise in the data or data loss but might also reflect the use of different cognitive strategies.

Connectivity analysis: DCM

DCM can be applied to test specific hypotheses concerning the presence, direction and the modulators of effective connectivity between a set of predefined brain regions. DCM is described in detail elsewhere (Friston et al., 2003; Stephan et al., 2010). In brief, neural interactions between regions are expressed by differential equations, which describe (i) how the activity in one brain region causes dynamics (i.e. rate of change) in another brain region and (ii) how these interactions change under the influence of experimental conditions. Here,

we compared conditions for emotional and neutral pictures while taking into account if a picture was later recalled or not. DCM strives for neurophysiological interpretability by making an explicit distinction between the "neural level" and the "hemodynamic level" (Penny et al., 2004). This is achieved by inverting a biophysically motivated and parameterized forward model which links the modeled neural dynamics to the measured hemodynamic time courses (Friston et al., 2003). The connectivity parameters can therefore be interpreted as an influence between neural populations (Stephan et al., 2010). Our inference on connectivity depends on the underlying mathematical assumptions incorporated in the parameterization of DCM. These assumptions have been critically assessed (Daunizeau et al., 2011).

Connectivity analysis: DCM – model space

We explored all pairwise connections between the cerebellar ROI and the remaining 28 ROIs by defining a series of two node DCMs where the ROI located in the cerebellum was systematically paired with one of the other ROIs. Connectivity parameters represent the net connectivity between ROIs, i.e. the they do not take into account whether or not the influence between two ROIs is mediated by additional regions, unless these additional regions are explicitly included in the DCM model. Since the DCMs tested here include only two nodes, they do not take into account if the influence between the cerebellum and a second ROI is mediated by additional regions. The values of our connectivity parameters therefore potentially reflect both direct and indirect connections.

We applied bilinear, deterministic DCM with two-states (version DCM12) (Marreiros et al., 2008). We specified reciprocal intrinsic connections between each ROI. Extrinsic inputs to ROIs drive the network and quantify how ROIs respond to external stimuli. Four different input regressors were defined containing (1) emotional and neutral pictures, (2) scrambled pictures, (3) button presses and (4) rating scale presentation. Each of the input regressors could enter the network at all ROIs. The strength of the intrinsic connections between ROIs could be modulated by the following conditions: (1) emotional recalled pictures, (2) emotional non-recalled pictures, (3) neutral recalled pictures and (4) neutral non-recalled pictures.

For a Bayesian perspective on multiple comparison, see (Berry & Hochberg, 1999; Friston & Penny, 2003). Importantly, we replicated the results of the discovery sample in a second sample.

Connectivity analysis: DCM – model estimation

We used an efficient post hoc model selection, which requires the estimation of only one full model to find (1) the model evidence for all possible connection architectures with Bayesian model selection (BMS), (2) posterior probabilities resulting from family level inferences to determine the probability for a contrast of parameter estimates, and (3) Bayesian parameter averages (BPA) over all possible models showing if a contrast of parameter estimates differs from zero (Friston et al., 2011; Hillebrandt et al., 2013; Rosa et al., 2012). As we used fixed-effects BMS, we assumed that the optimal model is the same for each subject in the population (Stephan et al., 2010). Estimation of DCM models was performed at sciCORE (http://scicore.unibas.ch/) scientific computing core facility at University of Basel.

Connectivity analysis: DCM – parameter analysis

We use Bayesian inference to assess if connection strength is increased during successful emotional memory encoding. Specifically, we used the posterior expectations and posterior covariances to compute the posterior probability that the contrast between modulators of connection strength is bigger than zero. The contrast for successful emotional memory encoding was built by subtracting the modulators of the following conditions: (*recalled emotional pictures – non-recalled emotional pictures) – (recalled neutral pictures – non-recalled neutral pictures)*. First, within the discovery sample, we identified those connections that had a posterior probability of the contrast greater than 0.99. Second, we analyzed these connections in the replication sample, testing if they too have a posterior probability of the contrast greater than 0.99. In descriptive terms, the applied probability threshold of 0.99 can be interpreted as providing very strong evidence for an effect (Kass & Raftery, 1995; Masson, 2011). Calculations with regard to connection strength were based on the strength of the contrast in the replication sample.

Connections were visualized using the circlize library in R (Gu et al., 2014).

Segmentation of anatomical image

Each participant's anatomical image was automatically segmented into cortical and subcortical structures using FreeSurfer v4.5 (Fischl et al., 2002). Labelling of the cortical gyri was based on the Desikan-Killiany atlas (Desikan et al., 2006), yielding 35 cortical and 7 subcortical regions per hemisphere. Note that the applied segmentation and labeling

technique provides an accuracy comparable to manual labeling by experts (Desikan et al., 2006; Fischl et al., 2002).

Anatomical localication of ROIs based on a population-averaged anatomical probabilistic atlas

Segmentations of cortical and subcortical structures retrieved from FreeSurfer (see paragraph "*Segmentation of anatomical image"*) were used to build a population-average probabilistic anatomical atlas, based on data of 1,000 out of the 1,418 subjects. Individual segmented anatomical images were normalized to the study-specific anatomical template space using the subject's previously computed warp field, and affine-registered to the MNI space. Nearest-neighbor interpolation was applied, in order to preserve labeling of the different structures. The normalized segmentations were finally averaged across subjects, in order to create a population-average probabilistic atlas. Each voxel of the template could consequently be assigned a probability of belonging to a given anatomical structure.

This population-average probabilistic atlas was used to report the anatomical location of coordinates and ROIs. Percentages per coordinate denote the population-average probability of an anatomical label. Furthermore, we report the average percentage of regional correspondence per ROI. Per ROI, we determined which anatomical labels are spanned by its voxels. We then summed up the probabilities per label across all voxels within the ROI and divided the sum by the overall number of voxels in the mask. A 100% correspondence would occur if all voxels of a ROI would be located within the same anatomical region, and each voxel itself had a probability of 100% of being located in this region.

Acknowledgments:

We thank Elmar Merkle, Christoph Stippich and Oliver Bieri for granting access to the fMRI facilities of the University Hospital Basel. This work was funded by the Swiss National Science Foundation (Sinergia grant CRSI33_130080 to D.Q. and A.P.). M.F. was funded by the Research Fund for Junior Researchers of the University of Basel (grant DPE2141). Calculations were performed at sciCORE (http://scicore.unibas.ch/) scientific computing core facility at University of Basel. The authors declare no competing financial interests.

Study 4: SELERA – selection rate antecedents

Title:

Neurofunctional peculiarities in emotion responsivity are linked to peculiarities in an emotion-related behavioral phenotype in healthy young individuals

Teaser:

LASSO and prediction modeling reveal that network responsivity during negative picture encoding is linked to an emotion-related behavioral phenotype, which may be a neurofunctional marker for being in an antecedant stage to develop a mental disorder.

Authors:

Léonie Geissmann[1,2], Annette Milnik[2,3], David Coynel[1,2], Dominique J.-F. de Quervain[1,2,4]

Affiliations:

[1]Division of Cognitive Neuroscience, Department of Psychology, University of Basel, Birmannsgasse 8, 4055 Basel, Switzerland, [2]Transfaculty Research Platform Molecular and Cognitive Neurosciences (MCN), University of Basel, Birmannsgasse 8, 4055 Basel, Switzerland, [3]Division of Molecular Neuroscience, Department of Psychology, University of Basel, Birmannsgasse 8, 4055 Basel, Switzerland, [d]Psychiatric University Clinics, University of Basel, 4055 Basel, Switzerland, [4]Psychiatric University Clinics, University of Basel, Switzerland

Abstract

Mental disorders often develop gradually rather than abruptly. Aberrant emotion processing is a core feature across mental disorders. In a large sample of healthy individuals aged in the age range of onset for many mental disorders, some may be in the antecedent stage to developing a mental disorder. This study aimed to answer (i) whether there are individuals with peculiarities in emotion responsivity on a neurofunctional level, and (ii) whether such peculiarities are linked to emotion-related behavioral phenotypes. Utilizing LASSO and prediction modeling found FCN responsivity during negative picture encoding to be linked to a behavioral phenotype of emotion processing. Future studies could investigate associations with genetic markers and perform similar studies in individuals with mental disorders.

Introduction

Rationale: Theoretical background

Age of onset of most mental disorders is between ages 20 and 30 (Kessler et al., 2007). Most mental disorders do not emerge abruptly but rather evolve gradually from an antecedent stage (Dandash et al., 2017; Golonka et al., 2017; Salvatore et al., 2021). Major diagnostic systems may not adequately capture the organization of neural circuits and their associated maladaptive behaviors (Morris & Cuthbert, 2012). Mirroring the fact that most patients experience symptoms not adequately captured by one diagnosis (Caspi et al., 2020; Hudson et al., 2007), mental disorders are polygenic (Selzam et al., 2018; Wang et al., 2017), highlighting the multidimensional nature of mental disorders. With the centrality of emotion processing deficits in mental disorders, underlying mechanisms may be represented on a liability spectrum (Kret & Ploeger, 2015). Emotion responsivity, likely characterized by inter-individual variability, describes the emotional response to an emotional event (similar to FCN responsivity in Study 2).

It is unfortunate that many individuals in the antecedent stage leading to a mental disorder are overlooked due to not meeting diagnostic criteria (Addington et al., 2013), or because their clinically significant impairment in everyday functioning may not manifest overtly despite causing significant burden (Figure 5.1).

Given the high prevalence of mental disorders (Zuberi et al., 2021), in a large sample of over 1,000 healthy individuals with a mean age of 22 years, one may assume that some individuals may currently be in an antecedent stage.

Overall research questions

The overall objective was to enlighten characteristics in healthy individuals with peculiar emotion-related FCN responsivity, in accord with the dimensional conceptualization of mental disorders.

1. (i) Are there individuals with peculiar network engagement relative to the total sample? Which are the most-commonly activated FCNs in negative picture encoding?
2. (ii) If so, are they characterized by peculiarities in emotion-related behavioral phenotypes? Is the strength of recruiting these networks related to the perceived strength of arousal of our participants?

Figure 5.1

Depiction of a hypothetical course of developing a mental disorder

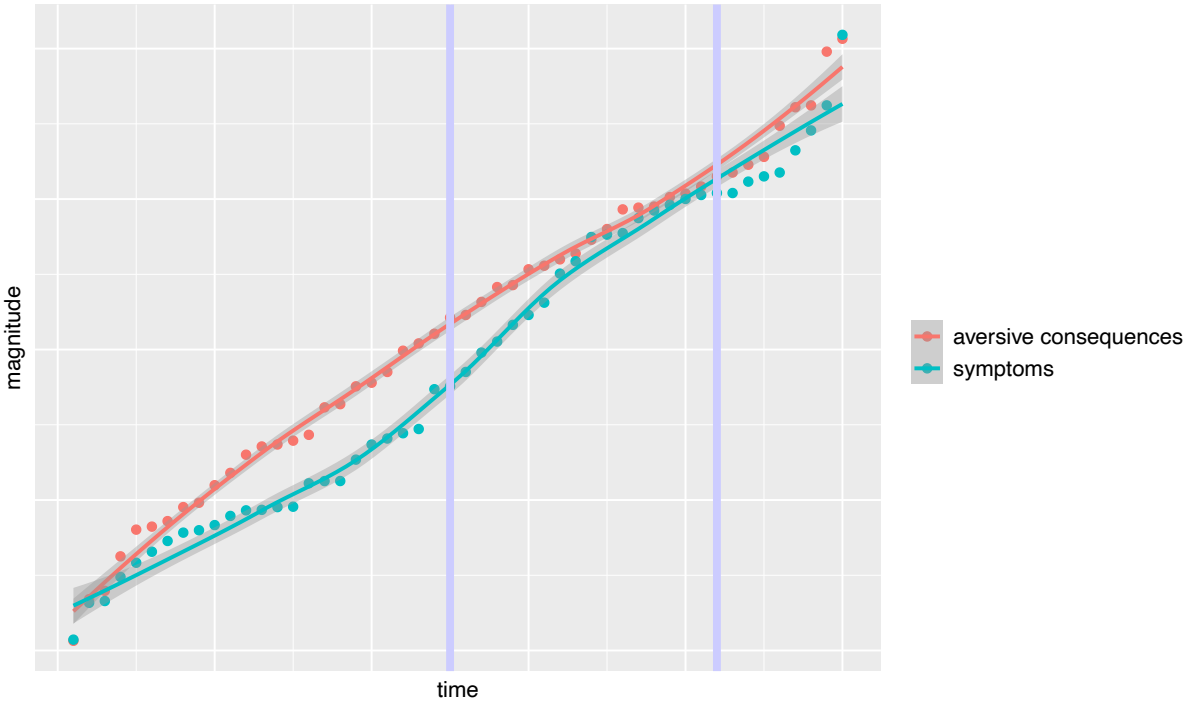

Note. In this example, the vertical line on the left represents a hypothetical starting point at which a person's symptoms and their aversive consequences have reached a degree at which professional intervention is required. The vertical line on the right represents the hypothetical point at which the person meets the diagnostic criteria for a mental disorder. The zone between the two vertical lines is illustrates the antecedent stage.

Rationale: methods

Investigating FCNs instead of voxels may have the advantage of enhanced interpretability and comply with the understanding of brain function as a network. Machine learning may be a reasonable starting point (Yarkoni & Westfall, 2017) as it can, e.g., take inter-individual differences into account while also returning group-statistics. Given the innovative nature of the procedure, multiple validation steps were added.

The sample consisted of a discovery (n = 575) and replication (n = 572) sample, based on data from Study 2, i.e., subjects were drawn from the same sample, network responsivity during encoding was calculated in a similar manner, with the difference being that network responsivity encompassed responsivity to negative picture encoding only (instead of encoding of pictures of all valences as in Study 2). The starting point was the total of 60 ICs calculated

and validated in Study 2. The network-based first-level beta-values (i.e., estimates) for each subject were those from the regressor negative picture encoding.

Methods

The procedure involved three levels: (i) single-subject, (ii) group-level, and (iii) association with behavior.

Level 1: Single-subject

Overview of level 1

The Least Absolute Shrinkage and Selection Operator (LASSO) penalized regression was used to select, for a given subject, a set of FCNs associated with encoding negative pictures. To summarize, first, a statistical model (i.e., a learner) was constructed in two thirds of the fMRI data to figure out an ideal lambda, and then have the model predict negative picture encoding based on each IC's single-subject time courses. By using cross-validation (CV) procedurs, this resulted in a single-subject selection rate for each IC, reflecting the variable importance of this IC to explain variance in the outcome variable negative picture encoding. The final model's performance was tested in the remaining one third of the unseen fMRI data.

Step 1: Selection of the tuning parameter lambda for single-subject LASSO models

For each subject, their fMRI design matrix (SPM-mat files) (Friston et al., 2007) was merged into one data set with the subject's IC time courses, as calculated with dual regression (see Study 2). Two thirds of this data (i.e., time points 1 to 280) were used for model training, and the remaining third (i.e., time points 281 to 420) for testing of the model's performance. Then, using the training data, a penalized regression model LASSO was constructed, for each subject, to tune the parameter lambda to enhance model quality, using the R package glm.net (Friedman et al., 2010) with 10-fold CV. The function cv.glmnet was used, with the following parameter settings: alpha set to 1, family set to Gaussian. The outcome variable was negative picture encoding.

Step 2: Calculation of single-subject IC selection rates using LASSO with the lambda value

Next, by using the lambda obtained in step 1, LASSO models were estimated by applying a simple block bootstrapping procedure. For doing so, we divided the training data into 28

equally sized non-overlapping blocks and recreated the training data by randomly resampling this data (sampling with replacement). We repeated this procedure 10 times.

For each model, the ICs were either set to zero by LASSO (i.e., unselected), or not set to zero (i.e., selected) based on the informativeness of the outcome variable (i.e., negative picture encoding). Based on this, each IC had a selection rate that represented the average of the 10 repetitions it was not set to zero, henceforth referred to as single-subject selection rate. For example, if IC 10's first-level regressor negative picture encoding for subject *j* was not set to zero 8 times, then the selection rate for IC 10 in subject *i* was 8/10 = 80 %.

For model testing, the ICs with a single-subject selection rate above 60 % were considered as "selected". With the selected ICs, we ran linear regression models with the selected ICs as predictors and the negative picture encoding as outcome variable in the training data. The model performance was then estimated in the test data. Performance r^2 was quantified as the square of the Pearson correlation *r* between predicted and observed values in the test data of each subject.

Level 2: Group-level

The next step aimed at mapping the distribution each IC's single-subject selection rates, to further use this distribution for outlier assessment. ICs with a mean selection rate above 65 % on group-level were considered as important. Note that the term important is used in the sense of variable importance (Wei et al., 2015). Next, the R package e1071 (Meyer et al., 2021) was used for an additional outlier analysis based on skewness of each IC's group-based selection rate distribution. ICs with a minimal skewness of -0.5 were rated as moderately negatively skewed, indicating that there was a robust selection of this IC on group-level, with only few outliers. All procedures were done separately in the discovery and replication sample, allowing then to assess whether the same final set of ICs was considered as important for the next step.

Level 3: Association with behavior

Level 3 used a correlational approach. Correlational models using Pearson's correlation were used to assess the association between single-subject selection rate (corrected for age and sex) and the behavioral phenotypes, wherein each behavioral phenotype was modeled in separate models. The models were tested for statistical significance using univariate *t*-tests.

Note that only those ICs which were found to be important (i.e., high group-level selection rate as assessed by skewness and mean) were modeled. Further, this subset included only the replicable ICs. All procedures were done separately in the discovery (n = 575) and in the replication (n = 572) sample.

The behavioral variable hypothesized to capture emotion responsivity was arousal rating for negative pictures, as a trait-related measure that is more intermediate than a retrospective self-rating questionnaire.

Hypotheses

As a bottom line, for each of the ICs found to be important for encoding negative pictures in both discovery and replication sample, the following hypotheses were tested:

1. Hypothesis (i): There is an association between arousal ratings for negative pictures and selection rate.

Results

Level 1: Single-subject

The percentage of ICs selected to be important (i.e., not set to zero by LASSO i.e., single-subject selection rates) ranged from 2 to 90 % across all participants. The average performance (r^2 between predicted and observed values) of these models in the test data was fair in the discovery (M = 0.102, SD = 0.059, 25th percentile = 0.055, 75th percentile = 0.138) and the replication sample (M = 0.104, SD = 0.062, 25th percentile = 0.059, 75th percentile = 0.143), confirming that the bootstrapping procedure served its purpose.

Level 2: Group-level

Group-level variable selection found four networks to be important for negative picture encoding: ICs 12, 21, 28 and 47 (Figures 5.2 and 5.3A-D, Table 5.1A-C, Supplementary Figure S1), in both replication and discovery sample, based on the group-level selection rates' mean and skewness. These four ICs were treated as FCNs of interest for the succeeding analyses.

Level 3: Association with behavior

1. Hypothesis (i): Arousal ratings for negative pictures were positively associated with the selection rates of IC 12 (discovery sample: $t(574) = 2.606$, $p = 0.009$; replication sample: $t(571) = 3.542$, $p = 0.0004$), and negatively linked to the selection rates of IC 28 (discovery: $t(574) = -2.661$, $p = 0.00801$; replication: $t(571) = -2.043$, $p = 0.0415$. Neither IC 21 (discovery sample: $t(574) = 1.112$, $p = 0.266$; replication sample: $t(571) = 0.269$, $p = 0.788$) nor IC 47 (discovery sample: $t(574) = 1.938$, $p = 0.053$; replication sample: $t(571) = 1.809$, $p = 0.071$) were linked to arousal ratings for negative pictures.

Figure 5.2

The four ICs with high importance for encoding negative pictures, replicated in both discovery (n = 582) and replication (n = 576) samples

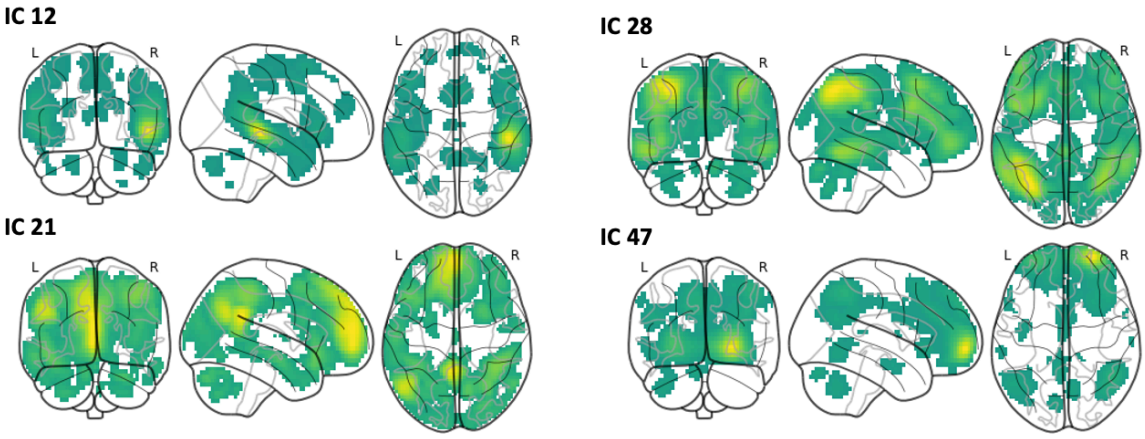

Note. ICs 12 and 28 were positively and negatively, respectively, linked to arousal ratings for negative pictures There was no such association for ICs 21 and 47.

Table 5.1A

Descriptive statistics of the group-level selection rates for ICs 1 to 20

IC	M_D	M_R	SD_D	SD_R	*skew-ness*$_D$	*skew-ness*$_R$
1	0.428	0.422	0.354	0.354	0.315	0.305
2	0.543	0.531	0.279	0.279	-0.151	-0.059
3	0.469	0.489	0.308	0.305	0.187	0.101
4	0.366	0.372	0.300	0.300	0.538	0.473
5	0.525	0.504	0.298	0.291	-0.056	0.084
6	0.553	0.563	0.305	0.294	-0.206	-0.074
7	0.542	0.540	0.294	0.285	-0.110	-0.159
8	0.437	0.410	0.284	0.284	0.269	0.413
9	0.460	0.468	0.345	0.327	0.214	0.214
10	0.540	0.539	0.293	0.279	-0.111	-0.082
11	0.442	0.450	0.282	0.293	0.253	0.185
12	**0.666**	**0.676**	**0.290**	**0.282**	**-0.569**	**-0.536**
13	0.446	0.471	0.278	0.283	0.217	0.142
14	0.583	0.573	0.295	0.294	-0.220	-0.223
15	0.351	0.353	0.289	0.293	0.576	0.578
16	0.520	0.509	0.315	0.295	0.033	0.056
17	0.441	0.381	0.288	0.281	0.242	0.484
18	0.614	0.595	0.303	0.304	-0.391	-0.275
19	0.448	0.449	0.308	0.320	0.174	0.170
20	0.453	0.457	0.280	0.281	0.124	0.123

Note. D = discovery sample; R = replication sample.

Table 5.1B

Descriptive statistics of the group-level selection rates for ICs 21 to 40

IC	M_D	M_R	SD_D	SD_R	*skew-ness*$_D$	*skew-ness*$_R$
21	**0.757**	**0.779**	**0.281**	**0.269**	**-1.107**	**-1.232**
22	0.520	0.504	0.298	0.303	-0.073	0.014
23	0.556	0.562	0.320	0.311	-0.144	-0.151
24	0.383	0.392	0.293	0.290	0.491	0.437
25	0.405	0.396	0.304	0.305	0.423	0.420
26	0.573	0.552	0.287	0.304	-0.170	-0.094
27	0.484	0.481	0.289	0.283	0.048	0.145
28	**0.780**	**0.791**	**0.268**	**0.266**	**-1.284**	**-1.319**
29	0.421	0.407	0.310	0.300	0.324	0.379
30	0.460	0.445	0.283	0.290	0.180	0.266
31	0.476	0.477	0.284	0.286	0.026	0.031
32	0.319	0.321	0.307	0.304	0.763	0.749
33	0.363	0.351	0.295	0.299	0.596	0.623
34	0.393	0.400	0.297	0.311	0.399	0.412
35	0.408	0.376	0.316	0.300	0.414	0.524
36	0.499	0.477	0.319	0.301	0.050	0.094
37	0.573	0.566	0.287	0.289	-0.184	-0.193
38	0.568	0.536	0.305	0.306	-0.269	-0.099
39	0.460	0.452	0.293	0.283	0.112	0.218
40	0.534	0.513	0.289	0.281	-0.102	-0.008

Note. D = discovery sample; R = replication sample.

Table 5.1C

Descriptive statistics of the group-level selection rates for ICs 41 to 60

IC	M_D	M_R	SD_D	SD_R	*skew-ness*$_D$	*skew-ness*$_D$
41	0.513	0.509	0.287	0.289	0.014	0.042
42	0.516	0.512	0.294	0.297	-0.016	-0.088
43	0.412	0.435	0.297	0.288	0.320	0.258
44	0.519	0.512	0.279	0.284	0.009	0.027
45	0.594	0.589	0.284	0.269	-0.313	-0.228
46	0.303	0.298	0.296	0.276	0.798	0.813
47	**0.686**	**0.687**	**0.307**	**0.297**	**-0.733**	**-0.660**
48	0.464	0.468	0.301	0.292	0.180	0.178
49	0.443	0.450	0.296	0.291	0.267	0.140
50	0.391	0.400	0.289	0.284	0.501	0.355
51	0.479	0.458	0.304	0.292	0.107	0.224
52	0.458	0.452	0.292	0.288	0.162	0.255
53	0.447	0.471	0.284	0.283	0.158	0.182
54	0.456	0.469	0.284	0.284	0.202	0.121
55	0.528	0.549	0.291	0.276	-0.058	-0.074
56	0.500	0.418	0.295	0.290	0.015	0.352
57	0.489	0.493	0.287	0.295	0.024	0.020
58	0.455	0.451	0.292	0.289	0.212	0.214
59	0.456	0.463	0.294	0.287	0.174	0.186
60	0.400	0.349	0.283	0.284	0.394	0.665

Note. D = discovery sample; R = replication sample.

Figure 5.3A-B

*Group-based selection rates for ICs 12 and 21 shown in panels **A** and **B**, respectively*

A

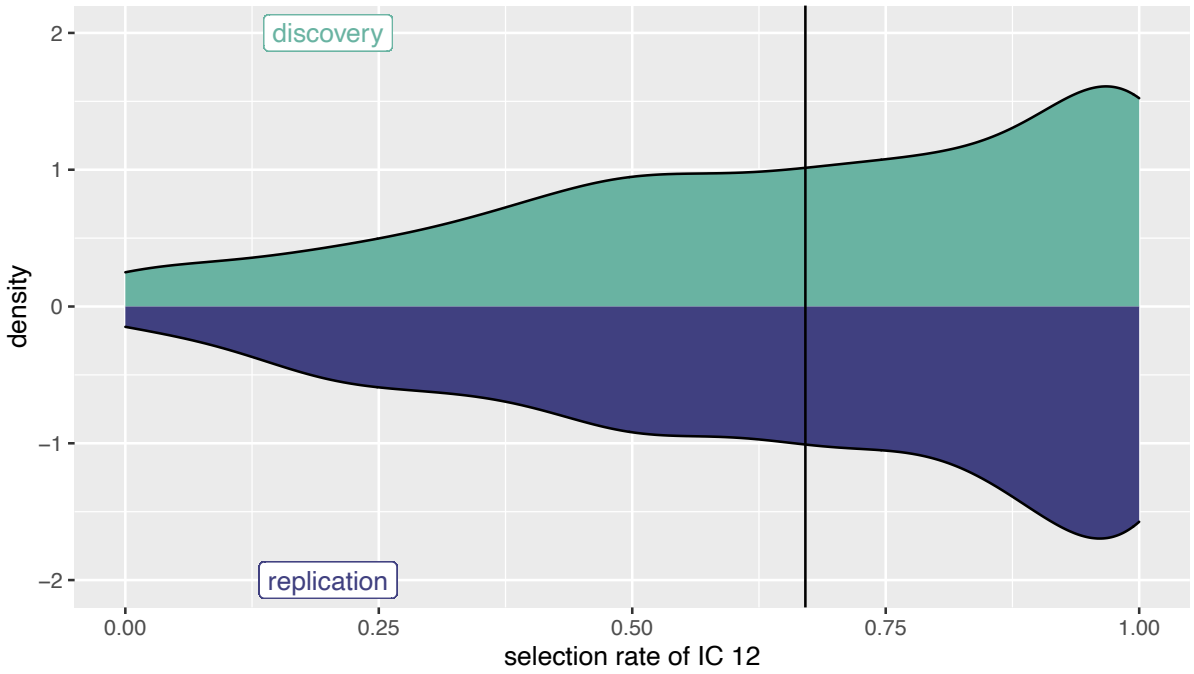

B

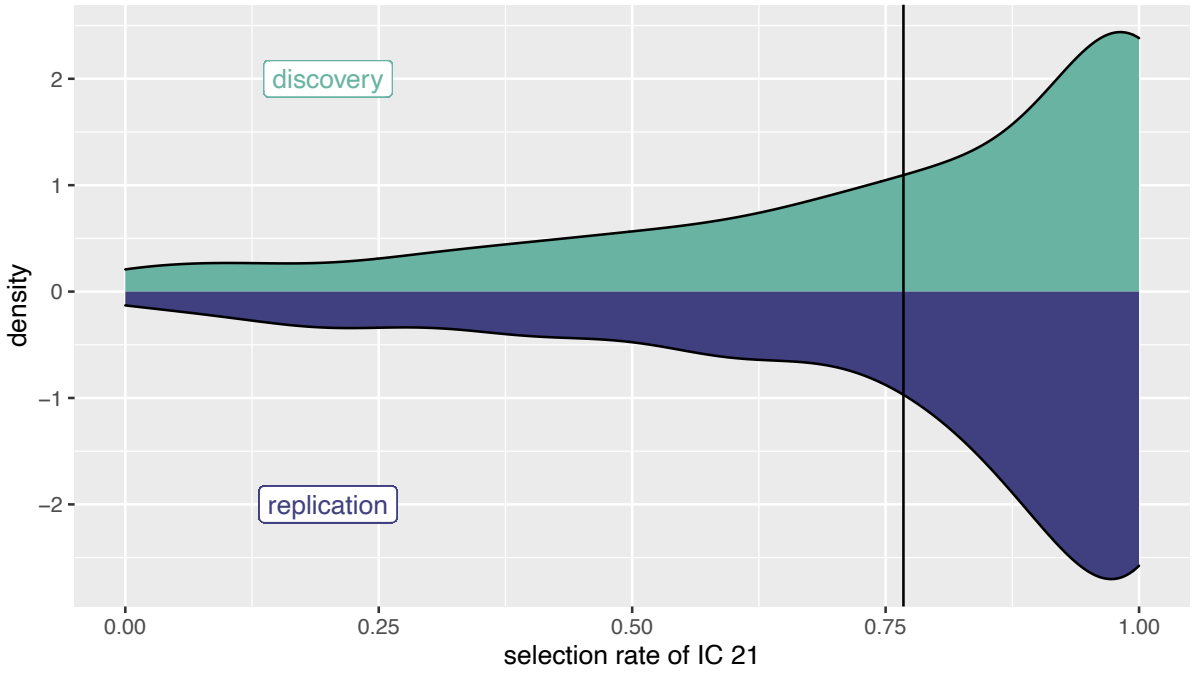

Note. The selection rates represent the importance of the ICs for encoding negative pictures on group-level. These four ICs had high importance in both the discovery (*n* = 575) as well as the replication (*n* = 572) samples. See Supplementary Figure S1 for additional ICs. The vertical line represents the mean.

Figure 5.3C-D

Figure 5.3C-D

*Group-based selection rates for ICs 28 and 47 shown in panels **C** and **D**, respectively*

C

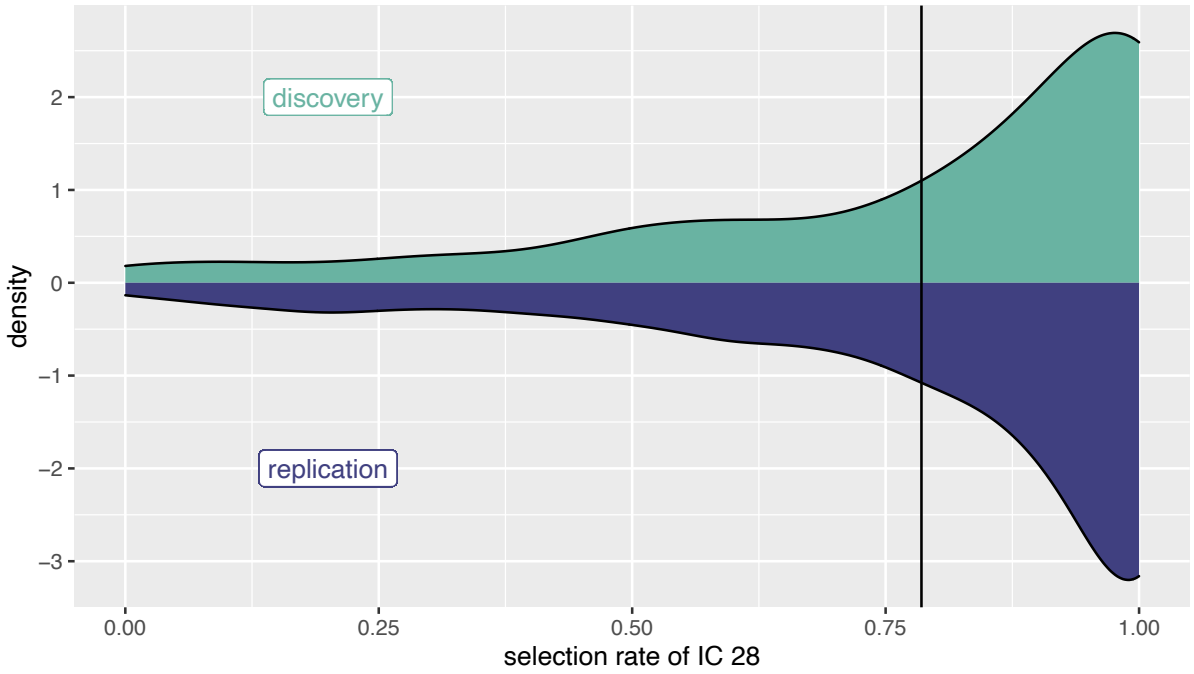

D

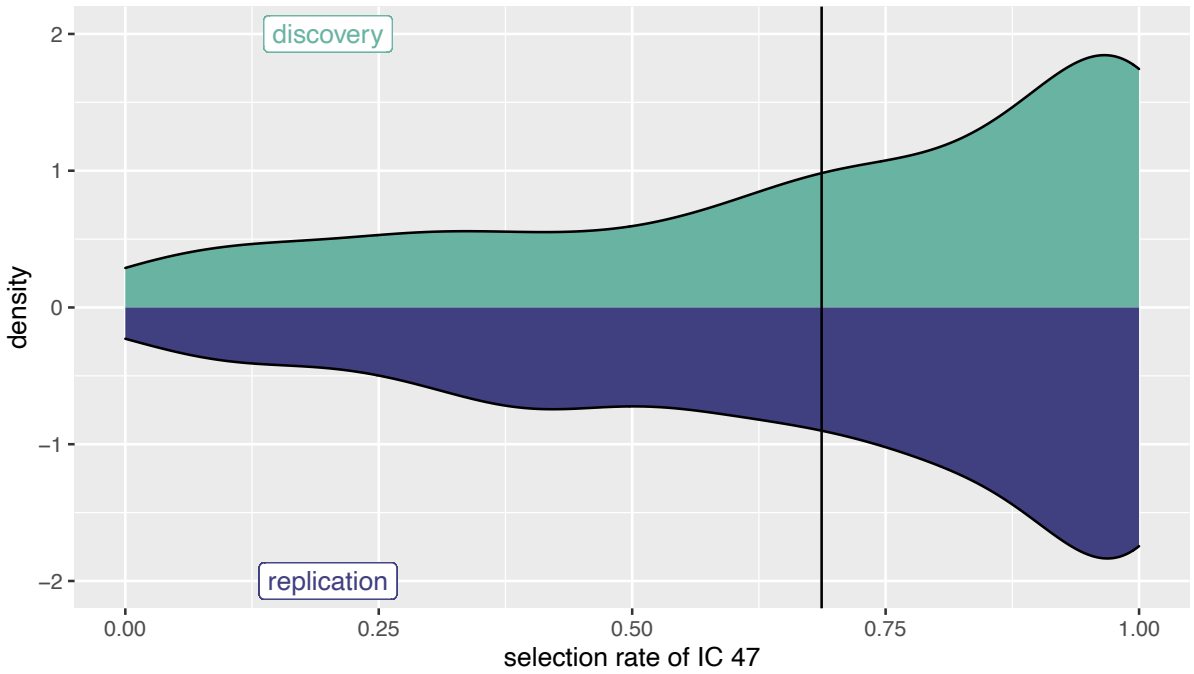

Note. The selection rates represent the importance of the ICs for encoding negative pictures on group-level. These four ICs had high importance in both the discovery (*n* = 575) as well as the replication (*n* = 572) samples. See Supplementary Figure S1 for additional ICs. The vertical line represents the mean.

Discussion

This study assessed which FCNs are particularly responsive to negative picture encoding across a large sample of healthy individuals. Four FCNs were found to be important for negative picture encoding in an encoding task in both the discovery and replication sample. Embedding this insight with the findings of Study 2, among the four FCNs, IC 21 was associated with free recall performance of pictures in Study 2. This IC was further associated with free recall performance of emotional pictures (not mentioned in Study 2). Note that the brain-behavior correlations in Study 2 were based on the complete sample and not limited to the subjects used in this study (here *n* = 1,147, split into discovery and replication sample). All four networks were robust in that they were spatially reproducible (see Study 2, Supplementary information). IC 12 largerly overlaps with the insula, middle superior temporal gyrus, precuneus and posterior cingulate cortex, which are all brain regions found to be affected in MDs such as attention deficit hyperactivity disoder, autism spectrum disorder, bipolar disorder, major depressive disorder, and schizophrenia (Wang et al., 2017). IC 28 notably included the inferior temporal gyrus, inferior parietal gyrus, cuneus and frontal gyrus, as well as the angular gyrus, which has been related to schizophrenia (Wang et al., 2017). IC 47 majorly covered the orbitofrontal cortex, as well as mediofrontal and superior-temporal parts of the brain in the right and left hemisphere, respectively. IC 21 is described in further detail in Study 2.

After determining the importance of the ICs for negative picture encoding, this study found two of these important ICs to be linked to arousal ratings of negative pictures in both samples. The underlying notion could be that negative arousal ratings capture a phenotype that puts one at greater liability to mental disorders, as it reflects immediate emotion processing. These included IC 12 and IC 28.

IC 12 largely overlaps with brain regions known to be implicated in executive function (Cui et al., 2020), while executive function itself is associated with most major neuropsychiatric disorders (Cui et al., 2020). Cui and colleagues (2020) have found that as early as during youth, FCNs spanning association cortices are linked to executive functioning, in line with the notion that neuroimaging markers of cognitive functions linked to mental disorders may be present when there is likely no such current diagnosis. Neither IC 21 nor IC 47 were consistently (i.e., in both replication and discovery samples) linked to the two

behavioral phenotypes. It could be hypothesized that the spatial coverage of IC 21 was too broad to capture the specificity of the phenotype.

To recapitulate, emotion responsivity circumscribes the emotional response to an event that may vary between individuals in terms of intensity, speed to reach peak, and speed to return to baseline. The complexity of emotional responses forms part of a liability spectrum for mental disorders in general (Kret & Ploeger, 2015). Arousal is listed as a construct in the Research Domain Criteria matrix (Morris & Cuthbert, 2012), highlighting its importance in characterizing the spectrum of neurobiological traits underlying mental disorders. Arousal has the advantage of being a more intermediate construct than retrospectively self-reported negative emotional reactivity.

As a limitation, given the cross-sectional study design, this study did not test whether the emotion-related behavioral phenotypes are indicative of being in an antecedent stage to develop a mental disorder. Therefore, the results are preliminary.

To conclude, the first finding was that some healthy individuals are characterized by peculiar network engagement relative to the total sample. The second finding was that there is an association between peculiar network engagement in a subset of relevant networks and behavioral phenotypes related to emotion processing. Future research could investigate associatons with genetic markers, as well as perform out-of-sample analyses to check whether FCNs with brain-behavior correlations stand out in populations of individuals with mental disorders.

Discussion

Study 1: Considerations

Consideration 1: What does the resting-state measure and what makes it so relevant?

The state of mind during a state of resting

During states of resting, i.e., nonattendance in an active task and absence of external stimulation (Barkhof et al., 2014), meaningful patterns of brain activity emerge spontaneously across cortical and subcortical structures. The vast majority of the brain's metabolic resources are devoted to maintaining spontaneous activity rather than supporting evoked responses (Uddin et al., 2019). Whether engaging in a task or wakefully resting, the majority of the body's energy budget is invested in resting potentials and infra-slow signaling (< 0.1 Hz). At the same time, 25 to 40 % of it is used for housekeeping functions with the remaining up to 10 % being devoted to the metabolically expensive spikes (Howarth et al., 2012; Pezzulo et al., 2021).

Rather than primarily stimulus-driven or reflexive, cognitive function arises from the brain's intrinsically self-organizing character (Alderson et al., 2020), wherein the brain's interacting units form whole-brain patterns due to their mutual constraints (Bressler & Tognoli, 2006). Cognition has been defined as the real-time expression of distributed local areas whose states of mutual coordination are adjusted dynamically over time (Alderson et al., 2020; Bressler & Tognoli, 2006). Neuroimaging data suggest that changes in blood flow and metabolism during task activation are relatively small (Pezzulo et al., 2021). During the resting-state, the brain partakes in sophisticated cognitive functions, such as self-referential processing, mental scenario stimulation, integration of episodic memory, emphasizing and abstract thinking (van den Heuvel & Hulshoff Pol, 2010).

These cognitive functions are, however, not constrained to the resting-state. In line with this, resting-state networks are conserved during task states (Damoiseaux et al., 2006), but not perfectly so, with between-task variability in their exact constellation (Fornito et al., 2012; Laird et al., 2011; Utevsky et al., 2014).

Seemingly obvious in a laboratory setting, the distinction between a state of resting and task in terms of cognitive function might be obfuscated in a naturalistic environment. In support of this, single-unit neuron recording indicates that the brain activity of two monkeys may be affected differently by slight adjustments to a resting-state protocol (Dąbrowska et al., 2021). The state of the mind during the resting-state might be more nuanced than generally assumed.

Potential functions of the brain as a network during rest

Aside from the biological explanation of mechanisms during the resting-state, one may ask what the merits of the brain as a system of networks are. A system that navigates within a limited space has distinct states that may be activated during different tasks and stimuli while maintaining a common core to ensure the maintenance of whole-brain network configuration (Zimmern, 2020), enabling efficient situational reconfigurations. The intrinsic core of the system might thus represent a dynamic regime that balances counteracting tendencies towards integration and segregation such that local areas are permitted to express their intrinsic functionality yet also couple together and coordinate globally (Alderson et al., 2020). The dynamic regime of brain architecture might be driven by the following three: (i) anatomical connectivity between regions, (ii) relatively state-invariant intrinsic correlation patterns, and (iii) an individual's history of co-activations across the lifespan (Dosenbach et al., 2006; Gratton et al., 2016).

In order to readily reconfigure in adaptive ways, the intrinsic core might strive for a state of metastability. Metastability is defined as a coupled or collective oscillatory activity that falls outside its equilibrium state for dwell times that depend on distance from equilibrium (Kelso, 1995), corresponding to an optimal exploration of the dynamical repertoire inherent in the static structural linkages of the anatomy where the probability of network switching is maximal (Alderson et al., 2020; Cabral et al., 2011).

The brain's functional architecture, as observed with neuroimaging methods, is backed up by research in other fields. Shaped by evolution (Xu et al., 2020), neural plasticity throughout an individual's life span and the features of the structural connectome, the repertoire of possible FCN configurations of an individual at a given time of their life is constrained. In support of the modular structure of the brain and its intrinsic core is the finding that inter-areal couplings of long-range temporal correlations and the propagation of neuronal avalanches are most pronounced in the predominant pathways of FC (Zhigalov et al., 2017) and that spatial organization of FCNs corresponds to gene expression networks such that the spatial organization of FCNs corresponds to regions with more highly correlated gene expression than expected by chance (Richiardi et al., 2015).

Moreover, signal propagation in a system can be enhanced by the existence of an optimal background noise intensity, suggesting that the overall structure of the whole

functional connectome contributes to task-related cognitive function. This might not be apparent in conventional fMRI analysis paradigms such as the mass-univariate general linear model (GLM) for associating individual brain regions with specific tasks or stimuli. In line with this, widespread increases in metastability may indicate that most of the brain is involved during tasks (Alderson et al., 2020).

Collectively, the elaborate network-based view on the essence of states of resting and task may not only offer substantial insights into human brain function but also make demands for a multitude of nascent techniques.

Spontaneous brain activity from a generative top-down modeling perspective

The mechanics supporting the brain's constant challenge of deciphering and processing information may be conceptualized as statistical learning (Wang et al., 2017). The functional importance of spontaneous activity may be illustrated in terms of top-down generative models (Pezzulo et al., 2021). This model phrases the brain as an organ that forms generative models to continuously generate predictions in the service of perception and adaptive behavior (Pezzulo et al., 2015).

During rest, the input of new data is generally low. Therefore, this is the phase during which the generative model undergoes "offline" abstraction and integration, whereas, during states of task, data is collected "online". The online data collection ought to occur in an adaptive manner enabled by the the offline period, which has served the purpose of making sense of prior experience (Figure 6.1).

The adaptiveness is enabled by continuous model enhancement, which functions in a top-down manner by making sense of already collected data. This happens during rest, and is predictive as it is supposed to optimize future behavior during states of task, according to an individual's requirements when immersed in a new environment. Generative refers to the fact that data is generated for use in the future. In that sense, the brain as a generative model provides top-down predictive signals for perception, cognition, and action, wherein during states of little to no externally incoming data, top-down dynamics optimize the generative models for future interactions (as discussed in detail in Pezzulo, 2021).

Figure 6.1

Illustration of spontaneous brain activity from a top-down modeling perspective

Note. During an engagement in a task (left), such as food seeking, the brain is prepared to allow the being to act in adaptive ways, e.g., by optimizing attention attribution. New data is collected during task execution which renders the models more complex. During rest (right), there is little incoming data, as sensory input is limited, which is when the brain engages in dimensionality reduction and model simplification to allow to react in the most adaptive ways in the future.

Interpreting the findings from a generative top-down modeling perspective

The top-down generative model perspective on brain function may explain why resting-state functional connectivity measures remain unaffected by exposure to stimuli well-known to provoke differential brain responses. This distinguished response, which critically involves the amygdala (Banks et al., 2007; Eippert et al., 2007; Erk et al., 2010; Fastenrath et al., 2014; Murty et al., 2010; Rasch et al., 2009; Townsend et al., 2013), allows for adaptive behavior given the context (Figure 6.2). Depending on the functional processing cascade as seen during integration enabled by the amygdala's widespread connectivity across the brain, the resultant behavioral response can vary a lot (see Introduction).

Our study protocol was designed to make participants feel at ease, safe, and well-informed. For example, participants were made familiar with the environment, spent about an hour prior to the first MRI scan with the investigator, and had time to ask questions. They were aware of the possibility of withdrawing from the study at any time without giving a reason. This may have affected the participants' top-down generative predictive models in the brain: With that little probability of proximal threats, the brain may have devoted its computations to engage in model simplification during the second rs-fMRI session rather than, for example, externally driven data collection. The latter may have affected brain connectivity differently. As a speculation, in a different setting, rs-FC, after encountering highly aversive pictures, may have been affected in that the emotion-regulating effect of interacting with the investigator may not have exerted a dampening effect.

Figure 6.2

Exemplification of the spectrum of cognitive processes related to the resting-state

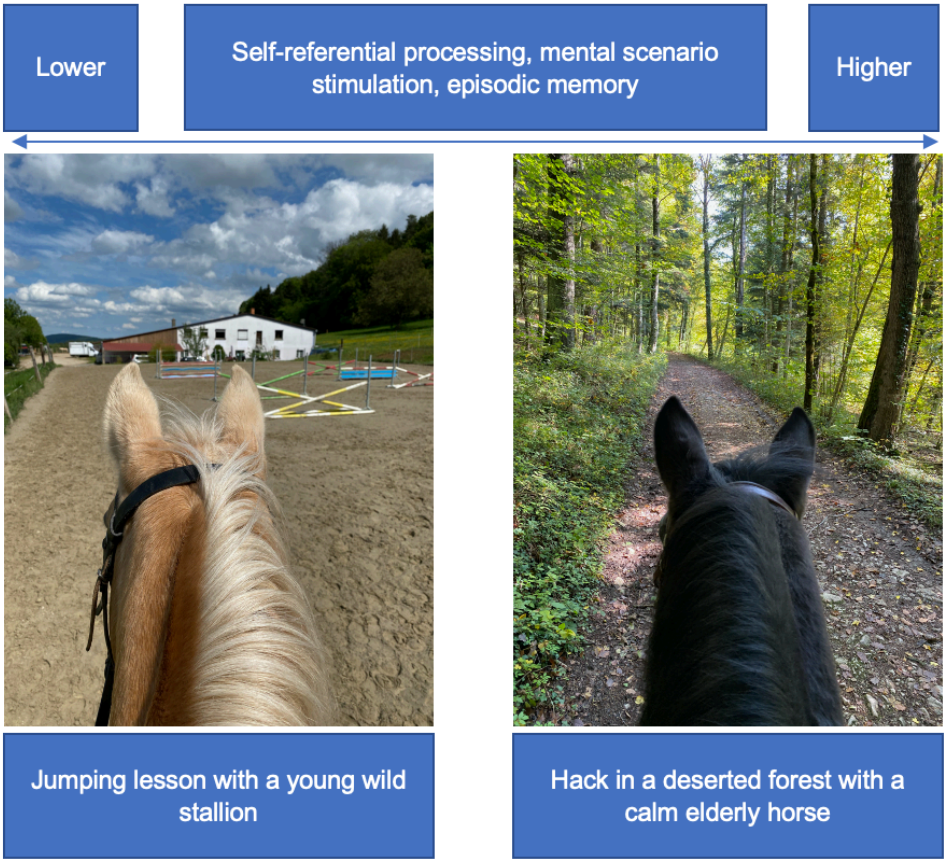

Note. In situations characterized by high predictability, high stability, and low probability of imminent threat (right), one might partake in cognitive processing typically related to the resting-state more than in situations with low predictability, high changeability, and high probability of imminent threat (left).

In full awareness of their speculative character, the reflections offered here ought to show that conclusions based on data may benefit greatly from detailed conceptual contemplations beyond that of statistical power.

Consideration 2: The statistical power and goodness of theoretical background

The power of the study

The chance of finding a significant between-group difference when an actual difference exists is related to sample size, the absolute size of group differences, the intrinsic variability of measurements and the rejection threshold alpha for the null hypothesis (Dansereau et al., 2017). The goodness of a theory to fit the facts is critical to consider regarding sample size, and predictions about absolute mean group differences may be near-impossible (Szucs & Ioannidis, 2017). Intrinsic variability may be minimized by sound experimental setup, pre-processing, elaborate and appropriate analytic approaches that allow for data quality, and limiting confounding factors, such as fluctuations in vigilance (Tagliazucchi & Laufs, 2014). Hence, we implemented complementary analytical methods, a repeated-measures design outlined at accounting for baseline differences in rs-FC, and set up the picture encoding task according to previous research showing that it robustly elicits differential brain activity (Fastenrath et al., 2014). Regardless, with statistical power being a key criterion for all these measures to serve their purpose, replication of the study with a larger sample would be required for statistically backed up rejection or acceptance of our hypotheses.

Study 2: Considerations

Consideration 1: Using static FCNs

One main focus of our study on brain-behavior correlations is FCN responsivity. Information processing in the brain prompted by stimuli exposure follows an incremental hierarchical flow along a temporal dimension. The longer an epoch is, the more brain regions a FCN may include (Sanchez-Rodriguez et al., 2021). However, given the rapid nature of memory encoding processes (Viskontas et al., 2006), these larger FCNs may not capture the entirety of the brain's fine-grained functional network topology during shorter episodes, i.e., the network's rapidly fluctuating dynamics. Therefore, the question about the epoch length for which our detected brain-behavior correlation-ICs applies remains an open question. Each IC with brain-

behavior correlations may have its unique epoch length and dynamics following the immediate responsivity reaction.

Consideration 2: Correlations between behavior and FCNs versus voxels

We queried all ICs present during the encoding task for brain-behavior correlations and not only those that include brain regions with subsequent memory effects. Relationships between the magnitude of neural activation and functional role may not always follow easily linearly discernible patterns. Following this, it has recently been found that dopamine neurons in the ventral tegmental area contribute to short-term memory during the relay period, despite low activity during that time (Choi et al., 2020). Most of the brain is involved during tasks (Alderson et al., 2020), indicating that the network-based approach to brain-behavior correlations and the voxel-based approach to brain-behavior correlations cannot be seamlessly compared as they may not capture the same concept.

Consideration 3: Temporal resolution and temporal hierarchy of network responsivity

It is important to note that network responsivity, i.e., a static task-based FCN's reaction to a stimulus, may not be the only FCN behavior related to episodic memory recall. The importance of bridging networks and their characteristics across multiple time scales regarding memory and FCN dynamics is supported by a line of research. Early phase synchronization between sensory areas reflects multi-sensory integration, which captures attention and results in memory improvement (Wang et al., 2018). Power increases during successful item encoding in the slow theta range occurs within the first 1,000 ms after item presentation, specifically in the posterior hippocampus (Lin et al., 2017). Increases in hippocampal power predict episodic memory performance, preferentially in the slow 2-5 Hz range (Choi et al., 2020), and even pre-encoding hippocampal spike activity 1,000 to 2,000 ms before stimulus presentation are predictive of better memory (Urgolites et al., 2020). The vascular response of the BOLD signals is characterized by a large signal magnitude peak 5 to 6 s after stimulation, which differs a lot from the occurrence of above-mentioned neural events (Dowdle et al., 2021).

Consideration 4: Breaking down which neurocognitive phenotypes the individual FCNs are important for in the context of episodic memory

Further, the precise neurocognitive phenotypes underlying the link between encoding and later recall performance are not perceptible from our paradigm. Among the many potential mediating roles of neurocognitive traits important for episodic memory are reward region connectivity (Frank et al., 2019), flexibility in DMN and its relation to the degree of difficulty of a working memory task (Vatansever et al., 2015), visual attention (Nenert et al., 2014), the coordination of attentional resources to govern intruding thoughts during encoding (Zhang et al., 2020), and DMN-related information integration (Smallwood et al., 2016). Further, even if the roles of the FCNs in cognition were known, inter-individual differences may still be possible. For example, the finding that the extended frontoparietal network's reactivity to pictures is associated with inter-individual differences in memory recall performance does not necessarily indicate that the network fulfills the same purpose in all individuals. The distinct degrees of involvement of the FCNs with brain-behavior correlations in those elements (i.e., neurocognitive traits) of episodic memory encoding needs to be clarified further.

Consideration 5: The set of FCNs

One may wonder why we detected only a small percentage of the total of our ICA's networks to be related to inter-individual differences in episodic memory performance. The vast majority of the brain's metabolic resources are devoted to maintaining spontaneous activity rather than supporting evoked responses (Uddin et al., 2019). Findings provided by studies looking into relations between genetics, development, and FCNs (Richiardi et al., 2015; Xu et al., 2020; Zhigalov et al., 2017) and state-dependent reconfigurations of FCNs (Zimmern, 2020) all indicate that the overall structure of the whole functional connectome, and not only the brain-behavior correlation-ICs, might to some part contribute to episodic memory performance. The ICs with brain-behavior correlations are implicated explicitly in their distinguished responsivity to stimuli during encoding, meaning that the associations we discovered need to be interpreted in the face of how we defined responsivity. The FCNs for which we found brain-behavior correlations might not be the only essential FCNs that are associated with inter-individual differences in episodic memory performance.

Consideration 6: Effect sizes of the subsequent memory effects

Study 2 contributes to the field by investigating well-established subsequent memory effects in a large single-site sample. Correspondingly, the effect sizes of the subsequent memory effects in the brain regions previously not reported are smaller than those in brain regions that previous studies had revealed. On the one hand, it has been argued that by increasing sample size enough, one is guaranteed that H_0 can be rejected even with tiny effect sizes (Szucs & Ioannidis, 2017). On the other hand, small effect sizes only imply that the effect is small in the whole group and the statistical framework used, and not that these effects are any less meaningful for individuals of that group. For one, this is due to the mass univariate voxel-wise testing in the subsequent memory paradigms, which does not allow for direct conclusions about interactions between the voxels. For another, these tests assume that the sample is homogeneous enough to underline the effects of interest. However, an alternative explanation might be provided by a potential presence of meaningful subgroups, wherein the population-level effects being reversed is known under the term Simpson's paradoxon (Pearl, 2014). Another possibility is the existence of a continuum for different subgroups. When the variables making that continuum have not been measured or do not follow the assumptions underlying the mass univariate approach, they may not be evidently distinguishable. Along similar lines, even when the paradigm is well-established, such as in the case of the subsequent memory effects, the *p*-values cannot be compared across studies as they depend on sample and effect size (Szucs & Ioannidis, 2017). Beyond statistical terms, factors concerning the whole study design may matter. It has been suggested that reasonably powered studies (i.e., large sample size) may provide clarity and be a helpful heuristic when theoretical predictions are not precise (Szucs & Ioannidis, 2017).

Studies 1 and 2: Methodological-operationalizational considerations

Consideration 1: Strengths of ICA

Predicated on the idea that during states of tasks, brain configurations function in a network way, we applied an explorative data-driven procedure (ICA). Validation of the networks, which we achieved by verifying their reproducibility and checking for their association to the task with brain-behavior correlations (network responsivity), showed that this approach is suitable.

Decomposition of brain activity into 60 networks was highly reproducible in our study (Figure 6.3, Table 6.1, Supplementary Figure S4 Study 2), allowing us to circumvent difficulties of ROI-based FCN definitions, such as reliance on the problematic assumption of universality of FCN structure regarding different tasks and individuals. Along similar lines, RSN templates for investigating task questions does not comply with their non-uniformity across different tasks (Fornito et al., 2012; Laird et al., 2011; Utevsky et al., 2014). A line of benefits arises from the ICA's characteristic of decomposing data in a bottom-up data-driven manner. The brain is a complex system in which individual components are characterized by multiplicity, connotating that intermingled neuronal populations within one region can have distinct structural connections and that they may form unique functional assemblies. For example, the hippocampus is composed of subregions that differ in cellular organization and connectivity (Eldridge et al., 2005).

Figure 6.3

ICs with a particularly low and high spatial reproducibility

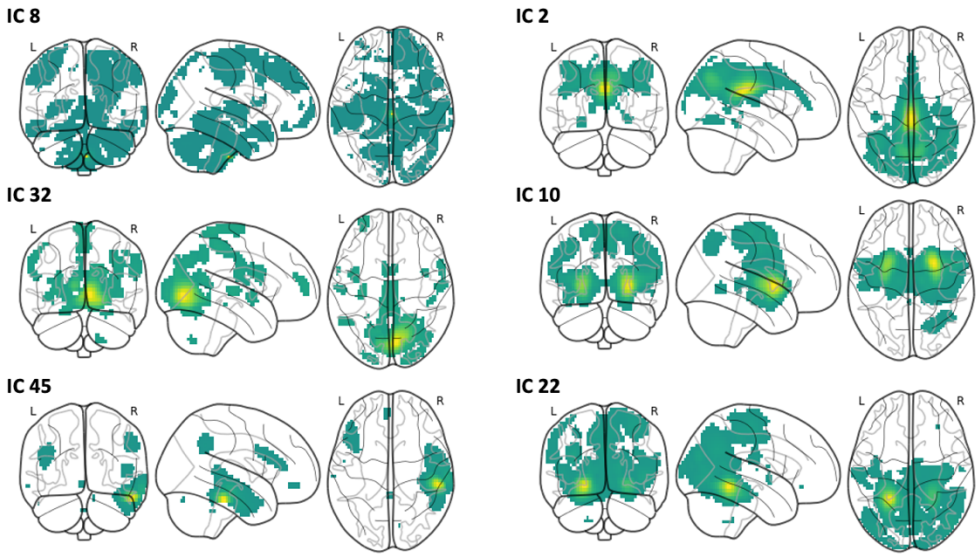

Note. The brain maps show ICs from Study 2 with a particularly low and high spatial reproducibility (left and right columns, respectively). The between-sample correlation values are provided in Table 6.1 (for calculation, see Study 2).

There is ambiguity regarding what constitutes a large-scale FCN. The exact setup of functional assemblies as the building blocks that form the backbone of FCNs across the brain is largely context-sensitive. Despite general agreement on the taxonomy of well-known FCNs

(Smith et al., 2009; Uddin et al., 2019), their occurrence is not uniform across contexts. For example, the DMN may fractionate into subnetworks in a context-specific and stimulus-sensitive manner.

Table 6.1

Between-sample correlation values of ICs with particularly low and high spatial reproducibility

IC	Correlation value (|*r*|)
2	0.987
8	0.437
10	0.977
22	0.972
32	0.347
45	0.333

Note. Matching brain maps are shown in Figure 6.2. See Study 2 for calculation of *r* and Study 2 Supplementary Table S1 for correlation values of each of the 60 ICs.

Template-directed approaches rely on previously described FCNs. They are typically oriented on topological landmarks such as brain regions (i.e., nodes). They may therefore ignore the context-specificity of the FCNs. Along similar lines, many template-based approaches require anatomical delineation of brain regions, which may miss out on the observation that many brain regions may better be described in terms of gradients without clear boundaries. This becomes even more important when moving from the individual-space to the group-space due to the richness of inter-individual differences in brain morphology. Therefore, a particular advantage of ICA is that it does not call for a priori node definition, a liberty that can cleverly handle subject-specific individuality in brain morphology.

In case of ICA, a priori arbitrary thresholding of what defines a connection between nodes is redundant. Definitions often include prior assumptions about the existence of structural connections, which allow for physical proximity rules related to cognitive efficiency and community detection algorithms depending on the chosen null model and a resolution parameter when there is no mathematical ground truth to be used for reference (Sanchez-Rodriguez et al., 2021).

ICA offers full brain coverage, whereas, among many taxonomies of FCNs, full brain coverage is not met, with subcortical regions potentially not being incorporated at all (Uddin et al., 2019). By potentially including non-brain matter, ICA offers a way to model noise

elaborately. Further denoising of inter-individual variance in the BOLD signal may be achieved by experimentally locking individuals' brain activity to the task (Greene et al., 2020).

Consideration 2: Different ways of investigating similar questions

The conclusions we draw from fMRI-based characteristics of FCNs rely on complex modeling of pre-processed fMRI data, which in one way or another involves dimensionality reduction or some other abstraction of lower-level characteristics. Thereby, the spatial resolution and abstraction of the underlying brain activity decrease, leading to loss of data granularity, narrowing down the scope of interpretations drawn based on further analyses. Network-based approaches may not be able to answer all questions regarding brain function.

An example is given by the default mode network (DMN), which is among the most thoroughly investigated FCNs. In humans, functions of the DMN are thought to include moral reasoning, model building, and prospection (Buckner et al., 2008). However, other species thought to lack such higher cognitive abilities have a DMN (Mantini et al., 2011), the question as to why cannot be answered readily when looking at characteristics of the network (e.g., importance of certain network members, interactions with other networks). Rather, such a question might be better approached with methods that focus on the DMN's members (i.e. brain regions or functional units). Ultimately merging different spatial scales and measurement methods into one framework is essential, as shown by a recent finding that cytoarchitectonic properties of the retrosplenial cortex may distinguish regional, layer, and cell-type specific connectivity of the mouse DMN (Whitesell et al., 2021).

Consideration 3: A network is a network because of its members

Moreover, in some way, region-localizationist approaches might favor an interpretation that is more straightforward and more clearly comparable between studies. In task-based fMRI studies, region-localizationist approaches typically involve the mass-univariate voxel-based GLM, in which the BOLD response of each voxel in the brain - or a region of interest - to certain stimuli or tasks get tested in a two-stage procedure. The first step involves inferential statistics on a single-subject level, wherein the sample is the totality of stimuli presented. This step is applied to each subject separately, to then proceed to use the derived estimates on a group-based level (i.e., second-level) to investigate the univariate involvement of voxels in the task of interest (Friston et al., 2007).

This class of approaches has contributed tremendously to our understanding of brain function and has laid the groundwork for network-based approaches. Still, potential pitfalls to this procedure are common knowledge, such as problems arising from statistical thresholding, the shape of the hemodynamic response, or spatial voxel assignment (Dubois & Adolphs, 2016). Region-localizationist approaches provide a level of understanding not given by an approach that investigates a construct that inherently includes higher-order interactions – whether these interactions are modeled or not - such as FCNs derived from ICA or usage of out-of-sample FCN templates. For example, if looking at one region of interest, the impact of falsely delineating that region's location in each subject might be less grave than falsely delineating all regions of a network. As each approach has benefits and pitfalls, they make useful complements. Characterization of functions of localized brain regions is of equal importance as investigation of coordinated activity across the whole brain (Yang et al., 2014) as functional integration and functional specialization inherently depend on each other (Friston et al., 2007).

Outlooks and limitations

Outlook 1: Multifunctionality and interdependencies between brain circuits

The detection of neurobiological underpinnings of complex behavior is not automatically the equivalent of understanding it (Krakauer et al., 2017). Delving deeper into the multifunctionality, temporal hierarchy, and interdependencies of different brain circuits could provide more clarity. For one, similar behavior could originate from different brain circuits; for another, one FCN or brain region could produce different behaviors (Krakauer et al., 2017). Regarding Study 2, the finding that the responsivity of six FCNs while encoding pictures is important for the amount of later recalled pictures implies neither specialization nor absolute necessity of any one of the 6 FCNs. The relatively small variance explained by the ICs (up to roughly 6 %) is in line with this, suggesting that other important neurofunctional mechanisms have not been captured in Study 2. To be explored in future studies is what other cognitive functions these six FCNs fulfill.

Throughout the human cerebral cortex, information processing follows a spatial hierarchy, with primary sensory regions having shorter processing timescales than the longer timescales in higher-order cortical regions (Raut et al., 2020). Given this temporal hierarchy, interdependency between brain circuits can be assumed. A worthwhile challenge could be to

reframe the current findings in a more complex model which may include, for example, interactions between FCNs.

Outlook 2: Additional network modeling approaches

The brain's architecture can be formally described as a complex system consisting of nodes and their edges (Power et al., 2011), thought to constitute brain regions and their connections, respectively (Figure 6.4). This type of network-based viewpoint allows for quantification of hierarchy and substructure within the brain, therewith identification of hubs and critical nodes, and determination of information flow (Power et al., 2011). Hubs describe nodes with a critical role in integrating and distributing information by minimizing the distance between nodes, lowering the metabolic cost of information transfer, such as seen in subcortical structures. Subcortical structures can provide short-cuts between lower sensory areas and higher-cortical areas to promote higher cognitive function (Fransson & Thompson, 2020). Hubs have been suggested to possess the ability to modify interactions between distributed systems allowing for the completion of complex tasks (Gratton et al., 2016). The constellations of hubs is dynamic and adjusts based on task state (Fransson & Thompson, 2020). It would be interesting to investigate the exact nodal structure of the FCNs of Study 2, for example with the usage of graph modeling (Power et al., 2011).

Figure 6.4

Resting-state fMRI data modeled as graphs based on 264 putative functional areas to reveal functional connectivity networks (Power et al., 2011)

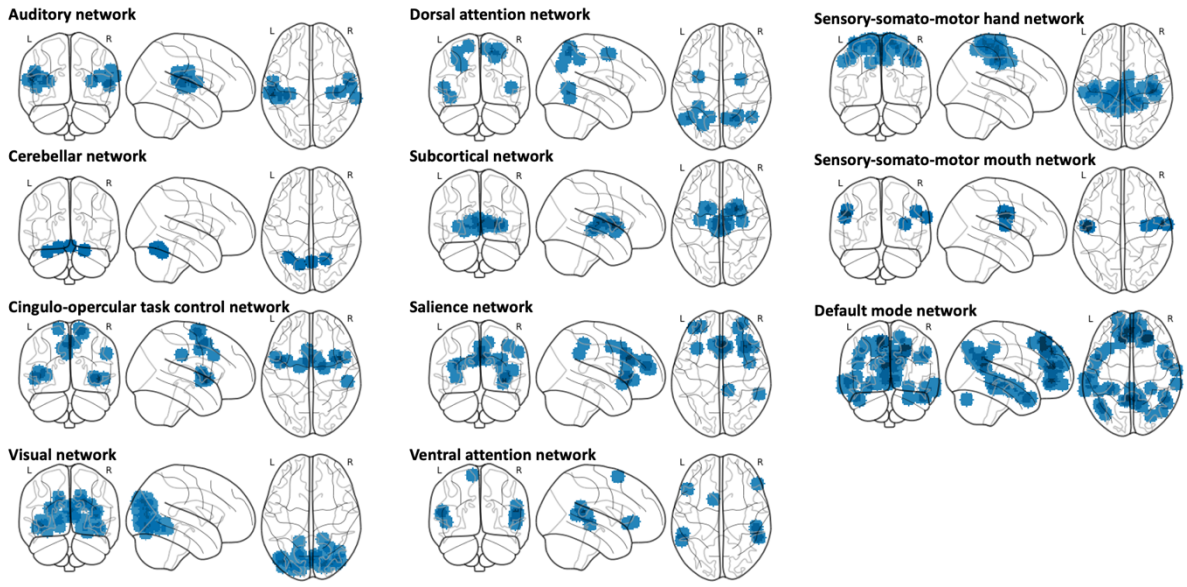

Outlook 3: Prediction modeling to strengthen our findings on inter-individual differences

It has been argued that prediction modeling may be necessary to ensure the generalizability of the results of brain-behavior correlations to out-of-sample individual subjects (Dubois & Adolphs, 2016). Prediction modeling as an expansion of our studies could be a direction worth exploring. Despite the attractivity of using the sample of Study 2 for this endeavor, the potential issue of double dipping (Kriegeskorte et al., 2009) would need to be considered, as conducting similar analyses on one sample repeatedly may lead to a bias of results.

Outlook 4: The experimental paradigm

Humans integrate various sensory information to produce a unitary experience of the external world. Accordingly, there has been a growing consensus on the importance of including the study of behavior closer to its natural occurrence, which could, for example, be afforded by virtual reality experiments (Faul et al., 2020). In their fMRI-based study on fear-conditioning, Faul and colleagues (2020) used virtual reality to show that the spatial proximity of threat affects learning and extinction. Moreover, presence versus absence of conspecifics might affect neural activity, which could be relevant for investigating episodic memory and emotion processing (Mulej Bratec et al., 2020). With a bearing on Study 1, the division between resting-state and task-state in a natural environment, which is what we ultimately wish to generalize our findings to, might not be evident. Different emotion processing types might have distinct time scales (Hollenstein, 2015). The effectiveness of emotion regulation strategies might be linked to inter-individual differences and rely more on flexibility rather than rigid selection of one and the best emotion regulation strategy (Fernandez et al., 2016). Complementing laboratory-based experimental studies with more naturalistic ones could fuel future advances in the study of adaptive human behavior.

Strengths

Strength 1: Fundamental findings

The most prevalent fMRI-based paradigm involves the assessment of differences in the central tendency of one or more dependent variables based on differences between conditions or groups (Cooper et al., 2019) to answer fundamental questions, such as the involvement of

different brain regions in subsequent memory effects in Study 2, or the effects of emotion processing on rs-FC in Study 1.

Strength 2: Finding a balance of parameters in a multi-dimensional feature space

Nevertheless, this group of statistical approaches may encourage a discrete conception of behavioral variables because the independent variable is modeled as discrete (e.g., experimental conditions A and B, groups A and B). This may cause oversimplification and negligence of inter-individual differences.

An individual could be profiled as a unique setup of features sampled from an infinite number of features. However, by tailoring a model to one individual, an issue of inference may arise, in that the function of the features in the model of that individual can only be asserted after observing a large array of samples of that individual to then embed the profile into a larger context. If it were only a snapshot, neither the stability of an individual's profile (i.e., model) nor its functional consequences would be evident. Put differently, an individual's profile captures the setup of features in one moment. However, because there is no link to future, past, nor other individuals, it cannot be used to provide a meaningful bigger picture. To put it into context with the profile of other individuals or other contexts of that individual, a representative subset of features needs to be selected and assessed for its distribution.

To conclude, for understanding and making use of a high-dimensional snapshot of one individual, group-based studies are fundamental. A balanced and well-reflected set of features comprehensible enough from the full scope of possible features is a necessity for that transition. A particular strength of both our studies has been the elaborate reduction of dimensionality of the brain's functional architecture to a comprehensible set of FCNs, while involving multiple validation steps.

Strength 3: A balanced and highly representative sample

Appropriate variability in sample characteristics

Study 2 substantially adds to research about episodic memory by exploring a carefully validated reduced feature space in a sample that is preeminent beyond its large size. A large sample size is required to increase statistical power (Dubois & Adolphs, 2016). Additionally, validity and reliability, i.e., whether we are measuring what we intend to and whether the findings are stable in the face of presumable irrelevant variations, respectively, are seminal

(Dubois & Adolphs, 2016). These, among others, critically hinge on sample characteristics. The sample of Study 2 is characterized by an outstanding balance between homogeneity and informative variability in terms of the behavior investigated.

In this context, with regards to the null hypothesis statistical testing, studying a sample of healthy individuals has the major advantage of grounding hypotheses on a null hypothesis that is representative of a large part of the population. Rejection of H_0 is frequently misunderstood as accepting a specific H_1 (Szucs & Ioannidis, 2017). Therefore, an H_0 based on a sample with relevant variance is critical. Even if H_1 captures a true effect, it does not indicate that there are no other true alternative hypotheses or that the group effects stem from differences in the grouping variable. This makes it all the more important to have a well-balanced sample in terms of variability.

The benefits of the age range in our sample

Noteworthy in this context is the age range of our samples. Over the life span, cortical development progresses from lower-order, primary and unimodal cortices to higher-order, transmodal cortices (Sydnor et al., 2021). Phylogenetically older, lower-order functional systems undergo refinement in childhood. In contrast, evolutionarily newer systems, which serve higher-order faculties, continue to mature, wherein restructuring of functional system connections takes place until adulthood, leading to greater between-individual functional connectome distinctiveness (Sydnor et al., 2021). Correspondingly, the age of onset for many mental disorders is in the early third decade of life (Kessler et al., 2007). This indicates that the age range of our samples may be particularly well-suited for researching basic mechanisms, as these require similar variance (in the case of one-sample tests), as well as for investigating inter-individual differences, which requires meaningful variability. Multiple lines of evidence support the claim that maturational variability within higher-order association cortices is causally related to inter-individual variability in psychological functioning and psychiatric illness (Sydnor et al., 2021).

Conclusion on sample characteristics to investigate complex behavior

To conclude, for understanding complex behavior at group-level and the level of inter-individual differences, a sample needs not only to be large enough to be statistically well-powered (Dubois & Adolphs, 2016), but it needs to have certain characteristics such as

sufficient homogeneity yet also representative and informative variability. This can be achieved with a large population of healthy individuals aged in the critical range of neurodevelopment likely to be relevant for psychiatric illness and critical behavioral phenotypes such as episodic memory and emotion processing.

Strength 4: Complementary approaches

As discussed, each approach has its advantages and pitfalls. It is a strength that this PhD project has addresses episodic memory and emotion processing with different approaches.

Overall conclusions

The view of the brain functioning as a network has garnered considerable attention over the past years. This PhD project has corroborated further support for the meaningfulness of this notion, during states of resting and engagement in an episodic memory encoding task. The illuminating results foster our understanding of emotion processing and episodic memory, which are vital across the spectrum of mental health and mental disorders.

While much had been known about immediate brain activity changes induced by emotional stimuli, the subsequent temporal unfolding of emotions had yet to be explored. Study 1, employing a resting-state fMRI paradigm, sought to fill this gap. We found that resting-state networks, as well as the amygdala's low-frequency oscillations, appear to be unaffected by preceding exposure to widely used emotionally aversive visual stimuli in healthy young adults.

Study 2 has offered, for the first time, robust insights into brain regions and networks involved in inter-individual differences in episodic memory and compared these neurofunctional underpinnings with those of successful memory encoding on the subjects' group-level. Study 2 managed to unravel basic memory function common to a group of individuals as well as inter-individual differences ocurring in that group of individuals.

Learning more about episodic memory and emotion processing in the healthy is a premise upon which our understanding of mental disorders is based. Identifying neurofunctional markers based on inter-individual differences in memory may open the possibility for studying associations with other individual phenotypes, such as psychological traits, genetic or epigenetic makeup, or individual metabolomic profiles.

Supplementary material: Study 1

Supplementary Figure S1

Brain maps thresholded at F < 7 illustrating voxels with different FC to the amygdala depending on segmentation method (FreeSurfer vs. FSL First) at baseline resting-state ($F_{min}(2,29) = 8.85$, minimum number of voxels in one cluster = 56), depicted in axial slices (Z = 26.40 to Z = 57.20 in MNI space)

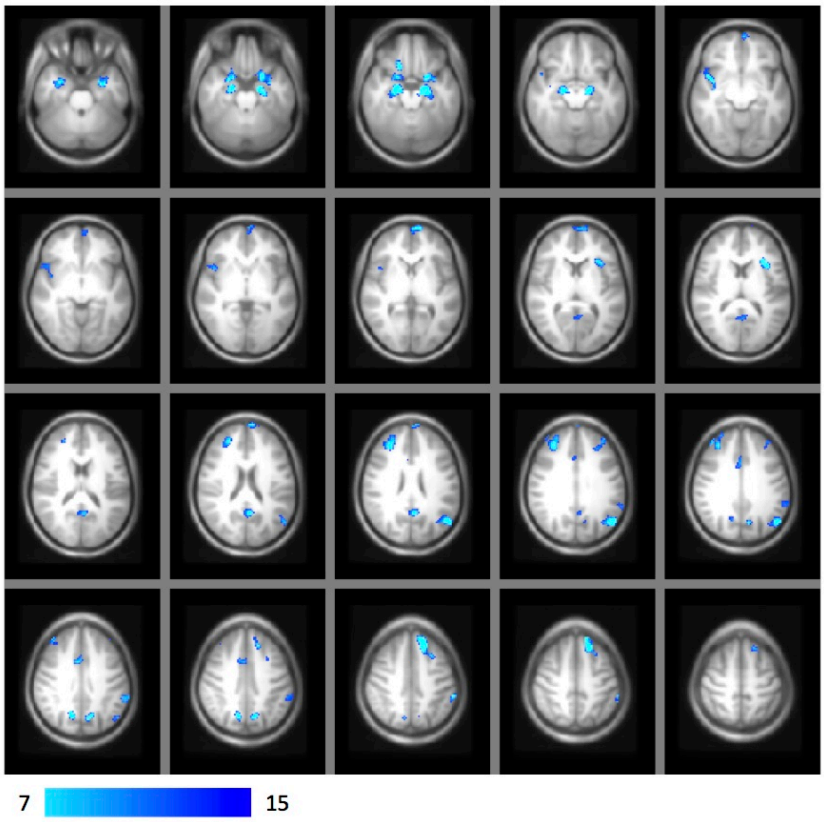

Supplementary Figures S2A-O

Brain maps depicting the spatial overlap of the 10 template networks (green) with the 20 ICs derived from our data (blue), encompassing axial slices (Z = 26.40 to Z = 57.20 in MNI space).

Note. Indices and details on strength of cross-correlation are used in accordance with the denotations in Table 2. 2A: VN1-IC4; 2B: VN1-IC8; 2C: VN2-IC8; 2D: VN3-IC10; 2E: VN3-IC12; 2F: DMN-IC3; 2G: CN-IC15; 2H: CN-IC18; 2I: SMN-IC5; 2J: ADT-IC12; 2K: ECN-IC2; 2L: ECN-IC7; 2M: LFPN-IC2; 2N: LFPN-IC11; 2O: RFPN-IC14. Abbreviations: IC=independent component (from our data); VN=visual network; DMN=default mode network; CN=cerebellum network; SMN=sensorimotor network; ADT=auditory network; ECN=executive control network; LFPN=left frontoparietal network; RFPN=right frontoparietal network.

Supplementary Figure S2A

VN1-IC4

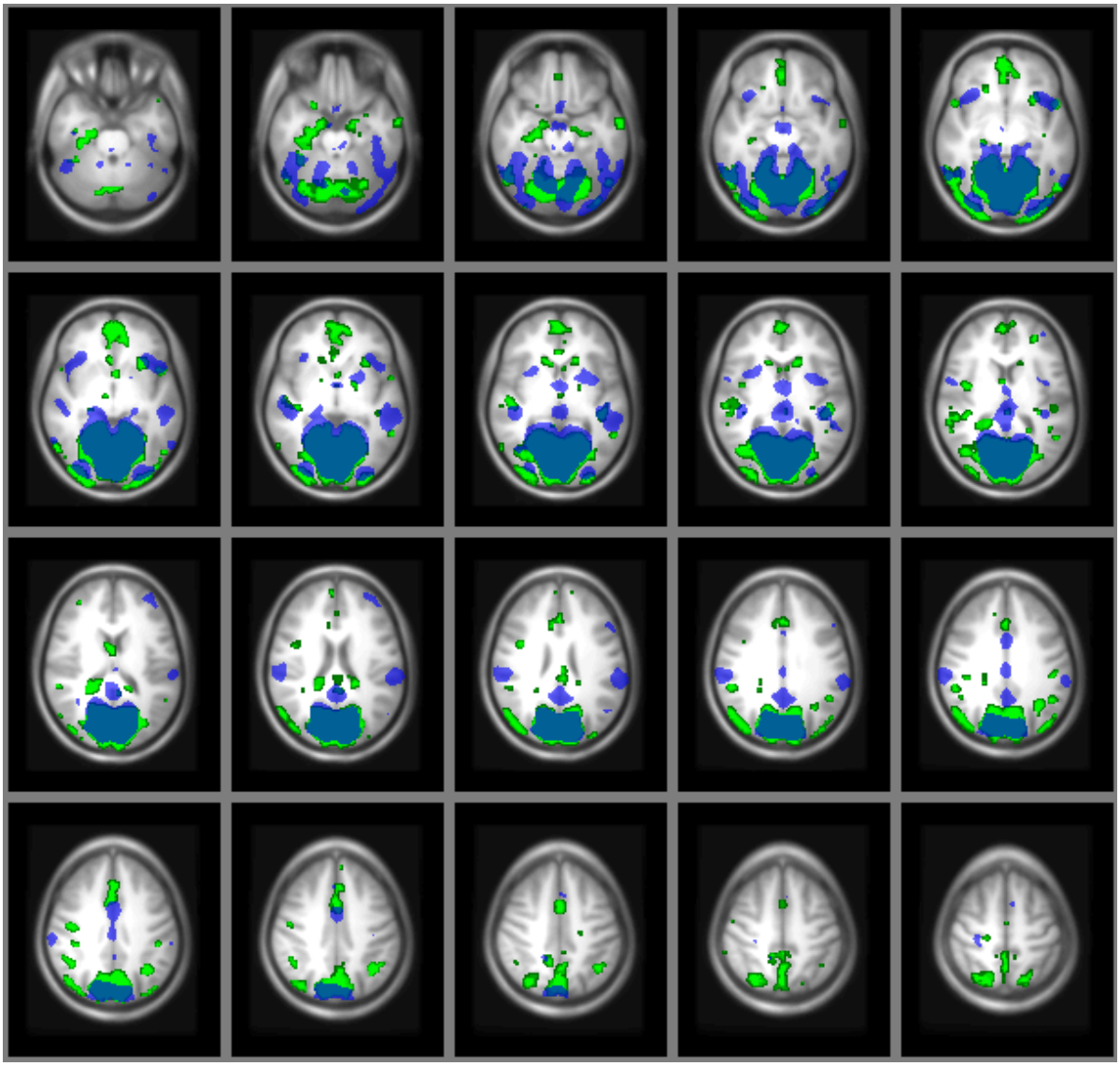

Supplementary Figure S2B

VN1-IC8

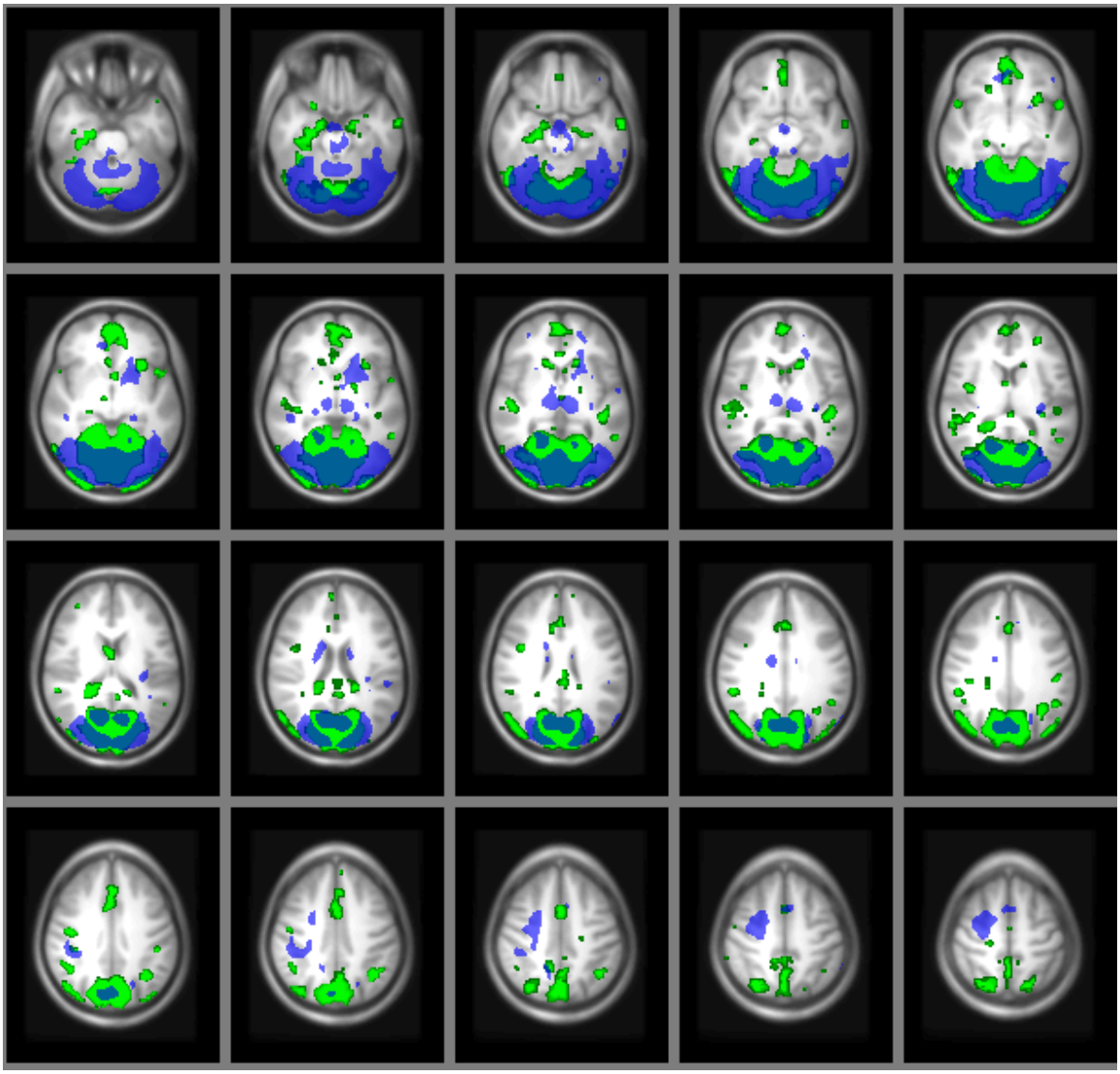

Supplementary Figure S2C

VN2-IC8

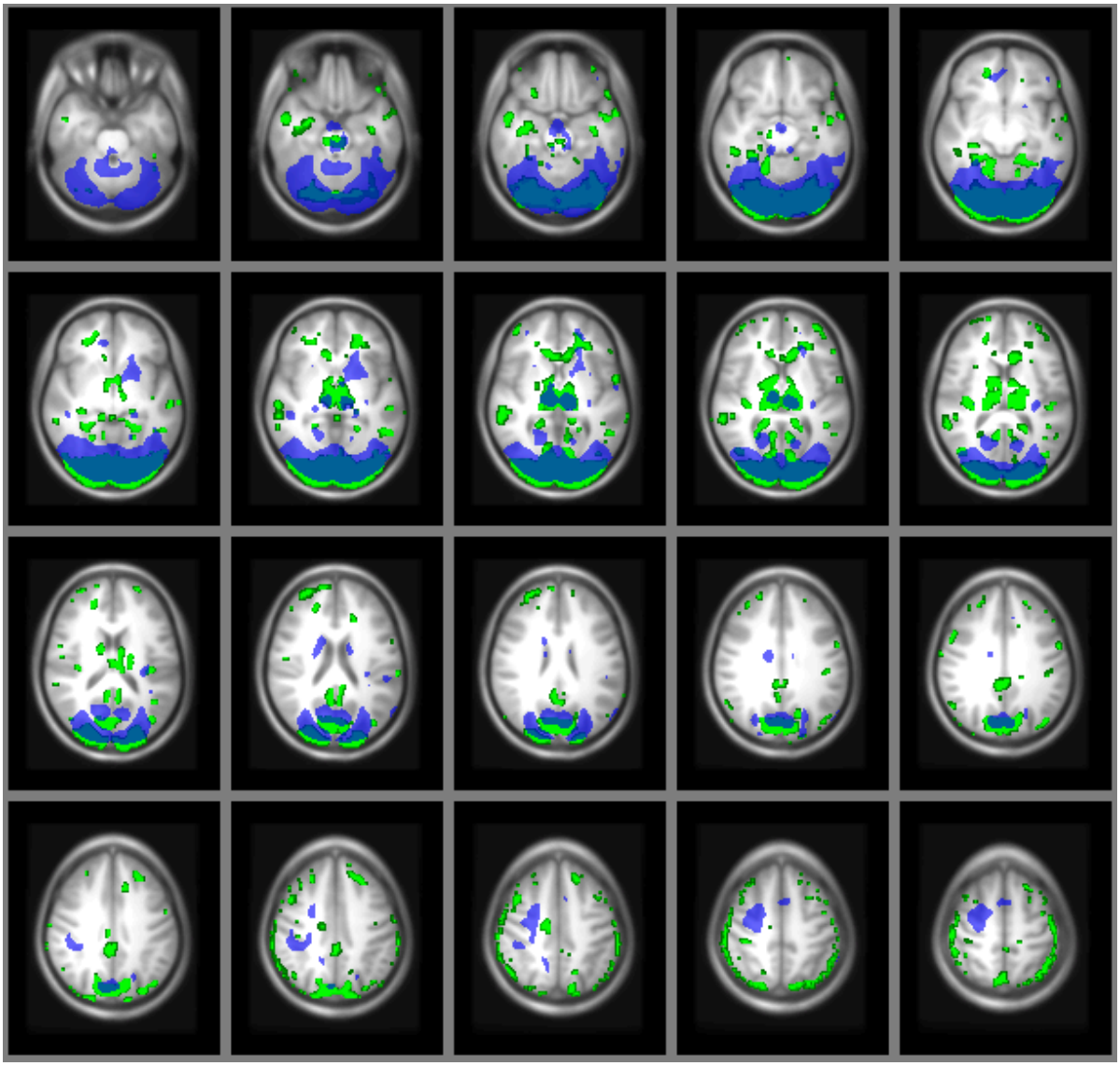

Supplementary Figure S2D

VN3-IC10

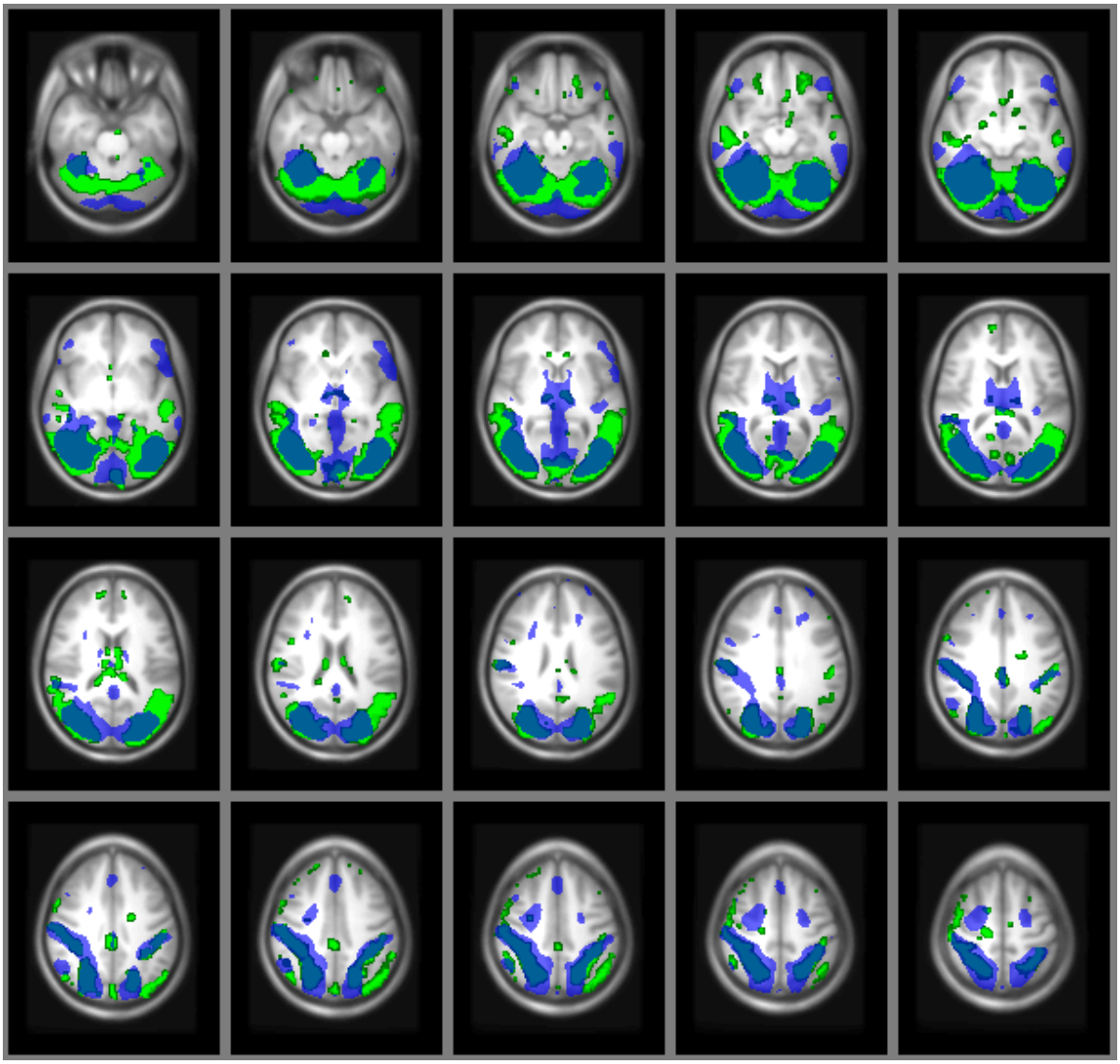

Supplementary Figure S2E

VN3-IC12

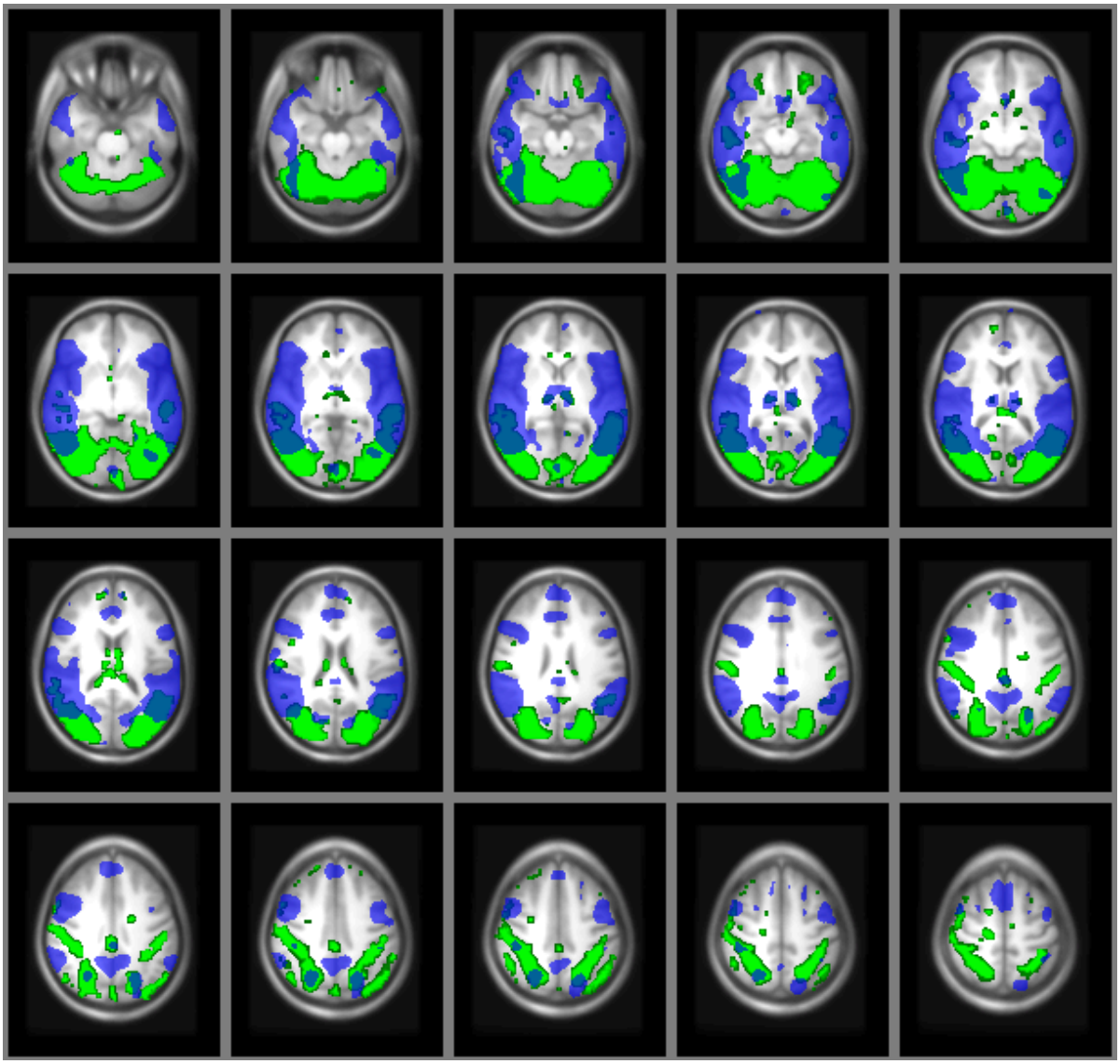

Supplementary Figure S2F

DMN-IC3

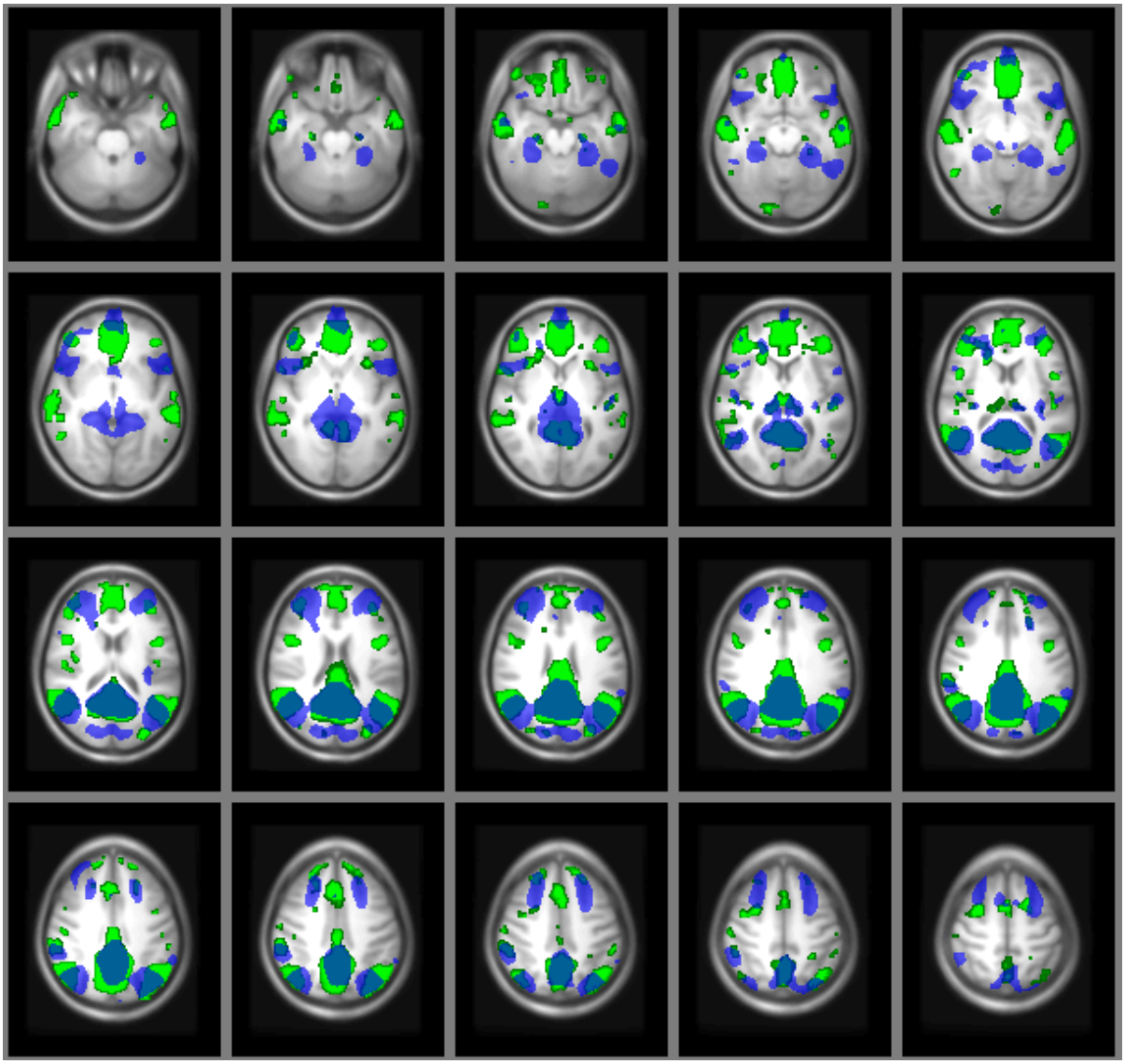

Supplementary Figure S2G

CN-IC15

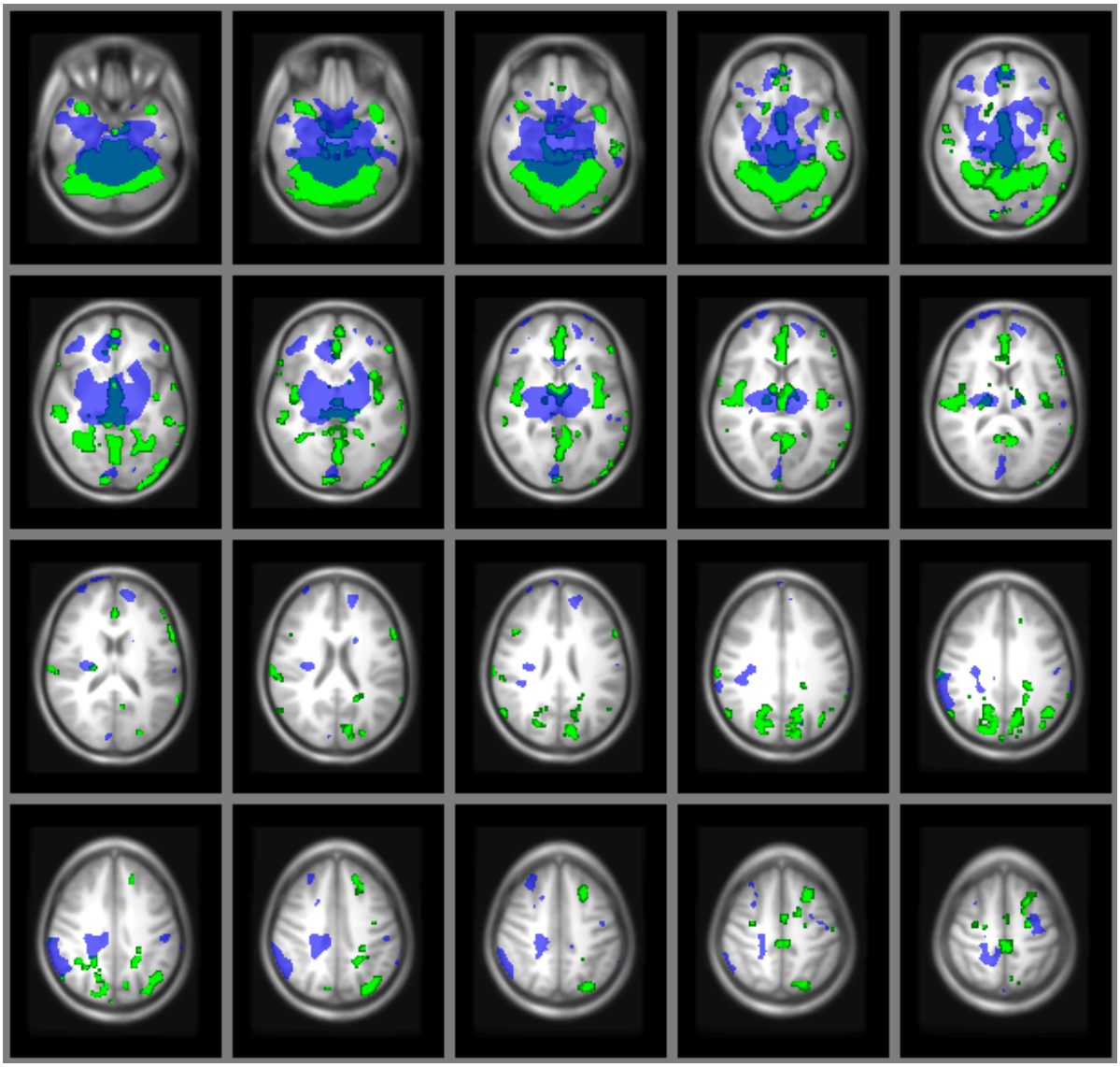

Supplementary Figure S2H

CN-IC18

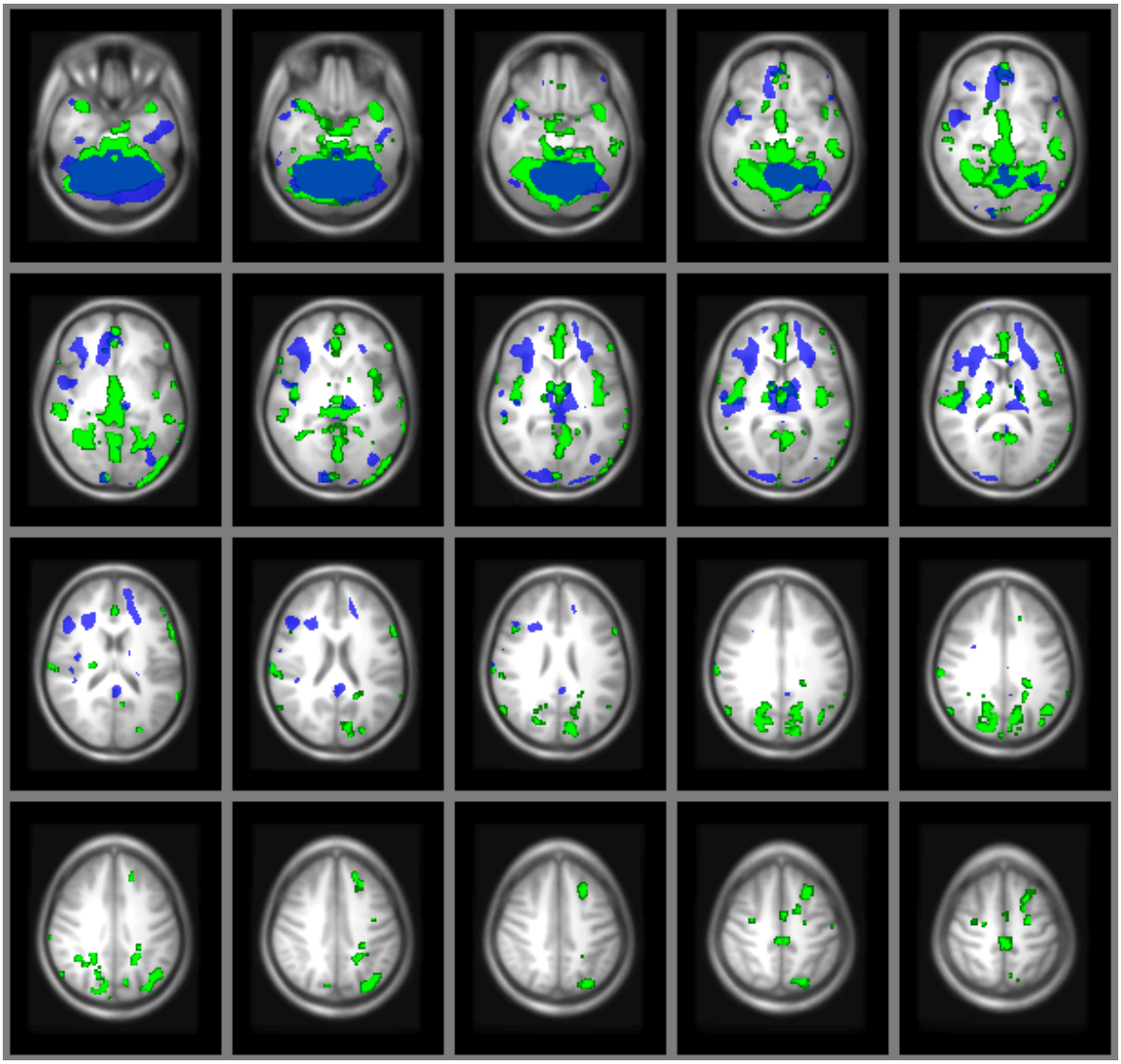

Supplementary Figure S2I

SMN-IC5

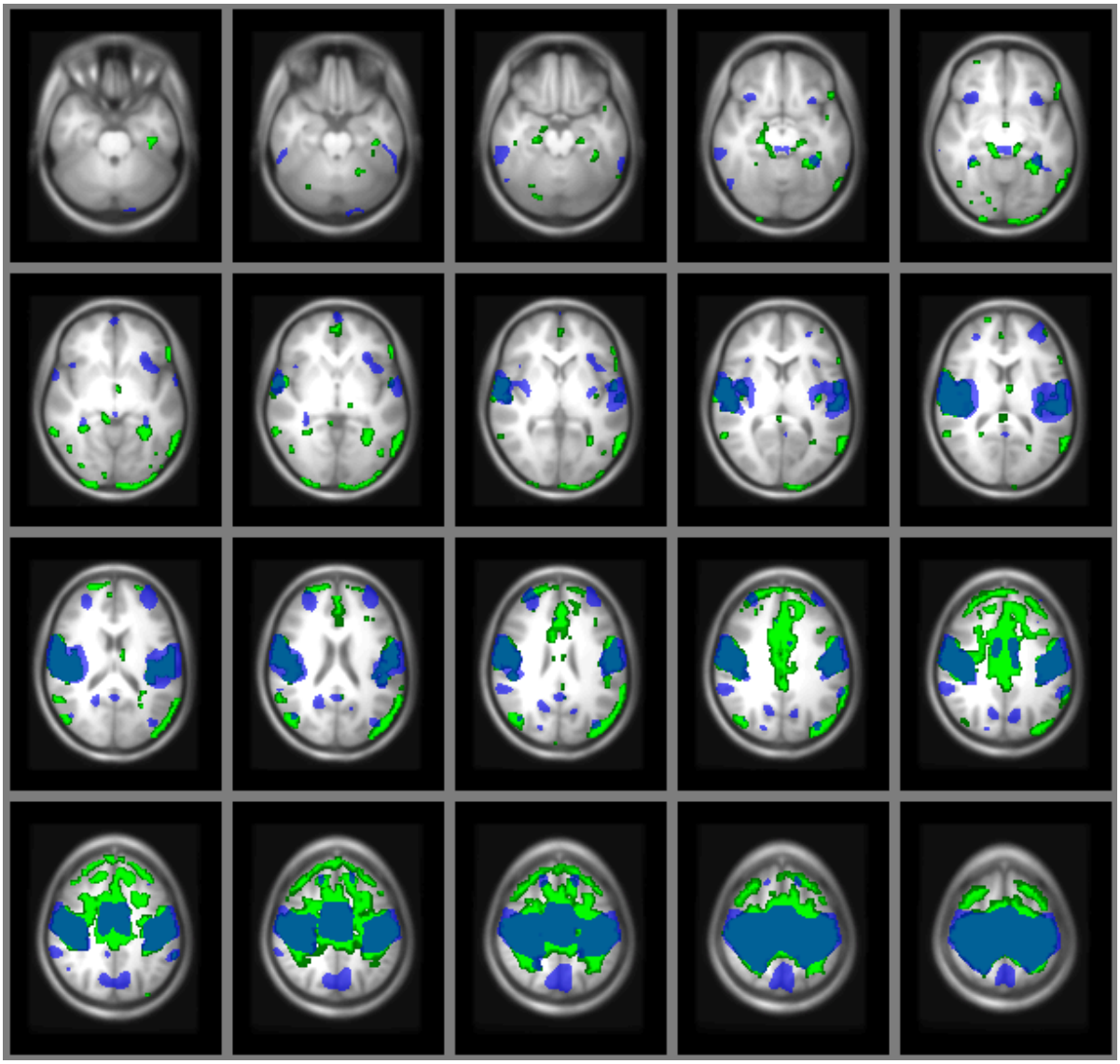

Supplementary Figure S2J

ADT-IC12

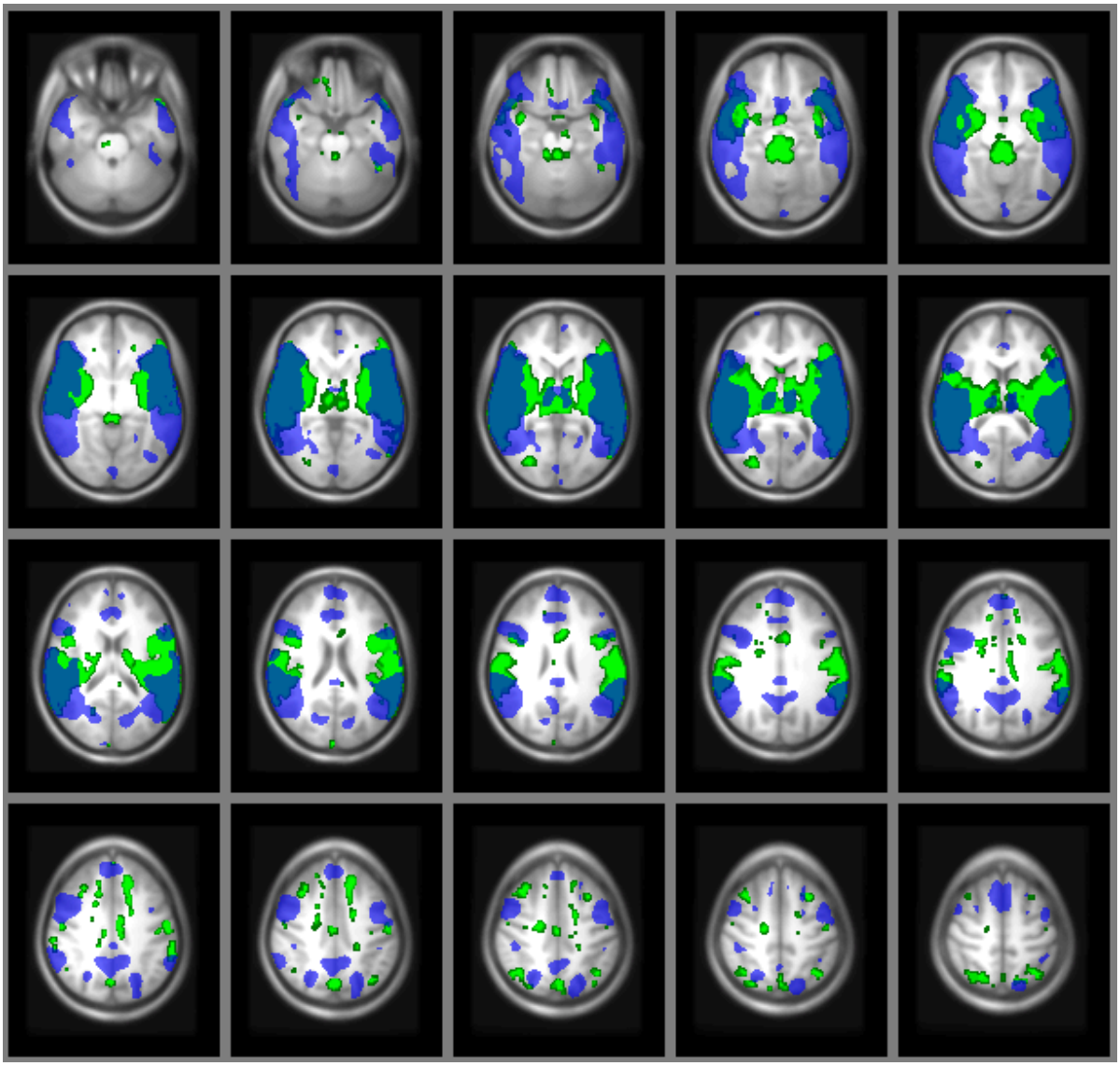

Supplementary Figure S2K

ECN-IC2

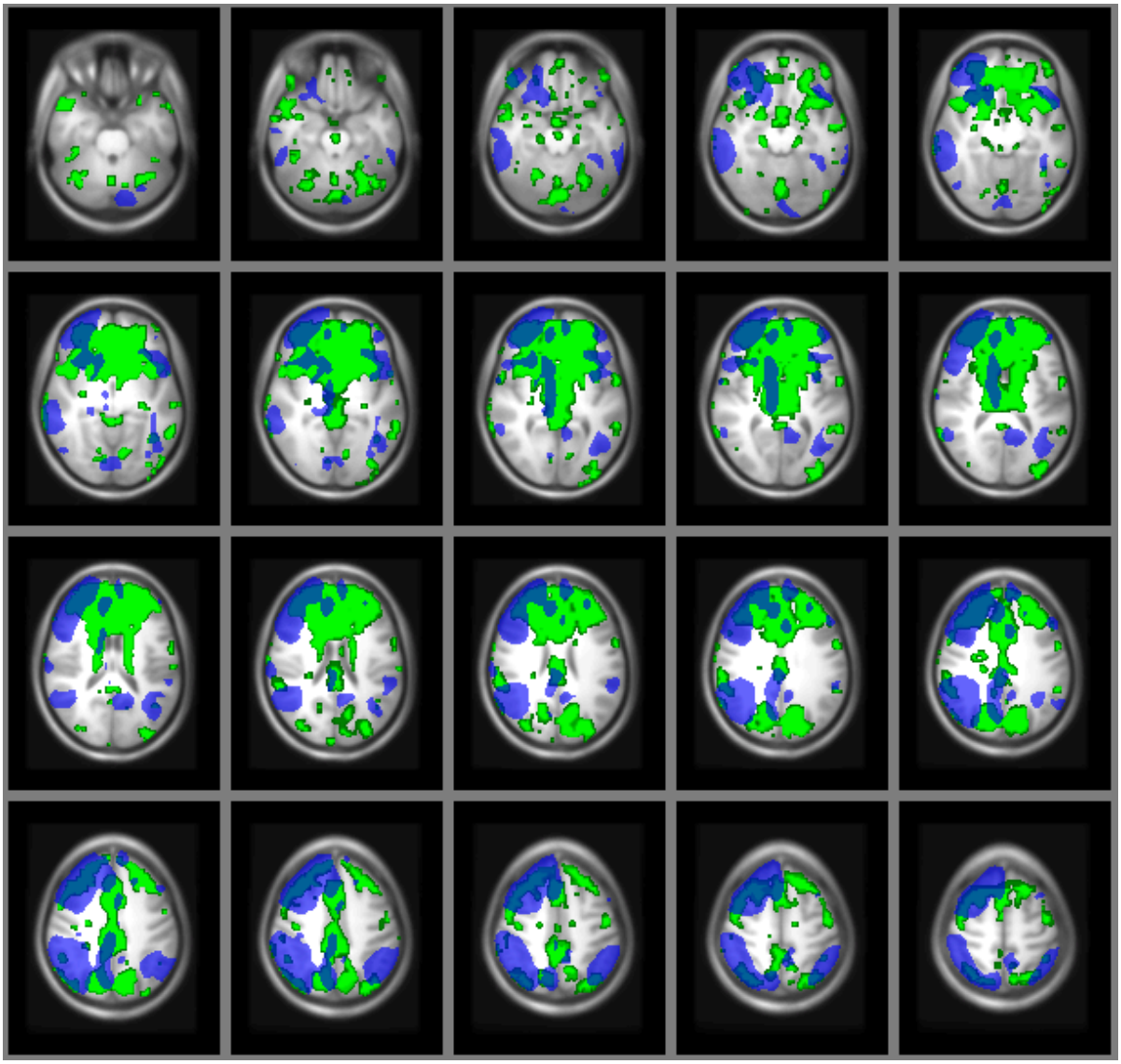

Supplementary Figure S2L

ECN-IC7

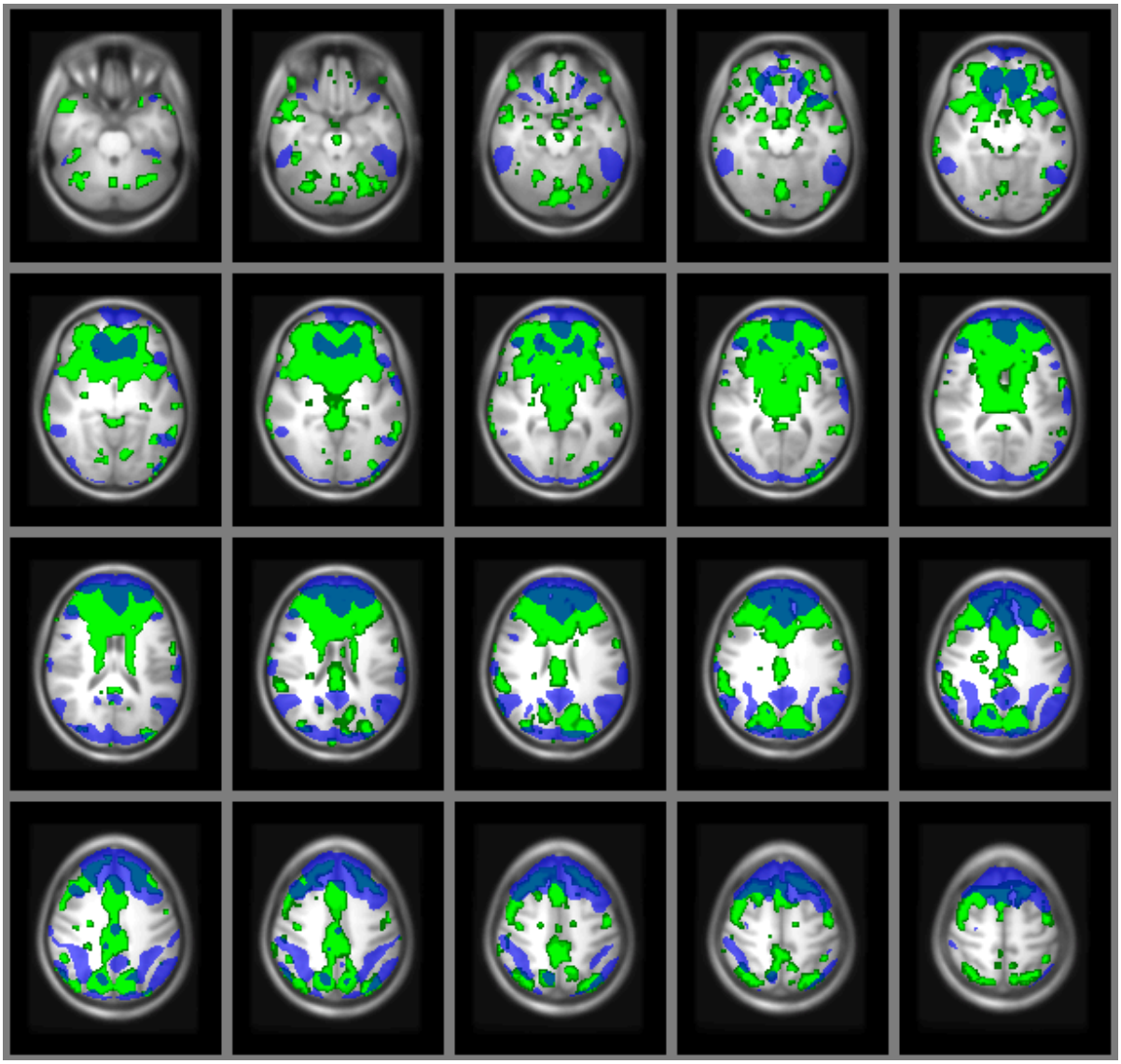

Supplementary Figure S2M

LFPN-IC2

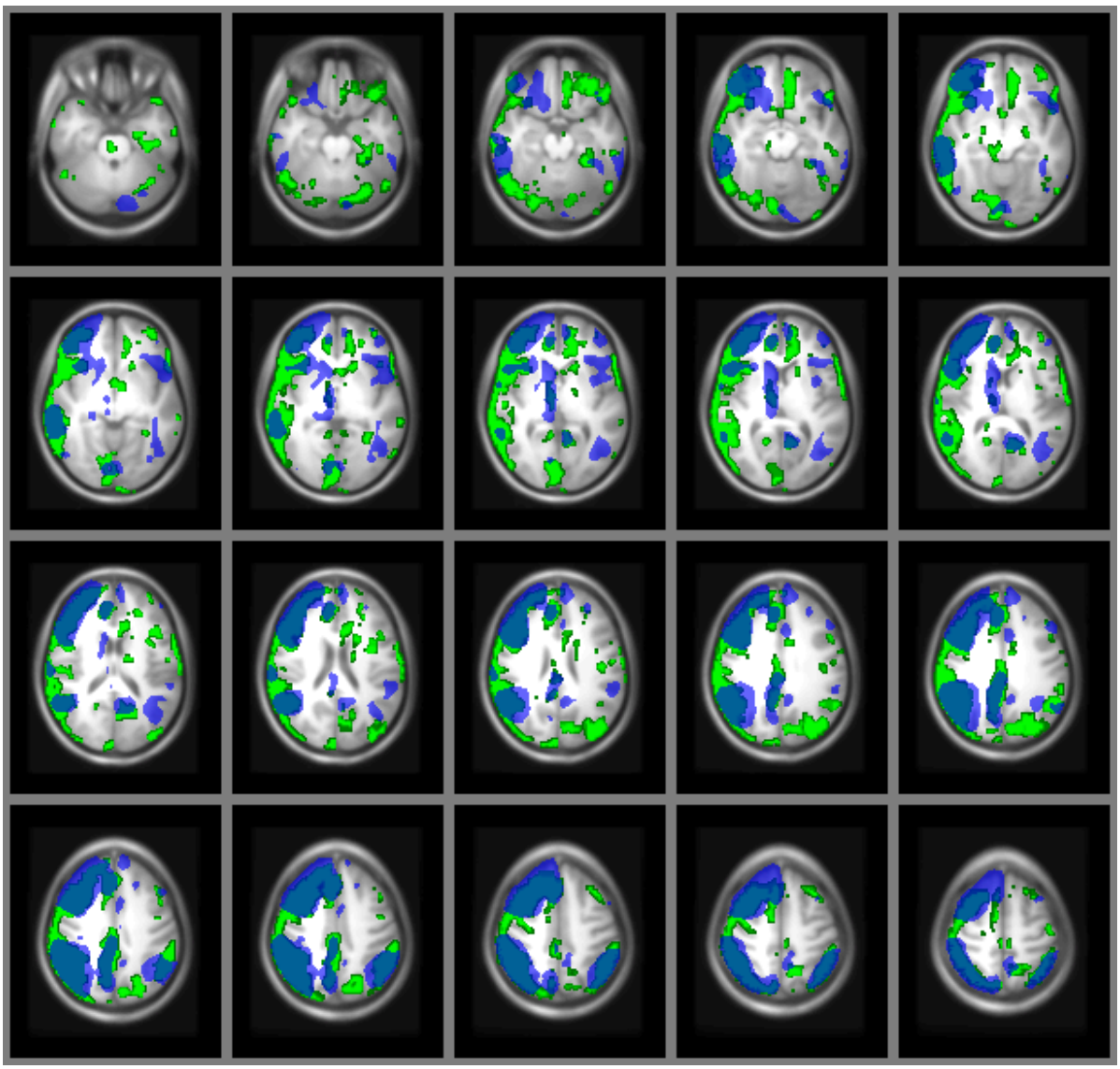

Supplementary Figure S2N

LFPN-IC11

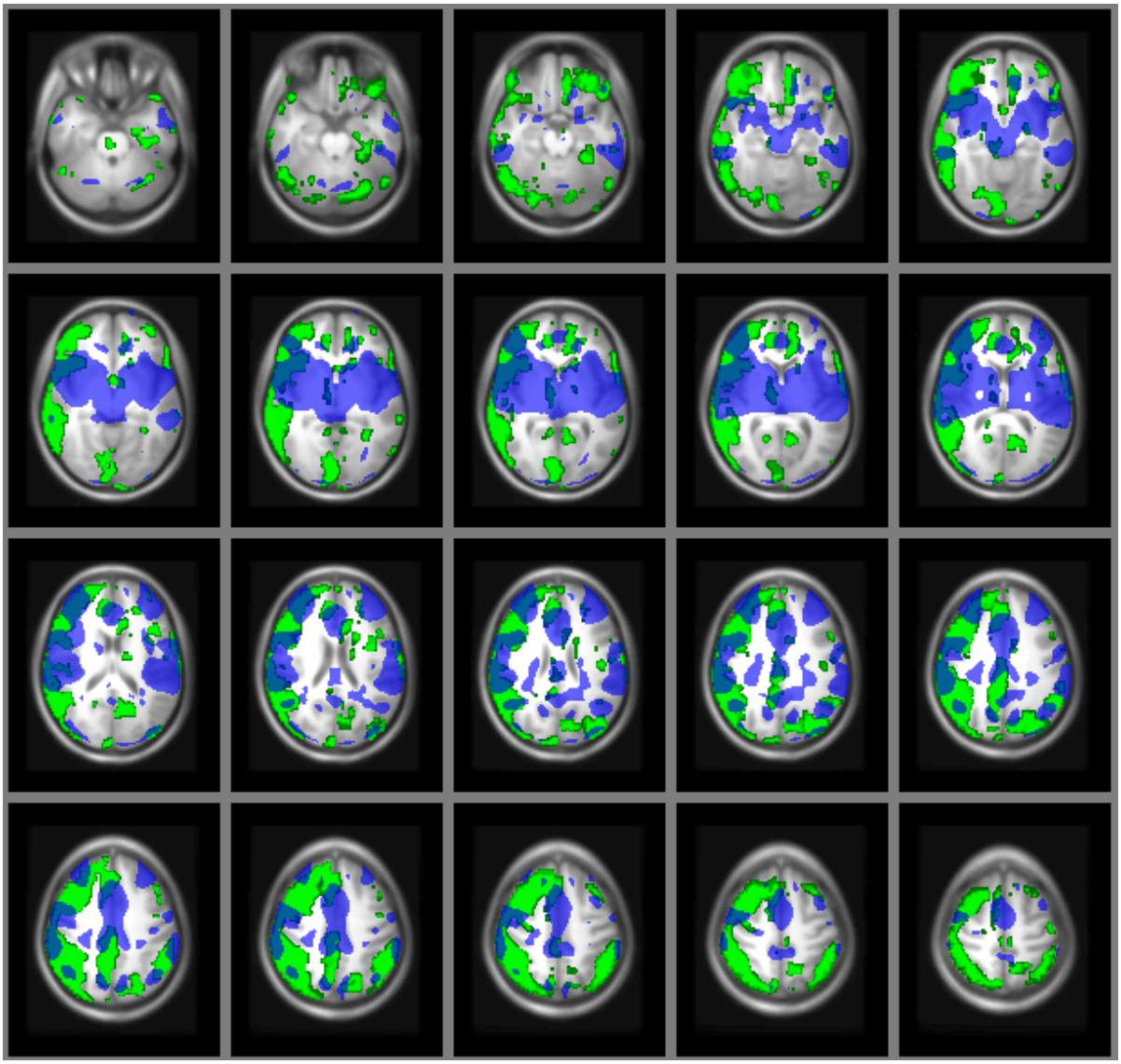

Supplementary Figure S2O

RFPN-IC14

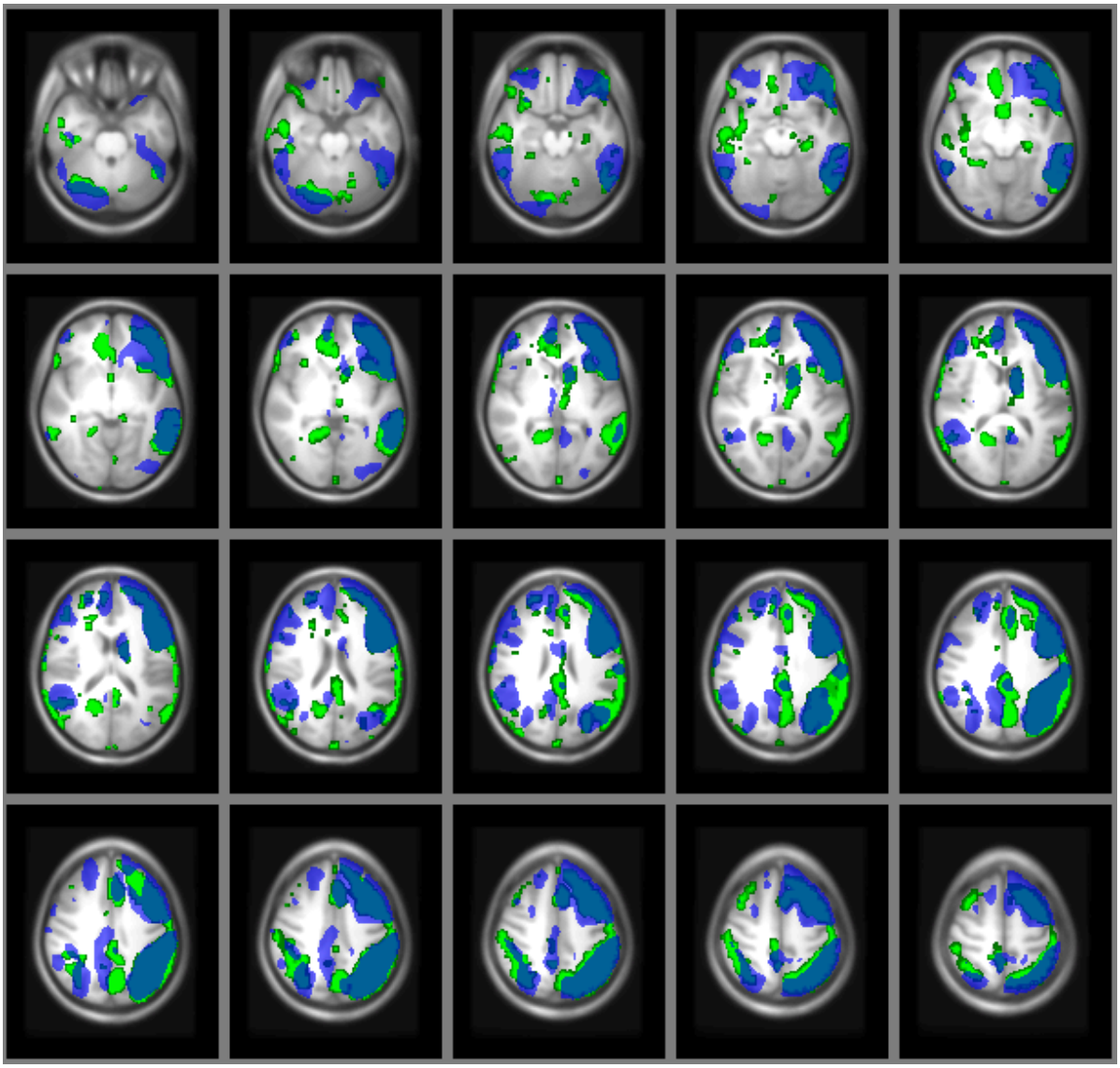

Supplementary Table S1

Description of questionnaires in this study, ordered in the way they were completed

Abbreviation	Questionnaire	Measure	Scoring
EHI	Edinburgh Handedness Inventory (Oldfield, 1971)	Handedness	10 items
ESS	Epworth Sleepiness Scale (Johns, 1991)	Chance of dozing in general	7 items, maximal score 21, relative cutoff 9 (variable)
STAI trait	State-Trait-Angstinventar (Laux et al., 1981)	Levels of anxiety in general	20 items, maximal score 80
NEO-FFI	NEO-Fünffaktoren-Inventar (Borkenau & Ostendorf, 1993)	Personality comparted into neuroticism, extraversion, openness, agreeableness and conscientiousness	60 items, maximal 48 per factor
AIM	Affect Intensity Measure (Larsen & Diener, 1987)	Affective reagibility in general, subdivided into negative affect intensity (NI), positive affect intensity (PI) and serenity	29 items, maximal total score 116, NI 40, PI 40, serenity 36)
ADS	Allgemeine Depressionsskala (Hautzinger & Bailer, 1993)	Depression scores in the last 7 days	20 items (long version), maximal score 60, recommended cutoff 23
STAI state	State-Trait-Angstinventar (Laux et al., 1981)	Momentary levels of anxiety	20 items, maximal score 80

Supplementary Table S2

Normative arousal and valence scores of an American sample (Lang et al., 2005)*, in which a rating scale from 1 to 9 was used, for the pictures utilized in the main task and the preceding training in our study*

		Negative pictures	**Neutral pictures**
	Rating	***M(SD)***	***M(SD)***
Main task	Arousal	5.76(2.19)	3.61(1.99)
	Valence	2.47(1.49)	5.23(1.35)
Training	Arousal		3.14(2.06)
	Valence		5.59(1.18)

Note. Numbers represent the mean *(M)* and standard deviation *(SD)* of the negative and neutral IAPS pictures individually, as used in the negative- and neutral-group, respectively.

Supplementary material: Study 2

Supplementary Figure S1

Statistical brain map of the group-based subsequent memory effects

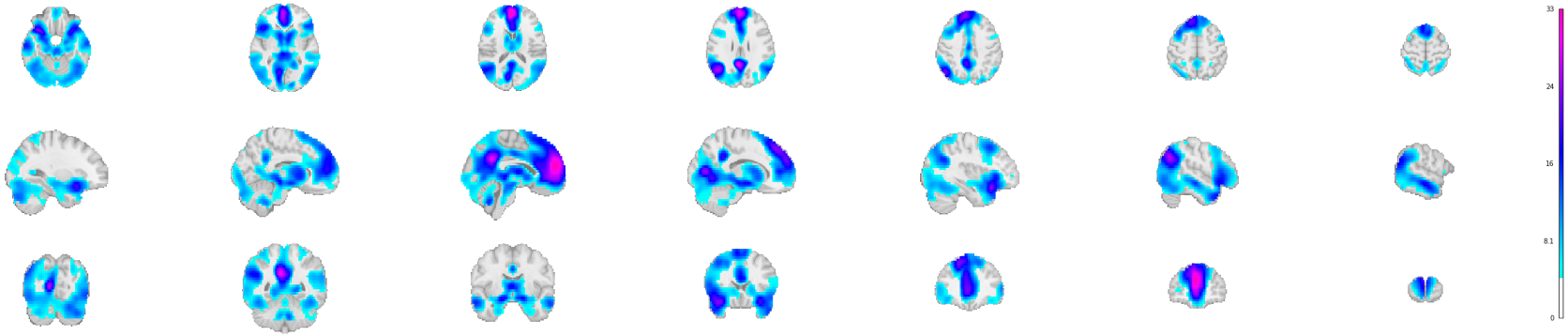

Note. The images are corrected for multiple comparison at the whole-brain level (two-sided *FWE* $p < 0.05$).

Supplementary Figure S2

Voxel intensity value distribution of the subsequent memory effects

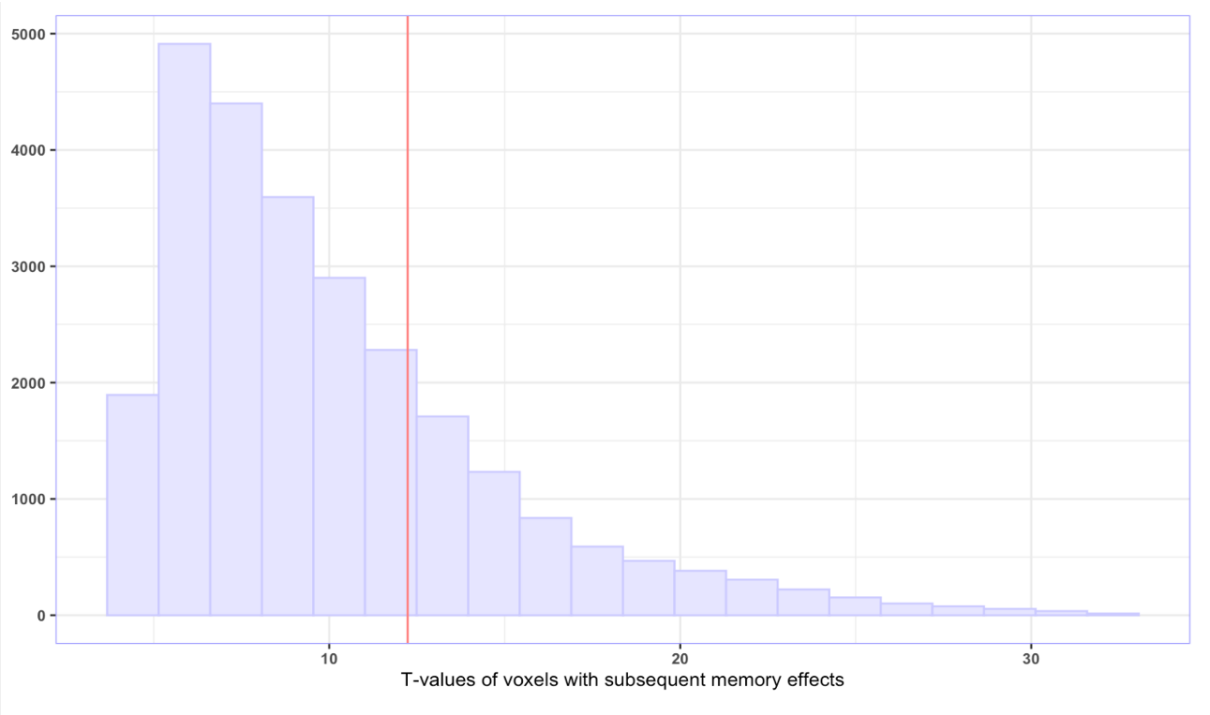

Note. The voxels included are the ones that passed statistical significance. The red line indicates the 75th percentile with a value of 12.235.

Supplementary Figure S3A

The full set of ICs during picture encoding

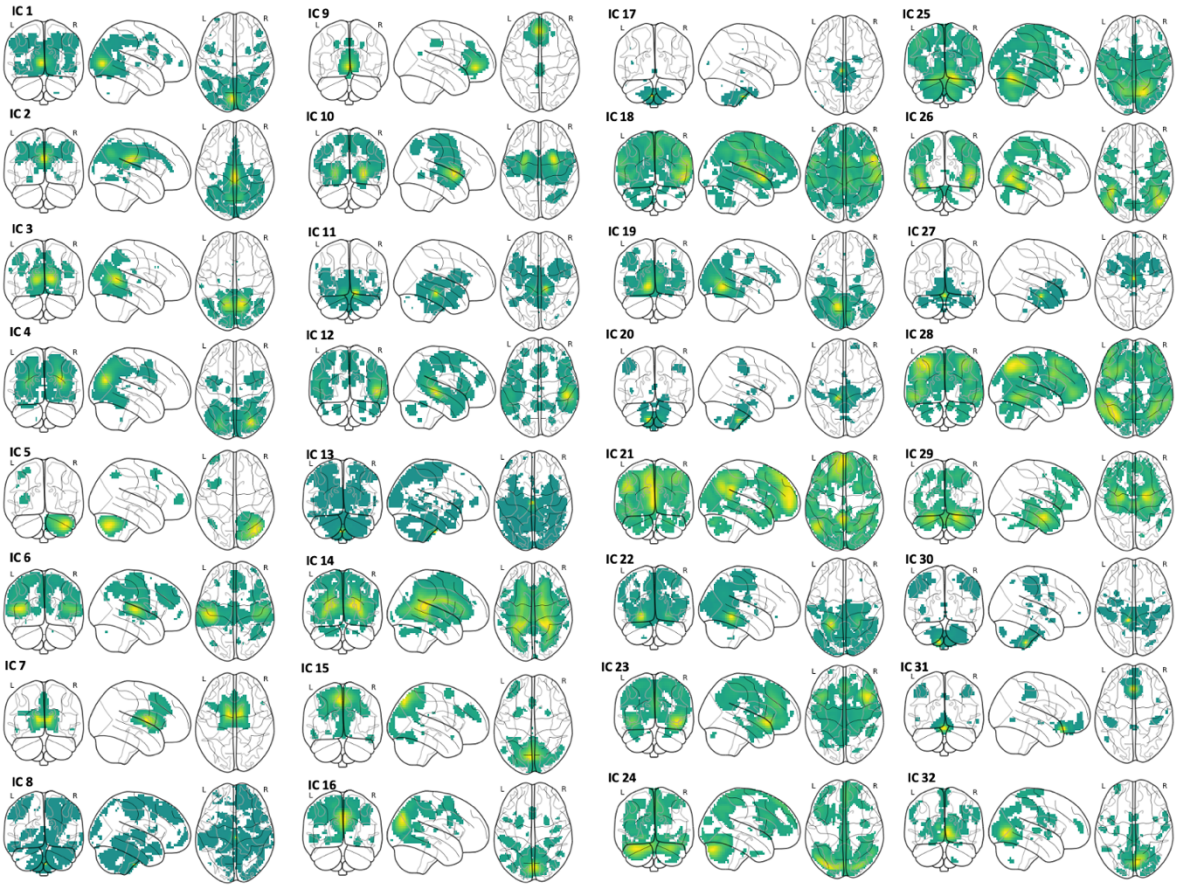

Note. We used group-based ICA to decompose the functional data during picture encoding into 60 ICs. ICs 1 to 32 and ICs 33 to 60 are illustrated in **(A)** and **(B)**, respectively.

Supplementary Figure S3B

The full set of ICs during picture encoding

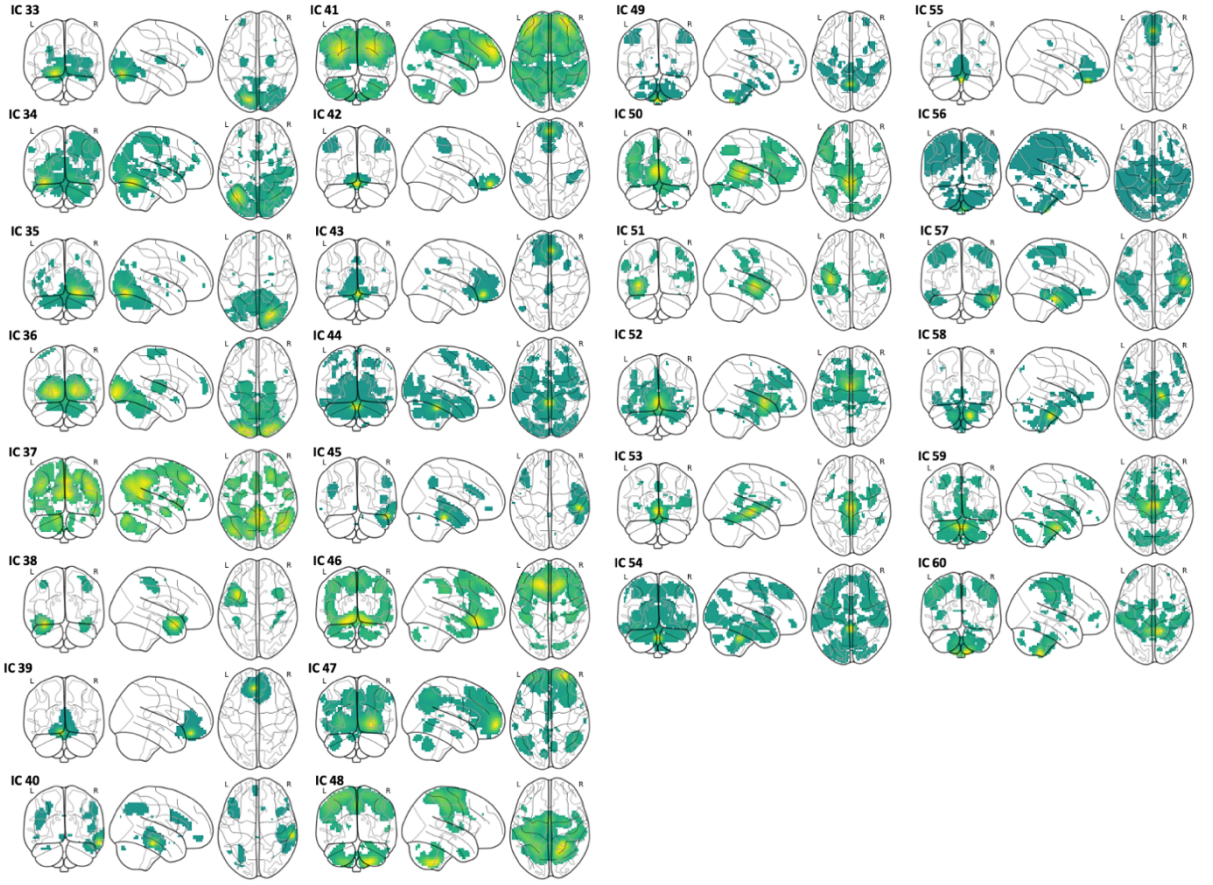

Note. We used group-based ICA to decompose the functional data during picture encoding into 60 ICs. ICs 1 to 32 and ICs 33 to 60 are illustrated in **(A)** and **(B)**, respectively.

Supplementary Figure S4

Illustration of the cross-correlation values between the ICA solution in subsample 1 and subsample 2

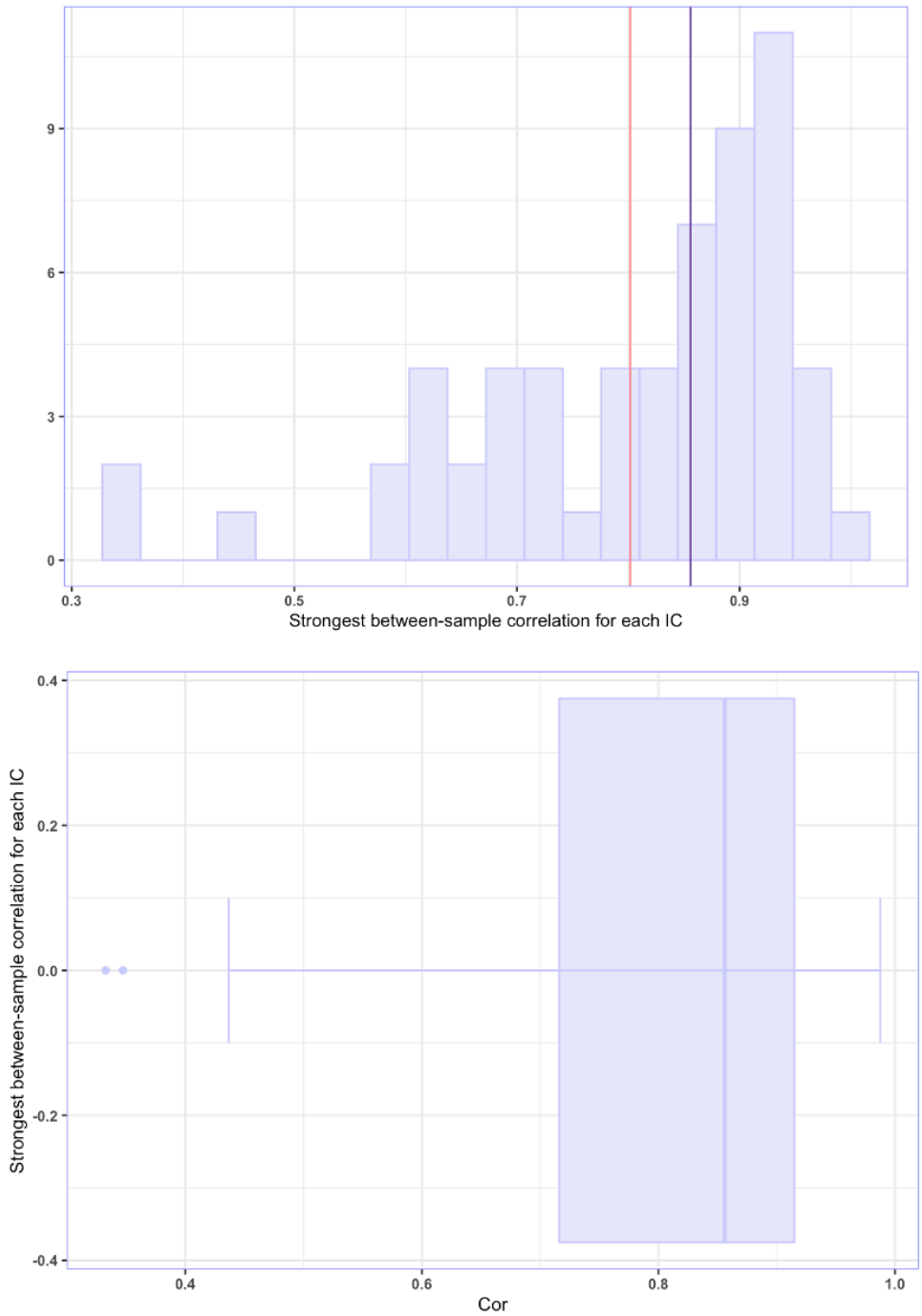

Note. Fifty out of 60 ICs surpassed $|r|_{max}$ >= 0.65, including all non-artefactual ICs with brain-behavior correlations. The distribution was left-skewed. The vertical lines in histogram (top figure) represent the mean (blue) and median (red) with values of 0.856 and 0.802, respectively. The left and right whiskers in boxplot (bottom figure) extend from the hinge to the lowest and highest value within 1.5 times of the interquartile range, respectively.

Supplementary Figure S5A

Comparison of the ICs with resting-state networks

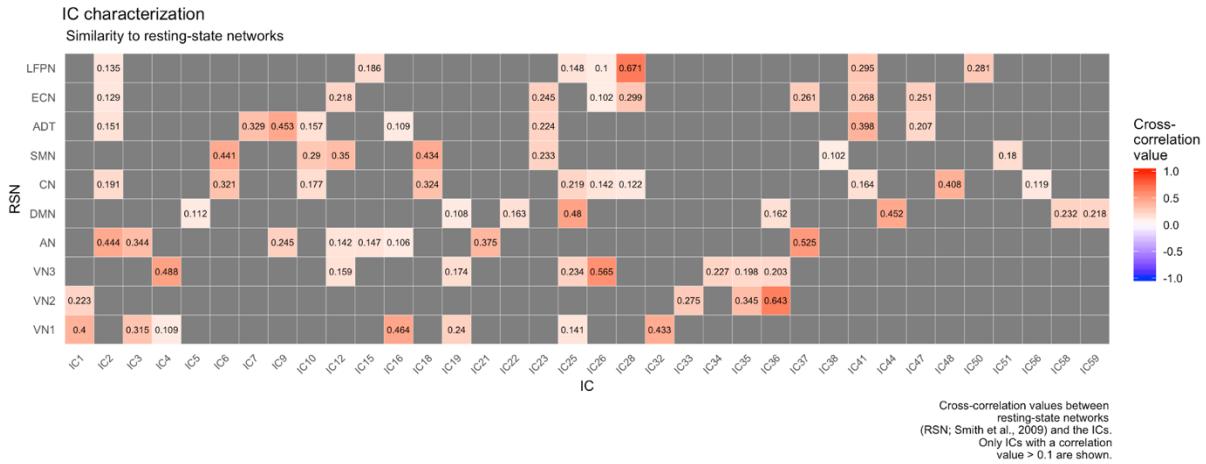

Supplementary Figure S5B

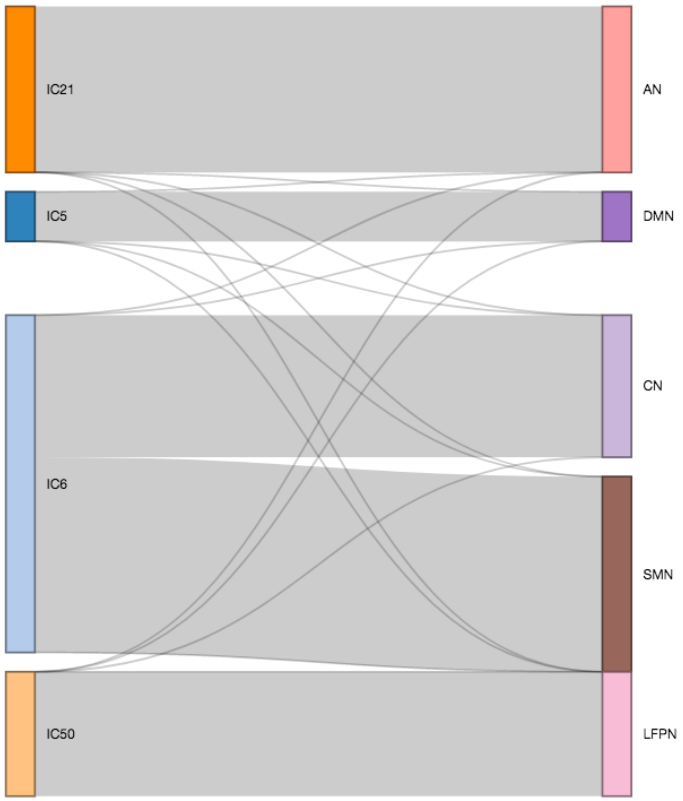

Note. To characterize the ICs extracted from subsample 1 further, we compared their spatial appearance with that of taxonomic resting-state networks (see Materials and Methods), as illustrated in the **(A)** cross-correlation matrix and **(B)** sankey plot, restricted to ICs associated with inter-individual differences in memory performance. VN = visual network; AN = attention network; DMN = default mode network; CN = cerebellar network; SMN = sensorimotor network; ADT = auditory network; ECN = executive control network; LFPN = left frontoparietal network.

Supplementary Figure S6

Comparison of the ICs with resting-state networks

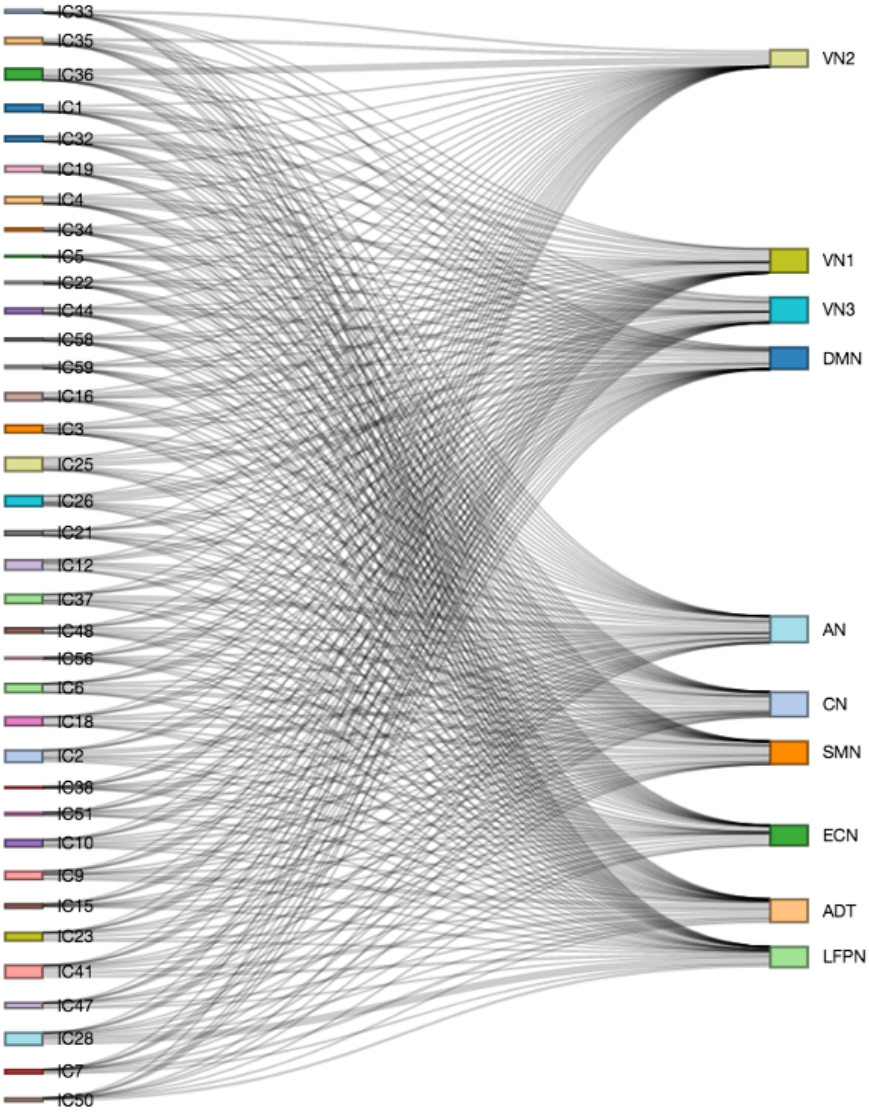

Note. To characterize the ICs extracted from subsample 1 further, we compared their spatial appearance with that of taxonomic resting-state networks (see Materials and Methods), as illustrated in the sankey plot, where only ICs with a cross-correlation value above 0.1 are shown. VN = visual network; AN = attention network; DMN = default mode network; CN = cerebellar network; SMN = sensorimotor network; ADT = auditory network; ECN = executive control network; LFPN = left frontoparietal network.

Supplementary Figure S7A

The ICs with brain-behavior correlations

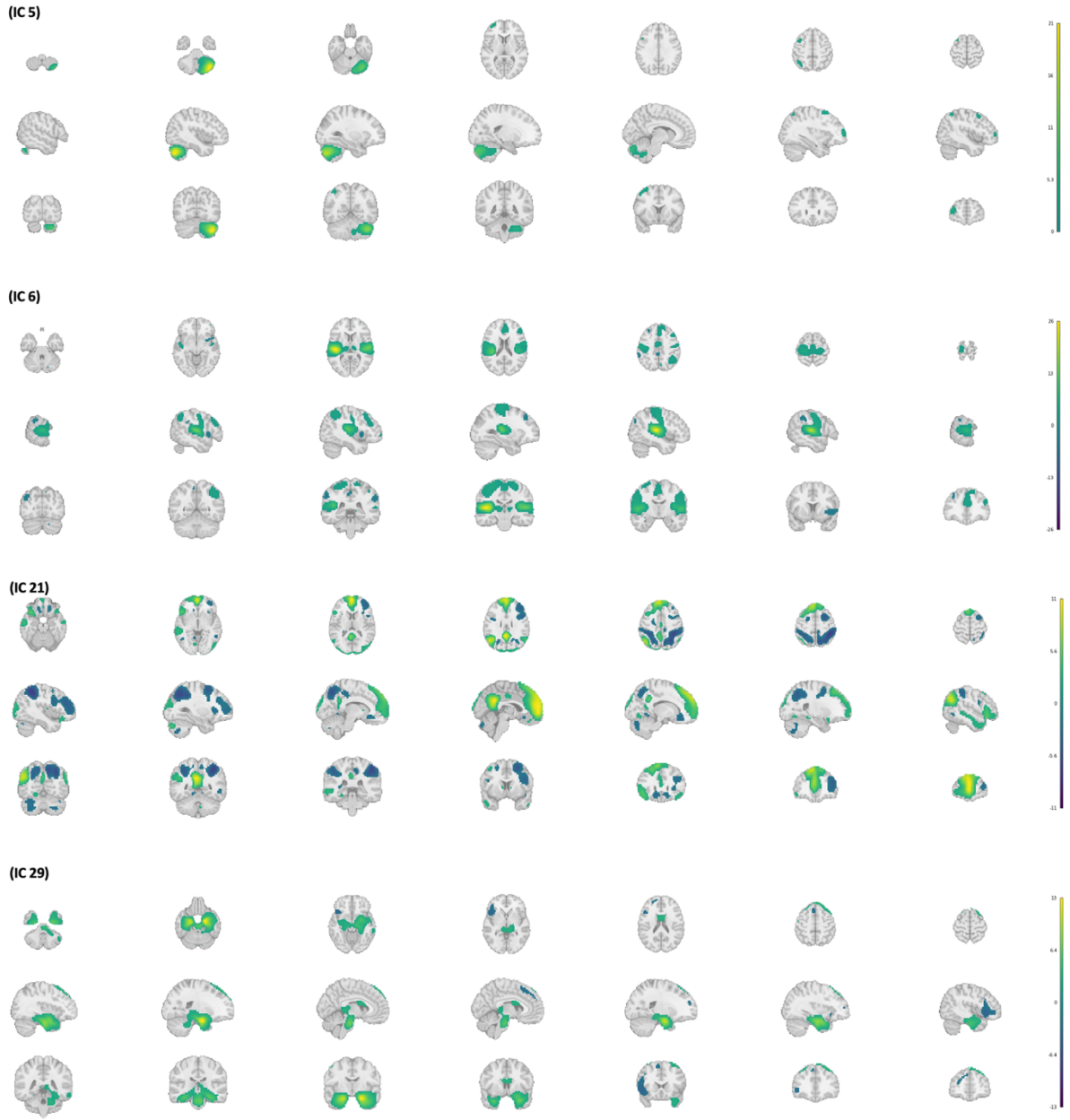

Note. Z-values run along a spectrum from yellow to dark green, respectively, high to low values. See **(A)** for ICs 5, 6, 21 and 29, and **(B)** for ICs 42 and 50, and 54.

Supplementary Figure S7B

The ICs with brain-behavior correlations

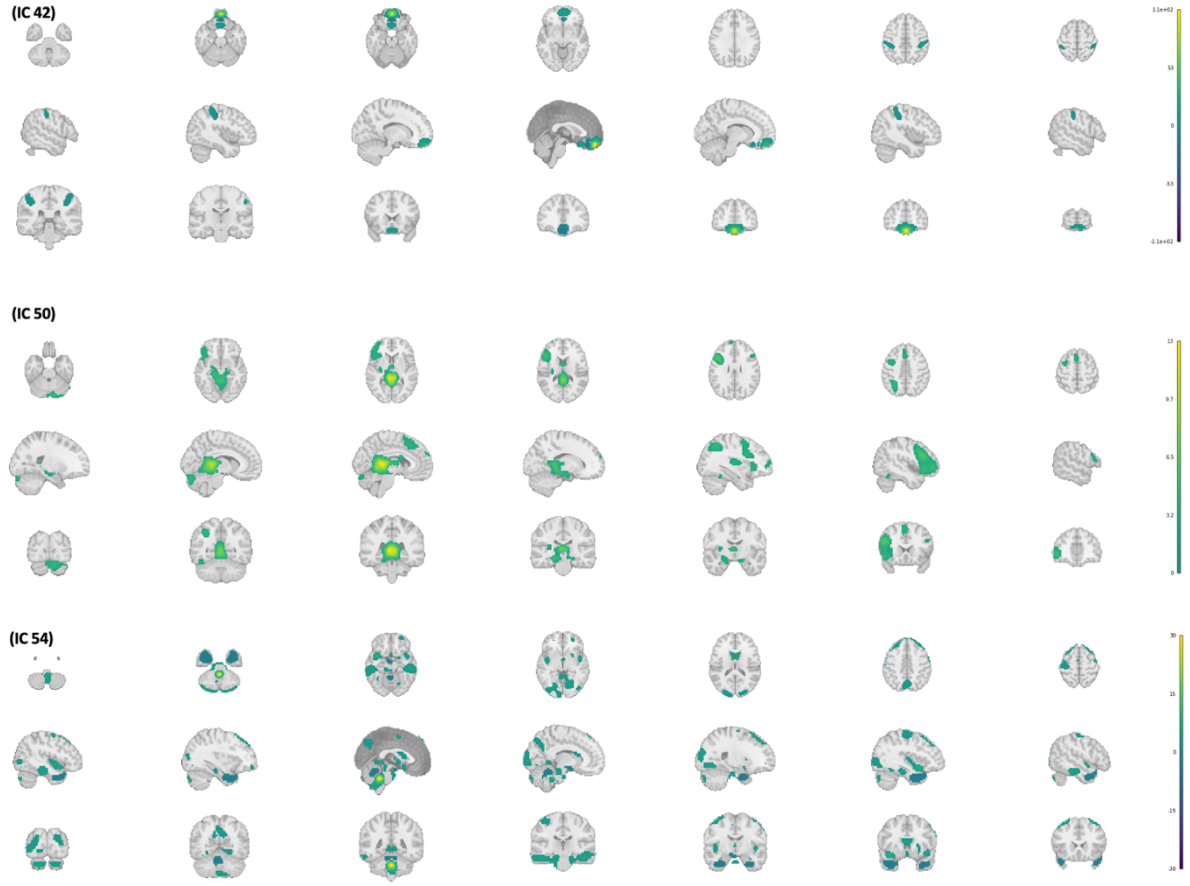

Note. Z-values run along a spectrum from yellow to dark green, respectively, high to low values. See **(A)** for ICs 5, 6, 21 and 29, and **(B)** for ICs 42 and 50, and 54.

Supplementary Figure S8

Closer inspection of IC 54

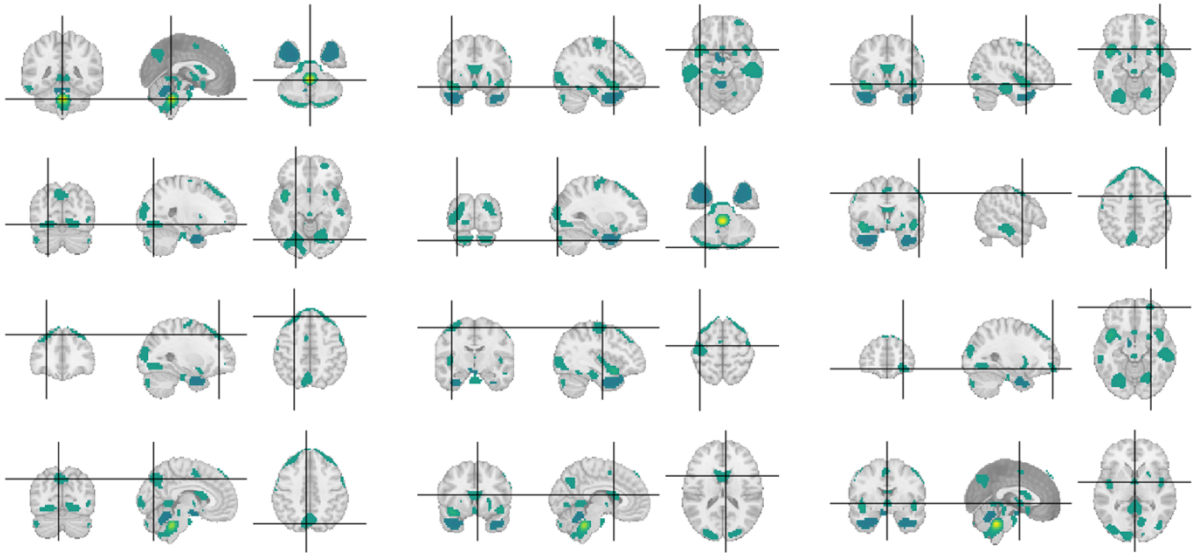

Note. We decided not to include this IC for further interpretation of the brain-behavior correlation due to its fragmented anatomical distribution with clear non-brain matter and the typical ring known indicative of motion artifacts. Color codes run along a spectrum from yellow to dark green, respectively, high to low values.

Supplementary Table S1

Between-sample spatial correlations of the ICs

(A)

Dataset	Min (|*r*|)	Max (|*r*|)	Median (|*r*|)	*M* (|*r*|)	*SD* (|*r*|)
All 60 ICs	0.333	0.987	0.856	0.802	0.150
ICs with brain-behavior correlations	0.641	0.931	0.786	0.796	0.122

(B)

IC 1 – IC 30		IC 31 – IC 60	
IC	**Correlation value (|*r*|)**	**IC**	**Correlation value (|*r*|)**
IC1	0.87	IC31	0.920
IC2	0.987	IC32	0.347
IC3	0.921	IC33	0.864
IC4	0.954	IC34	0.768
IC5	0.696	IC35	0.854
IC6	0.925	IC36	0.913
IC7	0.614	IC37	0.889
IC8	0.437	IC38	0.812
IC9	0.914	IC39	0.943
IC10	0.977	IC40	0.661
IC11	0.963	IC41	0.881
IC12	0.946	IC42	0.931
IC13	0.840	IC43	0.930
IC14	0.917	IC44	0.691
IC15	0.923	IC45	0.333
IC16	0.894	IC46	0.692
IC17	0.767	IC47	0.885
IC18	0.891	IC48	0.624
IC19	0.879	IC49	0.940
IC20	0.793	IC50	0.786
IC21	0.697	IC51	0.876
IC22	0.972	IC52	0.612
IC23	0.776	IC53	0.820
IC24	0.729	IC54	0.641
IC25	0.736	IC55	0.855
IC26	0.865	IC56	0.726
IC27	0.896	IC57	0.829
IC28	0.614	IC58	0.857
IC29	0.898	IC59	0.722
IC30	0.591	IC60	0.598

Note. **(A)** Descriptive statistics of the spatial correlation between ICs extracted from subsample 1 and subsample 2, as given for the complete set of 60 ICs and the ICs with brain-behavior correlations. **(B)** For each IC obtained from subsample 1, the highest between-sample voxel correlations with the ICs extracted from subsample 2 are shown.

Supplementary Table S2

Comparison of the brain-behavior correlations of the network-based and voxel-based approaches

(A)

Voxel-based brain-behavior correlation cluster	IC5	IC6	IC21	IC29	IC42	IC50
1	0	0	0	131	0	70
2	0	2	95	0	0	74
3	0	0	0	82	0	24
4	0	0	54	0	82	0
5	43	0	24	0	0	10
6	0	0	25	0	0	0
7	6	0	6	0	0	0
8	0	2	7	0	0	4
9	0	0	3	0	0	0
10	0	0	0	0	0	0
11	2	0	2	0	0	0
12	0	0	2	0	0	0
13	1	0	0	1	0	0
14	0	0	0	0	0	1
15	0	0	0	0	0	0

(B)

Brain region largely covered by the cluster	Voxel-based brain-behavior correlation cluster	Cluster is covered by IC(s):
Medial temporal lobe (left)	1	10, 11, 13, 14, 22, 25, 27, 29, 38, 41, 44, 50, 51, 53, 54, 56, 59
Medial temporal lobe (right)	3	10, 11, 13, 14, 22, 25, 29, 41, 50, 54, 57, 59
Cerebellum	11	5, 21, 24, 30, 46, 54
Cerebellum	7	5, 20, 21, 25, 37, 44, 49, 54, 58, 60
Cerebellum	5	5, 12, 13, 21, 24, 25, 26, 28, 30, 35, 36, 37, 46, 50, 54, 56
Medial prefrontal cortex	4	9, 21, 31, 39, 42, 43, 45, 46, 47
Superior frontal gyrus (left)	8	6, 21, 41, 46, 50
Superior frontal gyrus (left)	6	9, 14, 18, 21, 28, 37, 41, 46, 56
Precuneus / isthmus cingulate	2	2, 3, 6, 14, 15, 18, 19, 21, 22, 28, 34, 37, 50, 54, 56

Note. **(A)** Absolute number of voxels of the voxel-based brain-behavior correlation clusters included in each of the ICs with brain-behavior correlations. **(B)** Overview of the voxel-based brain-behavior correlation cluster's coverage by the ICs.

Supplementary material: Study 3

Figure S1

Sample quantiles of the behavioral effect of emotional memory enhancement versus theoretical quantiles from a normal distribution

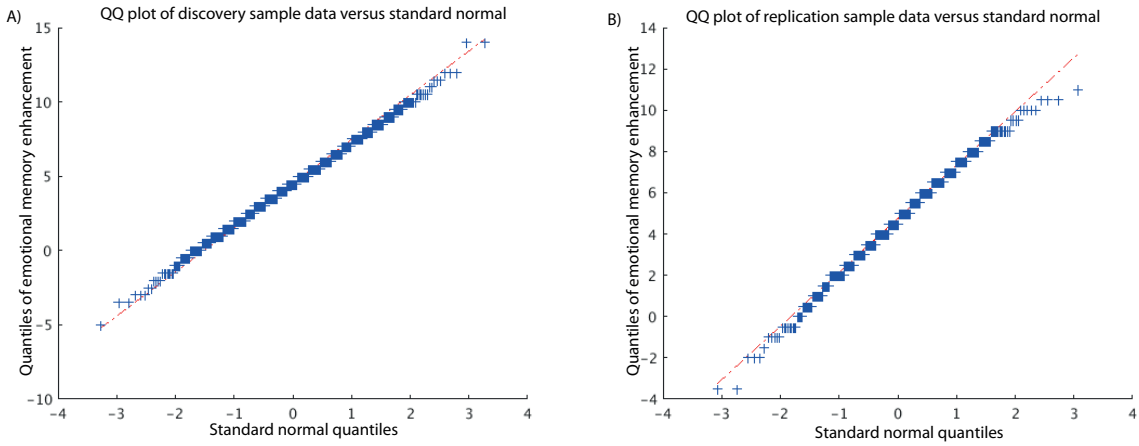

Note. Panels A and B show results for discovery and replication sample, respectively.

Figure S2

Voxels that show increased activation for successful emotional memory encoding within the discovery sample ($P_{whole\text{-}brain\text{-}FWE\text{-}corrected} < 0.05$, N = 945)

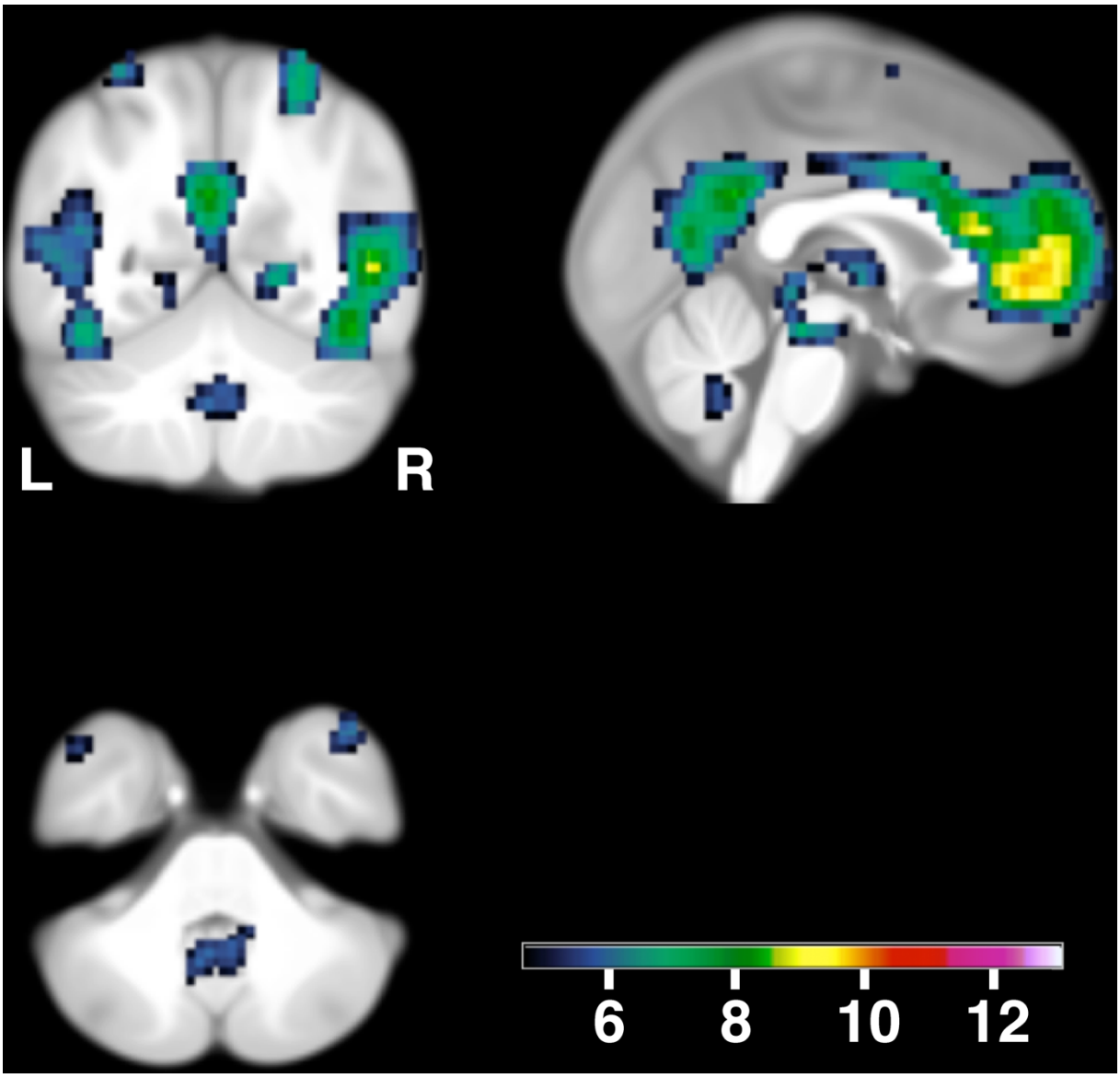

Note. Different colors denote different ROIs. Different colors denote different regions.

Figure S3

The figure depicts the result of the parcellation, where 29 spatially coherent regions of interest (ROIs) were identified

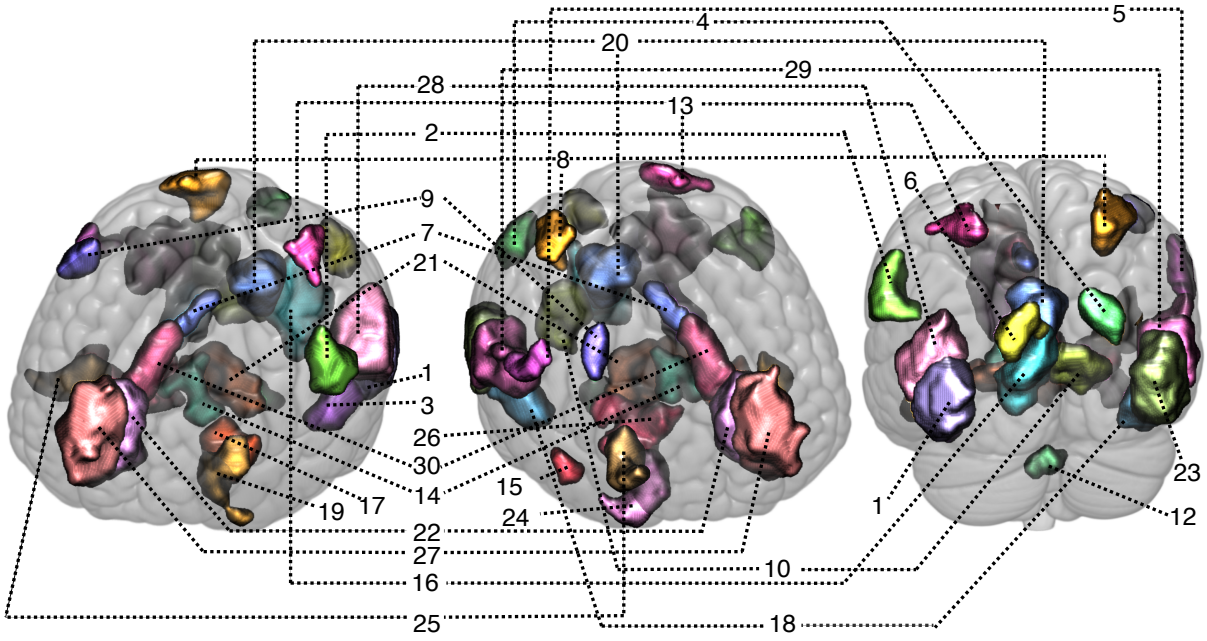

Note. Different colors denote different ROIs. See Table S5 for anatomical correspondence per ROI.

Figure S4.

Result of the parcellation, where 29 spatially coherent regions of interest (ROIs) were identified

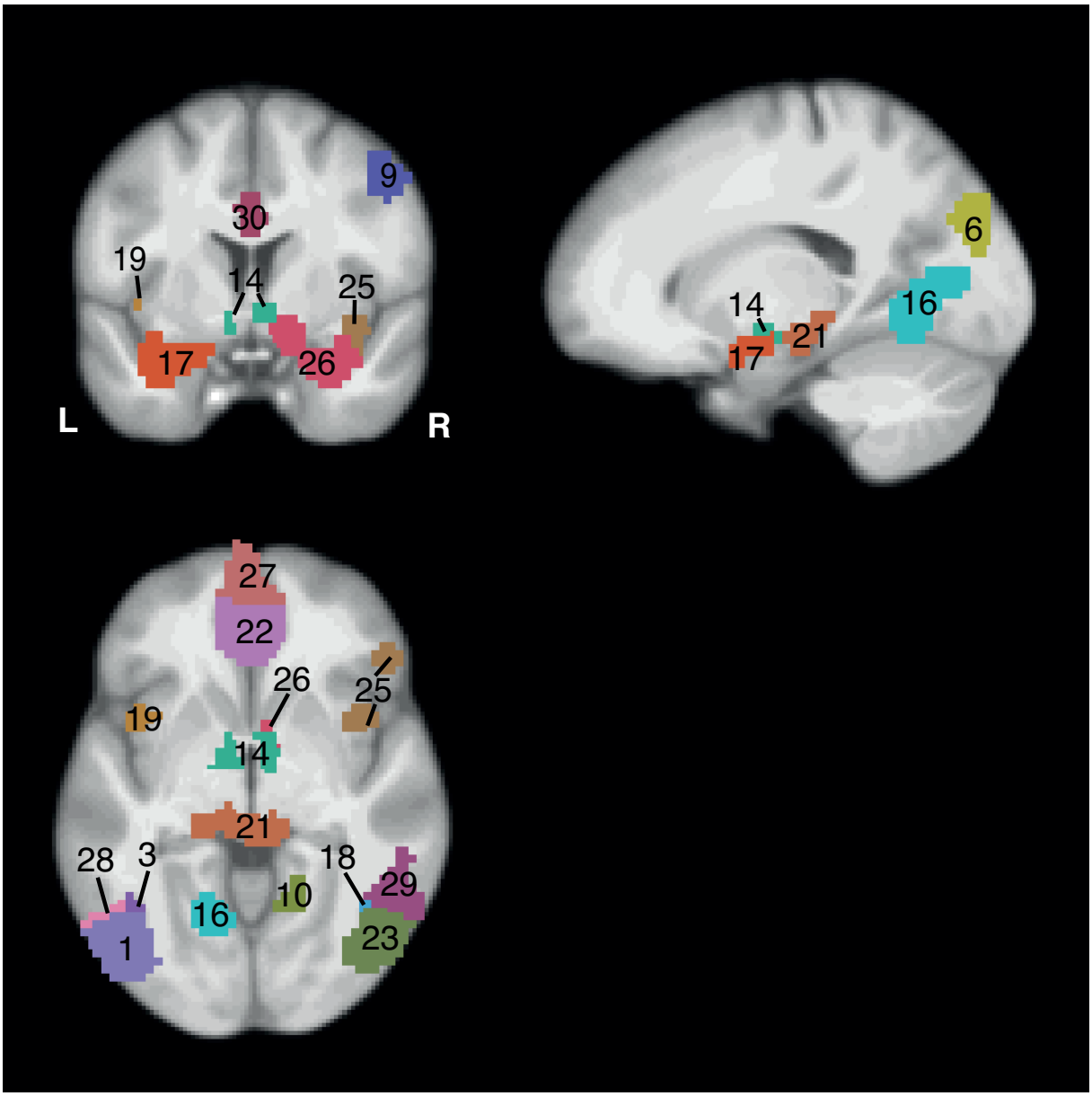

Note. The figure depicts ROIs: 1, 3, 6, 9, 10, 14, 16, 17, 18, 19, 21, 22, 23, 25, 26, 28, 29, 30. Different colors denote different regions.

Figure S5

Result of the parcellation, where 29 spatially coherent regions of interest (ROIs) were identified

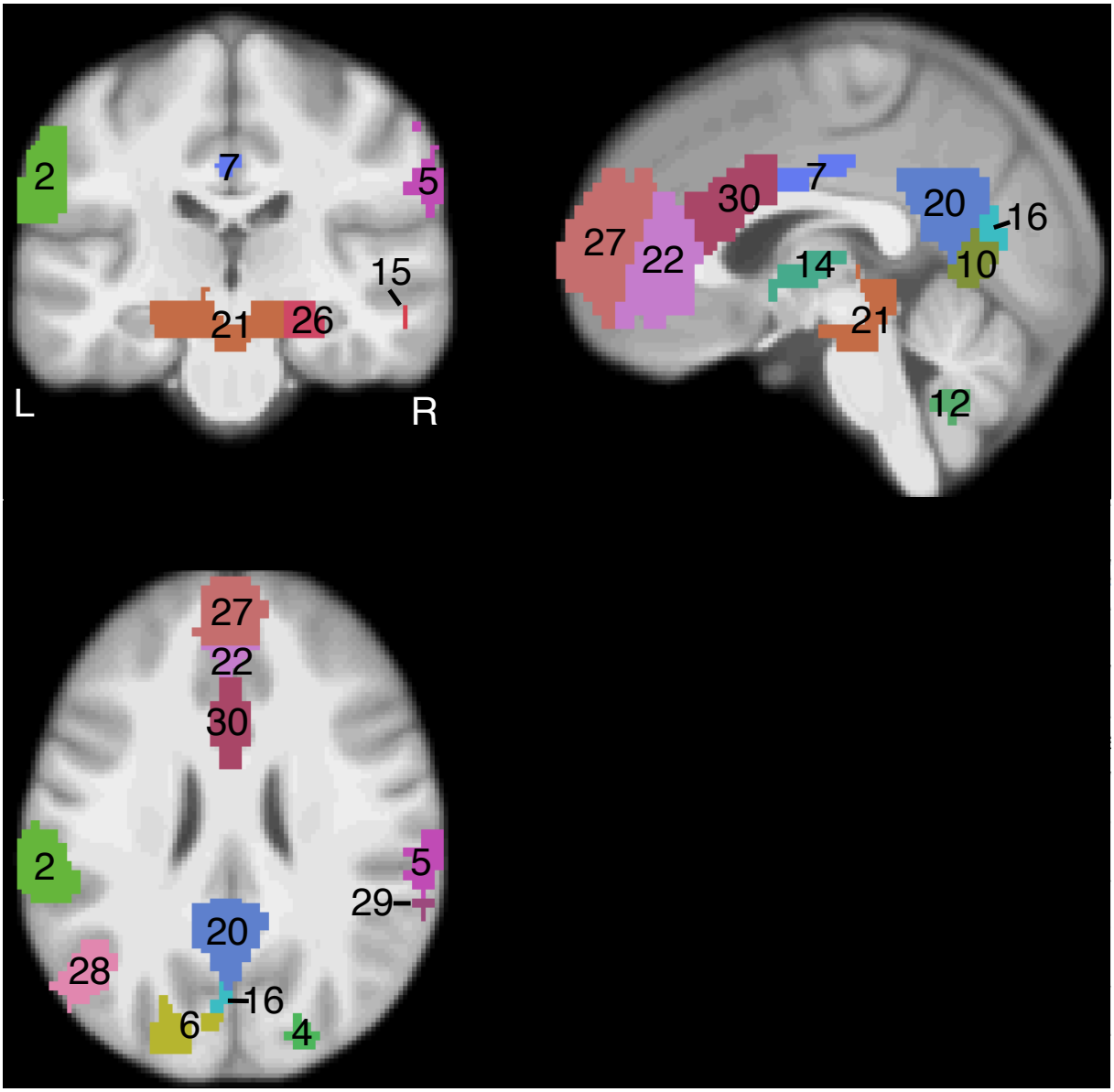

Note. The figure depicts ROIs: 2, 4, 5, 6, 7, 10, 12, 14, 15, 16, 21, 22, 26, 27, 28, 30. Different colors denote different regions.

Figure S6

Result of the parcellation, where 29 spatially coherent regions of interest (ROIs) were identified

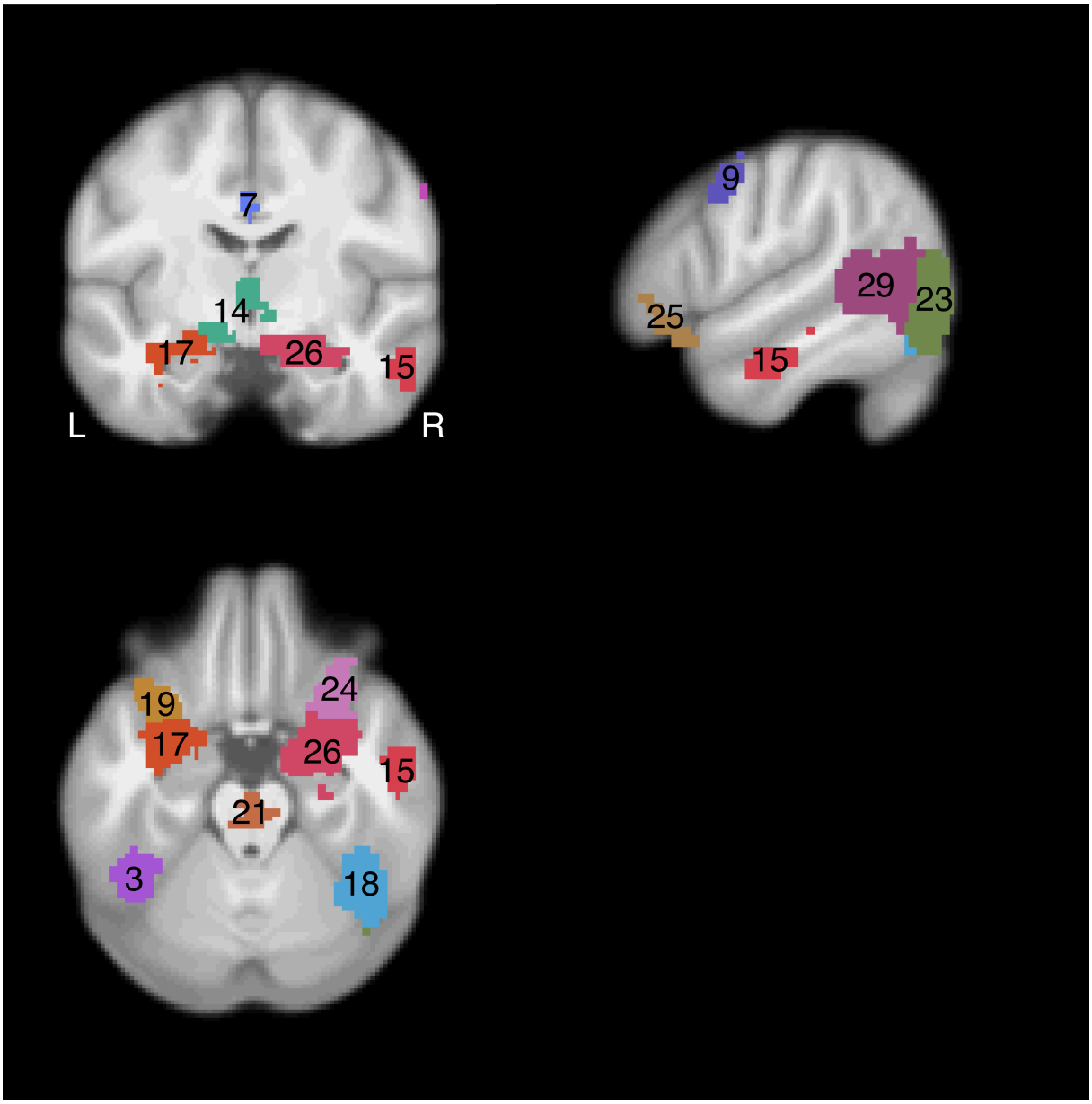

Note. The figure depicts ROIs: 3, 7, 9, 14, 15, 17, 18, 19, 21, 23, 24, 25, 26, 29. Different colors denote different regions.

Figure S7

Result of the parcellation, where 29 spatially coherent regions of interest (ROIs) were identified

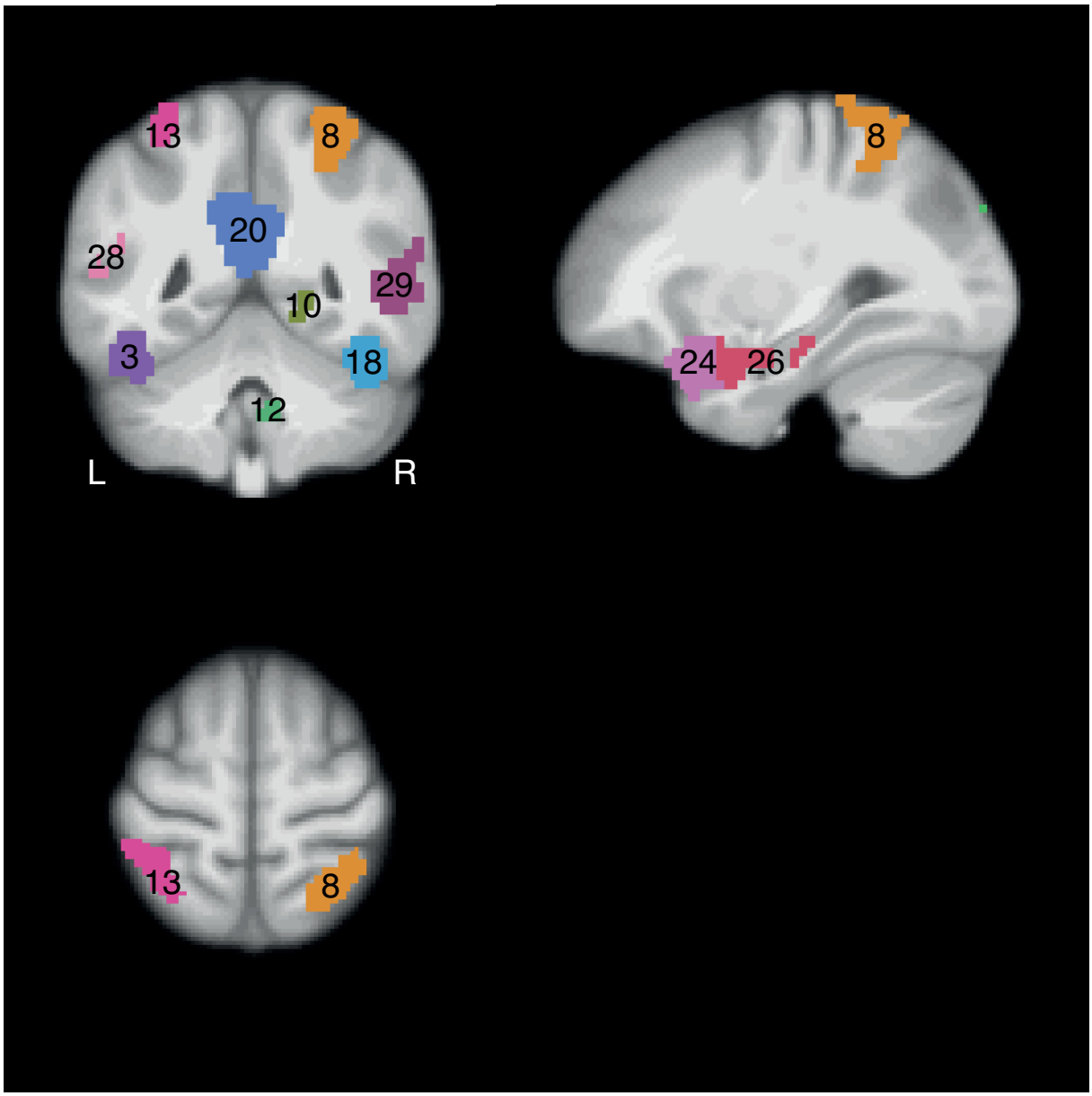

Note. The figure depicts ROIs: 3, 8, 10, 12, 13, 18, 20, 24, 26, 28, 29. Different colors denote different regions.

Table S1

Number of subjects per DCM between replicating ROIs

DCM model (R12 and one other ROI)	Sample size in discovery sample	Sample size in replication sample
R1 and R12	901	433
R2 and R12	899	429
R3 and R12	899	429
R4 and R12	862	419
R5 and R12	852	411
R6 and R12	894	422
R8 and R12	881	426
R9 and R12	798	378
R10 and R12	899	432
R14 and R12	902	432
R15 and R12	837	410
R16 and R12	902	433
R17 and R12	899	432
R18 and R12	902	432
R19 and R12	901	433
R20 and R12	902	433
R21 and R12	902	433
R22 and R12	902	433
R23 and R12	902	433
R24 and R12	901	433
R26 and R12	902	433
R27 and R12	902	433
R28 and R12	902	433
R29 and R12	902	433
R30 and R12	899	432

Note. The table lists the sample size after the exclusion of subjects from whom time courses could not be successfully extracted. Sample size without exclusions due to unsuccessful time course extraction: Discovery sample N = 945; replication sample N = 473. Table refers to Materials and Methods, paragraph "*Time course extraction from ROIs"*.

Table S2

Percentage of subjects per replicating ROI that had to be excluded as they did not show robust activation (Table refers to Materials and Methods, paragraph "Time course extraction from ROIs").

ROI	Percentage of excluded subjects in discovery sample	Percentage of excluded subjects in replication sample
1	0.11 %	0 %
2	0.42 %	0.85 %
3	0.42 %	0.85 %
4	4.87 %	3.59 %
5	5.92 %	5.29 %
6	1.27 %	2.54 %
8	2.54 %	1.69 %
9	11.64 %	14.16 %
10	0.32 %	0.21 %
12	4.55 %	8.46 %
14	0 %	0.21 %
15	7.20 %	5.92 %
16	0 %	0 %
17	0.32 %	0.21 %
18	0 %	0.21 %
19	0.11 %	0 %
20	0 %	0 %
21	0 %	0 %
22	0 %	0 %
23	0 %	0 %
24	0.11 %	0 %
26	0 %	0 %
27	0 %	0 %
28	0 %	0 %
29	0 %	0 %
30	0.32 %	0.21 %

Table S3

Increased activity during successful emotional memory encoding in the discovery sample (*N* = 945)

ROI from parcellation	Maximum t value within ROI	Regional correspondence of the local maxima within ROI	MNI coordinates at maximum		
			X	Y	Z
1	12.0263	ctx-lh-inferiorparietal (1%) ctx-lh-inferiortemporal (11%) ctx-lh-lateraloccipital (54%) ctx-lh-middletemporal (5%)	-49.5	-74.25	0
2	7.0601	ctx-lh-postcentral (3%) ctx-lh-supramarginal (80%)	-63.25	-27.5	28
3	8.6389	ctx-lh-fusiform (36%) ctx-lh-inferiortemporal (33%)	-44	-46.75	-20
4	7.2131	ctx-rh-superiorparietal (59%)	16.5	-85.25	40
5	6.6197	ctx-rh-postcentral (8%) ctx-rh-supramarginal (30%)	66	-16.5	40
6	6.6173	ctx-lh-lateraloccipital (1%) ctx-lh-superiorparietal (29%)	-19.25	-85.25	32
7	6.3562	ctx-lh-posteriorcingulate (56%) ctx-rh-posteriorcingulate (14%)	0	0	36
8	7.1087	ctx-rh-superiorparietal (59%)	27.5	-55	64
9	6.4531	ctx-rh-caudalmiddlefrontal (4%) ctx-rh-precentral (50%)	46.75	0	56
10	7.5141	ctx-lh-precuneus (1%) ctx-rh-cuneus (10%) ctx-rh-lingual (23%) ctx-rh-pericalcarine (5%) ctx-rh-precuneus (2%)	2.75	-63.25	12
12	5.7674	Right-Cerebellum-Cortex (1%) Left-Cerebellum-Cortex (97%) Vermis IX (76%), Left IX (14%)[1]	-2.75	-55	-40
13	6.3208	ctx-lh-superiorparietal (26%)	-30.25	-55	68
14	7.6908	Left-Pallidum (5%) Left-VentralDC (15%)	-8.25	-5.5	-8
15	5.9768	ctx-rh-middletemporal (56%)	57.75	-8.25	-20
16	8.3868	ctx-lh-lingual (3%) ctx-lh-pericalcarine (46%)	-13.75	-74.25	8
17	8.3571	ctx-lh-insula (6%)	-33	0	-20
18	10.9539	ctx-rh-fusiform (10%) ctx-rh-inferiortemporal (20%) ctx-rh-lateraloccipital (19%) ctx-rh-middletemporal (1%)	46.75	-63.25	-8
19	7.4373	ctx-lh-lateralorbitofrontal (21%) ctx-lh-insula (54%)	-30.25	13.75	-16
20	8.8163	ctx-lh-isthmuscingulate (55%) ctx-lh-precuneus (17%)	-5.5	-49.5	28
21	8.527	Brain-Stem (24%) Right-VentralDC (61%)	13.75	-22	-12

22	10.537	ctx-lh-medialorbitofrontal (3%) ctx-lh-rostralanteriorcingulate (68%) ctx-lh-superiorfrontal (10%)	-2.75	44	0
23	11.869	ctx-rh-inferiortemporal (23%) ctx-rh-lateraloccipital (35%) ctx-rh-middletemporal (8%)	52.25	-66	-4
24	8.3787	ctx-rh-lateralorbitofrontal (67%) ctx-rh-insula (12%)	30.25	16.5	-20
25	7.9919	ctx-rh-insula (90%)	35.75	11	-12
26	9.1318	Right-Amygdala (98%)	19.25	-5.5	-16
27	10.1738	ctx-lh-medialorbitofrontal (6%) ctx-lh-rostralanteriorcingulate (10%) ctx-lh-superiorfrontal (51%)	-2.75	52.25	4
28	10.7336	ctx-lh-inferiorparietal (4%) ctx-lh-inferiortemporal (16%) ctx-lh-lateraloccipital (13%) ctx-lh-middletemporal (37%)	-52.25	-68.75	4
29	10.4155	ctx-rh-inferiorparietal (2%) ctx-rh-inferiortemporal (18%) ctx-rh-lateraloccipital (10%) ctx-rh-middletemporal (34%)	52.25	-60.5	0
30	9.0748	ctx-lh-caudalanteriorcingulate (6%) ctx-rh-caudalanteriorcingulate (29%) ctx-rh-corpuscallosum (1%) CC_Anterior (3%)	2.75	27.5	16

Note. Table shows the local maxima per region of interest (ROI). Regions are in accordance to FreeSurfer nomenclature. Percentages denote the share of participants with a certain label located at a given coordinate (see Materials and Methods, paragraph "*Anatomical localication of ROIs based on a population-averaged anatomical probabilistic atlas*"). [1] Assignment based on FSL atlas "Cerebellar Atlas in MNI152 space after normalization with FNIRT" (Diedrichsen et al., 2009).

Table S4

Increased activity during successful emotional memory encoding in the replication sample (N = 473)

ROI from parcellation	Maximum t value within ROI	Regional correspondence of the local maxima within ROI	MNI coordinates at maximum		
			X	Y	Z
1	8.3442	ctx-lh-fusiform (4%) ctx-lh-inferiortemporal (12%) ctx-lh-lateraloccipital (43%) ctx-lh-middletemporal (1%)	-46.75	-71.5	-4
2	4.9721	ctx-lh-supramarginal (55%)	-55	-35.75	28
3	6.9116	ctx-lh-fusiform (47%) ctx-lh-inferiortemporal (16%) ctx-lh-lateraloccipital (7%)	-44	-63.25	-12
4	6.1305	ctx-rh-superiorparietal (56%)	22	-85.25	44
5	4.6385	ctx-rh-postcentral (2%) ctx-rh-supramarginal (24%)	66	-19.25	44
6	4.9083	ctx-lh-inferiorparietal (3%) ctx-lh-superiorparietal (67%)	-19.25	-85.25	40
7	4.285 †	ctx-lh-posteriorcingulate (56%) ctx-rh-posteriorcingulate (14%)	0	0	36
8	4.4662	ctx-rh-superiorparietal (46%)	33	-52.25	68
9	5.4453	ctx-rh-caudalmiddlefrontal (4%) ctx-rh-precentral (70%)	49.5	2.75	48
10	5.2734	ctx-rh-lingual (43%)	8.25	-60.5	4
12	5.122	Right-Cerebellum-Cortex (93%) Left-Cerebellum-Cortex (6%) Right IX (75%), Vermis IX (22%), Vermis VIIIb (2%) [1]	2.75	-57.75	-44
13 †	3.5337	ctx-lh-superiorparietal (43%)	-30.25	-49.5	60
14	6.2463	Left-Pallidum (1%) Left-Amygdala (6%) Left-VentralDC (49%)	-13.75	-5.5	-12
15	5.626	ctx-rh-middletemporal (68%) ctx-rh-superiortemporal (2%)	55	-8.25	-20
16	6.1707	ctx-lh-cuneus (2%) ctx-lh-lingual (1%) ctx-lh-pericalcarine (54%)	-8.25	-74.25	12
17	8.051	Left-Amygdala (92%)	-19.25	-5.5	-16
18	8.1444	ctx-rh-fusiform (10%) ctx-rh-inferiortemporal (20%) ctx-rh-lateraloccipital (19%) ctx-rh-middletemporal (1%)	46.75	-63.25	-8
19	5.5845	ctx-lh-lateralorbitofrontal (64%) ctx-lh-insula (11%)	-30.25	16.5	-16
20	6.8923	ctx-lh-isthmuscingulate (7%) ctx-lh-precuneus (39%) ctx-rh-precuneus (10%)	0	-55	28
21	5.406	Brain-Stem (95%)	5.5	-30.25	-4

22	7.362	ctx-lh-medialorbitofrontal (1%) ctx-lh-rostralanteriorcingulate (52%) ctx-lh-superiorfrontal (27%)	-2.75	46.75	4
23	8.8366	ctx-rh-fusiform (5%) ctx-rh-inferiortemporal (19%) ctx-rh-lateraloccipital (34%) ctx-rh-middletemporal (2%)	49.5	-66	-8
24	5.6773	ctx-rh-lateralorbitofrontal (22%) ctx-rh-insula (50%)	27.5	13.75	-16
25	3.8598 †	ctx-rh-lateralorbitofrontal (5%) ctx-rh-parsorbitalis (40%) ctx-rh-parstriangularis (17%)	46.75	27.5	-8
26	6.836	Right-Hippocampus (1%) Right-Amygdala (85%) Right-VentralDC (6%)	16.5	-5.5	-16
27	7.1583	ctx-lh-rostralanteriorcingulate (25%) ctx-lh-superiorfrontal (49%)	-2.75	49.5	8
28	7.7959	ctx-lh-inferiorparietal (4%) ctx-lh-inferiortemporal (16%) ctx-lh-lateraloccipital (13%) ctx-lh-middletemporal (37%)	-52.25	-68.75	4
29	7.4797	ctx-rh-inferiortemporal (27%) ctx-rh-lateraloccipital (8%) ctx-rh-middletemporal (21%)	55	-60.5	-4
30	6.0532	ctx-lh-caudalanteriorcingulate (42%) ctx-lh-corpuscallosum (2%) ctx-rh-caudalanteriorcingulate (2%) CC_Anterior (4%)	0	27.5	16

Note. Table shows the local maxima per region of interest (ROI). Regions are in accordance to FreeSurfer nomenclature. Percentages per coordinate denote the population-average probability of an anatomical label (see Materials and Methods, paragraph "*Anatomical localication of ROIs based on a population-averaged anatomical probabilistic atlas*"). [1] Assignment based on FSL atlas "Cerebellar Atlas in MNI152 space after normalization with FNIRT" (Diedrichsen et al., 2009). † Maxima for clusters 7, 13 and 25 did not reach significance threshold ($T = 4.4056$, $P < 0.05$, one-sided, Bonferroni corrected for 7635 tests).

Table S5

Number of voxels and anatomical correspondence per ROI

ROI from parcellation	Size of ROI	Anatomical correspondence of centroid [MNI]	Anatomical regions spanned by ROI	Average percentage regional correspondence
1	462	ctx-lh-lateraloccipital (53%) Left-Cerebral-White-Matter (36%) [-44 -77 0]	ctx-lh-fusiform ctx-lh-inferiortemporal ctx-lh-lateraloccipital Left-Cerebral-White-Matter ctx-lh-middletemporal ctx-lh-inferiorparietal	6.9 5.97 32.34 24.08 2.26 5.07
2	232	ctx-lh-postcentral (4%) ctx-lh-supramarginal (59%) Left-Cerebral-White-Matter (31%) [-60.5 -27.5 32]	ctx-lh-supramarginal ctx-lh-postcentral Left-Cerebral-White-Matter	44.83 8.46 14.25
3	181	ctx-lh-fusiform (59%) ctx-lh-inferiortemporal (10%) Left-Cerebral-White-Matter (22%) [-41.25 -52.25 -16]	Left-Cerebellum-Cortex ctx-lh-fusiform ctx-lh-inferiortemporal Left-Cerebral-White-Matter	8.81 32.74 24.09 21.1
4	127	ctx-rh-superiorparietal (42%) Right-Cerebral-White-Matter (53%) [19.25 -85.25 36]	Right-Cerebral-White-Matter ctx-rh-lateraloccipital ctx-rh-superiorparietal	31.58 2.64 39.21
5	101	ctx-rh-postcentral (1%) ctx-rh-supramarginal (64%) Right-Cerebral-White-Matter (31%) [63.25 -24.75 32]	Right-Cerebral-White-Matter ctx-rh-superiortemporal ctx-rh-supramarginal ctx-rh-postcentral	13.24 1.21 50.59 5.88
6	141	ctx-lh-superiorparietal (24%) Left-Cerebral-White-Matter (72%) [-16.5 -85.25 32]	Left-Cerebral-White-Matter ctx-lh-inferiorparietal ctx-lh-lateraloccipital ctx-lh-superiorparietal ctx-lh-cuneus	38.86 1.41 4.54 34.41 3.36
7	66	ctx-lh-posteriorcingulate (61%) Left-Cerebral-White-Matter (3%) ctx-rh-posteriorcingulate (17%) [0 -11 36]	ctx-rh-posteriorcingulate ctx-lh-posteriorcingulate Left-Cerebral-White-Matter	20.73 48.75 12.27
8	177	ctx-rh-postcentral (1%)	Right-Cerebral-White-Matter	18.24

		ctx-rh-superiorparietal (49%) Right-Cerebral-White-Matter (43%) [30.25 -49.5 64]	ctx-rh-superiorparietal ctx-rh-postcentral	42.09 1.67
9	76	ctx-rh-caudalmiddlefrontal (4%) ctx-rh-precentral (70%) Right-Cerebral-White-Matter (21%) [49.5 2.75 48]	Right-Cerebral-White-Matter ctx-rh-caudalmiddlefrontal ctx-rh-precentral	10.14 5.51 44.31
10	201	ctx-rh-lingual (24%) ctx-rh-pericalcarine (5%) Right-Cerebral-White-Matter (69%) [13.75 -63.25 4]	ctx-rh-lingual Right-Cerebral-White-Matter ctx-rh-pericalcarine ctx-rh-precuneus ctx-rh-cuneus	25.07 39.46 11.13 3.8 3.11
11	60	Left-Caudate (54%) Left-Cerebral-White-Matter (35%) [-16.5 -8.25 24]	Left-Cerebellum-Cortex ctx-rh-fusiform Right-Cerebral-White-Matter ctx-lh-middletemporal Left-Cerebral-White-Matter Left-Putamen ctx-lh-superiorfrontal ctx-lh-precentral ctx-rh-superiorfrontal	13.25 6.52 8.76 3.21 5.8 1.46 9.89 12.19 7
12	65	Right-Cerebellum-Cortex (41%) Left-Cerebellum-Cortex (59%) [0 -55 -40]	Left-Cerebellum-Cortex Left-Cerebellum-White-Matter Right-Cerebellum-Cortex Right-Cerebellum-White-Matter	38.82 3.96 46.53 6
13	110	ctx-lh-postcentral (2%) ctx-lh-superiorparietal (47%) [-33 -46.75 68]	Left-Cerebral-White-Matter ctx-lh-superiorparietal ctx-lh-postcentral	7.16 32.43 3.27
14	147	Left-Thalamus-Proper (53%) Left-Cerebral-White-Matter (1%) Left-VentralDC (31%) [-2.75 -5.5 -4]	Left-VentralDC Left-Cerebral-White-Matter Left-Pallidum Left-Thalamus-Proper Right-Cerebral-White-Matter Right-Thalamus-Proper Right-VentralDC	15.25 19.22 4.65 26.01 7.01 17.33 1.64
15	61	ctx-rh-middletemporal (29%) Right-Cerebral-White-Matter (71%) [57.75 -11 -20]	Right-Cerebral-White-Matter ctx-rh-middletemporal ctx-rh-superiortemporal	40.22 44.95 5.74
16	354	ctx-lh-cuneus (4%)	Left-Cerebellum-Cortex	2.69

		ctx-lh-lingual (22%) ctx-lh-pericalcarine (33%) Left-Cerebral-White-Matter (18%) [-8.25 -68.75 8]	ctx-lh-lingual Left-Cerebral-White-Matter ctx-lh-pericalcarine ctx-lh-precuneus ctx-lh-cuneus	18.92 36.72 10.09 5.69 7.68
17	205	Left-Amygdala (54%) [-27.5 -2.75 -20]	Left-Cerebral-White-Matter ctx-lh-temporalpole Left-Amygdala ctx-lh-superiortemporal Left-Hippocampus ctx-lh-insula Left-Putamen	25.56 1.06 19.39 3.57 1.93 7.44 1.12
18	261	ctx-rh-fusiform (53%) ctx-rh-inferiortemporal (10%) ctx-rh-lateraloccipital (2%) Right-Cerebral-White-Matter (30%) [44 -55 -16]	Right-Cerebellum-Cortex ctx-rh-fusiform ctx-rh-inferiortemporal Right-Cerebral-White-Matter ctx-rh-lateraloccipital	9.77 33.55 14.49 27.58 3.35
19	210	ctx-lh-lateralorbitofrontal (13%) ctx-lh-superiortemporal (6%) [-35.75 13.75 -20]	Left-Cerebral-White-Matter ctx-lh-middletemporal ctx-lh-superiortemporal ctx-lh-temporalpole ctx-lh-lateralorbitofrontal ctx-lh-insula	7.79 3.71 11.93 3.69 20.11 20.82
20	348	ctx-lh-isthmuscingulate (44%) ctx-lh-precuneus (38%) Left-Cerebral-White-Matter (3%) [-2.75 -52.25 28]	ctx-rh-precuneus ctx-lh-isthmuscingulate ctx-lh-precuneus Left-Cerebral-White-Matter ctx-rh-isthmuscingulate Right-Cerebral-White-Matter	13.26 14.17 24.89 16.85 7.93 3.49
21	303	Brain-Stem (95%) Left-VentralDC (5%) [-2.75 -27.5 -12]	Brain-Stem Right-VentralDC Left-VentralDC Left-Cerebral-White-Matter Left-Hippocampus Left-Thalamus-Proper Right-Thalamus-Proper	39.72 10.37 19.28 2.76 4.83 4.21 1.17
22	604	ctx-lh-rostralanteriorcingulate (45%) ctx-lh-superiorfrontal (2%)	Left-Cerebral-White-Matter ctx-lh-medialorbitofrontal ctx-lh-rostralanteriorcingulate	13.67 6.44 14.73

		ctx-rh-rostralanteriorcingulate (11%) [0 41.25 4]	ctx-rh-rostralanteriorcingulate	10.75
			ctx-rh-medialorbitofrontal	4.24
			Right-Cerebral-White-Matter	7.11
			ctx-rh-superiorfrontal	6.67
			ctx-lh-superiorfrontal	9.46
			CC_Anterior	1.3
			ctx-rh-caudalanteriorcingulate	3.06
			ctx-lh-caudalanteriorcingulate	3.48
23	487	ctx-rh-inferiorparietal (3%) ctx-rh-inferiortemporal (3%) ctx-rh-lateraloccipital (56%) Right-Cerebral-White-Matter (26%) [46.75 -71.5 0]	ctx-rh-lateraloccipital	32.03
			ctx-rh-fusiform	3.3
			Right-Cerebral-White-Matter	29.37
			ctx-rh-inferiortemporal	4.77
			ctx-rh-middletemporal	3.28
			ctx-rh-inferiorparietal	12.83
24	259	ctx-rh-superiortemporal (44%) ctx-rh-temporalpole (31%) [35.75 16.5 -28]	ctx-rh-temporalpole	8.46
			ctx-rh-middletemporal	6.76
			ctx-rh-superiortemporal	15.08
			Right-Cerebral-White-Matter	10.79
			ctx-rh-lateralorbitofrontal	19.56
			ctx-rh-insula	5.51
25	232	ctx-rh-parsorbitalis (1%) ctx-rh-insula (47%) [44 16.5 -8]	ctx-rh-insula	27.66
			ctx-rh-superiortemporal	6.7
			Right-Cerebral-White-Matter	13.36
			ctx-rh-lateralorbitofrontal	2.13
			ctx-rh-parsorbitalis	4.8
			ctx-rh-parstriangularis	11.41
			ctx-rh-parsopercularis	3.76
26	357	Right-Cerebral-White-Matter (1%) Right-Amygdala (74%) [22 -2.75 -16]	Right-Cerebral-White-Matter	19.26
			Right-Amygdala	13.32
			ctx-rh-lateralorbitofrontal	1.15
			Right-Hippocampus	10.68
			ctx-rh-superiortemporal	1.02
			ctx-rh-insula	4.61
			Right-VentralDC	13.29
			Right-Putamen	4.76
			Right-Accumbens-area	1.7
			Right-Pallidum	3.1
27	654	ctx-lh-superiorfrontal (29%)	ctx-rh-medialorbitofrontal	2.65

		ctx-rh-superiorfrontal (4%) [0 57.75 16]	ctx-lh-medialorbitofrontal	3.18
			Left-Cerebral-White-Matter	9.66
			Right-Cerebral-White-Matter	7.24
			ctx-lh-superiorfrontal	23.64
			ctx-rh-superiorfrontal	21.83
28	503	ctx-lh-bankssts (3%) ctx-lh-inferiorparietal (48%) ctx-lh-lateraloccipital (2%) ctx-lh-middletemporal (11%) ctx-lh-supramarginal (2%) Left-Cerebral-White-Matter (12%) [-49.5 -63.25 16]	Left-Cerebral-White-Matter	25.19
			ctx-lh-inferiortemporal	2.54
			ctx-lh-lateraloccipital	3.39
			ctx-lh-middletemporal	11.21
			ctx-lh-bankssts	4.14
			ctx-lh-inferiorparietal	30.18
			ctx-lh-supramarginal	2.66
29	431	ctx-rh-bankssts (7%) ctx-rh-inferiorparietal (25%) ctx-rh-middletemporal (6%) Right-Cerebral-White-Matter (58%) [55 -52.25 12]	ctx-rh-middletemporal	14.45
			ctx-rh-inferiortemporal	2.45
			ctx-rh-lateraloccipital	1.54
			Right-Cerebral-White-Matter	26.83
			ctx-rh-bankssts	14.3
			ctx-rh-inferiorparietal	23.02
			ctx-rh-supramarginal	3.67
30	220	ctx-lh-caudalanteriorcingulate (55%) Left-Cerebral-White-Matter (1%) ctx-rh-caudalanteriorcingulate (10%) [0 16.5 28]	Right-Cerebral-White-Matter	10.88
			CC_Mid_Anterior	2.79
			CC_Anterior	3.22
			Left-Cerebral-White-Matter	13.16
			ctx-rh-caudalanteriorcingulate	16.86
			ctx-lh-caudalanteriorcingulate	19.71
			ctx-lh-superiorfrontal	2.43
			ctx-rh-posteriorcingulate	3.39
			ctx-lh-posteriorcingulate	5.41

Note. Percentages per centroid denote the population-average probability of an anatomical label. The average percentage of regional correspondence denotes the proportion of voxels mapping to a specific anatomical region. A 100 % correspondence would occur if all voxels of a parcellation would be located within an anatomical region such as the brain stem, and each voxel itself had a probability of 100 % of being located in the brain stem. Within a specific voxel, probabilities across anatomical labels do not necessarily sum to 100 %, and therefore anatomical correspondence per ROI may not sum to 100 %. Regions are in accordance to FreeSurfer nomenclature. The procedure is described in Materials and Methods, paragraph "*Anatomical localication of ROIs based on a population-averaged anatomical probabilistic atlas"*. Regional probabilities smaller than 1 % are not shown.

Table S6

Strength of directed connections from the cerebellum (R12) to other ROIs

	12
2	0.11921
3	0.093783
4	0.61016
5	0.27471
7	0.16686
9	0.36561
14	0.12886
20	0.06998
21	0.14973
22	0.13135
24	0.43569
25	0.19362
26	0.074432
28	0.184
29	0.074452
30	0.30206

Note. Table lists connections for the discovery sample. Connection strength as shown in the table represents the change in connection strength during "successful emotional memory encoding" (posterior probability > 0.99).

Table S7

Strength of directed connections from other ROIs to the cerebellum (R12)

	3	6	9	10	19	21	22	23	24	25	28	30
1	0.051	0.10	0.12	0.15	0.15	0.11	0.24	0.040	0.59	0.09	0.26	0.16
2	472	967	144	855	171	905	779	656	631	727	612	022

Note. Table lists connections for the discovery sample. Connection strength as shown in the table represents the change in connection strength during "successful emotional memory encoding" (posterior probability > 0.99).

Table S8

Strength of directed connections from the cerebellum (R12) to other ROIs

	12
2	0.25584
4	0.18826
7	0.098119
9	0.77797
14	0.15531
20	0.12753
21	0.2837
22	0.059954
25	0.18126
26	0.64998
28	0.0925
29	0.11791
30	0.090504

Note. Table lists connections for the replication sample. Connection strength as shown in the table represents the change in connection strength during "successful emotional memory encoding" (posterior probability > 0.99).

Table S9

Strength of directed connections from other ROIs to the cerebellum (R12)

	9	**10**	**22**	**23**	**25**
12	0.35532	0.072462	0.18277	0.25333	0.25304

Note. Table lists connections for the replication sample. Connection strength as shown in the table represents the change in connection strength during "successful emotional memory encoding" (posterior probability > 0.99).

Supplementary material: Study 4

Supplementary Figure S1A-F

Group-based selection rates of ICs found to be associated with inter-individual differences in memory performance (in Study 2)

Note. The vertical line indicates the mean of the group-based selection rate (see Table 5.1). ICs with a mean selection rate above 65 % were considered as important.

A

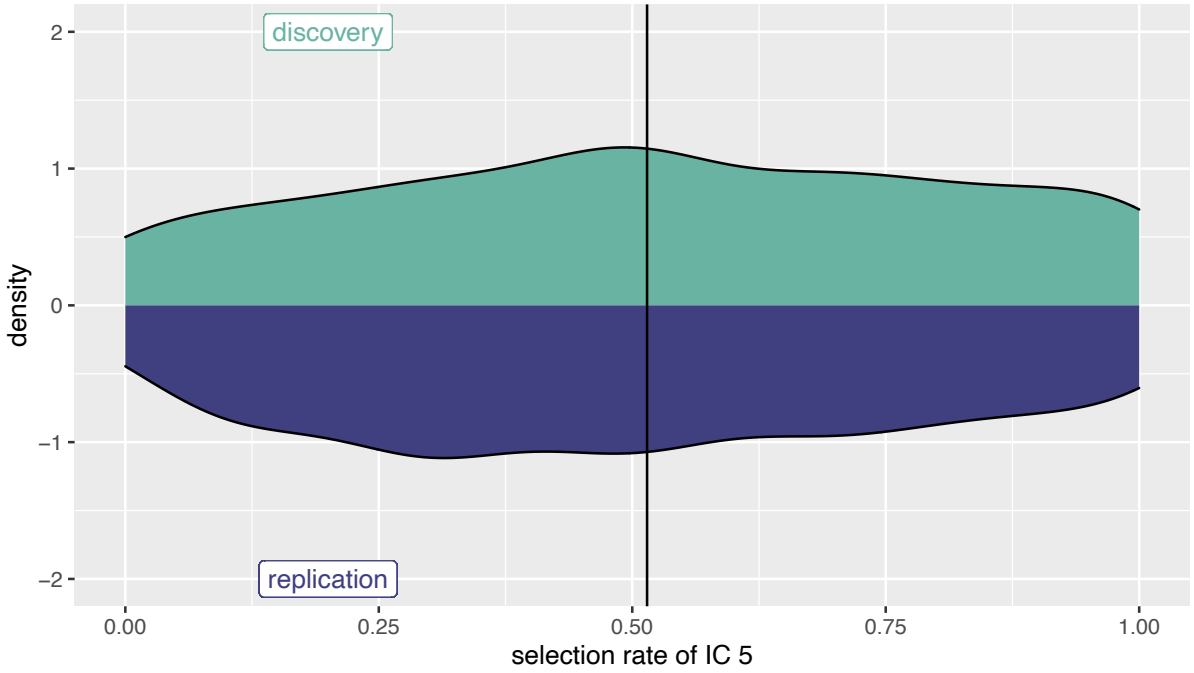

B

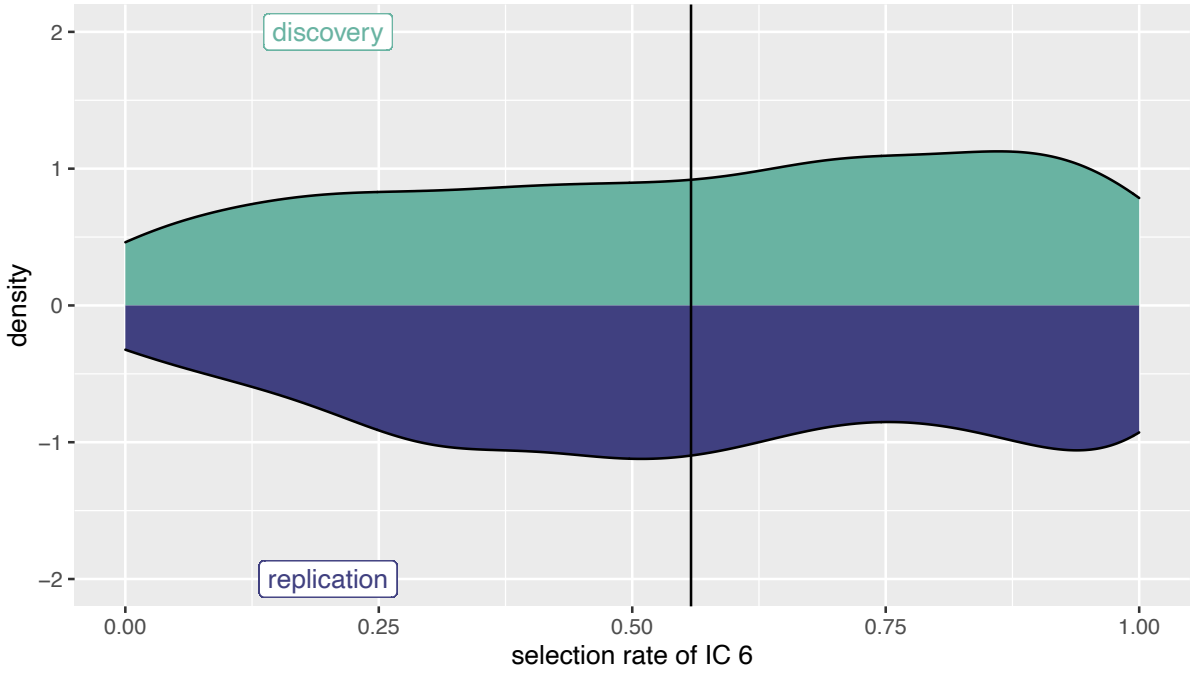

C

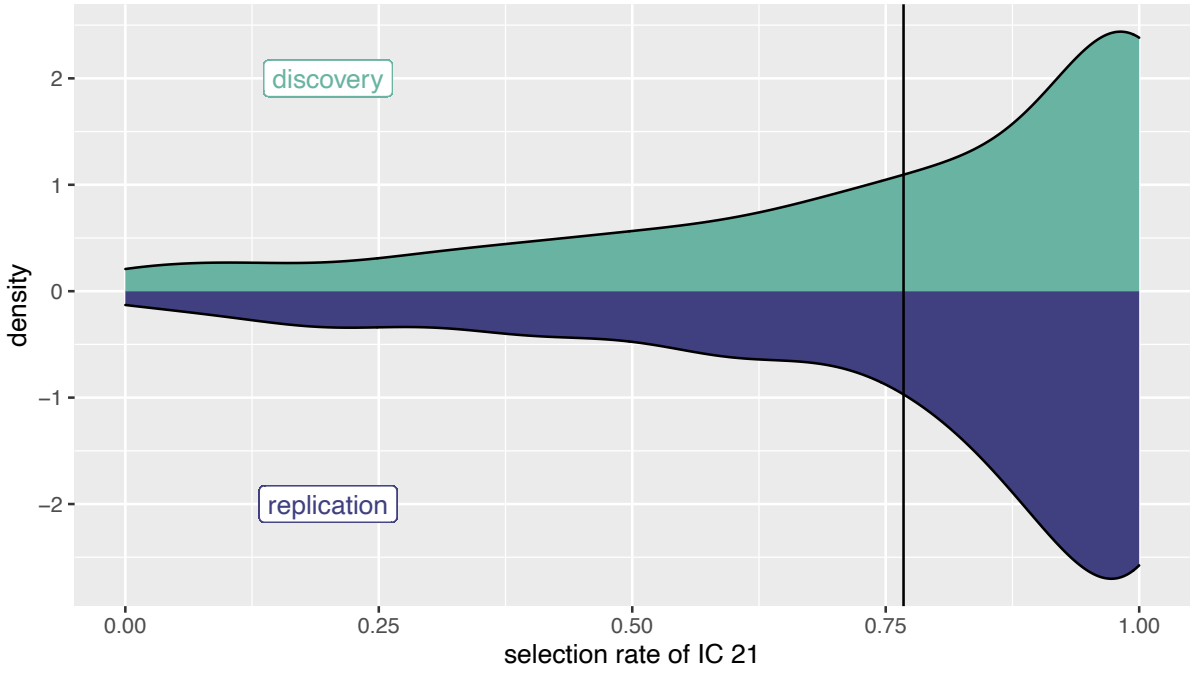
discovery
replication
density
2
1
0
−1
−2
0.00
0.25
0.50
0.75
1.00
selection rate of IC 21

D

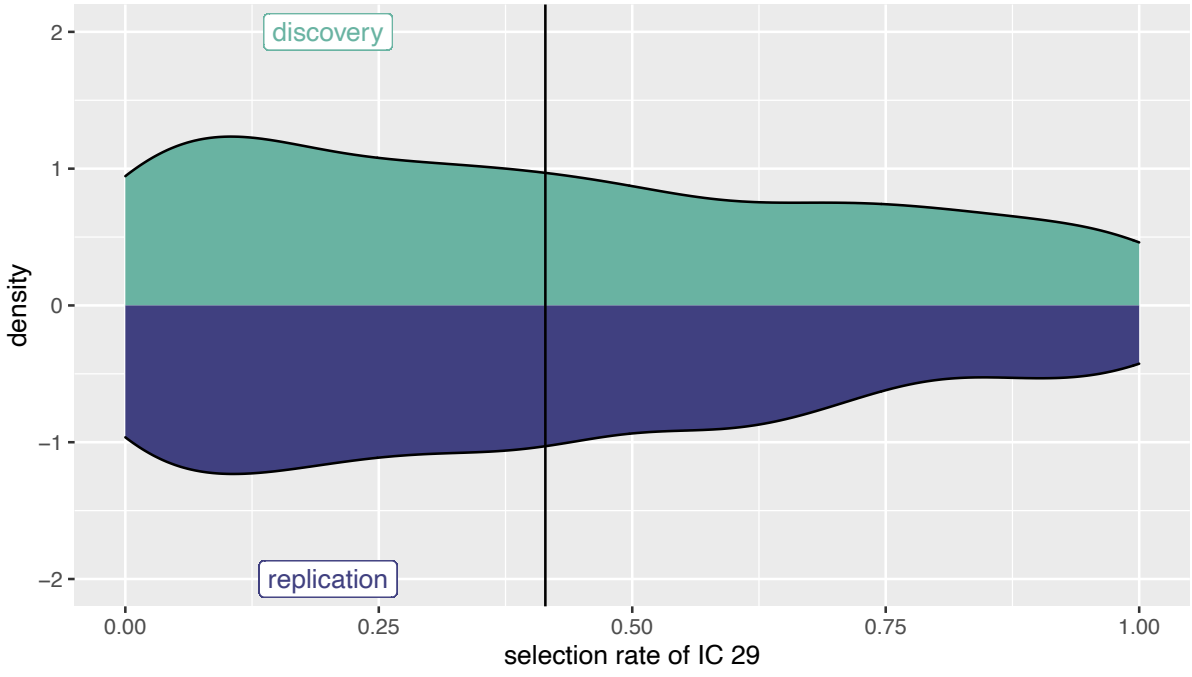
discovery
replication
density
2
1
0
−1
−2
0.00
0.25
0.50
0.75
1.00
selection rate of IC 29

E

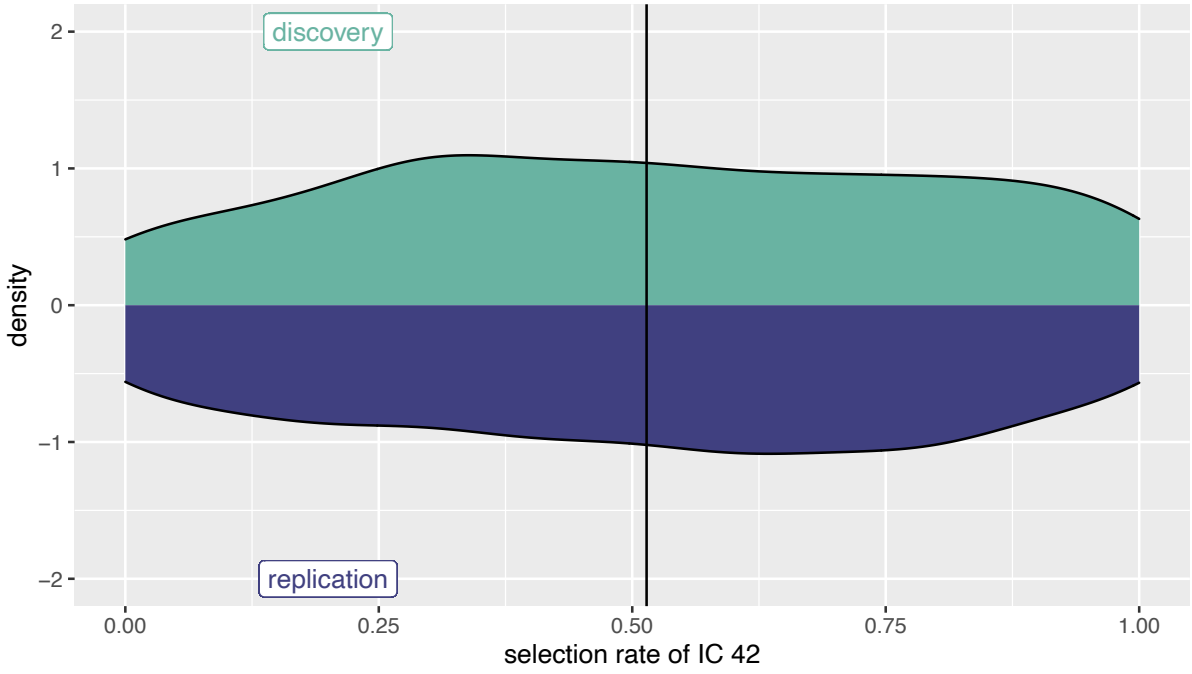
discovery
replication
density
2
1
0
−1
−2
0.00
0.25
0.50
0.75
1.00
selection rate of IC 42

F

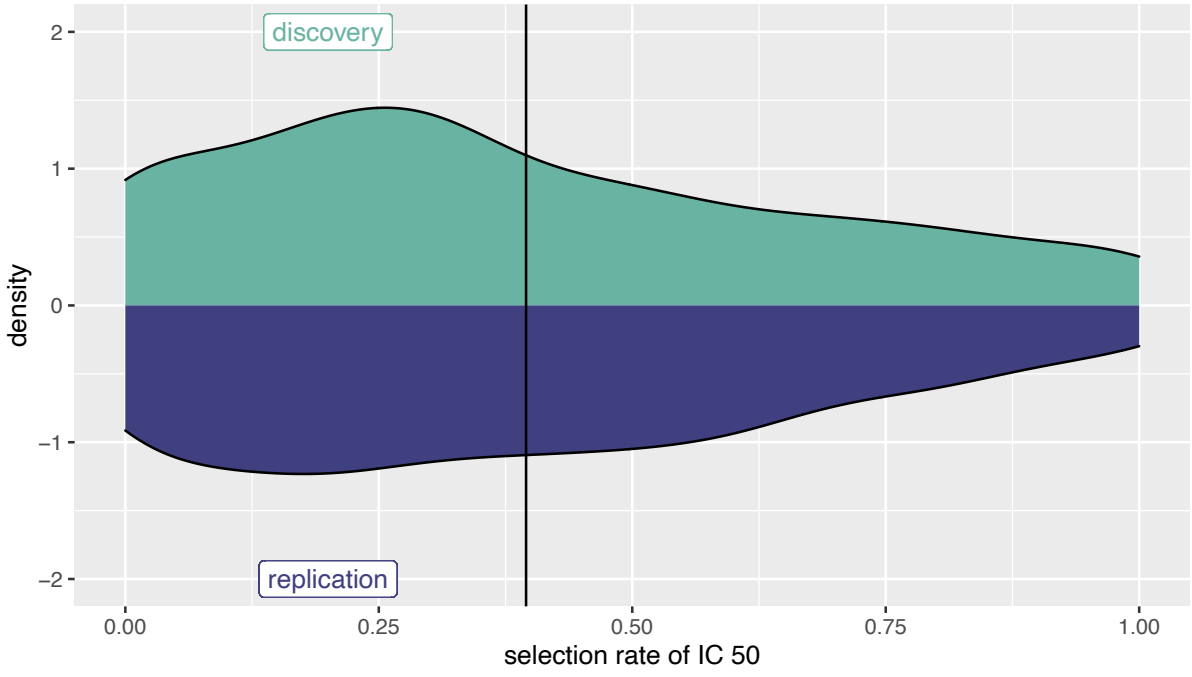
discovery
replication
density
2
1
0
−1
−2
0.00
0.25
0.50
0.75
1.00
selection rate of IC 50

References

Adamaszek, M., D'Agata, F., Ferrucci, R., Habas, C., Keulen, S., Kirkby, K. C., Leggio, M., Mariën, P., Molinari, M., Moulton, E., Orsi, L., Van Overwalle, F., Papadelis, C., Priori, A., Sacchetti, B., Schutter, D. J., Styliadis, C., & Verhoeven, J. (2017). Consensus Paper: Cerebellum and Emotion. *Cerebellum*, *16*(2), 552–576. https://doi.org/10.1007/s12311-016-0815-8

Adhikari, A., Topiwala, M. A., & Gordon, J. A. (2011). Single units in the medial prefrontal cortex with anxiety-related firing patterns are preferentially influenced by ventral hippocampal activity. *Neuron*, *71*(5), 898–910. https://doi.org/10.1016/j.neuron.2011.07.027

Alberini, C. M., & LeDoux, J. E. (2013). Memory reconsolidation. *Current Biology*, *23*(17), R746–R750. https://doi.org/10.1016/j.cub.2013.06.046

Alderson, T. H., Bokde, A. L. W., Kelso, J. A. S., Maguire, L., & Coyle, D. (2020). Metastable neural dynamics underlies cognitive performance across multiple behavioural paradigms. *Human Brain Mapping*, *41*(12), 3212–3234. https://doi.org/10.1002/hbm.25009

Allen, P. J., Josephs, O., & Turner, R. (2000). A method for removing imaging artifact from continuous EEG recorded during functional MRI. *NeuroImage*, *12*(2), 230–239. https://doi.org/10.1006/nimg.2000.0599

Allen, T. A., & Fortin, N. J. (2013). The evolution of episodic memory. *Proceedings of the National Academy of Sciences*, *110*(Supplement 2), 10379–10386. https://doi.org/10.1073/pnas.1301199110

Anderson, K. M., Ge, T., Kong, R., Patrick, L. M., Spreng, R. N., Sabuncu, M. R., Yeo, B. T. T., & Holmes, A. J. (2021). Heritability of individualized cortical network topography. *Proceedings of the National Academy of Sciences of the United States of America*, *118*(9), e201627118. https://doi.org/10.1073/pnas.2016271118

Andrews-Hanna, J. R., Snyder, A. Z., Vincent, J. L., Lustig, C., Head, D., Raichle, M. E., & Buckner, R. L. (2007). Disruption of large-scale brain systems in advanced aging. *Neuron*, *56*(5), 924–935. https://doi.org/10.1016/j.neuron.2007.10.038.

Ashburner, J. (2007). A fast diffeomorphic image registration algorithm. *NeuroImage*, *38*(1), 95–113. https://doi.org/10.1016/j.neuroimage.2007.07.007

Bandelow, B., Krause, J., Wedekind, D., Broocks, A., Hajak, G., & Rüther, E. (2005). Early traumatic life events, parental attitudes, family history, and birth risk factors in patients with borderline personality disorder and healthy controls. *Psychiatry Research*, *134*(2), 169–179. https://doi.org/10.1016/j.psychres.2003.07.008

Banks, S. J., Eddy, K. T., Angstadt, M., Nathan, P. J., & Luan Phan, K. (2007). Amygdala-frontal connectivity during emotion regulation. *Social Cognitive and Affective Neuroscience*, *2*(4), 303–312. https://doi.org/10.1093/scan/nsm029

Barkhof, F., Haller, S., & Rombouts, S. A. R. B. (2014). Resting-state functional MR imaging: A new window to the brain. *Radiology*, *272*(1), 29–49. https://doi.org/10.1148/radiol.14132388

Baron-Cohen, S., Ring, H. A., Bullmore, E. T., Wheelwright, S., Ashwin, C., & Williams, S. C. R. (2000). The amygdala theory of autism. *Neuroscience & Biobehavioral Reviews*, *24*(3), 355–364. https://doi.org/10.1016/S0149-7634(00)00011-7

Bauman, M. L., & Kemper, T. L. (2005). Neuroanatomic observations of the brain in autism: a review and future directions. *International Journal of Developmental Neuroscience*, *23*(2), 183–187. https://doi.org/10.1016/j.ijdevneu.2004.09.006

Baumann, O., & Mattingley, J. B. (2012). Functional topography of primary emotion

processing in the human cerebellum. *NeuroImage*, *61*(4), 805–811. https://doi.org/10.1016/j.neuroimage.2012.03.044
Beckmann, C. F., Mackay, C. E., Filippini, N., & Smith, S. M. (2009). Group comparison of resting-state FMRI data using multi-subject ICA and dual regression. *OHBM*. https://doi.org/10.1073/pnas.0811879106
Beckmann, C. F., & Smith, S. M. (2004). Probabilistic independent component analysis for functional magnetic resonance imaging. *IEEE Transactions On Medical Imaging*, *23*(2), 137–152. https://doi.org/10.1016/B978-0-444-64148-9.00019-3
Behzadi, Y., Restom, K., Liau, J., & Liu, T. T. (2007). A component based noise correction method (CompCor) for BOLD and perfusion based fMRI. *NeuroImage*, *37*(1), 90–101. https://doi.org/10.1016/j.neuroimage.2007.04.042
Bernardi, G., Ricciardi, E., Sani, L., Gaglianese, A., Papasogli, A., Ceccarelli, R., Franzoni, F., Galetta, F., Santoro, G., Goebel, R., & Pietrini, P. (2013). How skill expertise shapes the brain functional architecture: An fMRI study of visuo-spatial and motor processing in professional racing-car and naïve drivers. *PLoS One*, *8*(10), e77764. https://doi.org/10.1371/journal.pone.0077764
Berry, D. A., & Hochberg, Y. (1999). Bayesian perspectives on multiple comparisons. *Journal of Statistical Planning and Inference*, *82*(1), 215–227. https://doi.org/10.1016/S0378-3758(99)00044-0
Beversdorf, D. Q., Anderson, J. M., Manning, S. E., Anderson, S. L., Nordgren, R. E., Felopulos, G. J., Nadeau, S. E., Heilman, K. M., & Bauman, M. L. (1998). The effect of semantic and emotional context on written recall for verbal language in high functioning adults with autism spectrum disorder. *Journal of Neurology, Neurosurgery, and Psychiatry*, *65*(5), 685–692. https://doi.org/10.1136/jnnp.65.5.685
Biswal, B., Mennes, M., Zuo, X.-N., Gohel, S., Kelly, C., Smith, S. M., Beckmann, C. F., Adelstein, J. S., Buckner, R. L., Colcombe, S., Dogonowski, A.-M., Ernst, M., Fair, D., Hampson, M., Hoptman, M. J., Hyde, J. S., Kiviniemi, V. J., Kötter, R., Li, S.-J., … Milham, M. P. (2010). Toward discovery science of human brain function. *Proceedings of the National Academy of Sciences of the United States of America*, *107*(10), 4734–4739. https://doi.org/10.1073/pnas.0911855107
Biswal, B., Yetkin, F. Z., Haughton, V. M., & Hyde, J. S. (1995). Functional connectivity in the motor cortex of resting human brain using echo-planar MRI. *Magnetic Resonance in Medicine*, *34*(4), 537–541. https://doi.org/10.1002/mrm.1910340409
Borkenau, P., & Ostendorf, F. (1993). *NEO-Fünf-Faktoren-Inventar (NEO-FFI) nach Costa und McCrae*. Hogrefe.
Bostan, A. C., & Strick, P. L. (2018). The basal ganglia and the cerebellum: Nodes in an integrated network. *Nature Reviews Neuroscience*, *19*(6), 338–350. https://doi.org/10.1038/s41583-018-0002-7
Bravo-Rivera, C., & Sotres-Bayon, F. (2020). From isolated emotional memories to their competition during conflict. *Frontiers in Behavioral Neuroscience*, *14*, 36. https://doi.org/10.3389/fnbeh.2020.00036
Bressler, S. L., & Tognoli, E. (2006). Operational principles of neurocognitive networks. *International Journal of Psychophysiology*, *60*(2), 139–148. https://doi.org/10.1016/j.ijpsycho.2005.12.008
Brissenden, J. A., Levin, E. J., Osher, D. E., Halko, M. A., & Somers, D. C. (2016). Functional evidence for a cerebellar node of the dorsal attention network. *The Journal of Neuroscience*, *36*(22), 6083–6096. https://doi.org/10.1523/JNEUROSCI.0344-16.2016
Buckner, R. L., Andrews-Hanna, J. R., & Schacter, D. L. (2008). The brain's default network:

anatomy, function, and relevance to disease. *Annals of the New York Academy of Sciences*, *1124*, 1–38. https://doi.org/10.1196/annals.1440.011

Bunford, N., Hernández-Pérez, R., Farkas, E. B., Cuaya, L. V., Szabó, D., Szabó, Á. G., Gácsi, M., Miklósi, Á., & Andics, A. (2020). Comparative brain imaging reveals analogous and divergent patterns of species and face sensitivity in humans and dogs. *The Journal of Neuroscience*, *40*(43), 8396–8408. https://doi.org/10.1523/JNEUROSCI.2800-19.2020

Cabral, J., Hugues, E., Sporns, O., & Deco, G. (2011). Role of local network oscillations in resting-state functional connectivity. *NeuroImage*, *57*(1), 130–139. https://doi.org/10.1016/j.neuroimage.2011.04.010

Cahill, L., Uncapher, M., Kilpatrick, L., Alkire, M. T., & Turner, J. (2004). Sex-related hemispheric lateralization of amygdala function in emotionally influenced memory: an FMRI investigation. *Learning & Memory*, *11*(3), 261–266. https://doi.org/10.1101/lm.70504

Calhoon, G. G., & Tye, K. M. (2015). Resolving the neural circuits of anxiety. *Nature Neuroscience*, *18*(10), 1394–1404. https://doi.org/10.1038/nn.4101

Camchong, J., Stenger, A., & Fein, G. (2013). Resting-state synchrony during early alcohol abstinence can predict subsequent relapse. *Cerebral Cortex*, *23*(9), 2086–2099. https://doi.org/10.1093/cercor/bhs190

Canli, T., Zhao, Z., Brewer, J., Gabrieli, J. D. E., & Cahill, L. (2000). Event-related activation in the human amygdala associates with later memory for individual emotional experience. *The Journal of Neuroscience*, *20*(19), RC99. https://doi.org/10.1523/JNEUROSCI.20-19-j0004.2000

Caspi, A., Houts, R. M., Ambler, A., Danese, A., Elliott, M. L., Hariri, A., Harrington, H., Hogan, S., Poulton, R., Ramrakha, S., Rasmussen, L. J. H., Reuben, A., Richmond-Rakerd, L., Sugden, K., Wertz, J., Williams, B. S., & Moffitt, T. E. (2020). Longitudinal assessment of mental health disorders and comorbidities across 4 decades among participants in the Dunedin Birth Cohort Study. *JAMA Network Open*, *3*(4), e203221. https://doi.org/10.1001/jamanetworkopen.2020.3221

Cass, D. K., Thomases, D. R., Caballero, A., & Tseng, K. Y. (2013). Developmental disruption of gamma-aminobutyric acid function in the medial prefrontal cortex by noncontingent cocaine exposure during early adolescence. *Biological Psychiatry*, *74*(7), 490–501. https://doi.org/10.1016/j.biopsych.2013.02.021

Chai, X. J., Ofen, N., Gabrieli, J. D. E., & Whitfield-Gabrieli, S. (2014). Development of deactivation of the default-mode network during episodic memory formation. *NeuroImage*, *84*, 932–938. https://doi.org/10.1016/j.neuroimage.2013.09.032

Chai, X. J., Whitfield-Gabrieli, S., Shinn, A. K., Nieto-Castanon, A., Mccarthy, J. M., & Cohen, B. M. (2011). Abnormal medial prefrontal cortex resting-state connectivity in bipolar disorder and schizophrenia. *Neuropsychopharmacology*, *36*, 2009–2017. https://doi.org/10.1038/npp.2011.88

Chakraborty, R., Vijay Kumar, M. J., & Clement, J. P. (2021). Critical aspects of neurodevelopment. *Neurobiology of Learning and Memory*, *180*, 107415. https://doi.org/10.1016/j.nlm.2021.107415

Chan, R. W., Leong, A. T. L., Ho, L. C., Gao, P. P., Wong, E. C., Dong, C. M., Wang, X., He, J., Chan, Y. S., Lim, L. W., & Wu, E. X. (2017). Low-frequency hippocampal–cortical activity drives brain-wide resting-state functional MRI connectivity. *Proceedings of the National Academy of Sciences of the United States of America*, *114*(33), E6972–E6981. https://doi.org/10.1073/pnas.1703309114

Chao-Gan, Y., & Yu-Feng, Z. (2010). DPARSF: A MATLAB toolbox for “pipeline” data analysis

of resting-state fMRI. *Frontiers in Systems Neuroscience*, *4*, 13. https://doi.org/10.3389/fnsys.2010.00013

Cheng, D. T., Disterhoft, J. F., Power, J. M., Ellis, D. A., & Desmond, J. E. (2008). Neural substrates underlying human delay and trace eyeblink conditioning. *Proceedings of the National Academy of Sciences of the United States of America*, *105*(23), 8108–8113. https://doi.org/10.1073/pnas.0800374105

Cheng, D. T., Meintjes, E. M., Stanton, M. E., Desmond, J. E., Pienaar, M., Dodge, N. C., Power, J. M., Molteno, C. D., Disterhoft, J. F., Jacobson, J. L., & Jacobson, S. W. (2014). Functional MRI of cerebellar activity during eyeblink classical conditioning in children and adults. *Human Brain Mapping*, *35*(4), 1390–1403. https://doi.org/10.1002/hbm.22261

Choi, J. Y., Jang, H. J., Ornelas, S., Fleming, W. T., Fürth, D., Au, J., Bandi, A., Engel, E. A., & Witten, I. B. (2020). A Comparison of Dopaminergic and Cholinergic Populations Reveals Unique Contributions of VTA Dopamine Neurons to Short-Term Memory. *Cell Reports*, *33*(11), 108492. https://doi.org/10.1016/j.celrep.2020.108492

Clewett, D., Schoeke, A., & Mather, M. (2013). Amygdala functional connectivity is reduced after the cold pressor task. *Cognitive, Affective, & Behavioral Neuroscience*, *13*(3), 501–518. https://doi.org/10.3758/s13415-013-0162-x

Coffman, K. A., Dum, R. P., & Strick, P. L. (2011). Cerebellar vermis is a target of projections from the motor areas in the cerebral cortex. *Proceedings of the National Academy of Sciences of the United States of America*, *108*(38), 16068–16073. https://doi.org/10.1073/pnas.1107904108

Cohen, J. (1988). *Statistical Power Analysis for the Behavioral Sciences*. Routledge. https://doi.org/10.4324/9780203771587

Cohen, N., Pell, L., Edelson, M. G., Ben-Yakov, A., Pine, A., & Dudai, Y. (2015). Peri-encoding predictors of memory encoding and consolidation. *Neuroscience and Biobehavioral Reviews*, *50*, 128–142. https://doi.org/10.1016/j.neubiorev.2014.11.002

Cole, M. W., Reynolds, J. R., Power, J. D., Repovs, G., Anticevic, A., & Braver, T. S. (2013). Multi-task connectivity reveals flexible hubs for adaptive task control. *Nature Neuroscience*, *16*(9), 1348–1355. https://doi.org/10.1038/nn.3470.Multi-task

Cooper, S. R., Jackson, J. J., Barch, D. M., & Braver, T. S. (2019). Neuroimaging of individual differences: A latent variable modeling perspective. *Neuroscience and Biobehavioral Reviews*, *98*, 29–46. https://doi.org/10.1016/j.neubiorev.2018.12.022

Courchesne, E., Yeung-Courchesne, R., Hesselink, J. R., & Jernigan, T. L. (1988). Hypoplasia of cerebellar vermal lobules VI and VII in autism. *New England Journal of Medicine*, *318*(21), 1349–1354. https://doi.org/10.1056/NEJM198805263182102

Craddock, R. C., James, G. A., Holtzheimer III, P. E., Hu, X. P., & Mayberg, H. S. (2012). A whole brain fMRI atlas generated via spatially constrained spectral clustering. *Human Brain Mapping*, *33*(8), 1914–1928. https://doi.org/10.1002/hbm.21333

Cui, Z., Li, H., Xia, C. H., Larsen, B., Adebimpe, A., Baum, G. L., Cieslak, M., Gur, R. E., Gur, R. C., Moore, T. M., Oathes, D. J., Alexander-Bloch, A. F., Raznahan, A., Roalf, D. R., Shinohara, R. T., Wolf, D. H., Davatzikos, C., Bassett, D. S., Fair, D. A., … Satterthwaite, T. D. (2020). Individual Variation in Functional Topography of Association Networks in Youth. *Neuron*, *106*(2), 340-353.e8. https://doi.org/10.1016/j.neuron.2020.01.029

Dąbrowska, P. A., Voges, N., von Papen, M., Ito, J., Dahmen, D., Riehle, A., Brochier, T., & Grün, S. (2021). On the Complexity of Resting State Spiking Activity in Monkey Motor Cortex. *Cerebral Cortex Communications*, *2*(3). https://doi.org/10.1093/texcom/tgab033

Dahlgren, K., Ferris, C., & Hamann, S. (2020). Neural correlates of successful emotional episodic encoding and retrieval: An SDM meta-analysis of neuroimaging studies. *Neuropsychologia*, *143*, 107495. https://doi.org/10.1016/j.neuropsychologia.2020.107495

Damasio, A. R., Grabowski, T. J., Bechara, A., Damasio, H., Ponto, L. L. B., Parvizi, J., & Hichwa, R. D. (2000). Subcortical and cortical brain activity during the feeling of self-generated emotions. *Nature Neuroscience*, *3*(10), 1049–1056. https://doi.org/10.1038/79871

Damoiseaux, J. S., Rombouts, S. A. R. B., Barkhof, F., Scheltens, P., Stam, C. J., Smith, S. M., & Beckmann, C. F. (2006). Consistent resting-state networks across healthy subjects. *Proceedings of the National Academy of Sciences of the United States of America*, *103*(37), 13848–13853. https://doi.org/10.1073/pnas.0601417103

Dandash, O., Pantelis, C., & Fornito, A. (2017). Dopamine, fronto-striato-thalamic circuits and risk for psychosis. *Schizophrenia Research*, *180*, 48–57. https://doi.org/10.1016/J.SCHRES.2016.08.020

Dansereau, C., Benhajali, Y., Risterucci, C., Pich, E. M., Orban, P., Arnold, D., & Bellec, P. (2017). Statistical power and prediction accuracy in multisite resting-state fMRI connectivity. *NeuroImage*, *149*, 220–232. https://doi.org/10.1016/j.neuroimage.2017.01.072

Darwin, C. (1979). *The Origin of Species*. Avenel Books.

Daunizeau, J., David, O., & Stephan, K. E. (2011). Dynamic causal modelling: A critical review of the biophysical and statistical foundations. *NeuroImage*, *58*(2), 312–322. https://doi.org/10.1016/j.neuroimage.2009.11.062

de Quervain, D. J.-F., Kolassa, I.-T., Ackermann, S., Aerni, A., & Boesiger, P. (2012). PKCα is genetically linked to memory capacity in healthy subjects and to risk for posttraumatic stress disorder in genocide survivors. *Proceedings of the National Academy of Sciences of the United States of America*, *109*, 8746–8751. https://doi.org/10.1073/pnas.1200857109/-/DCSupplemental.www.pnas.org/cgi/doi/10.1073/pnas.1200857109

de Quervain, D. J.-F., Kolassa, I.-T., Ertl, V., Onyut, P. L., Neuner, F., Elbert, T., & Papassotiropoulos, A. (2007). A deletion variant of the α2b-adrenoceptor is related to emotional memory in Europeans and Africans. *Nature Neuroscience*, *10*(9), 1137–1139. https://doi.org/10.1038/nn1945

de Quervain, D. J. F., Schwabe, L., & Roozendaal, B. (2017). Stress, glucocorticoids and memory: implications for treating fear-related disorders. *Nature Reviews Neuroscience*, *18*(1), 7–19. https://doi.org/10.1038/nrn.2016.155

Deco, G., Jirsa, V. K., & McIntosh, A. R. (2011). Emerging concepts for the dynamical organization of resting-state activity in the brain. *Nature Reviews Neuroscience*, *12*(1), 43–56. https://doi.org/10.1038/nrn2961

Deligianni, F., Centeno, M., Carmichael, D. W., & Clayden, J. D. (2014). Relating resting-state fMRI and EEG whole-brain connectomes across frequency bands. *Frontiers in Neuroscience*, *8*, 258. https://doi.org/10.3389/fnins.2014.00258

Denis, D., Kim, S. Y., Kark, S. M., Daley, R. T., Kensinger, E. A., & Payne, J. D. (2021). Slow oscillation-spindle coupling is negatively associated with emotional memory formation following stress. *The European Journal of Neuroscience*, Advance online publication. https://doi.org/10.1111/ejn.15132

Deruelle, C., Hubert, B., Santos, A., & Wicker, B. (2008). Negative emotion does not enhance recall skills in adults with autistic spectrum disorders. *Autism Research*, *1*(2), 91–96.

https://doi.org/10.1002/aur.13
Desikan, R. S., Ségonne, F., Fischl, B., Quinn, B. T., Dickerson, B. C., Blacker, D., Buckner, R. L., Dale, A. M., Maguire, R. P., Hyman, B. T., Albert, M. S., & Killiany, R. J. (2006). An automated labeling system for subdividing the human cerebral cortex on MRI scans into gyral based regions of interest. *NeuroImage*, *31*(3), 968–980. https://doi.org/10.1016/j.neuroimage.2006.01.021
Di, X., & Biswal, B. B. (2015). Characterizations of resting-state modulatory interactions in the human brain. *Journal of Neurophysiology*, *114*(5), 2785–2796. https://doi.org/10.1152/jn.00893.2014
Dickerson, B. C., Salat, D. H., Greve, D. N., Chua, E. F., Rand-Giovannetti, E., Rentz, D. M., Bertram, L., Mullin, K., Tanzi, R. E., Blacker, D., Albert, M. S., & Sperling, R. A. (2005). Increased hippocampal activation in mild cognitive impairment compared to normal aging and AD. *Neurology*, *65*(3), 404–411. https://doi.org/10.1212/01.wnl.0000171450.97464.49
Diedrichsen, J., Balsters, J. H., Flavell, J., Cussans, E., & Ramnani, N. (2009). A probabilistic MR atlas of the human cerebellum. *NeuroImage*, *46*(1), 39–46. https://doi.org/10.1016/j.neuroimage.2009.01.045
Dolcos, F., Katsumi, Y., Weymar, M., Moore, M., Tsukiura, T., & Dolcos, S. (2017). Emerging directions in emotional episodic memory. *Frontiers in Psychology*, *8*, 1867. https://doi.org/10.3389/fpsyg.2017.01867
Dolcos, F., LaBar, K. S., & Cabeza, R. (2005). Remembering one year later: role of the amygdala and the medial temporal lobe memory system in retrieving emotional memories. *Proceedings of the National Academy of Sciences of the United States of America*, *102*(7), 2626–2631. https://doi.org/10.1073/pnas.0409848102
Dosenbach, N. U. F., Visscher, K. M., Palmer, E. D., Miezin, F. M., Wenger, K. K., Kang, H. C., Burgund, E. D., Grimes, A. L., Schlaggar, B. L., & Petersen, S. E. (2006). A core system for the implementation of task sets. *Neuron*, *50*(5), 799–812. https://doi.org/10.1016/j.neuron.2006.04.031
Dowdle, L. T., Ghose, G., Chen, C. C. C., Ugurbil, K., Yacoub, E., & Vizioli, L. (2021). Statistical power or more precise insights into neuro-temporal dynamics? Assessing the benefits of rapid temporal sampling in fMRI. *Progress in Neurobiology*, *207*, 102171. https://doi.org/10.1016/j.pneurobio.2021.102171
Drysdale, A. T., Grosenick, L., Downar, J., Dunlop, K., Mansouri, F., Meng, Y., Fetcho, R. N., Zebley, B., Oathes, D. J., Etkin, A., Schatzberg, A. F., Sudheimer, K., Keller, J., Mayberg, H. S., Gunning, F. M., Alexopoulos, G. S., Fox, M. D., Pascual-Leone, A., Voss, H. U., … Liston, C. (2017). Resting-state connectivity biomarkers define neurophysiological subtypes of depression. *Nature Medicine*, *23*(1), 28–38. https://doi.org/10.1038/nm.4246
Dubois, J., & Adolphs, R. (2016). Building a Science of Individual Differences from fMRI. In *Trends in Cognitive Sciences* (Vol. 20, Issue 6, pp. 425–443). https://doi.org/10.1016/j.tics.2016.03.014
Egli, T., Coynel, D., Spalek, K., Fastenrath, M., Freytag, V., Heck, A., Loos, E., Auschra, B., Papassotiropoulos, A., de Quervain, D. J.-F., & Milnik, A. (2018). Identification of two distinct working memory-related brain networks in healthy young Adults. *ENeuro*, *5*(1), ENEURO.0222-17.2018. https://doi.org/10.1523/ENEURO.0222-17.2018
Eippert, F., Veit, R., Weiskopf, N., Erb, M., Birbaumer, N., & Anders, S. (2007). Regulation of emotional responses elicited by threat-related stimuli. *Human Brain Mapping*, *28*(5), 409–423. https://doi.org/10.1002/hbm.20291

El Zein, M., Wyart, V., & Grèzes, J. (2015). Anxiety dissociates the adaptive functions of sensory and motor response enhancements to social threats. *ELife*, *4*, e10274. https://doi.org/10.7554/eLife.10274

Eldridge, L. L., Engel, S. A., Zeineh, M. M., Bookheimer, S. Y., & Knowlton, B. J. (2005). A dissociation of encoding and retrieval processes in the human hippocampus. *The Journal of Neuroscience*, *25*(13), 3280–3286. https://doi.org/10.1523/JNEUROSCI.3420-04.2005

Engen, H. G., & Anderson, M. C. (2018). Memory Control: A Fundamental Mechanism of Emotion Regulation. *Trends in Cognitive Sciences*, *22*(11), 982–995. https://doi.org/10.1016/j.tics.2018.07.015

Erk, S., Mikschl, A., Stier, S., Ciaramidaro, A., Gapp, V., Weber, B., & Walter, H. (2010). Acute and sustained effects of cognitive emotion regulation in major depression. *The Journal of Neuroscience*, *30*(47), 15726–15734. https://doi.org/10.1523/JNEUROSCI.1856-10.2010

Fair, D., Cohen, A. L., Dosenbach, N. U. F., Church, J. A., Miezin, F. M., Barch, D. M., Raichle, M. E., Petersen, S. E., & Schlaggar, B. L. (2008). The maturing architecture of the brain's default network. *Proceedings of the National Academy of Sciences of the United States of America*, *105*(10), 4028–4032. https://doi.org/10.1073/pnas.0800376105

Fastenrath, M., Coynel, D., Spalek, K., Milnik, A., Gschwind, L., Roozendaal, B., Papassotiropoulos, A., & de Quervain, D. J.-F. (2014). Dynamic modulation of amygdala-hippocampal connectivity by emotional arousal. *The Journal of Neuroscience*, *34*(42), 13935–13947. https://doi.org/10.1523/JNEUROSCI.0786-14.2014

Faul, L., Stjepanović, D., Stivers, J. M., Stewart, G. W., Graner, J. L., Morey, R. A., & LaBar, K. S. (2020). Proximal threats promote enhanced acquisition and persistence of reactive fear-learning circuits. *Proceedings of the National Academy of Sciences of the United States of America*, *117*(28), 16678–16689. https://doi.org/10.1073/pnas.2004258117

Fernandez, K. C., Jazaieri, H., & Gross, J. J. (2016). Emotion Regulation: A Transdiagnostic Perspective on a New RDoC Domain. *Cognitive Therapy and Research*, *40*(3), 426–440. https://doi.org/10.1007/s10608-016-9772-2

Ferreira, L. K., & Busatto, G. F. (2013). Resting-state functional connectivity in normal brain aging. *Neuroscience and Biobehavioral Reviews*, *37*(3), 384–400. https://doi.org/10.1016/j.neubiorev.2013.01.017

Filippini, N., Macintosh, B. J., Hough, M. G., Goodwin, G. M., Frisoni, G. B., Smith, S. M., Matthews, P. M., Beckmann, C. F., & Mackay, C. E. (2009). Distinct patterns of brain activity in young carriers of the APOE-4 allele. *Proceedings of the National Academy of Sciences of the United States of America*, *106*(17), 7209–7214. https://doi.org/10.1073/pnas.0811879106

Finn, E. S., Scheinost, D., Finn, D. M., Shen, X., Papademetris, X., & Constable, R. T. (2017). Can brain state be manipulated to emphasize individual differences in functional connectivity? *NeuroImage*, *160*, 140–151. https://doi.org/10.1016/j.neuroimage.2017.03.064

Fischl, B., Salat, D. H., Busa, E., Albert, M., Dieterich, M., Haselgrove, C., Van Der Kouwe, A., Killiany, R., Kennedy, D., Klaveness, S., Montillo, A., Makris, N., Rosen, B., & Dale, A. M. (2002). Whole brain segmentation: automated labeling of neuroanatomical structures in the human brain. *Neuron*, *33*(3), 341–355. https://doi.org/10.1016/S0896-6273(02)00569-X

Fjell, A. M., Sneve, M. H., Grydeland, H., Storsve, A. B., Lange, A. G. De, Amlien, I. K., Røgeberg, O. J., & Walhovd, K. B. (2015). Functional connectivity change across multiple

cortical networks relates to episodic memory changes in aging. *Neurobiology of Aging*, *36*(12), 3255–3268. https://doi.org/10.1016/j.neurobiolaging.2015.08.020

Fonseca, R., Vabulas, R. M., Hartl, F. U., Bonhoeffer, T., & Nägerl, U. V. (2006). A balance of protein synthesis and proteasome-dependent degradation determines the maintenance of LTP. *Neuron*, *52*(2), 239–245. https://doi.org/10.1016/j.neuron.2006.08.015

Fornito, A., Harrison, B. J., Zalesky, A., & Simons, J. S. (2012). Competitive and cooperative dynamics of large-scale brain functional networks supporting recollection. *Proceedings of the National Academy of Sciences of the United States of America*, *109*(31), 12788–12793. https://doi.org/10.1073/pnas.1204185109

Fornito, A., Zalesky, A., & Breakspear, M. (2015). The connectomics of brain disorders. *Nature Reviews Neuroscience*, *16*(3), 159–172. https://doi.org/10.1038/nrn3901

Frank, L. E., Preston, A. R., & Zeithamova, D. (2019). Functional connectivity between memory and reward centers across task and rest track memory sensitivity to reward. *Cognitive, Affective and Behavioral Neuroscience*, *19*(3), 503–522. https://doi.org/10.3758/s13415-019-00700-8

Fransson, P., Skiöld, B., Horsch, S., Nordell, A., Blennow, M., Lagercrantz, H., & Aden, U. (2007). Resting-state networks in the infant brain. *Proceedings of the National Academy of Sciences of the United States of America*, *104*(39), 15531–15536. https://doi.org/10.1073/pnas.0704380104

Fransson, P., & Thompson, W. H. (2020). Temporal flow of hubs and connectivity in the human brain. *NeuroImage*, *223*, 117348. https://doi.org/10.1016/j.neuroimage.2020.117348

Friedman, J. H., Hastie, T., & Tibshirani, R. (2010). Regularization Paths for Generalized Linear Models via Coordinate Descent. *Journal of Statistical Software*, *33*(1), 1–22. https://doi.org/10.18637/jss.v033.i01

Friston, K. J., Harrison, L., & Penny, W. (2003). Dynamic causal modelling. *NeuroImage*, *19*(4), 1273–1302. https://doi.org/10.1016/S1053-8119(03)00202-7

Friston, K. J., Li, B., Daunizeau, J., & Stephan, K. E. (2011). Network discovery with DCM. *NeuroImage*, *56*(3), 1202–1221. https://doi.org/10.1016/j.neuroimage.2010.12.039

Friston, K. J., & Penny, W. (2003). Posterior probability maps and SPMs. *NeuroImage*, *19*(3), 1240–1249. https://doi.org/10.1016/S1053-8119(03)00144-7

Friston, K. J., Penny, W. D., Ashburner, J., Kiebel, S., & Nichols, T. E. (2007). *Statistical Parametric Mapping: The Analysis of Functional Brain Images*. Academic Press.

Friston, K. J., Williams, S., Howard, R., Frackowiak, R. S., & Turner, R. (1996). Movement-related effects in fMRI time-series. *Magnetic Resonance in Medicine*, *35*(3), 346–355. https://doi.org/10.1002/mrm.1910350312

Gale, G. D., Anagnostaras, S. G., Godsil, B. P., Mitchell, S., Nozawa, T., Sage, J. R., Wiltgen, B., & Fanselow, M. S. (2004). Role of the basolateral amygdala in the storage of fear memories across the adult lifetime of rats. *The Journal of Neuroscience*, *24*(15), 3810–3815. https://doi.org/10.1523/JNEUROSCI.4100-03.2004

Gaudio, S., Piervincenzi, C., Beomonte Zobel, B., Romana Montecchi, F., Riva, G., Carducci, F., & Cosimo Quattrocchi, C. (2015). Altered resting state functional connectivity of anterior cingulate cortex in drug naïve adolescents at the earliest stages of anorexia nervosa. *Scientific Reports*, *5*(2014), 10818. https://doi.org/10.1038/srep10818

Gediminas, L., Fastenrath, M., Coynel, D., Freytag, V., Gschwind, L., Heck, A., Jessen, F., Maier, W., Milnik, A., Riedel-Heller, S. G., Scherer, M., Spalek, K., Vogler, C., Wagner, M., Wolfsgruber, S., Papassotiropoulos, A., & de Quervain, D. J.-F. (2015).

Computational dissection of human episodic memory reveals mental process-specific genetic profiles. *Proceedings of the National Academy of Sciences of the United States of America*, *112*(35), E4939–E4948. https://doi.org/10.1073/pnas.1500860112

Geissmann, L., Gschwind, L., Schicktanz, N., Deuring, G., Rosburg, T., Schwegler, K., Gerhards, C., Milnik, A., Pflueger, M. O., Mager, R., de Quervain, D. J. F., & Coynel, D. (2018). Resting-state functional connectivity remains unaffected by preceding exposure to aversive visual stimuli. *NeuroImage*, *167*, 354–365. https://doi.org/10.1016/j.neuroimage.2017.11.046

Gerhard, D. M., Meyer, H. C., & Lee, F. S. (2021). An adolescent sensitive period for threat responding: impacts of stress and sex. *Biological Psychiatry*, *89*(7), 651–658. https://doi.org/10.1016/j.biopsych.2020.10.003

Geschwind, D. H., & Rakic, P. (2013). Cortical evolution: Judge the brain by its cover. *Neuron*, *80*(3), 633–647. https://doi.org/10.1016/j.neuron.2013.10.045

Ghashghaei, H. T., & Barbas, H. (2002). Pathways for emotion: Interactions of prefrontal and anterior temporal pathways in the amygdala of the rhesus monkey. *Neuroscience*, *115*(4), 1261–1279. https://doi.org/10.1016/S0306-4522(02)00446-3

Gilmore, A. W., Nelson, S. M., & McDermott, K. B. (2015). A parietal memory network revealed by multiple MRI methods. *Trends in Cognitive Sciences*, *19*(9), 534–543. https://doi.org/10.1016/j.tics.2015.07.004

Gogolla, N. (2017). The insular cortex. *Current Biology*, *27*(12), R580–R586. https://doi.org/10.1016/j.cub.2017.05.010

Golier, J. a, Yehuda, R., Bierer, L. M., Mitropoulou, V., New, A. S., Schmeidler, J., Silverman, J. M., & Siever, L. J. (2003). The relationship of borderline personality disorder to posttraumatic stress disorder and traumatic events. *The American Journal of Psychiatry*, *160*(11), 2018–2024. https://doi.org/10.1176/appi.ajp.160.11.2018

Golonka, K., Mojsa-Kaja, J., Popiel, K., Marek, T., & Gawlowska, M. (2017). Neurophysiological markers of emotion processing in burnout syndrome. *Frontiers in Psychology*, *8*, 2155. https://doi.org/10.3389/fpsyg.2017.02155

Gong, Q., Li, L., Du, M., Pettersson-Yeo, W., Crossley, N., Yang, X., Li, J., Huang, X., & Mechelli, A. (2014). Quantitative prediction of individual psychopathology in trauma survivors using resting-state fMRI. *Neuropsychopharmacology*, *39*(3), 681–687. https://doi.org/10.1038/npp.2013.251

Gratton, C., Laumann, T. O., Gordon, E. M., Adeyemo, B., & Petersen, S. E. (2016). Evidence for Two Independent Factors that Modify Brain Networks to Meet Task Goals. *Cell Reports*, *17*(5), 1276–1288. https://doi.org/10.1016/j.celrep.2016.10.002

Greene, A. S., Gao, S., Noble, S., Scheinost, D., & Constable, R. T. (2020). How tasks change whole-brain functional organization to reveal brain-phenotype relationships. *Cell Reports*, *32*(8), 108066. https://doi.org/10.1016/j.celrep.2020.108066.

Gu, Z., Gu, L., Eils, R., Schlesner, M., & Brors, B. (2014). circlize Implements and enhances circular visualization in R. *Bioinformatics (Oxford, England)*, *30*(19), 2811–2812. https://doi.org/10.1093/bioinformatics/btu393

Guell, X., Schmahmann, J. D., Gabrieli, J. D. E., & Ghosh, S. S. (2018). Functional gradients of the cerebellum. *ELife*, *7*, e36652. https://doi.org/10.7554/eLife.36652

Habas, C., Kamdar, N., Nguyen, D., Prater, K., Beckmann, C. F., Menon, V., & Greicius, M. D. (2009). Distinct cerebellar contributions to intrinsic connectivity networks. *The Journal of Neuroscience*, *29*(26), 8586–8594. https://doi.org/10.1523/JNEUROSCI.1868-09.2009

Hamann, S. (2001). Cognitive and neural mechanisms of emotional memory. *Trends in Cognitive Sciences*, *5*(9), 394–400. https://doi.org/10.1016/S1364-6613(00)01707-1

Hamann, S. B., Ely, T. D., Grafton, S. T., & Kilts, C. D. (1999). Amygdala activity related to enhanced memory for pleasant and aversive stimuli. *Nature Neuroscience*, *2*(3), 289–293. https://doi.org/10.1038/6404

Hautzinger, M., & Bailer, M. (1993). *Allgemeine Depressionsskala*. Beltz Verlag.

Heath, R. G. (1973). Fastigial nucleus connections to the septal region in monkey and cat: a demonstration with evoked potentials of a bilateral pathway. *Biological Psychiatry*, *6*, 193–196.

Heath, R. G., Dempesy, C. W., Fontana, C. J., & Myers, W. A. (1978). Cerebellar stimulation: effects on septal region, hippocampus, and amygdala of cats and rats. *Biological Psychiatry*, *13*(5), 501–529.

Heck, A., Fastenrath, M., Ackermann, S., Auschra, B., Bickel, H., Coynel, D., Gschwind, L., Jessen, F., Kadzszkiewicz, H., Maier, W., Milnik, A., Pentzek, M., Riedel-Heller, S., Ripke, S., Spalek, K., Sullivan, P., Vogler, C., Wagner, M., Weyerer, S., … Papassotiropoulos, A. (2014). Converging genetic and functional brain imaging evidence links neuronal excitability to working memory, psychiatric disease, and brain activity. *Neuron*, *81*(5), 1203–1213. https://doi.org/10.1016/j.neuron.2014.01.010

Hegerl, U., Stein, M., Mulert, C., Mergl, R., Olbrich, S., Dichgans, E., Rujescu, D., & Pogarell, O. (2008). EEG-vigilance differences between patients with borderline personality disorder, patients with obsessive-compulsive disorder and healthy controls. *European Archives of Psychiatry and Clinical Neuroscience*, *258*(3), 137–143. https://doi.org/10.1007/s00406-007-0765-8

Hermans, E. J., van Marle, H. J. F., Ossewaarde, L., Henckens, M. J. A. G., Qin, S., van Kesteren, M. T. R., Schoots, V. C., Cousijn, H., Rijpkema, M., Oostenveld, R., & Fernández, G. (2011). Stress-related noradrenergic activity prompts large-scale neural network reconfiguration. *Science*, *334*(6059), 1151–1153. https://doi.org/10.1126/science.1209603

Hillebrandt, H., Dumontheil, I., Blakemore, S.-J., & Roiser, J. P. (2013). Dynamic causal modelling of effective connectivity during perspective taking in a communicative task. *NeuroImage*, *76*, 116–124. https://doi.org/10.1016/j.neuroimage.2013.02.072

Hjelmervik, H., Hausmann, M., Osnes, B., Westerhausen, R., & Specht, K. (2014). Resting states are resting traits - an fMRI study of sex differences and menstrual cycle effects in resting state cognitive control networks. *PLoS ONE*, *9*(7), 32–36. https://doi.org/10.1371/journal.pone.0103492

Höistad, M., & Barbas, H. (2008). Sequence of information processing for emotions through pathways linking temporal and insular cortices with the amygdala. *NeuroImage*, *40*(3), 1016–1033. https://doi.org/10.1016/j.neuroimage.2007.12.043.

Hollenstein, T. (2015). This Time, It's Real: Affective Flexibility, Time Scales, Feedback Loops, and the Regulation of Emotion. *Emotion Review*, *7*(4), 308–315. https://doi.org/10.1177/1754073915590621

Howarth, C., Gleeson, P., & Attwell, D. (2012). Updated energy budgets for neural computation in the neocortex and cerebellum. *Journal of Cerebral Blood Flow and Metabolism*, *32*(7), 1222–1232. https://doi.org/10.1038/jcbfm.2012.35

Hudson, J. I., Hiripi, E., Pope, H. G., & Kessler, R. C. (2007). The prevalence and correlates of eating disorders in the National Comorbidity Survey Replication. *Biological Psychiatry*, *61*(3), 348–358. https://doi.org/10.1016/j.biopsych.2006.03.040

Iannetti, G. D., Niazy, R. K., Wise, R. G., Jezzard, P., Brooks, J. C. W., Zambreanu, L., Vennart, W., Matthews, P. M., & Tracey, I. (2005). Simultaneous recording of laser-evoked brain potentials and continuous, high-field functional magnetic resonance imaging in

humans. *NeuroImage*, *28*(3), 708–719. https://doi.org/10.1016/j.neuroimage.2005.06.060
Insel, T. R. (2006). From species differences to individual differences. *Molecular Psychiatry*, *11*(5), 424. https://doi.org/10.1038/sj.mp.4001826
Ito, T. (1984). *The cerebellum and neural control*. Raven Press.
James L., M., Larry, C., & Benno, R. (1996). Involvement of the amygdala in memory storage: Interaction with other brain systems. *Proceedings of the National Academy of Sciences of the United States of America*, *93*(24), 13508–13514. https://doi.org/10.1073/pnas.93.24.13508
Janak, P. H., & Tye, K. M. (2015). From circuits to behaviour in the amygdala. *Nature*, *517*(7534), 284–292. https://doi.org/10.1038/nature14188
Jarovi, J., Volle, J., Yu, X., Guan, L., & Takehara-Nishiuchi, K. (2018). Prefrontal Theta Oscillations Promote Selective Encoding of Behaviorally Relevant Events. *ENeuro*, *5*(6), ENEURO.0407-18.2018. https://doi.org/10.1523/ENEURO.0407-18.2018
Jenkinson, M., Beckmann, C. F., Behrens, T. E. J., Woolrich, M. W., & Smith, S. M. (2012). FSL. *NeuroImage*, *62*(2), 782–790. https://doi.org/10.1016/j.neuroimage.2011.09.015
Jiang, L., Kundu, S., Lederman, J. D., López-Hernández, G. Y., Ballinger, E. C., Wang, S., Talmage, D. A., & Role, L. W. (2016). Cholinergic Signaling Controls Conditioned Fear Behaviors and Enhances Plasticity of Cortical-Amygdala Circuits. *Neuron*, *90*(5), 1057–1070. https://doi.org/10.1016/j.neuron.2016.04.028
Johns, M. W. (1991). A new method for measuring daytime sleepiness: The Epworth sleepiness scale. *Sleep*, *14*(6), 540–545.
Josselyn, S. A., & Frankland, P. W. (2018). Memory Allocation: Mechanisms and Function. *Annual Review of Neuroscience*, *41*(1), 389–413. https://doi.org/10.1146/annurev-neuro-080317-061956
Jung, W. H., Kang, D.-H., Kim, E., Shin, K. S., Jang, J. H., & Kwon, J. S. (2013). Abnormal corticostriatal-limbic functional connectivity in obsessive-compulsive disorder during reward processing and resting-state. *NeuroImage. Clinical*, *3*, 27–38. https://doi.org/10.1016/j.nicl.2013.06.013
Kanske, P., Heissler, J., Schönfelder, S., Bongers, A., & Wessa, M. (2011). How to regulate emotion? Neural networks for reappraisal and distraction. *Cerebral Cortex*, *21*(6), 1379–1388. https://doi.org/10.1093/cercor/bhq216
Kass, R. E., & Raftery, A. E. (1995). Bayes Factors. *Journal of the American Statistical Association*, *90*(430), 773–795. https://doi.org/10.1080/01621459.1995.10476572
Kelso, J. A. (1995). *Dynamic patterns: The self-organization of brain and behavior*. The MIT Press.
Kerr, K. L., Avery, J. A., Barcalow, J. C., Moseman, S. E., Bodurka, J., Bellgowan, P. S. F., & Simmons, W. K. (2015). Trait impulsivity is related to ventral ACC and amygdala activity during primary reward anticipation. *Social Cognitive and Affective Neuroscience*, *10*(1), 36–42. https://doi.org/10.1093/scan/nsu023
Kessler, R. C., Angermeyer, M., Anthony, J. C., DE Graaf, R., Demyttenaere, K., Gasquet, I., DE Girolamo, G., Gluzman, S., Gureje, O., Haro, J. M., Kawakami, N., Karam, A., Levinson, D., Medina Mora, M. E., Oakley Browne, M. A., Posada-Villa, J., Stein, D. J., Adley Tsang, C. H., Aguilar-Gaxiola, S., … Ustün, T. B. (2007). Lifetime prevalence and age-of-onset distributions of mental disorders in the World Health Organization's World Mental Health Survey Initiative. *World Psychiatry : Official Journal of the World Psychiatric Association (WPA)*, *6*(3), 168–176.
Kiebel, S. J., Klöppel, S., Weiskopf, N., & Friston, K. J. (2007). Dynamic causal modeling: A

generative model of slice timing in fMRI. *NeuroImage*, *34*(4), 1487–1496. https://doi.org/10.1016/j.neuroimage.2006.10.026
Kim, H. (2011). Neural activity that predicts subsequent memory and forgetting: A meta-analysis of 74 fMRI studies. *NeuroImage*, *54*(3), 2446–2461. https://doi.org/10.1016/j.neuroimage.2010.09.045
Kim, H. (2019). Neural correlates of explicit and implicit memory at encoding and retrieval: A unified framework and meta-analysis of functional neuroimaging studies. *Biological Psychology*, *145*, 96–111. https://doi.org/10.1016/j.biopsycho.2019.04.006
Kim, J., Chun, J., Park, C., Cho, H., Choi, J., Yang, S., Ahn, K., & Kim, D. J. (2019). The correlation between the frontostriatal network and impulsivity in internet gaming disorder. *Scientific Reports*, *9*(1), 1191. https://doi.org/10.1038/s41598-018-37702-4
Kim, M. J., Loucks, R. A., Palmer, A. L., Brown, A. C., Solomon, K. M., Marchante, A. N., & Whalen, P. J. (2011). The structural and functional connectivity of the amygdala: from normal emotion to pathological anxiety. *Behavioural Brain Research*, *223*(2), 403–410. https://doi.org/10.1016/j.bbr.2011.04.025
Kim, S.-Y., Adhikari, A., Lee, S. Y., Marshel, J. H., Kim, C. K., Mallory, C. S., Lo, M., Pak, S., Mattis, J., Lim, B. K., Malenka, R. C., Warden, M. R., Neve, R., Tye, K. M., & Deisseroth, K. (2013). Diverging neural pathways assemble a behavioural state from separable features in anxiety. *Nature*, *496*(7444), 219–223. https://doi.org/10.1038/nature12018
Kim, S. Y., & Payne, J. D. (2020). Neural correlates of sleep, stress, and selective memory consolidation. *Current Opinion in Behavioral Sciences*, *33*, 57–64. https://doi.org/10.1016/j.cobeha.2019.12.009
King, M., Hernandez-Castillo, C. R., Poldrack, R. A., Ivry, R. B., & Diedrichsen, J. (2019). Functional boundaries in the human cerebellum revealed by a multi-domain task battery. *Nature Neuroscience*, *22*(8), 1371–1378. https://doi.org/10.1038/s41593-019-0436-x
Klein, A., Andersson, J., Ardekani, B. A., Ashburner, J., Avants, B., Chiang, M.-C., Christensen, G. E., Collins, D. L., Gee, J., Hellier, P., Song, J. H., Jenkinson, M., Lepage, C., Rueckert, D., Thompson, P., Vercauteren, T., Woods, R. P., Mann, J. J., & Parsey, R. V. (2009). Evaluation of 14 nonlinear deformation algorithms applied to human brain MRI registration. *NeuroImage*, *46*(3), 786–802. https://doi.org/10.1016/j.neuroimage.2008.12.037
Klumpers, L. E., Cole, D. M., Khalili-Mahani, N., Soeter, R. P., te Beek, E. T., Rombouts, S. a R. B., & van Gerven, J. M. a. (2012). Manipulating brain connectivity with δ^9-tetrahydrocannabinol: A pharmacological resting state FMRI study. *NeuroImage*, *63*(3), 1701–1711. https://doi.org/10.1016/j.neuroimage.2012.07.051
Koziol, L. F., Budding, D., Andreasen, N., D'Arrigo, S., Bulgheroni, S., Imamizu, H., Ito, M., Manto, M., Marvel, C., Parker, K., Pezzulo, G., Ramnani, N., Riva, D., Schmahmann, J., Vandervert, L., & Yamazaki, T. (2014). Consensus Paper: The Cerebellum's Role in Movement and Cognition. *The Cerebellum*, *13*(1), 151–177. https://doi.org/10.1007/s12311-013-0511-x
Krakauer, J. W., Ghazanfar, A. A., Gomez-Marin, A., MacIver, M. A., & Poeppel, D. (2017). Neuroscience Needs Behavior: Correcting a Reductionist Bias. *Neuron*, *93*(3), 480–490. https://doi.org/10.1016/j.neuron.2016.12.041
Kranz, M. B., Voss, M. W., Id, G. E. C., & Banducci, S. E. (2018). The cortical structure of functional networks associated with age-related cognitive abilities in older adults. *PLoS ONE*, *13*(9), e0204280. https://doi.org/10.1371/journal.pone.0204280
Kret, M. E., & Ploeger, A. (2015). Emotion processing deficits: a liability spectrum providing

insight into comorbidity of mental disorders. *Neuroscience and Biobehavioral Reviews*, *52*, 153–171. https://doi.org/10.1016/j.neubiorev.2015.02.011

Kriegeskorte, N., Simmons, W. K., Bellgowan, P. S. F., & Baker, C. I. (2009). Circular analysis in systems neuroscience: the dangers of double dipping. *Nature Neuroscience*, *12*(5), 535–540. https://doi.org/10.1038/nn.2303.Circular

Krishnan, G. P., González, O. C., & Bazhenov, M. (2018). Origin of slow spontaneous resting-state neuronal fluctuations in brain networks. *Proceedings of the National Academy of Sciences of the United States of America*, *115*(26), 6858–6863. https://doi.org/10.1073/pnas.1715841115

Kunwar, P. S., Zelikowsky, M., Remedios, R., Cai, H., Yilmaz, M., Meister, M., & Anderson, D. J. (2015). Ventromedial hypothalamic neurons control a defensive emotion state. *ELife*, *4*, e06633. https://doi.org/10.7554/eLife.06633

Kurth, F., Zilles, K., Fox, P. T., Laird, A. R., & Eickhoff, S. B. (2010). A link between the systems: functional differentiation and integration within the human insula revealed by meta-analysis. *Brain Structure & Function*, *214*(5–6), 519–534. https://doi.org/10.1007/s00429-010-0255-z

LaBar, K. S., & Cabeza, R. (2006). Cognitive neuroscience of emotional memory. *Nature Reviews Neuroscience*, *7*(1), 54–64. https://doi.org/10.1038/nrn1825

Laird, A. R., Fox, M. P., Eickhoff, S. B., Turner, J. A., Ray, K. L., McKay, R. D., Glahn, D. C., Beckmann, C. F., Smith, S. M., & Fox, P. T. (2011). Behavioral interpretations of intrinsic connectivity networks. *Journal of Cognitive Neuroscience*, *23*(12), 4022–4037. https://doi.org/10.1162/jocn_a_00077

Lang, P. J., Bradley, M. M., & Cuthbert, B. N. (2005). *International affective picture system (IAPS): Affective ratings of pictures and instruction manual* (Technical).

Lange, I., Kasanova, Z., Goossens, L., Leibold, N., De Zeeuw, C. I., van Amelsvoort, T., & Schruers, K. (2015). The anatomy of fear learning in the cerebellum: A systematic meta-analysis. *Neuroscience and Biobehavioral Reviews*, *59*, 83–91. https://doi.org/10.1016/j.neubiorev.2015.09.019

Larsen, R. J., & Diener, E. (1987). Affect intensity as an individual difference characteristic: A review. *Journal of Research in Personality*, *21*(1), 1–39. https://doi.org/10.1016/0092-6566(87)90023-7

Laux, L., Glanzmann, P., Schaffner, P., & Spielberger, C. D. (1981). *Das State-Trait-Angstinventar. Theoretische Grundlagen und Handanweisung*. Beltz Test GmbH.

Lebreton, M., Bavard, S., Daunizeau, J., & Palminteri, S. (2019). Assessing inter-individual differences with task-related functional neuroimaging. *Nature Human Behaviour*, *3*(9), 897–905. https://doi.org/10.1038/s41562-019-0681-8

LeDoux, J. (2003). The Emotional Brain, Fear, and the Amygdala. *Cellular and Molecular Neurobiology*, *23*(4), 727–738. https://doi.org/10.1023/A:1025048802629

LeDoux, J. (2014). Coming to terms with fear. *Proceedings of the National Academy of Sciences of the United States of America*, *111*(8), 2871–2878. https://doi.org/10.1073/pnas.1400335111

Lee, T., & Kim, J. J. (2004). Differential effects of cerebellar, amygdalar, and hippocampal lesions on classical eyeblink conditioning in rats. *The Journal of Neuroscience*, *24*(13), 3242–3250. https://doi.org/10.1523/JNEUROSCI.5382-03.2004

Leff, A. P., Schofield, T. M., Stephan, K. E., Crinion, J. T., Friston, K. J., & Price, C. J. (2008). The cortical dynamics of intelligible speech. *The Journal of Neuroscience*, *28*(49), 13209–13215. https://doi.org/10.1523/JNEUROSCI.2903-08.2008

Lemon, N., Aydin-Abidin, S., Funke, K., & Manahan-Vaughan, D. (2009). Locus coeruleus

activation facilitates memory encoding and induces hippocampal LTD that depends on β-Adrenergic receptor activation. *Cerebral Cortex*, *19*(12), 2827–2837. https://doi.org/10.1093/cercor/bhp065

Light, G. A., Williams, L. E., Minow, F., Sprock, J., Rissling, A., Sharp, R., Swerdlow, N. R., & Braff, D. L. (2010). Electroencephalography (EEG) and Event-Related Potentials (ERPs) with Human Participants. *Current Protocols in Neuroscience*, *52*(1), 6.25.1-6.25.24. https://doi.org/10.1002/0471142301.ns0625s52

Lin, J.-J., Rugg, M. D., Das, S., Stein, J., Rizzuto, D. S., Kahana, M. J., & Lega, B. C. (2017). Theta band power increases in the posterior hippocampus predict successful episodic memory encoding in humans. *Hippocampus*, *27*(10), 1040–1053. https://doi.org/10.1002/hipo.22751

Liu, L., Tan, J., & Chen, A. (2015). Linking inter-individual differences in the perceptual load effect to spontaneous brain activity. *Frontiers in Human Neuroscience*, *9*, 1–7. https://doi.org/10.3389/fnhum.2015.00409

Logothetis, N. K. (2003). The underpinnings of the BOLD functional magnetic resonance imaging signal. *The Journal of Neuroscience*, *23*(10), 3963–3971. https://doi.org/10.1523/JNEUROSCI.23-10-03963.2003

Majerus, S., Salmon, E., & Attout, L. (2013). The importance of encoding-related neural dynamics in the prediction of inter-individual differences in verbal working memory performance. *PLoS ONE*, *8*(7), e69278. https://doi.org/10.1371/journal.pone.0069278

Manning, J., Reynolds, G., Saygin, Z. M., Hofmann, S. G., Pollack, M., Gabrieli, J. D. E., & Whitfield-Gabrieli, S. (2015). Altered resting-state functional connectivity of the frontal-striatal reward system in social anxiety disorder. *PLoS ONE*, *10*(4), e0125286. https://doi.org/10.1371/journal.pone.0125286

Mantini, D., Gerits, A., Nelissen, K., Durand, J.-B., Joly, O., Simone, L., Sawamura, H., Wardak, C., Orban, G. A., Buckner, R. L., & Vanduffel, W. (2011). Default mode of brain function in monkeys. *The Journal of Neuroscience*, *31*(36), 12954–12962. https://doi.org/10.1523/JNEUROSCI.2318-11.2011

Marreiros, A. C., Kiebel, S. J., & Friston, K. J. (2008). Dynamic causal modelling for fMRI: A two-state model. *NeuroImage*, *39*(1), 269–278. https://doi.org/10.1016/j.neuroimage.2007.08.019

Martini, M., Martini, C., Maran, T., & Sachse, P. (2018). Effects of post-encoding wakeful rest and study time on long-term memory performance. *Journal of Cognitive Psychology*, *30*(5–6), 558–569. https://doi.org/10.1080/20445911.2018.1506457

Martı, M., & Colom, R. (2013). Correlation between corpus callosum shape and cognitive performance in healthy young adults. *Brain Structure and Function*, *218*, 721–731. https://doi.org/10.1007/s00429-012-0424-3

Maschke, M., Schugens, M., Kindsvater, K., Drepper, J., Kolb, F. P., Diener, H.-C., Daum, I., & Timmann, D. (2002). Fear conditioned changes of heart rate in patients with medial cerebellar lesions. *Journal of Neurology, Neurosurgery, and Psychiatry*, *72*(1), 116–118. https://doi.org/10.1136/jnnp.72.1.116

Masson, M. E. J. (2011). A tutorial on a practical Bayesian alternative to null-hypothesis significance testing. *Behavior Research Methods*, *43*(3), 679–690. https://doi.org/10.3758/s13428-010-0049-5

McGaugh, J. L. (2000). Memory--a Century of Consolidation. *Science*, *287*(5451), 248–251. https://doi.org/10.1126/science.287.5451.248

McGaugh, J. L. (2003). *The Making of Lasting Memory*. Weidenfeld & Nicolson.

McGaugh, J. L. (2004). The amygdala modulates the consolidation of memories of

emotionally arousing experiences. *Annual Review of Neuroscience*, *27*, 1–28. https://doi.org/10.1146/annurev.neuro.27.070203.144157
McKeown, M. J., & Sejnowski, T. J. (1998). Independent component analysis of fMRI data: examining the assumptions. *Human Brain Mapping*, *6*(5–6), 368–372.
Menon, V., & Uddin, L. Q. (2010). Saliency, switching, attention and control: a network model of insula function. *Brain Structure and Function*, *214*(5), 655–667. https://doi.org/10.1007/s00429-010-0262-0
Meyer, D., Dimitriadou, E., Hornik, K., Weingessel, A., & Leisch, F. (2021). *e1071: Misc Functions of the Department of Statistics, Probability Theory Group (Formerly: E1071),* (R package version 1.7-9).
Mickley Steinmetz, K. R., & Kensinger, E. A. (2009). The effects of valence and arousal on the neural activity leading to subsequent memory. *Psychophysiology*, *46*(6), 1190–1199. https://doi.org/10.1111/j.1469-8986.2009.00868.x
Mohammad, F., Aryal, S., Ho, J., Stewart, J. C., Norman, N. A., Tan, T. L., Eisaka, A., & Claridge-Chang, A. (2016). Ancient Anxiety Pathways Influence Drosophila Defense Behaviors. *Current Biology*, *26*(7), 981–986. https://doi.org/10.1016/j.cub.2016.02.031
Moosmann, M., Schönfelder, V. H., Specht, K., Scheeringa, R., Nordby, H., & Hugdahl, K. (2009). Realignment parameter-informed artefact correction for simultaneous EEG-fMRI recordings. *NeuroImage*, *45*(4), 1144–1150. https://doi.org/10.1016/j.neuroimage.2009.01.024
Moreno-Juan, V., Filipchuk, A., Antón-Bolaños, N., Mezzera, C., Gezelius, H., Andrés, B., Rodríguez-Malmierca, L., Susín, R., Schaad, O., Iwasato, T., Schüle, R., Rutlin, M., Nelson, S., Ducret, S., Valdeolmillos, M., Rijli, F. M., & López-Bendito, G. (2017). Prenatal thalamic waves regulate cortical area size prior to sensory processing. *Nature Communications*, *8*(1), 14172. https://doi.org/10.1038/ncomms14172
Morey, R. A., Petty, C. M., Xu, Y., Hayes, J. P., Wagner, H. R., Lewis, D. V, LaBar, K. S., Styner, M., & McCarthy, G. (2009). A comparison of automated segmentation and manual tracing for quantifying hippocampal and amygdala volumes. *NeuroImage*, *45*(3), 855–866. https://doi.org/10.1016/j.neuroimage.2008.12.033
Morris, S. E., & Cuthbert, B. N. (2012). Research Domain Criteria: cognitive systems, neural circuits, and dimensions of behavior. *Dialogues in Clinical Neuroscience*, *14*(1), 29–37. https://doi.org/10.31887/DCNS.2012.14.1/smorris
Mulej Bratec, S., Bertram, T., Starke, G., Brandl, F., Xie, X., & Sorg, C. (2020). Your presence soothes me: a neural process model of aversive emotion regulation via social buffering. *Social Cognitive and Affective Neuroscience*, *15*(5), 561–570. https://doi.org/10.1093/scan/nsaa068
Murray, E. A., Wise, S. P., & Graham, K. S. (2018). Representational specializations of the hippocampus in phylogenetic perspective. *Neuroscience Letters*, *680*, 4–12. https://doi.org/10.1016/j.neulet.2017.04.065
Murty, V. P., Ritchey, M., Adcock, R. A., & LaBar, K. S. (2010). fMRI studies of successful emotional memory encoding: A quantitative meta-analysis. *Neuropsychologia*, *48*(12), 3459–3469. https://doi.org/0.1016/j.neuropsychologia.2010.07.030
Nakagawa, Y., & Shimogori, T. (2012). Diversity of thalamic progenitor cells and postmitotic neurons. *European Journal of Neuroscience*, *35*(10), 1554–1562. https://doi.org/10.1111/j.1460-9568.2012.08089.x
Narayanan, A. S., & Rothenfluh, A. (2016). I Believe I Can Fly!: Use of Drosophila as a Model Organism in Neuropsychopharmacology Research. *Neuropsychopharmacology*, *41*(6), 1439–1446. https://doi.org/10.1038/npp.2015.322

Nenert, R., Allendorfer, J. B., & Szaflarski, J. P. (2014). A model for visual memory encoding. *PLoS ONE*, *9*(10), e107761. https://doi.org/10.1371/journal.pone.0107761

Niazy, R. K., Beckmann, C. F., Iannetti, G. D., Brady, J. M., & Smith, S. M. (2005). Removal of FMRI environment artifacts from EEG data using optimal basis sets. *NeuroImage*, *28*(3), 720–737. https://doi.org/10.1016/j.neuroimage.2005.06.067

Nyberg, L., Karalija, N., Salami, A., Andersson, M., Wåhlin, A., & Kaboovand, N. (2016). Dopamine D2 receptor availability is linked to hippocampal – caudate functional connectivity and episodic memory. *Proceedings of the National Academy of Sciences of the United States of America*, *113*(28), 7918–7923. https://doi.org/10.1073/pnas.1606309113

Oertel-Knöchel, V., Reinke, B., Matura, S., Prvulovic, D., Linden, D. E. J., & van de Ven, V. (2015). Functional connectivity pattern during rest within the episodic memory network in association with episodic memory performance in bipolar disorder. *Psychiatry Research*, *231*(2), 141–150. https://doi.org/10.1016/j.pscychresns.2014.11.014

Okon-Singer, H., Hendler, T., Pessoa, L., & Shackman, A. J. (2015). The neurobiology of emotion-cognition interactions: fundamental questions and strategies for future research. *Frontiers in Human Neuroscience*, *9*, 58. https://doi.org/10.3389/fnhum.2015.00058

Olbrich, S., Mulert, C., Karch, S., Trenner, M., Leicht, G., Pogarell, O., & Hegerl, U. (2009). EEG-vigilance and BOLD effect during simultaneous EEG/fMRI measurement. *NeuroImage*, *45*(2), 319–332. https://doi.org/10.1016/j.neuroimage.2008.11.014

Oldfield, R. C. (1971). The assessment and analysis of handedness: The Edinburgh inventory. *Neuropsychologia*, *9*(1), 97–113.

Padilla-Coreano, N., Bolkan, S. S., Pierce, G. M., Blackman, D. R., Hardin, W. D., Garcia-Garcia, A. L., Spellman, T. J., & Gordon, J. A. (2016). Direct Ventral Hippocampal-Prefrontal Input Is Required for Anxiety-Related Neural Activity and Behavior. *Neuron*, *89*(4), 857–866. https://doi.org/10.1016/j.neuron.2016.01.011

Park, A. T., Leonard, J. A., Saxler, P. K., Cyr, A. B., Gabrieli, J. D. E., & Mackey, A. P. (2018). Amygdala–medial prefrontal cortex connectivity relates to stress and mental health in early childhood. *Social Cognitive and Affective Neuroscience*, *13*(4), 430–439. https://doi.org/10.1093/scan/nsy017

Pascalis, O., de Martin de Viviés, X., Anzures, G., Quinn, P. C., Slater, A. M., Tanaka, J. W., & Lee, K. (2011). Development of face processing. *Wiley Interdisciplinary Reviews. Cognitive Science*, *2*(6), 666–675. https://doi.org/10.1002/wcs.146

Passamonti, L., Rowe, J. B., Ewbank, M., Hampshire, A., Keane, J., & Calder, A. J. (2008). Connectivity from the ventral anterior cingulate to the amygdala is modulated by appetitive motivation in response to facial signals of aggression. *NeuroImage*, *43*(3), 562–570. https://doi.org/10.1016/j.neuroimage.2008.07.045

Patenaude, B., Smith, S. M., Kennedy, D. N., & Jenkinson, M. (2011). A Bayesian model of shape and appearance for subcortical brain segmentation. *NeuroImage*, *56*(3), 907–922. https://doi.org/10.1016/j.neuroimage.2011.02.046

Pearl, J. (2014). Comment: Understanding Simpson's Paradox. *The American Statistician*, *68*(1), 8–13. https://doi.org/10.1080/00031305.2014.876829

Penny, W. D., Stephan, K. E., Mechelli, A., & Friston, K. J. (2004). Modelling functional integration: a comparison of structural equation and dynamic causal models. *NeuroImage*, *23*, S264–S274. https://doi.org/10.1016/j.neuroimage.2004.07.041

Perusini, J. N., & Fanselow, M. S. (2015). Neurobehavioral perspectives on the distinction between fear and anxiety. *Learning and Memory*, *22*(9), 417–425.

https://doi.org/10.1101/lm.039180.115
Peterburs, J., & Desmond, J. E. (2016). The role of the human cerebellum in performance monitoring. *Current Opinion in Neurobiology*, *40*, 38–44. https://doi.org/10.1016/j.conb.2016.06.011
Pezzulo, G., Rigoli, F., & Friston, K. (2015). Active Inference, homeostatic regulation and adaptive behavioural control. *Progress in Neurobiology*, *134*, 17–35. https://doi.org/10.1016/j.pneurobio.2015.09.001
Pezzulo, G., Zorzi, M., & Corbetta, M. (2021). The secret life of predictive brains: what's spontaneous activity for? *Trends in Cognitive Sciences*, *25*(9), 730–743. https://doi.org/10.1016/j.tics.2021.05.007
Phan, K. L., Wager, T., Taylor, S. F., & Liberzon, I. (2002). Functional neuroanatomy of emotion: a meta-analysis of emotion activation studies in PET and fMRI. *NeuroImage*, *16*(2), 331–348. https://doi.org/10.1006/nimg.2002.1087
Phelps, E. A., & LeDoux, J. E. (2005). Contributions of the amygdala to emotion processing: From animal models to human behavior. *Neuron*, *48*(2), 175–187. https://doi.org/10.1016/j.neuron.2005.09.025
Pi, G., Gao, D., Wu, D., Wang, Y., Lei, H., Zeng, W., Gao, Y., Yu, H., Xiong, R., Jiang, T., Li, S., Wang, X., Guo, J., Zhang, S., Yin, T., He, T., Ke, D., Li, R., Li, H., … Wang, J. (2020). Posterior basolateral amygdala to ventral hippocampal CA1 drives approach behaviour to exert an anxiolytic effect. *Nature Communications*, *11*(1), 183. https://doi.org/10.1038/s41467-019-13919-3
Power, J. D., Cohen, A. L., Nelson, S. M., Wig, G. S., Barnes, K. A., Church, J. A., Vogel, A. C., Laumann, T. O., Miezin, F. M., Schlaggar, B. L., & Petersen, S. E. (2011). Functional network organization of the human brain. *Neuron*, *72*(4), 665–678. https://doi.org/10.1016/j.neuron.2011.09.006
Prerau, M. J., Hartnack, K. E., Obregon-Henao, G., Sampson, A., Merlino, M., Gannon, K., Bianchi, M. T., Ellenbogen, J. M., & Purdon, P. L. (2014). Tracking the sleep onset process: An empirical model of behavioral and physiological dynamics. *PLoS Computational Biology*, *10*(10), e1003866. https://doi.org/10.1371/journal.pcbi.1003866
Purdon, P. L., & Weisskoff, R. M. (1998). Effect of temporal autocorrelation due to physiological noise and stimulus paradigm on voxel-level false-positive rates in fMRI. *Human Brain Mapping*, *6*(4), 239–249. https://doi.org/10.1002/(SICI)1097-0193(1998)6:4<239::AID-HBM4>3.0.CO;2-4
Quaedflieg, C. W. E. M., Van De Ven, V., Meyer, T., Siep, N., Merckelbach, H., & Smeets, T. (2015). Temporal dynamics of stress-induced alternations of intrinsic amygdala connectivity and neuroendocrine levels. *PLoS ONE*, *10*(5), e0124141. https://doi.org/10.1371/journal.pone.0124141
R Core Team. (2015). *R: A Language and Environment for Statistical Computing* (0.99.441). R Foundation for Statistical Computing. http://www.r-project.org/
Radua, J., Sarró, S., Vigo, T., Alonso-Lana, S., Bonnín, C. M., Ortiz-Gil, J., Canales-Rodríguez, E. J., Maristany, T., Vieta, E., Mckenna, P. J., Salvador, R., & Pomarol-Clotet, E. (2014). Common and specific brain responses to scenic emotional stimuli. *Brain Structure and Function*, *219*(4), 1463–1472. https://doi.org/10.1007/s00429-013-0580-0
Rasch, B., Spalek, K., Buholzer, S., Luechinger, R., Boesiger, P., Papassotiropoulos, A., & de Quervain, D. J.-F. (2009). A genetic variation of the noradrenergic system is related to differential amygdala activation during encoding of emotional memories. *Proceedings of the National Academy of Sciences of the United States of America*, *106*(45), 19191–

19196. https://doi.org/10.1073/pnas.0907425106
Raut, R. V, Snyder, A. Z., & Raichle, M. E. (2020). Hierarchical dynamics as a macroscopic organizing principle of the human brain. *Proceedings of the National Academy of Sciences of the United States of America*, *117*(34), 20890–20897. https://doi.org/10.1073/pnas.2003383117
Razlighi, Q. R., Oh, H., Habeck, C., Shea, D. O., Gazes, E., Eich, T., Parker, D. B., Lee, S., & Stern, Y. (2017). Dynamic Patterns of Brain Structure – Behavior Correlation Across the Lifespan. *Cerebral Cortex*, *27*(7), 3586–3599. https://doi.org/10.1093/cercor/bhw179
Rechtschaffen, A., & Kales, A. (1968). *A Manual of Standardized Terminology, Techniques and Scoring System for Sleep Stages of Human Subjects*.
Reineberg, A. E., Gustavson, D. E., Benca, C., Banich, M. T., & Friedman, N. P. (2018). The Relationship Between Resting State Network Connectivity and Individual Differences in Executive Functions. *Frontiers in Psychology*, *9*, 1600. https://doi.org/10.3389/fpsyg.2018.01600
Richardson, F. M., Seghier, M. L., Leff, A. P., Thomas, M. S. C., & Price, C. J. (2011). Multiple routes from occipital to temporal cortices during reading. *The Journal of Neuroscience*, *31*(22), 8239–8247. https://doi.org/10.1523/JNEUROSCI.6519-10.2011
Richardson, M. P., Strange, B. A., & Dolan, R. J. (2004). Encoding of emotional memories depends on amygdala and hippocampus and their interactions. *Nature Neuroscience*, *7*(3), 278–285. https://doi.org/10.1038/nn1190
Richiardi, J., Altmann, A., Milazzo, A. C., Chang, C., Chakravarty, M. M., Banaschewski, T., Barker, G. J., Bokde, A. L. W., Bromberg, U., Büchel, C., Conrod, P., Fauth-Bühler, M., Flor, H., Frouin, V., Gallinat, J., Garavan, H., Gowland, P., Heinz, A., Lemaître, H., … Greicius, M. D. (2015). Correlated gene expression supports synchronous activity in brain networks. *Science*, *348*(6240), 1241–1244. https://doi.org/10.1126/science.1255905
Riedel, M. C., Ray, K. L., Dick, A. S., Sutherland, M. T., Hernandez, Z., Fox, P. M., Eickhoff, S. B., Fox, P. T., & Laird, A. R. (2015). Meta-analytic connectivity and behavioral parcellation of the human cerebellum. *NeuroImage*, *117*, 327–342. https://doi.org/10.1016/j.neuroimage.2015.05.008
Rodrigues, S. M., Schafe, G. E., & LeDoux, J. E. (2004). Molecular mechanisms underlying emotional learning and memory in the lateral amygdala. *Neuron*, *44*(1), 75–91. https://doi.org/10.1016/j.neuron.2004.09.014
Roozendaal, B., & Hermans, E. J. (2017). Norepinephrine effects on the encoding and consolidation of emotional memory: improving synergy between animal and human studies. *Current Opinion in Behavioral Sciences*, *14*, 115–122. https://doi.org/10.1016/j.cobeha.2017.02.001
Roozendaal, B., McEwen, B. S., & Chattarji, S. (2009). Stress, memory and the amygdala. *Nature Reviews Neuroscience*, *10*(6), 423–433. https://doi.org/10.1038/nrn2651
Roozendaal, B., & Mcgaugh, J. L. (2011). Memory modulation. *Behavioral Neuroscience*, *125*(6), 797–824. https://doi.org/10.1037/a0026187.MEMORY
Rosa, M. J., Friston, K., & Penny, W. (2012). Post-hoc selection of dynamic causal models. *Journal of Neuroscience Methods*, *208*(1), 66–78. https://doi.org/10.1016/j.jneumeth.2012.04.013
Roy, A. K., Shehzad, Z., Margulies, D. S., Kelly, a M. C., Uddin, L. Q., Gotimer, K., Biswal, B. B., Castellanos, F. X., & Milham, M. P. (2009). Functional connectivity of the human amygdala using resting state fMRI. *NeuroImage*, *45*(2), 614–626. https://doi.org/10.1016/j.neuroimage.2008.11.030

Sacchetti, B., Baldi, E., Lorenzini, C. A., & Bucherelli, C. (2002). Cerebellar role in fear-conditioning consolidation. *Proceedings of the National Academy of Sciences of the United States of America*, *99*(12), 8406–8411. https://doi.org/10.1073/pnas.112660399

Sacchetti, B., Sacco, T., & Strata, P. (2007). Reversible inactivation of amygdala and cerebellum but not perirhinal cortex impairs reactivated fear memories. *European Journal of Neuroscience*, *25*(9), 2875–2884. https://doi.org/10.1111/j.1460-9568.2007.05508.x

Sacchetti, B., Scelfo, B., & Strata, P. (2005). The Cerebellum: Synaptic Changes and Fear Conditioning. *The Neuroscientist*, *11*(3), 217–227. https://doi.org/10.1177/1073858405276428

Salay, L. D., Ishiko, N., & Huberman, A. D. (2018). A midline thalamic circuit determines reactions to visual threat. *Nature*, *557*(7704), 183–189. https://doi.org/10.1038/s41586-018-0078-2

Salehi, M., Karbasi, A., Barron, D. S., Scheinost, D., & Constable, R. T. (2020). Individualized functional networks reconfigure with cognitive state. *NeuroImage*, *206*, 116233. https://doi.org/10.1016/j.neuroimage.2019.116233

Salvatore, P., Baldessarini, R. J., Khalsa, H. K., & Tohen, M. (2021). Prodromal features in first-psychotic episodes of major affective and schizoaffective disorders. *Journal of Affective Disorders*, *295*, 1251–1258. https://doi.org/10.1016/j.jad.2021.08.099

Samu, D., Campbell, K. L., Tsvetanov, K. A., Shafto, M. A., Brayne, C., Bullmore, E. T., Calder, A. C., Cusack, R., Dalgleish, T., Duncan, J., Henson, R. N., Matthews, F. E., Marslen-Wilson, W. D., Rowe, J. B., Cheung, T., Davis, S., Geerligs, L., Kievit, R., McCarrey, A., … Tyler, L. K. (2017). Preserved cognitive functions with age are determined by domain-dependent shifts in network responsivity. *Nature Communications*, *8*, 14743. https://doi.org/10.1038/ncomms14743

Samuels, E. R., & Szabadi, E. (2008). Functional neuroanatomy of the noradrenergic locus coeruleus: its roles in the regulation of arousal and autonomic function part I: principles of functional organisation. *Current Neuropharmacology*, *6*, 235–253.

Sanchez-Rodriguez, L. M., Iturria-Medina, Y., Mouches, P., & Sotero, R. C. (2021). Detecting brain network communities: Considering the role of information flow and its different temporal scales. *NeuroImage*, *225*, 117431. https://doi.org/10.1016/j.neuroimage.2020.117431

Scheidegger, M., Walter, M., Lehmann, M., Metzger, C., Grimm, S., Boeker, H., Boesiger, P., Henning, A., & Seifritz, E. (2012). Ketamine decreases resting state functional network connectivity in healthy subjects: implications for antidepressant drug action. *PLoS One*, *7*(9), e44799. https://doi.org/10.1371/journal.pone.0044799

Schilbach, L. (2016). Towards a second-person neuropsychiatry. *Philosophical Transactions of the Royal Society B: Biological Sciences*, *371*(1686). https://doi.org/10.1098/rstb.2015.0081

Schmahmann, J. D., Guell, X., Stoodley, C. J., & Halko, M. A. (2019). The Theory and Neuroscience of Cerebellar Cognition. *Annual Review of Neuroscience*, *42*, 337–364. https://doi.org/10.1146/annurev-neuro-070918-050258

Schoenbaum, G., & Roesch, M. (2005). Orbitofrontal cortex, associative learning, and expectancies. *Neuron*, *47*, 633–636. https://doi.org/10.1016/j.neuron.2005.07.018

Schultz, C., & Engelhardt, M. (2014). Anatomy of the hippocampal formation. *Frontiers of Neurology and Neuroscience*, *34*, 6–17. https://doi.org/10.1159/000360925

Seeley, W. W., Menon, V., Schatzberg, A. F., Keller, J., Glover, G. H., Kenna, H., Reiss, A. L., & Greicius, M. D. (2007). Dissociable intrinsic connectivity networks for salience

processing and executive control. *The Journal of Neuroscience*, *27*(9), 2349–2356. https://doi.org/10.1523/JNEUROSCI.5587-06.2007
Seghier, M. L., & Price, C. J. (2010). Reading aloud boosts connectivity through the putamen. *Cerebral Cortex*, *20*(3), 570–582. https://doi.org/10.1093/cercor/bhp123
Sekeres, M. J., Winocur, G., & Moscovitch, M. (2018). The hippocampus and related neocortical structures in memory transformation. *Neuroscience Letters*, *680*, 39–53. https://doi.org/10.1016/j.neulet.2018.05.006
Selzam, S., Coleman, J. R. I., Caspi, A., Moffitt, T. E., & Plomin, R. (2018). A polygenic p factor for major psychiatric disorders. *Translational Psychiatry*, *8*(1), 205. https://doi.org/10.1038/s41398-018-0217-4
Seth, A. K. (2013). Interoceptive inference, emotion, and the embodied self. *Trends in Cognitive Sciences*, *17*(11), 565–573. https://doi.org/10.1016/j.tics.2013.09.007
Shalev, A. Y. (2009). Posttraumatic stress disorder (PTSD) and stress related disorders. *The Psychiatric Clinics of North America*, *32*(3), 687–704. https://doi.org/10.1016/j.psc.2009.06.001.
Sheline, Y. I., Price, J. L., Yan, Z., & Mintun, M. A. (2010). Resting-state functional MRI in depression unmasks increased connectivity between networks via the dorsal nexus. *Proceedings of the National Academy of Sciences of the United States of America*, *107*(24), 11020–11025. https://doi.org/10.1073/pnas.1000446107
Shin, J. D., & Jadhav, S. P. (2016). Multiple modes of hippocampal–prefrontal interactions in memory-guided behavior. *Current Opinion in Neurobiology*, *40*, 161–169. https://doi.org/10.1016/j.conb.2016.07.015
Sladky, R., Friston, K. J., Tröstl, J., Cunnington, R., Moser, E., & Windischberger, C. (2011). Slice-timing effects and their correction in functional MRI. *NeuroImage*, *58*(2), 588–594. https://doi.org/10.1016/j.neuroimage.2011.06.078
Smallwood, J., Karapanagiotidis, T., Ruby, F., Medea, B., Caso, I. De, Konishi, M., Wang, H. T., Hallam, G., Margulies, D. S., & Jefferies, E. (2016). Representing representation: Integration between the temporal lobe and the posterior cingulate influences the content and form of spontaneous thought. *PLoS ONE*, *11*(4), 1–19. https://doi.org/10.1371/journal.pone.0152272
Smith, S. M., Fox, P. T., Miller, K. L., Glahn, D. C., Fox, P. M., Mackay, C. E., Filippini, N., Watkins, K. E., Toro, R., Laird, A. R., & Beckmann, C. F. (2009). Correspondence of the brain's functional architecture during activation and rest. *Proceedings of the National Academy of Sciences of the United States of America*, *106*(31), 13040–13045. https://doi.org/10.1073/pnas.0905267106
Smith, S. M., Miller, K. L., Salimi-Khorshidi, G., Webster, M., Beckmann, C. F., Nichols, T. E., Ramsey, J. D., & Woolrich, M. W. (2011). Network modelling methods for FMRI. *NeuroImage*, *54*(2), 875–891. https://doi.org/10.1016/j.neuroimage.2010.08.063
Smith, D. V, Utevsky, A. V, Bland, A. R., Clement, N., Clithero, J. a, Harsch, A. E. ., McKell Carter, R., & Huettel, S. a. (2014). Characterizing individual differences in functional connectivity using dual-regression and seed-based approaches. *NeuroImage*, *95*, 1–12. https://doi.org/10.1016/j.neuroimage.2014.03.042
Sneve, M. H., Grydeland, H., Amlien, I. K., Langnes, E., Walhovd, K. B., & Fjell, A. M. (2017). Decoupling of large-scale brain networks supports the consolidation of durable episodic memories. *NeuroImage*, *153*, 336–345. https://doi.org/10.1016/j.neuroimage.2016.05.048
Sorg, C., Manoliu, A., Neufang, S., Myers, N., Peters, H., Schwerthöffer, D., Scherr, M., Mühlau, M., Zimmer, C., Drzezga, A., Förstl, H., Bäuml, J., Eichele, T., Wohlschläger, A.

M., & Riedl, V. (2013). Increased intrinsic brain activity in the striatum reflects symptom dimensions in schizophrenia. *Schizophrenia Bulletin*, *39*(2), 387–395. https://doi.org/10.1093/schbul/sbr184

Sotres-Bayon, F., Cain, C. K., & LeDoux, J. E. (2006). Brain mechanisms of fear extinction: historical perspectives on the contribution of prefrontal cortex. *Biological Psychiatry*, *60*(4), 329–336. https://doi.org/10.1016/j.biopsych.2005.10.012

Sotres-Bayon, F., & Quirk, G. J. (2010). Prefrontal control of fear: more than just extinction. *Current Opinion in Neurobiology*, *20*(2), 231–235. https://doi.org/10.1016/j.conb.2010.02.005

Spreen, O., & Strauss, E. (1991). *A Compendium of Neuropsychological Tests: Administration, Norms and Commentary*. Oxford University Press.

Squire, L. R., & Zola, S. M. (1998). Episodic memory, semantic memory, and amnesia. *Hippocampus*, *8*(3), 205–211. https://doi.org/https://doi.org/10.1002/(SICI)1098-1063(1998)8:3<205::AID-HIPO3>3.0.CO;2-I

Staresina, B. P., Alink, A., Kriegeskorte, N., & Henson, R. N. (2013). Awake reactivation predicts memory in humans. *Proceedings of the National Academy of Sciences of the United States of America*, *110*(52), 21159–21164. https://doi.org/10.1073/pnas.1311989110

Stephan, K. E., Penny, W. D., Moran, R. J., den Ouden, H. E. M., Daunizeau, J., & Friston, K. J. (2010). Ten simple rules for dynamic causal modeling. *NeuroImage*, *49*(4), 3099–3109. https://doi.org/10.1016/j.neuroimage.2009.11.015

Stoodley, C. J., & Schmahmann, J. D. (2010). Evidence for topographic organization in the cerebellum of motor control versus cognitive and affective processing. *Cortex*, *46*(7), 831–844. https://doi.org/10.1016/j.cortex.2009.11.008

Strata, P. (2015). The Emotional Cerebellum. *The Cerebellum*, *14*(5), 570–577. https://doi.org/10.1007/s12311-015-0649-9

Strick, P. L., Dum, R. P., & Fiez, J. A. (2009). Cerebellum and nonmotor function. *Annual Review of Neuroscience*, *32*, 413–434. https://doi.org/10.1146/annurev.neuro.31.060407.125606

Supple, W. F., & Leaton, R. N. (1990). Lesions of the cerebellar vermis and cerebellar hemispheres: Effects on heart rate conditioning in rats. *Behavioral Neuroscience*, *104*(6), 934–947. https://doi.org/10.1037/0735-7044.104.6.934

Sussman, T. J., Jin, J., & Mohanty, A. (2016). Top-down and bottom-up factors in threat-related perception and attention in anxiety. *Biological Psychology*, *121*, 160–172. https://doi.org/10.1016/j.biopsycho.2016.08.006

Sutherland, M. R., & Mather, M. (2018). Arousal (but not valence) amplifies the impact of salience. *Cognition and Emotion*, *32*(3), 616–622. https://doi.org/10.1080/02699931.2017.1330189

Sved, A. F., Cano, G., Passerin, A. M., & Rabin, B. S. (2002). The locus coeruleus, Barrington' s nucleus, and neural circuits of stress . *Physiology and Behavior*, *77*(4–5), 737–742. https://doi.org/10.1016/s0031-9384(02)00927-7

Sydnor, V. J., Larsen, B., Bassett, D. S., Alexander-bloch, A., Fair, D. A., Liston, C., Mackey, A. P., Milham, M. P., Pines, A., Roalf, D. R., Seidlitz, J., & Xu, T. (2021). Neurodevelopment of the association cortices: Patterns, mechanisms, and implications for psychopathology. *Neuron*, *109*. https://doi.org/10.1016/j.neuron.2021.06.016

Szucs, D., & Ioannidis, J. P. A. (2017). Empirical assessment of published effect sizes and power in the recent cognitive neuroscience and psychology literature. *PLoS Biology*, *15*(3), e2000797. https://doi.org/10.1371/journal.pbio.2000797

Tagliazucchi, E., & Laufs, H. (2014). Decoding wakefulness levels from typical fMRI resting-state data reveals reliable drifts between wakefulness and sleep. *Neuron*, *82*(3), 695–708. https://doi.org/10.1016/j.neuron.2014.03.020

Tagliazucchi, E., von Wegner, F., Morzelewski, A., Borisov, S., Jahnke, K., & Laufs, H. (2012). Automatic sleep staging using fMRI functional connectivity data. *NeuroImage*, *63*(1), 63–72. https://doi.org/10.1016/j.neuroimage.2012.06.036

Talmi, D., Anderson, A. K., Riggs, L., Caplan, J. B., & Moscovitch, M. (2008). Immediate memory consequences of the effect of emotion on attention to pictures. *Learning and Memory*, *15*(3), 172–182. https://doi.org/10.1101/lm.722908

Tambini, A., Ketz, N., & Davachi, L. (2010). Enhanced brain correlations during rest are related to memory for recent experiences. *Neuron*, *65*(2), 280–290. https://doi.org/10.1016/j.neuron.2010.01.001

Tavano, A., Grasso, R., Gagliardi, C., Triulzi, F., Bresolin, N., Fabbro, F., & Borgatti, R. (2007). Disorders of cognitive and affective development in cerebellar malformations. *Brain*, *130*(10), 2646–2660. https://doi.org/10.1093/brain/awm201

Thomason, M. E., Palopoli, A. C., Jariwala, N. N., Werchan, D. M., Chen, A., Adhikari, S., Espinoza-Heredia, C., Brito, N. H., & Trentacosta, C. J. (2021). Miswiring the brain: Human prenatal Δ9-tetrahydrocannabinol use associated with altered fetal hippocampal brain network connectivity. *Developmental Cognitive Neuroscience*, *51*, 101000. https://doi.org/10.1016/j.dcn.2021.101000

Timmann, D., Drepper, J., Frings, M., Maschke, M., Richter, S., Gerwig, M., & Kolb, F. P. (2010). The human cerebellum contributes to motor, emotional and cognitive associative learning. A review. *Cortex*, *46*(7), 845–857. https://doi.org/10.1016/j.cortex.2009.06.009

Todd, R., Schmitz, T., Susskind, J., & Anderson, A. (2013). Shared neural substrates of emotionally enhanced perceptual and mnemonic vividness. *Frontiers in Behavioral Neuroscience*, *7*, 40. https://doi.org/10.3389/fnbeh.2013.00040

Townsend, J. D., Torrisi, S. J., Lieberman, M. D., Sugar, C. A., Bookheimer, S. Y., & Altshuler, L. L. (2013). Frontal-amygdala connectivity alterations during emotion downregulation in bipolar I dosorder. *Biological Psychiatry*, *73*(2), 127–135. https://doi.org/10.1016/j.biopsych.2012.06.030

Train the Brain Consortium. (2017). Randomized trial on the effects of a combined physical/cognitive training in aged MCI subjects: the Train the Brain study. *Scientific Reports*, *7*(1), 39471. https://doi.org/10.1038/srep39471

Tsvetanov, K. A., Ye, Z., Hughes, L., Samu, D., Treder, M. S., Wolpe, N., Tyler, L. K., & Rowe, J. B. (2018). Activity and connectivity differences underlying inhibitory control across the adult life span. *The Journal of Neuroscience*, *38*(36), 7887–7900. https://doi.org/10.1523/JNEUROSCI.2919-17.2018

Tulving, E., & Markowitsch, H. J. (1998). Episodic and declarative memory: role of the hippocampus. *Hippocampus*, *8*(3), 198–204. https://doi.org/10.1002/(SICI)1098-1063(1998)8:3<198::AID-HIPO2>3.0.CO;2-G

Tye, K. M. (2018). Neural Circuit Motifs in Valence Processing. *Neuron*, *100*(2), 436–452. https://doi.org/10.1016/j.neuron.2018.10.001

Tye, K. M., Prakash, R., Kim, S.-Y., Fenno, L. E., Grosenick, L., Zarabi, H., Thompson, K. R., Gradinaru, V., Ramakrishnan, C., & Deisseroth, K. (2011). Amygdala circuitry mediating reversible and bidirectional control of anxiety. *Nature*, *471*(7338), 358–362. https://doi.org/10.1038/nature09820

Uddin, L. Q., Yeo, B. T. T., & Spreng, R. N. (2019). Towards a Universal Taxonomy of Macro-

scale Functional Human Brain Networks. *Brain Topography*, *32*(6), 926–942. https://doi.org/10.1007/s10548-019-00744-6

Urgolites, Z. J., Wixted, J. T., Goldinger, S. D., Papesh, M. H., Treiman, D. M., Squire, L. R., & Steinmetz, P. N. (2020). Spiking activity in the human hippocampus prior to encoding predicts subsequent memory. *Proceedings of the National Academy of Sciences of the United States of America*, *117*(24), 13767–13770. https://doi.org/10.1073/pnas.2001338117

Utevsky, A. V, Smith, D. V, & Huettel, S. A. (2014). Precuneus is a functional core of the default-mode network. *The Journal of Neuroscience*, *34*(3), 932–940. https://doi.org/10.1523/JNEUROSCI.4227-13.2014

Vaisvaser, S., Lin, T., Admon, R., Podlipsky, I., Greenman, Y., Stern, N., Fruchter, E., Wald, I., Pine, D. S., Tarrasch, R., Bar-Haim, Y., & Hendler, T. (2013). Neural traces of stress: cortisol related sustained enhancement of amygdala-hippocampal functional connectivity. *Frontiers in Human Neuroscience*, *7*, 313. https://doi.org/10.3389/fnhum.2013.00313

van den Heuvel, M. P., & Hulshoff Pol, H. E. (2010). Exploring the brain network: A review on resting-state fMRI functional connectivity. *European Neuropsychopharmacology*, *20*(8), 519–534. https://doi.org/10.1016/j.euroneuro.2010.03.008

van Marle, H. J. F., Hermans, E. J., Qin, S., & Fernández, G. (2010). Enhanced resting-state connectivity of amygdala in the immediate aftermath of acute psychological stress. *NeuroImage*, *53*(1), 348–354. https://doi.org/10.1016/j.neuroimage.2010.05.070

van Stegeren, A. H., Goekoop, R., Everaerd, W., Scheltens, P., Barkhof, F., Kuijer, J. P. A., & Rombouts, S. A. R. B. (2005). Noradrenaline mediates amygdala activation in men and women during encoding of emotional material. *NeuroImage*, *24*(3), 898–909. https://doi.org/10.1016/j.neuroimage.2004.09.011

Varangis, E., Habeck, C. G., Razlighi, Q. R., & Stern, Y. (2019). The effect of aging on resting state connectivity of predefined networks in the brain. *Frontiers in Aging Neuroscience*, *11*, 234. https://doi.org/10.3389/fnagi.2019.00234

Vatansever, D., Menon, D. K., Manktelow, A. E., Sahakian, B. J., & Stamatakis, E. A. (2015). Default mode dynamics for global functional integration. *The Journal of Neuroscience*, *35*(46), 15254–15262. https://doi.org/10.1523/JNEUROSCI.2135-15.2015

Veer, I. M., Oei, N. Y. L., Spinhoven, P., van Buchem, M. A., Elzinga, B. M., & Rombouts, S. A. R. B. (2011). Beyond acute social stress: Increased functional connectivity between amygdala and cortical midline structures. *NeuroImage*, *57*(4), 1534–1541. https://doi.org/10.1016/j.neuroimage.2011.05.074

Veer, I. M., Oei, N. Y. L., Spinhoven, P., van Buchem, M. a, Elzinga, B. M., & Rombouts, S. a R. B. (2012). Endogenous cortisol is associated with functional connectivity between the amygdala and medial prefrontal cortex. *Psychoneuroendocrinology*, *37*(7), 1039–1047. https://doi.org/10.1016/j.psyneuen.2011.12.001

Venkatraman, A., Edlow, B. L., & Immordino-Yang, M. H. (2017). The brainstem in emotion: A review. *Frontiers in Neuroanatomy*, *11*, 15. https://doi.org/10.3389/fnana.2017.00015

Verduyn, P., Delaveau, P., Rotge, J.-Y., Fossati, P., & Van Mechelen, I. (2015). Determinants of emotion duration and underlying psychological and neural mechanisms. *Emotion Review*, *7*(4), 330–335. https://doi.org/10.1177/1754073915590618

Viskontas, I. V., Knowlton, B. J., Steinmetz, P. N., & Fried, I. (2006). Differences in mnemonic processing by neurons in the human hippocampus and parahippocampal regions. *Journal of Cognitive Neuroscience*, *18*(10), 1654–1662. https://doi.org/10.1162/jocn.2006.18.10.1654

Vogt, B. A. (2014). Submodalities of emotion in the context of cingulate subregions. *Cortex*, *59*, 197–202. https://doi.org/10.1016/j.cortex.2014.04.002

Wahlstrom, K. L., Huff, M. L., Emmons, E. B., Freeman, J. H., Narayanan, N. S., McIntyre, C. K., & Lalumiere, R. T. (2018). Basolateral amygdala inputs to the medial entorhinal cortex selectively modulate the consolidation of spatial and contextual learning. *The Journal of Neuroscience*, *38*(11), 2698–2712. https://doi.org/10.1523/JNEUROSCI.2848-17.2018

Walter, H., von Kalckreuth, A., Schardt, D., Stephan, A., Goschke, T., & Erk, S. (2009). The temporal dynamics of voluntary emotion regulation. *PLoS One*, *4*(8), e6726. https://doi.org/10.1371/journal.pone.0006726

Wang, D., Clouter, A., Chen, Q., Shapiro, K. L., & Hanslmayr, S. (2018). Single-trial phase entrainment of theta oscillations in sensory regions predicts human associative memory performance. *The Journal of Neuroscience*, *38*(28), 6299–6309. https://doi.org/10.1523/JNEUROSCI.0349-18.2018

Wang, R., Shen, Y., Tino, P., Welchman, A. E., & Kourtzi, Z. (2017). Learning predictive statistics: strategies and brain mechanisms. *The Journal of Neuroscience*, *37*(35), 8412–8427. https://doi.org/10.1523/JNEUROSCI.0144-17.2017

Wang, T., Zhang, X., Li, A., Zhu, M., Liu, S., Qin, W., Li, J., Yu, C., Jiang, T., & Liu, B. (2017). Polygenic risk for five psychiatric disorders and cross-disorder and disorder-specific neural connectivity in two independent populations. *NeuroImage. Clinical*, *14*, 441–449. https://doi.org/10.1016/j.nicl.2017.02.011

Waugh, C. E., & Schirillo, J. a. (2012). Timing: A missing key ingredient in typical fMRI studies of emotion. *Behavioral and Brain Sciences*, *35*(3), 170–171. https://doi.org/10.1017/S0140525X11001646

Wei, P., Lu, Z., & Song, J. (2015). Variable importance analysis: A comprehensive review. *Reliability Engineering & System Safety*, *142*, 399–432. https://doi.org/10.1016/j.ress.2015.05.018

Whitesell, J. D., Liska, A., Coletta, L., Hirokawa, K. E., Bohn, P., Williford, A., Groblewski, P. A., Graddis, N., Kuan, L., Knox, J. E., Ho, A., Wakeman, W., Nicovich, P. R., Nguyen, T. N., van Velthoven, C. T. J., Garren, E., Fong, O., Naeemi, M., Henry, A. M., … Harris, J. A. (2021). Regional, Layer, and Cell-Type-Specific Connectivity of the Mouse Default Mode Network. *Neuron*, *109*(3), 545-559.e8. https://doi.org/10.1016/j.neuron.2020.11.011

Whitfield-Gabrieli, S., & Ford, J. M. (2012). Default mode network activity and connectivity in psychopathology. *Annual Review of Clinical Psychology*, *8*, 49–76. https://doi.org/10.1146/annurev-clinpsy-032511-143049

Whitfield-Gabrieli, S., Ghosh, S. S., Nieto-Castanon, A., Saygin, Z., Doehrmann, O., Chai, X. J., Reynolds, G. O., Hofmann, S. G., Pollack, M. H., & Gabrieli, J. D. (2016). Brain connectomics predict response to treatment in social anxiety disorder. *Molecular Psychiatry*, *21*(5), 680–685. https://doi.org/10.1038/mp.2015.109

Whitfield-Gabrieli, S., & Nieto-Castanon, A. (2012). Conn: A functional connectivity toolbox for correlated and anticorrelated brain networks. *Brain Connectivity*, *2*(3), 125–141. https://doi.org/10.1089/brain.2012.0073

Wilcox, C. E., Pommy, J. M., & Adinoff, B. (2016). Neural circuitry of impaired emotion regulation in substance use disorders. *The American Journal of Psychiatry*, *173*(4), 344–361. https://doi.org/10.1176/appi.ajp.2015.15060710

Winkler, A. M., Ridgway, G. R., Webster, M. A., Smith, S. M., & Nichols, T. E. (2014). Permutation inference for the general linear model. *NeuroImage*, *92*, 381–397. https://doi.org/10.1016/j.neuroimage.2014.01.060

Xie, C., Li, S. J., Shao, Y., Fu, L., Goveas, J., Ye, E., Li, W., Cohen, A. D., Chen, G., Zhang, Z., &

Yang, Z. (2011). Identification of hyperactive intrinsic amygdala network connectivity associated with impulsivity in abstinent heroin addicts. *Behavioural Brain Research*, *216*(2), 639–646. https://doi.org/10.1016/j.bbr.2010.09.004

Xie, X., Bratec, S. M., Schmid, G., Meng, C., Doll, A., Wohlschläger, A., Finke, K., Förstl, H., Zimmer, C., Pekrun, R., Schilbach, L., Riedl, V., & Sorg, C. (2016). How do you make me feel better? Social cognitive emotion regulation and the default mode network. *NeuroImage*, *134*, 270–280. https://doi.org//10.1016/j.neuroimage.2016.04.015

Xu, T., Nenning, K. H., Schwartz, E., Hong, S. J., Vogelstein, J. T., Goulas, A., Fair, D. A., Schroeder, C. E., Margulies, D. S., Smallwood, J., Milham, M. P., & Langs, G. (2020). Cross-species functional alignment reveals evolutionary hierarchy within the connectome. *NeuroImage*, *223*, 117346. https://doi.org/10.1016/j.neuroimage.2020.117346

Xue, A., Kong, R., Yang, Q., Eldaief, M. C., Angeli, P., DiNicola, L. M., Braga, R. M., Buckner, R. L., & Yeo, B. T. T. (2020). The detailed organization of the human cerebellum estimated by intrinsic functional connectivity within the individual. *Journal of Neurophysiology*, *125*(2), 358–384. https://doi.org/10.1152/jn.00561.2020

Xue, G. (2018). The neural representations underlying human episodic memory. *Trends in Cognitive Sciences*, *22*(6), 544–561. https://doi.org/10.1016/j.tics.2018.03.004

Yang, S., Yang, S., Moreira, T., Hoffman, G., Carlson, G. C., Bender, K. J., Alger, B. E., & Tang, C. M. (2014). Interlamellar CA1 network in the hippocampus. *Proceedings of the National Academy of Sciences of the United States of America*, *111*(35), 12919–12924. https://doi.org/10.1073/pnas.1405468111

Yang, Z., Xu, Y., Xu, T., Hoy, C. W., Handwerker, D. A., Chen, G., Northoff, G., Zuo, X.-N., & Bandettini, P. A. (2014). Brain network informed subject community detection in early-onset schizophrenia. *Scientific Reports*, *4*, 5549. https://doi.org/10.1038/srep05549

Yarkoni, T., & Westfall, J. (2017). Choosing Prediction Over Explanation in Psychology: Lessons From Machine Learning. *Perspectives on Psychological Science*, *12*(6), 1100–1122. https://doi.org/10.1177/1745691617693393

Yazar, Y., Bergström, Z. M., & Simons, J. S. (2017). Reduced multimodal integration of memory features following continuous theta burst stimulation of angular gyrus. *Brain Stimulation*, *10*(3), 624–629. https://doi.org/10.1016/j.brs.2017.02.011

Zhang, N., Rane, P., Huang, W., Liang, Z., Kennedy, D., Frazier, J. A., & King, J. (2010). Mapping resting-state brain networks in conscious animals. *Journal of Neuroscience Methods*, *189*(2), 186–196. https://doi.org/10.1016/j.jneumeth.2010.04.001

Zhang, Y., Jia, S., Zheng, Y., Yu, Z., Tian, Y., Ma, S., Huang, T., & Liu, J. K. (2020). Reconstruction of natural visual scenes from neural spikes with deep neural networks. *Neural Networks*, *125*, 19–30. https://doi.org/10.1016/j.neunet.2020.01.033

Zhigalov, A., Arnulfo, G., Nobili, L., Palva, S., & Palva, J. M. (2017). Modular co-organization of functional connectivity and scale-free dynamics in the human brain. *Network Neuroscience*, *1*(2), 143–165. https://doi.org/10.1162/netn_a_00008

Zimmern, V. (2020). Why brain criticality is clinically relevant: a scoping review. *Frontiers in Neural Circuits*, *14*, 54. https://doi.org/10.3389/fncir.2020.00054

Zotev, V., Phillips, R., Young, K. D., Drevets, W. C., & Bodurka, J. (2013). Prefrontal control of the amygdala during real-time fMRI neurofeedback training of emotion regulation. *PLoS ONE*, *8*(11), e79184. https://doi.org/10.1371/journal.pone.0079184

Zotev, V., Phillips, R., Yuan, H., Misaki, M., & Bodurka, J. (2014). Self-regulation of human brain activity using simultaneous real-time fMRI and EEG neurofeedback. *NeuroImage*, *85*(3), 985–995. https://doi.org/10.1016/j.neuroimage.2013.04.126

Zou, Q. H., Zhu, C. Z., Yang, Y., Zuo, X. N., Long, X. Y., Cao, Q. J., Wang, Y. F., & Zang, Y. F. (2008). An improved approach to detection of amplitude of low-frequency fluctuation (ALFF) for resting-state fMRI: Fractional ALFF. *Journal of Neuroscience Methods*, *172*(1), 137–141. https://doi.org/10.1016/j.jneumeth.2008.04.012

Zuberi, A., Waqas, A., Naveed, S., Hossain, M. M., Rahman, A., Saeed, K., & Fuhr, D. C. (2021). Prevalence of mental disorders in the WHO Eastern Mediterranean region: A systematic review and meta-analysis. *Frontiers in Psychiatry*, *12*, 665019. https://doi.org/10.3389/fpsyt.2021.665019

Declaration by candidate

I declare herewith that I have independently carried out the PhD thesis entitled „The brain's functional architecture and its links to emotion processing and episodic memory during the resting-state and an encoding task ". This thesis consists of original research articles that have been written in cooperation with the enlisted co-authors and have been published in peer-reviewed scientific journals. Only allowed resources were used and all references used were cited accordingly.

Date: _____

Signature: _____